Multifunctional Organic Field-Effect Transistors

Dissertation

zur Erlangung des Grades

“Doktor der Naturwissenschaften”

im Promotionsfach Chemie

Am Fachbereich Chemie, Pharmazie und Geowissenschaften

der Johannes Gutenberg-Universität Mainz und in Kooperation

mit dem Max-Planck-Institut für Polymerforschung in Mainz

Sten Gebel

geboren in Mainz, Deutschland

Mainz, 2025

1. Betreuer: [redacted]

2. Betreuer: [redacted]

1. Gutachter: [redacted]

2. Gutachterin: [redacted]

Tag der mündlichen Prüfung:

I hereby declare that I wrote the dissertation submitted without any unauthorized external assistance and used only sources acknowledged in this work. All textual passages which are appropriate verbatim or paraphrased from published and unpublished texts, as well as all information obtained from oral sources, are duly indicated and listed in accordance with bibliographical rules. In carrying out this research, I complied with the rules of standard scientific practice as formulated in the statutes of Johannes Gutenberg-University Mainz to ensure standard scientific practice.

…… ……

(Date, place) (Sten Gebel)

We make our world significant by the courage of

our questions and by the depth of our answers.

(Carl Sagan)

Acknowledgements

Firstly, I would like to thank my supervisor [redacted] for giving me the opportunity to carry out my PhD research in her newly formed Organic Bioelectronics Research Group at MPI-P. I am especially thankful not only for confronting me with plenty of challenges, which made me grow as a young researcher, but also for many opportunities to travel to international conferences, which I consider my personal highlights of my time as a PhD student. Secondly, I would like to thank [redacted] for providing the amazing facilities, the many constructive discussions during the work meetings and the contributions to my manuscripts. I would also like to express my gratitude to my former Master student and now fellow PhD student [redacted], who showed great dedication in the lab and therefore made significant contributions to the data presented in Chapter 5.

Furthermore, I would like to express my thankfulness to my collaborators for the following scientific contributions to the work presented in this dissertation or elsewhere: [redacted] and [redacted] for synthesizing and providing the DHA/VHF switches, [redacted], [redacted] and [redacted] for synthesizing and providing the SP/MC switches, [redacted] and [redacted] for carrying out the fs-TA measurements, including data analysis, [redacted] and [redacted] for supporting the XRD measurements at MPI-P and for carrying out the synchrotron GIWAXS measurements, including data analysis and [redacted] for supporting the EPR measurements. Additionally, I would like to thank [redacted], [redacted], [redacted], [redacted] and [redacted] for the technical support in the laboratories.

It goes without saying that probably none of this work would have been possible without the endless love and support from [redacted], [redacted] and [redacted]. Without them, I would be no one and I am incredibly grateful for having them in my life.

Abstract

Organic field-effect transistors (OFETs) enable large-area, flexible and wearable electronics. One promising approach to introduce additional functionalities for sensing and memory applications into these devices is the introduction of molecular photoswitches. These small organic molecules undergo reversible isomerization between two isomers when e.g. irradiated with light of different wavelength. The resulting reversible changes in molecular properties can be exploited to deliberately modify charge transport in OFETs and therefore enable optical control over device characteristics. After an introduction to OFETs and photoswitches (Chapter 1), Chapter 2 systematically analyzes how molecular switches can alter electrical characteristics of OFETs (literature review), while the following three chapters summarize and discuss the experimental results of this dissertation. In particular, this work addresses in detail the functionalization of OFETs and examines the effects of 1) embedding photoswitches into different functional layers of the transistor, and 2) employing different classes of photoswitches.

In Chapter 3, for the first time reversible switching of OFETs by blending dihydroazulene/vinylheptafulvene (DHA/VHF) photo-/thermoswitches into polythiophene-based conjugated polymers is presented. The reversible switching upon alternating UV light irradiation and thermal annealing is quantified by figures of merit. Irradiating the devices with different doses of UV light shows that the magnitude of switching directly depends on the respective UV dose, hence enabling a multi-level electronic system, that also shows long-term cyclability.

Chapter 4 demonstrates that stimuli-responsiveness of organic transistors is achieved by incorporating the DHA/VHF molecular switches into the gate dielectric. To systematically explore this approach, firstly the dielectric properties of the DHA/VHF blends with the dielectric polymer poly(methyl methacrylate) (PMMA) are evaluated using impedance spectroscopy. Afterwards, these switchable dielectric blends are employed as gate dielectrics in OFETs, allowing optical control over device characteristics and figures of merit.

Chapter 5 examines in detail how blends of spiropyran/merocyanine molecular switches and PMMA can be used to obtain precise control over the threshold voltage of OFETs. The functional blends are applied as gate dielectrics in polymer transistors and enable the deterministic control

over the threshold voltage via exposure to UV light. This control can be exerted after the fabrication of the device and can be reversed via thermal annealing. Furthermore, it is examined for the first time how the substitution of the photoswitches with alkyl chains of different lengths is affecting the light-responsiveness and the overall performance of the transistors.

Zusammenfassung

Organische Feldeffekttransistoren (OFETs) ermöglichen großflächige, flexible und tragbare Elektronik. Ein vielversprechender Ansatz zur Einführung zusätzlicher Funktionen für Sensor- und Speicheranwendungen in diese Bauelemente ist die Verwendung von molekularen Photoschaltern. Diese kleinen organischen Moleküle führen eine reversible Isomerisierung zwischen zwei Isomeren durch, wenn sie z. B. mit Licht unterschiedlicher Wellenlänge bestrahlt werden. Die daraus resultierenden reversiblen Änderungen der molekularen Eigenschaften können ausgenutzt werden, um den Ladungstransport in OFETs gezielt zu verändern und so optische Kontrolle über die Bauelementeigenschaften zu ermöglichen. Nach einer Einführung in OFETs und Photoschalter (Kapitel 1) wird in Kapitel 2 systematisch analysiert, wie molekulare Schalter die elektrischen Eigenschaften von OFETs verändern können (Literaturübersicht), während in den folgenden drei Kapiteln die experimentellen Ergebnisse dieser Dissertation zusammengefasst und diskutiert werden. Insbesondere befasst sich diese Arbeit ausführlich mit der Funktionalisierung von OFETs und untersucht die Auswirkungen von 1) der Einbettung von Photoschaltern in verschiedene Funktionsschichten des Transistors und 2) der Verwendung verschiedener Klassen von Photoschaltern.

In Kapitel 3 wird erstmals das reversible Schalten von OFETs durch Einbringen von Dihydroazulen/Vinylheptafulven (DHA/VHF)-Photo-/Thermoschaltern in konjugierte Polymere auf Polythiophenbasis vorgestellt. Die reversiblen Schaltvorgänge bei abwechselnder UV-Bestrahlung und thermischer Auslagerung werden mit Hilfe von Leistungskennzahlen quantifiziert. Die Bestrahlung der Bauelemente mit verschiedenen Dosen von UV-Licht zeigt, dass das Ausmaß des Schaltens direkt von der jeweiligen UV-Dosis abhängt. Dadurch wird ein mehrstufiges, elektronisches System ermöglicht, welches über eine hohe Zahl an Zyklen hinweg schaltbar bleibt.

In Kapitel 4 wird gezeigt, dass organische Transistoren durch das Einbringen von DHA/VHF-Molekularschaltern in das Dielektrikum des Bauteils stimulationsempfindlich werden. Um diesen Ansatz systematisch zu erforschen, werden zunächst die dielektrischen Eigenschaften der DHA/VHF-Gemische mit dem dielektrischen Polymer Polymethylmethacrylat (PMMA) mittels Impedanzspektroskopie analysiert. Anschließend werden diese schaltbaren dielektrischen

Gemische als Gate-Dielektrika in OFETs eingesetzt, was eine optische Kontrolle der Bauelementeigenschaften und der Leistungskennzahlen ermöglicht.

In Kapitel 5 wird untersucht, wie Gemische aus molekularen Spiropyran/Merocyanin-Schaltern und PMMA verwendet werden können, um eine präzise Kontrolle der Schwellspannung von OFETs zu erreichen. Die funktionalen Gemische werden als Gate-Dielektrika in Polymertransistoren eingesetzt und ermöglichen die Kontrolle der Schwellspannung durch Bestrahlung mit UV-Licht. Diese Kontrolle kann nach der Herstellung des Bauelements ausgeübt werden und lässt sich durch thermisches Auslagern wieder rückgängig machen. Darüber hinaus wird erstmals untersucht, wie sich das Verhalten der Transistoren, insbesondere die Lichtempfindlichkeit, durch das Anbringen unterschiedlich langer Alkylketten an die Photoschalter beeiflussen lässt.

Table of Contents

List of Abbreviations

AAP	arylazopyrazole
AFM	atomic force microscopy
AZB	azobenzene
BC	bottom-contact
BG	bottom-gate
BJT	bipolar junction transistor
COF	covalent organic framework
CPE	constant phase element
CTC	charge transfer complex
DAE	diarylethene
DASA	donor-acceptor Stenhouse adduct
DFT	density functional theory
DHA	dihydroazulene
DOS	density of states
DPP	diketopyrrolopyrrole
EDL	electric double layer
EISSA	Electrochemical Impedance Spectroscopy Spectrum Analyzer
EPR	electron paramagnetic resonance
FET	field-effect transistor
GIWAXS	grazing-incidence wide-angle X-ray scattering
HABI	hexaarylbiimidazole
HOMO	highest occupied molecular orbital
LUMO	lowest unoccupied molecular orbital
MC	merocyanine
MOSFET	metal-oxide-semiconductor field-effect transistor
NMR	nuclear magnetic resonance
NP	naphthopyran
OECT	organic electrochemical transistor
OFET	organic field-effect transistor

OLED	organic light-emitting diode
OSC	organic semiconductor
P3HT	poly(3-hexylthiophene-2,5-diyl)
PBTTT	poly[2,5-bis(3-tetradecylthiophen-2-yl)thieno[3,2-b]thiophene]
PDMS	poly(dimethylsiloxane)
PIL	polymeric ionic liquid
PMMA	poly(methyl methacrylate)
PTAA	poly(triarylamine)
PVP	poly(4-vinylphenol)
RRAM	resistive random-access memory
S/D	source/drain
SAM	self-assembled monolayer
SAND	self-assembled nanodielectric
SP	spiropyran
SPOx	spirooxazine
SRAM	static random-access memory
TC	top-contact
TFT	thin-film transistor
TG	top-gate
UV	ultraviolet
VHF	vinylheptafulvene
Vis	visible
WORM	write once read many
XRD	X-ray diffractometry

Chapter 1: Introduction

In 1977 Chiang et al. reported that the electrical conductivity of the semiconducting polymer polyacetylene could be modified over eleven orders of magnitude via doping, allowing for the controlled transition from insulating to semiconducting to metal-like properties [1]. This landmark discovery was honored with the Nobel Prize in Chemistry in the year 2000 and gave rise to the field of organic electronics. Key advantages of organic electronic materials include the vast possibilities to modify the properties of conductors and semiconductors via chemical design, as well as their mechanical flexibility and their solubility in common solvents. As a result, these materials are ideal candidates to realize low-cost fabrication of large-area devices using printing techniques such as inkjet or screen printing [2].

One core motivation of organic electronics research is to understand and control the manifold complex processes that govern device performance. Such devices can either be based on polymer semiconductors, as well as small molecule semiconductors, each providing their own advantages and challenges. As summarized in the literature, intense research efforts during the last decades have led to impressive developments in organic solar cells [3-5], organic light-emitting diodes [6-8] or organic field-effect transistors [9-11]. The physics behind these devices and the materials and processes that are used to fabricate them are outlined in numerous textbooks [12-14] and review articles [15-19] and therefore will not be discussed here extensively. Instead, this chapter will introduce the main topic of this dissertation, which are multifunctional organic field-effect transistors (OFETs) employing photoswitches. After a brief introduction to the basic principles of OFETs and photoswitches, a detailed literature survey will summarize the relevant articles focusing on the modification of charge transport in organic transistors caused by the isomerization of the switch.

1.1. Organic Field-Effect Transistors

The first field-effect behavior in an organic semiconductor device was reported by Ebisawa et al. in 1983 [20]. The authors exploited the electrical properties of polyacetylene/polysiloxane interfaces in order to fabricate a p-type depletion-mode transistor. However, the modulation of the

drain current was relatively low. Only a few years later, in 1986, Tsumura et al. published their results on the first successful fabrication and characterization of an organic field-effect transistor [21]. Their device utilized an electrochemically deposited polythiophene thin-film on top of an oxide-covered silicon wafer and was able to achieve a current modulation over more than two orders of magnitude and a charge carrier mobility of around 10^{-5} cm^2 V^{-1} s^{-1}. From this starting point onwards, the research on OFETs intensified, strongly driven by the development of new materials and more efficient fabrication techniques.

It can be stated that the charge carrier mobility (also called field-effect mobility) is one of the most important figures of merit of an organic field-effect transistor. Therefore, it can be used to monitor the progress in the field of OFET technologies over time. By establishing an improved physical understanding of transport and structure-property relationships, OFETs eventually started to outperform benchmark amorphous silicon-based devices (0.5-1 cm^2 V^{-1} s^{-1}) [10]. Nowadays, OFETs showing charge carrier mobilities of even more than 10 cm^2 V^{-1} s^{-1} are reported regularly [22]. However, the community has become more aware that regularly erroneous data analysis resulted in overestimation of mobility values, which has led to a more critical evaluation of high mobility values and transistor performance metrics in general [23, 24]. A re-evaluation of the literature of the past 30 years published by Paterson et al. in 2018 stated that the threshold of 10 cm^2 V^{-1} s^{-1} has been surpassed for p-type, but not for n-type organic semiconductors [25]. They also reported that evaporated small molecules show the highest mobilities and that blend systems containing small molecules and polymers yield the highest mobilities for solution-processed organic semiconductors. However, mobility is not the only device parameter to consider. Transistors have several other figures of merit such as on/off ratio, threshold voltage, subthreshold swing and contact resistance, among others. It is crucial to consider all of these parameters and even others metrics such as bias stress stability or environmental stability in order to obtain a comprehensive picture of the transistor performance and to properly evaluate the suitability for certain applications, e.g. as building blocks for digital logic circuits. However, it is even necessary to go beyond this standard electrical characterization in order to tap into the full potential of the organic transistor. Either by harnessing the intrinsic optoelectronic properties of the organic semiconductor, or by modifying the device with an additional functional component, it is possible to explore OFETs for applications such as sensors or memory devices. The objective of this dissertation is to evaluate one specific strategy to realize this goal, namely the incorporation of

stimuli-responsive molecular switches into OFETs for the development of multifunctional organic optoelectronic devices. Such devices will enable the next generation of lightweight and flexible electronic applications, including photodetectors, photomemories, light-switchable logic and neuromorphic circuits. However, before summarizing the relevant literature on this topic, a brief overview will be provided on how an organic field-effect transistor works and how relevant figures of merit can be extracted from its electrical characteristics.

OFET Architectures

Organic field-effect transistors are three-terminal devices consisting of electrically conductive electrodes, an insulating layer and a semiconducting (also called active) layer. In analogy to metal-oxide-semiconductor field-effect transistors (MOSFETs), the three electrodes are referred to as source, drain and gate. The latter is separated from the semiconductor by an insulator, also called gate dielectric. As mentioned above, the first OFET device was constructed by depositing the semiconductor on an oxide-covered doped silicon substrate on which source/drain electrodes had already been deposited. This particular device geometry is called bottom-gate bottom-contact and is shown schematically in **Figure 1.1a**. It can be convenient to use such an architecture, since the transistor can be fabricated in a single step by depositing the semiconductor on the pre-prepared substrate. Similarly, it is possible to first deposit the semiconductor on the gate dielectric and deposit the source/drain contacts afterwards. Such a geometry is called bottom-gate top-contact and is depicted in **Figure 1.1b**. Until today, bottom-gate OFETs are often realized with oxide-covered silicon substrates. However, charge transport in these devices is usually hindered by a high density of charge traps, i.e. silanol groups, which are forming in order to passivate dangling bonds on the silicon dioxide surface [26]. One possibility to avoid this issue is by utilizing polymer dielectrics such as Cytop or PMMA, which yield interfaces with lower trap densities [27-29]. Unfortunately, the surfaces of these polymers typically have low surface energies, making it challenging to deposit organic semiconductors from solution on top of them. An alternative device architecture (top-gate devices) overcomes this problem through deposition of the polymer dielectric on top of the semiconductor. This is possible, as long as the dielectric is coated from a solvent that is orthogonal to the semiconductor. As depicted in **Figure 1.1c-d** the top-gate architecture, similar to the bottom-gate architecture, can be combined with bottom or top source/drain electrodes. These four possible transistor architectures can also be divided into

staggered and coplanar architectures, where the former describes the scenario that source/drain electrodes and the dielectric are on opposite sides of the semiconductor (i.e. bottom-gate top-contact and top-gate bottom-contact), while the latter refers to devices where source/drain electrodes and the dielectric are on the same side of the semiconductor (i.e. bottom-gate bottom-contact and top-gate top-contact).

From the geometric considerations, it becomes clear that OFETs are complex devices containing several different interfaces. Even though all of these interfaces are affecting the overall performance of the transistor, the charge transport is mostly governed by the properties of the semiconductor-dielectric interface.

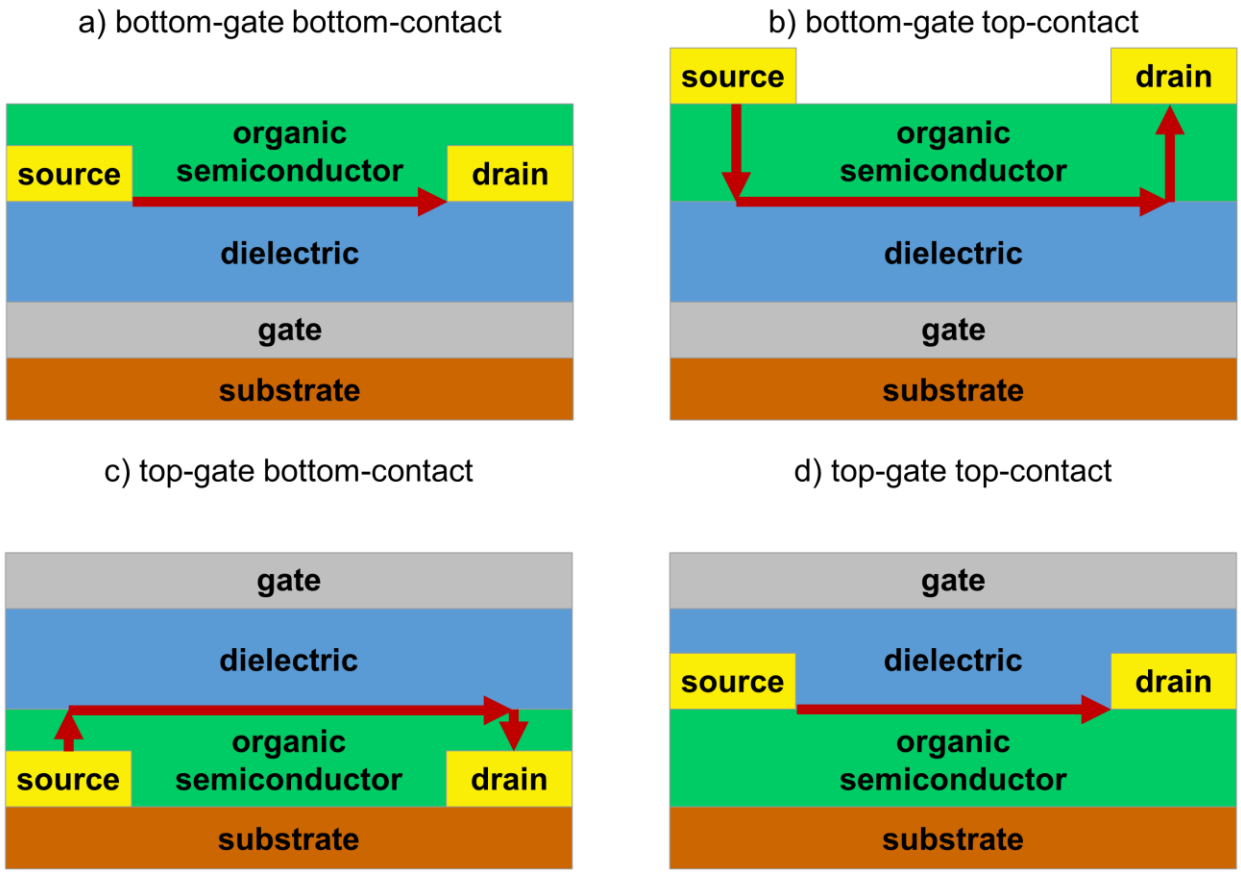

Figure 1.1: Typical device architectures of an organic field-effect transistor. a) Bottom-gate bottom-contact, b) bottom-gate top-contact, c) top-gate bottom-contact and d) top-gate top-contact. The red arrows schematically depict the charge flow from the source electrode across the semiconductor-dielectric interface to the drain electrode.

Charge Transport in OFETs

In any transistor, the charge transport between two electrodes can be controlled via a third electrode. Depending on how this control is achieved, transistors can be divided into two groups: Current-controlled bipolar junction transistors (BJTs) and voltage-controlled field-effect transistors (FETs). BJTs are composed of three doped semiconductor layers (either in an n-p-n or p-n-p configuration), which is difficult to realize using organic semiconductors and was only recently successfully demonstrated for the first time [30]. A FET operates via accumulation and depletion of charges within the channel between the source and drain, thereby controlling the conductivity between these two electrodes. This phenomenon occurs at the semiconductor-dielectric interface and is controlled via the application of a potential difference between the gate electrode and the source contact, also called gate-source bias V_{GS}. The gate dielectric in between the gate electrode and the semiconductor-dielectric interface can be considered as a parallel plate capacitor. By applying a bias to the gate electrode, (the source is typically held at ground potential) charge carriers can be injected from the source electrode and accumulate at the semiconductor-dielectric interface. This scenario is sketched in **Figure 1.2** for an OFET utilizing a p-type semiconductor.

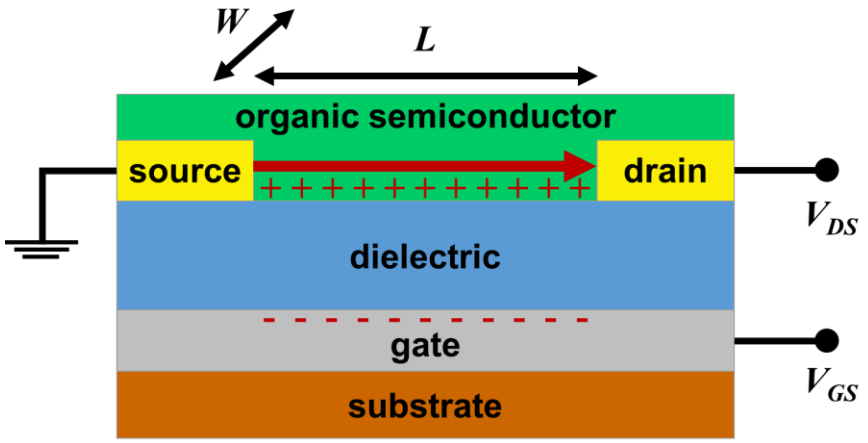

Figure 1.2: Schematic depiction of a p-type OFET with channel length L and channel width W under applied biases. The source electrode is grounded, while the drain-source bias V_{DS} is applied to the drain electrode and the gate-source bias V_{GS} is applied to the gate electrode. The latter induces positive charge carriers within the organic semiconductor (however only in the region with close proximity to the semiconductor-dielectric interface) which will move towards the drain electrode as a consequence of the difference in electric potential between the source and drain. Reproduced from [31].

In reality, the gate-source bias needs to exceed a certain threshold voltage V_{Th} in order to create mobile charge carriers. This is due to the presence of traps in proximity to the interface, which are capturing and therefore immobilizing the first injected charges. When a second potential difference is applied between the drain and the source electrode, also called drain-source bias V_{DS}, the mobile charge carriers will move from source to drain, where the drain current I_D is measured. Depending on the magnitude of V_{DS} the transistor either operates in the linear regime ($|V_{DS}| << |V_{GS} - V_{Th}|$) or the saturation regime ($|V_{DS}| > |V_{GS} - V_{Th}|$). The drain current in the linear regime $I_{D,lin}$ depends linearly on V_{DS} (see Equation 1), while the drain current in the saturation regime $I_{D,sat}$ does not depend on V_{DS} (see Equation 2). The drain currents in both regimes depend on the charge carrier mobility μ, the dimensions of the channel (width W and length L) and the area-normalized capacitance of the gate dielectric C_i.

$$I_{D,lin} = \mu \frac{W}{L} C_i (V_{GS} - V_{Th}) V_{DS} \tag{1}$$

$$I_{D,sat} = \mu \frac{W}{2L} C_i (V_{GS} - V_{Th})^2 \tag{2}$$

The transition point between the two regimes is reached when $|V_{DS}| = |V_{GS} - V_{Th}|$. This point is called pinch-off, since this is when the concentration of mobile charges becomes zero at the drain electrode. A further increase of the drain-source bias only extends the width of this depletion zone, but does not yield any further increase in the now space-charge limited drain current. The spatial distribution of charge carrier density and the corresponding I_D-V_{DS} characteristics are given in **Figure 1.3**.

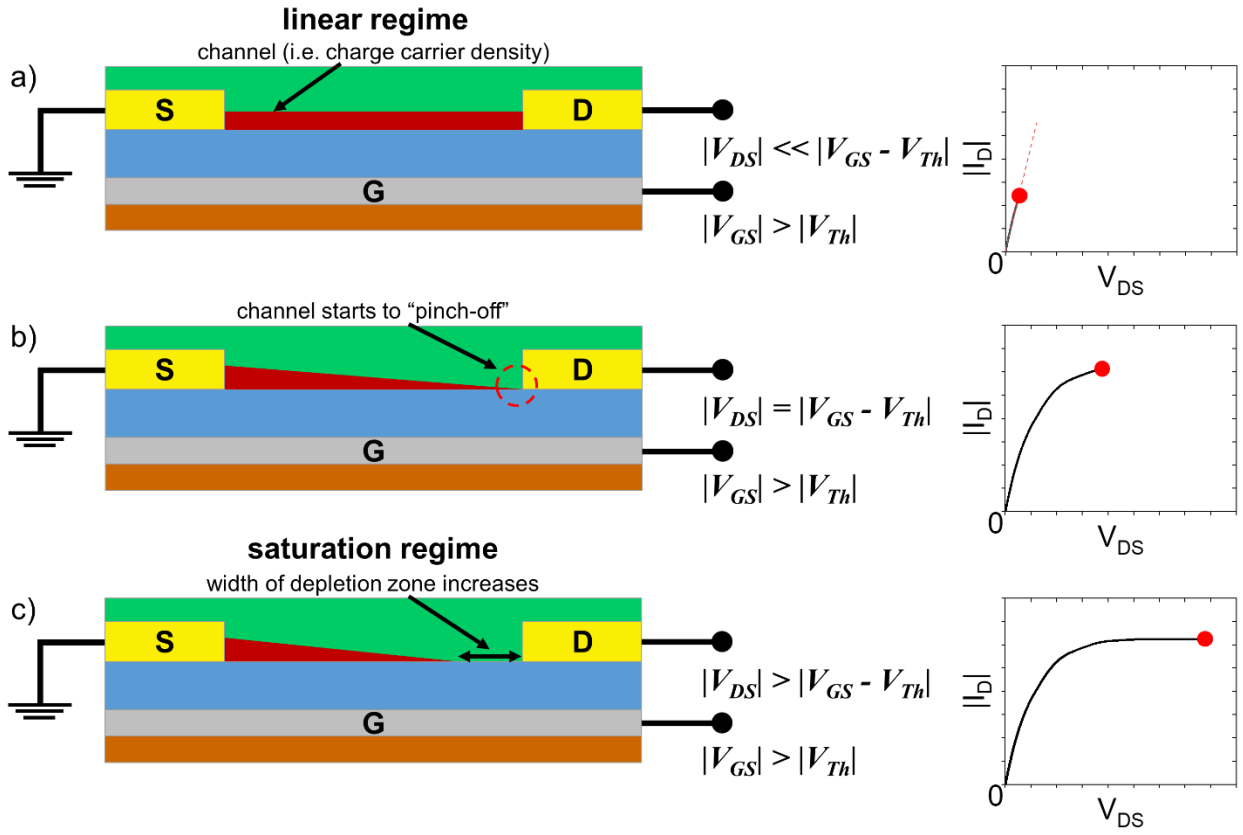

Figure 1.3: Operational regimes of an OFET. a) Linear regime, b) pinch-off and c) saturation regime. As soon as the applied gate-source bias V_{GS} exceeds the threshold voltage V_{Th}, charge carriers (indicated in red) start to accumulate at the semiconductor-dielectric interface. In the linear regime, the drain current I_D depends linearly on the applied drain-source bias V_{DS}. In the saturation regime however, the drain current does not depend on the drain-source bias, but only on the magnitude of the space-charge limited current between the pinch-off point and the drain electrode. The color coding of the individual components of the transistor is the same as in **Figure 1.2**. Adapted from [32].

The basic electrical measurements conducted on OFETs are usually transfer characteristics (measuring I_D, while sweeping V_{GS} and keeping V_{DS} constant) and output characteristics (measuring I_D, while sweeping V_{DS} and keeping V_{GS} constant). Plotting transfer characteristics on a linear-linear scale, allows for the extraction of field-effect mobility μ and threshold voltage V_{Th}, while a logarithmic-linear plot allows for the extraction of subthreshold swing SS, on-voltage V_{on}, on-current I_{on} and off-current I_{off} . The latter two can be used to calculate the on/off ratio. **Figure 1.4** shows typical transfer characteristics and how transistor figures of merit can be extracted from them. It should be noted that due to the quadratic dependence on V_{GS} (see Equation 2) linear-linear plots of transfer characteristics measured in the saturation regime display the square root of the drain current on the ordinate.

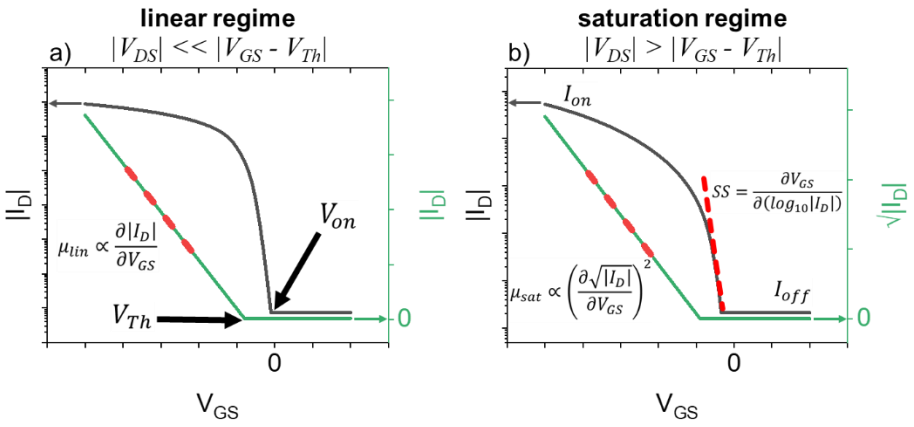

Figure 1.4: Typical transfer curves measured on a p-type OFET in the a) linear regime and b) saturation regime. These characteristics can be plotted either on a logarithmic (black lines) or on a linear (green lines) ordinate which allows for the extraction of device parameters such as on-current I_{on}, off-current I_{off}, on-voltage V_{on}, subthreshold swing SS and field-effect mobility μ, threshold voltage V_{Th} respectively. In order to calculate the field-effect mobilities, the capacitance of the gate dielectric and the device geometry need to be considered as given in Equations 1 and 2. It should be noted that the linear ordinate in the saturation regime does not display the drain current, but its square root. Threshold voltage, on-voltage, subthreshold swing, on-current and off-current are determined the same way in both regimes. Adapted from [16].

1.2. Photoswitches

Photochromic molecules, also called photoswitches, are small organic molecules, which can be reversibly converted between (at least) two different isomeric forms. This conversion can be triggered using light of different wavelengths (typically in the UV and visible range) and is accompanied by a change in color [33]. **Figure 1.5** displays an example of a photoswitch and shows how the transition between the two isomers is related to a change in the molecular structure and therefore in the optical properties.

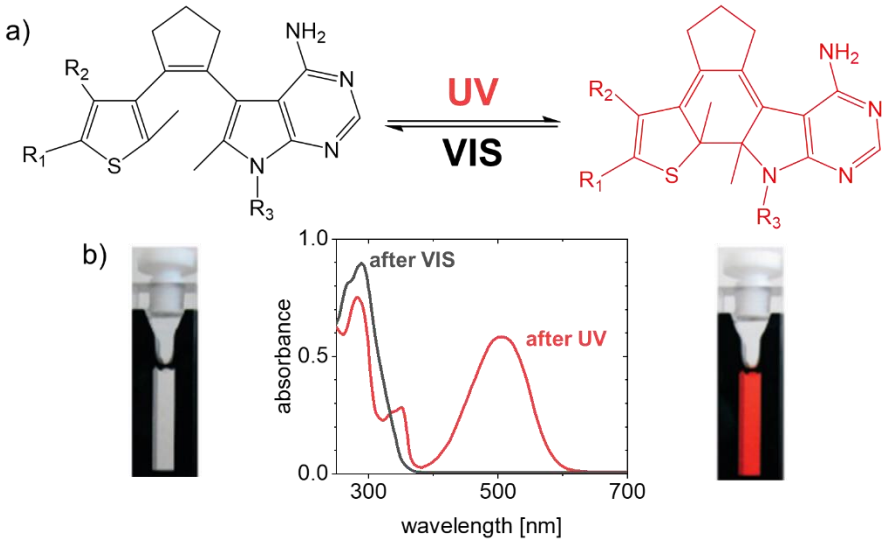

Figure 1.5: A typical photoswitch (diarylethene derivative with heteroaryl substitutions) showing photochromic behavior in solution. a) Molecular structures of both isomers. The reversible isomerization between these isomers is induced by irradiation with either UV or visible light. b) Photographs showing the coloration (after exposure to UV light) and the discoloration (after exposure to visible light) of the solution and the corresponding UV/Vis absorption spectra. The spectrum measured after exposure to UV light indicates the appearance of an absorption peak at around 500 nm, which correlates to the red color of the dissolved compound. Figures were either reproduced or adapted from [34].

Photochromic molecules are a subgroup of chromic molecules, which are materials that show a change in color due to the application of a certain stimulus. The range of possible stimuli beyond light includes temperature, electric field, application of solvents in liquid or vapor form, pH, ions or mechanical force, giving rise to the phenomena of thermochromism [35], electrochromism [36], solvatochromism [37], vapochromism [38], halochromism [39], ionochromism [40] and mechanochromism [41] among others. Besides their interesting chemical and physical properties, photoswitches have also attracted considerable attention as candidates to realize molecular machines. In 1999 Koumura et al. were the first to report a light-driven molecular motor, which was able to convert energy in the form of UV light or thermal stimulus into a unidirectional rotary motion via four discrete isomerization steps [42]. For this discovery and the subsequent developments, Bernard L. Feringa was honored with the Nobel Prize in Chemistry in 2016.

To date, a wide variety of photoswitches is known [43] and new ones are continuously synthesized [44-46]. Some recent trends regarding photoswitches include red-shifted switches that isomerize under visible and near-infrared light [47], switches with orthogonal stimuli [48], solid-to-liquid phase transition materials [49] and ferroelectric photoswitches [50-52]. Additionally, these

photoresponsive materials are in high demand as switchable fluorophores in bioimaging [53], in photopharmacology [54], and other applications in soft materials [55] and biological systems [56]. It becomes clear that photoswitches are fascinating materials, which draw significant attention from multidisciplinary research communities due to their wide range of possible applications.

The objective of this dissertation is to utilize the potential of photoswitches for one specific application, namely the modification of charge transport in OFETs, in order to develop novel concepts for optoelectronic devices such as photomemories or photodetectors. Prior to summarizing the current literature addressing this issue, the classes of photoswitches that are most relevant in this context will be introduced. These include azobenzenes, spirocompounds and diarylethenes.

Azobenzenes

The chemical compound diphenyldiazene, also called azobenzene, is a molecule containing two phenyl rings linked by an azo-bridge (nitrogen-nitrogen double bond) which was first synthesized and characterized in 1834 by Mitscherlich [57]. The term azobenzene however, is not only referring to the parent molecule, but in general to the whole class of substituted azo-compounds [58]. After the initial discovery, azo-compounds quickly found application as synthetic dyes with the first examples being aniline yellow and Bismarck brown reported in 1861 and 1863, respectively [59]. Further information about the rich history of these materials in general is well summarized in the literature [60]. In 1937, Hartley reported the groundbreaking discovery that azobenzene can reversibly isomerize between the *trans*- and the *cis*-form (some authors refer to them as *E*- and *Z*-isomers respectively) under application of light and heat [61]. The isomerization from the stable *trans*-isomer to the metastable *cis*-isomer is usually triggered by UV light, while the backreaction occurs spontaneously as soon as the light source is turned off, but can be accelerated by irradiation with visible light or by heating [62]. Expanding the range of possible applications for these photoswitches can be achieved by increasing the lifetime of the metastable *cis*-isomer through chemical design [63-66]. The reversible transformation between the two isomers of unsubstituted azobenzene is shown in **Figure 1.6**.

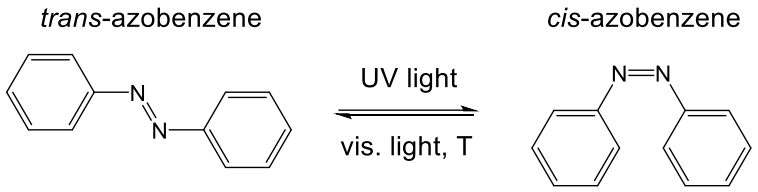

Figure 1.6: Molecular structure of the (parent) azobenzene photoswitch. The reversible isomerization from the *trans*- to the *cis*-isomer is induced by irradiation with UV light, while the backreaction from the *cis*- to the *trans*-isomer can be induced by irradiation with visible light or via thermal activation.

As a consequence of the isomerization, the molecule simultaneously experiences significant changes in its geometric conformation and its dipole moment [67]. As will be discussed below, it is these property changes in particular that make azobenzene photoswitches very attractive to realize stimuli-responsive organic electronic devices. Besides electronics, the vast range of possible applications, including biomedicine [68], solar energy storage [69], light-induced actuators [70] or mechanophores [71], indicates the immense importance of these materials. Some authors even claim that azobenzenes are the most studied photoswitches ever since [62].

Spiropyrans and Spirooxazines

The first account of the synthesis and characterization of spiropyrans was published in 1908 by Decker et al. [72]. Even though the thermochromic properties of these molecules were already noted in this early report, it was not until 1952 that Fischer et al. published results about a photochromic spiropyran derivative [73]. This finding and the subsequent proposal to use these materials as photochemical memories marked a new starting point for research on photoswitches [74]. It is interesting to note that the nowadays widely used term photochromism was coined by the same group that published these findings [75].

To date, the spiropyran derivative that is most commonly used to construct light-responsive organic electronic devices is the commercially available 1′,3′-dihydro-1′,3′,3′-trimethyl-6-nitrospiro[2*H*-1-benzopyran-2,2′-(2*H*)-indole]. This material (and its related compounds) are known to undergo a ring-opening reaction, which transforms the non-ionic spiropyran (SP) into the zwitterionic merocyanine (MC) under UV light irradiation. In the colorless SP isomer, the indoline and the chromene unit are connected through a spiro-carbon and are oriented perpendicular to each other. The MC isomer however is planar and fully conjugated which gives

rise to a dark blue/purple color [76]. Besides the considerable change in the size of the molecule, the isomerization also alters the dipole moment from around 4-6 D for SP to around 14-18 D for MC [77]. The backreaction occurs spontaneously and can be accelerated with visible light irradiation or heat. The reaction scheme of this isomerization is depicted in **Figure 1.7**.

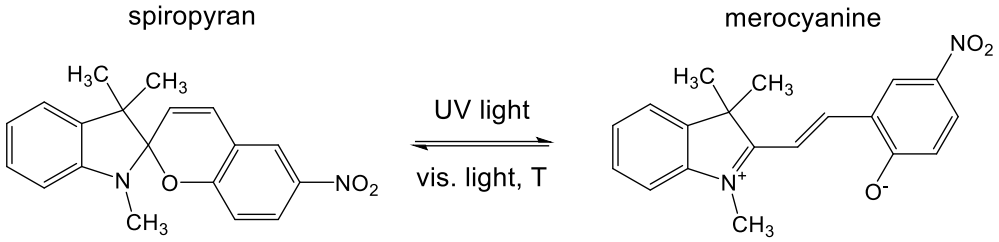

Figure 1.7: Molecular structure of the typical spiropyran photoswitch 1′,3′-dihydro-1′,3′,3′-trimethyl-6-nitrospiro[2*H*-1-benzopyran-2,2′-(2*H*)-indole]. The reversible isomerization from the non-ionic spiropyran to the zwitterionic merocyanine isomer is induced by irradiation with UV light, while the backreaction from the merocyanine to the spiropyran isomer can be induced by irradiation with visible light or via thermal activation.

A unique advantage of this system is its ability to respond to a wide range of stimuli comprising not only light, temperature and pH [78], but also the presence of metal ions [79], solvents of different polarity [80] or mechanical stress [81]. In addition, merocyanines tend to aggregate due to dipole-dipole interactions and π-π stacking which gives rise to phenomena such as bathochromic/hypsochromic shifts of the optical absorption in the case of J-aggregates [82]/H-aggregates [83] or photocontraction of liquid films [84].

A significant drawback of SP/MC photoswitches is their poor resistance against photo-oxidation leading to strong switching fatigue [85]. Several strategies have been proposed to overcome this issue, e.g. the use of near-infrared light instead of UV light (two-photon excitation instead of single-photon excitation) [86], the addition of antioxidant groups [87] or singlet oxygen quenchers [88]. However, switching experiments under the exclusion of air indicated that other mechanisms can additionally contribute to the fatigue [89]. Studies aiming to avoid aggregation of the MC isomers via immobilization and/or dilution of the photoswitch [90-93] were successful in reducing switching fatigue of SP/MC photoswitches.

A class of photochromic compounds that is closely related to spiropyrans are spirooxazines. The first reports of these materials were published in the 1960s and 1970s, many in the form of patents [94, 95]. Similar to spiropyrans, irradiation with UV light induces a ring opening reaction yielding

the merocyanine form [96]. **Figure 1.8** depicts the reversible isomerization of a typical spirooxazine photoswitch.

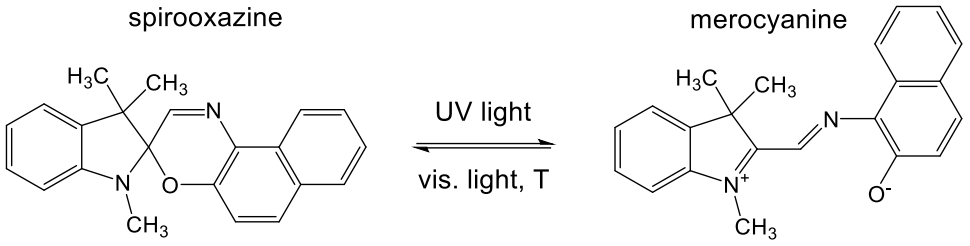

Figure 1.8: Molecular structure of the typical spirooxazine photoswitch 1,3-dihydro-1,3,3-trimethylspiro[2*H*-indole-2,3′-[3*H*]naphth[2,1-*b*][1,4]oxazine]. The reversible isomerization from the spirooxazine to the merocyanine isomer is induced by irradiation with UV light, while the backreaction from the merocyanine to the spirooxazine isomer can be induced by irradiation with visible light or via thermal activation.

In general, the photochemical properties of spirooxazines are similar to the ones of spiropyrans [97]. However, the main advantage over spiropyrans is their significantly higher resistance against switching fatigue [98-100].

While most of the early research efforts dedicated to spiropyrans and spirooxazines focused on possible memory applications [74, 101], attention has shifted more recently towards sensing [102-104] and biological applications such as drug delivery [105, 106].

Diarylethenes

In general, diarylethenes (DAEs) are molecules in which two aromatic groups are linked through a carbon-carbon double bond. The simplest DAE, stilbene is known to undergo a photocyclization reaction under UV light, with an isomerization from *trans*-/*E*-stilbene to *cis*-/*Z*-stilbene as an initial step to yield dihydrophenanthrene [107]. However, this photoisomer is not stable and returns back to stilbene in the dark as long as oxygen or other hydrogen acceptors are excluded. When the cyclization reaction of stilbene is triggered in air, phenanthrene will be formed and the photochromic properties are lost irreversibly. Motivated by this knowledge Irie et al. were the first to report the successful synthesis of air-stable, thermally irreversible photochromic DAEs in 1988 by replacing the benzene rings of stilbene with methyl-substituted heterocyclic rings [108]. The molecular structure of one of these molecules and its reversible cyclization reaction induced by UV light (ring-opening reaction induced by visible light) is shown in **Figure 1.9**.

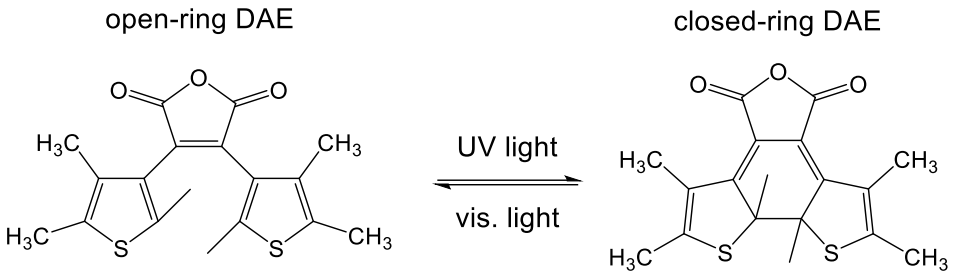

Figure 1.9: Molecular structure of one of the first DAE photoswitches reported by Irie et al. [108]. The reversible isomerization from the open-ring to the closed-ring isomer is induced by irradiation with UV light, while the backreaction from the closed-ring to the open-ring isomer is induced by irradiation with visible light. In contrast to other photoswitches, this compound and most other DAE photoswitches do not undergo any thermally activated isomerization reactions.

This discovery can be considered a significant breakthrough in photoswitch research, since some derivatives have been reported to reach very long lifetimes of both isomers on the timescale of 10^5 years (at 30 °C) [109] and cycle numbers of more than 10^4 times without significant degradation [110, 111]. Such excellent cycling stability can be observed even in solid state, since the isomerization causes only negligible changes in the size and structure of the molecule [112]. It is for such superior properties, further including fast response times of less than 10 ps [113, 114] and photocyclization quantum yields of close to 1 [115, 116] that these molecules gathered considerable attention [117-120]. In particular, they are promising candidates for optoelectronic devices such as optical memories and switches [121]. As will be discussed in the next chapter, indeed this potential has already been widely harnessed to realize a great amount of applications in the field of light-responsive organic electronic devices. Most of these devices exploit the fact that the π-conjugation of the open-ring and the closed-ring isomers differ greatly. The more extended π-electron system of the closed-ring isomer manifests itself in a lower bandgap and thereby a characteristic coloration [122]. It should be noted that to date, the term DAE photoswitch usually refers to compounds based on these molecules originally developed by Irie and coworkers and not anymore to other diarylethene compounds including stilbene. Some authors also use the term dithienylethenes for DAEs in which the alkene is substituted with thiophene moieties.

Chapter 2: Photoswitches in OFETs (Literature Review)

The application of photoswitches enables the realization of multifunctional organic electronic devices. Review articles on this matter are often focusing on two types of devices: 1) Molecular-junction-based devices employing the photoswitch as a single-molecule, as a self-assembled monolayer or as a thin-film. Herein, the electrical characteristics depend directly on the isomerization of the switch [123-126]. 2) Thin-film-based devices where the isomerization of the switch alters the semiconducting, conducting or dielectric properties of a second (host) material and thereby causes the alteration of device characteristics. This strategy has been realized successfully for combinations of photoswitches with organic semiconductors [127-132], carbon nanomaterials [133], 2D materials [134] and solution-processable semiconductors in general [77]. Review articles dedicated exclusively to photoswitches in OFETs have been published by Fu et al. in 2016 [135] and Xu et al. in 2021 [136]. These two articles categorize the published works based on straightforward criteria such as device architecture or the type of photoswitch. The following literature review aims to go beyond these obvious criteria and instead categorizes the literature based on the mechanism of charge transport modification. This provides a novel perspective on organic field-effect transistors functionalized with photoswitches and yields a more comprehensive understanding of how the isomerization of photoswitches modulates the charge transport in these devices.

The first report of reversible alteration of OFET characteristics through the isomerization of a photoswitch was published by Shen et al. in 2009 [137]. Since then to the best of my knowledge, a total of 75 research articles covering OFETs functionalized with photoswitches have been published (not including review articles). As shown in **Figure 2.1a**, the majority of these works focuses on three kinds of photoswitches, namely diarylethenes (28 articles), (indoline) spiropyrans/spirooxazines (27 articles) and azobenzenes (14 articles). Others such as stilbenes (two articles), arylazopyrazoles (two articles), hexaarylbiimidazoles (one article), naphthopyrans (one article) and donor-acceptor Stenhouse adducts (one article) have not been used as frequently. Further analysis of the literature with respect to device architecture and type of organic semiconductor reveals that most work has been conducted on bottom-gate instead of top-gate devices (72 vs. 4 articles, see **Figure 2.1b**) and that small molecule organic semiconductors have been preferred over polymer semiconductors (46 vs. 30 articles, see **Figure 2.1c**). It can be

concluded that top-gate OFETs using polymer semiconductors, which are the experimental focus of this dissertation, are currently underrepresented in the literature for photoswitch-functionalized organic field-effect transistors.

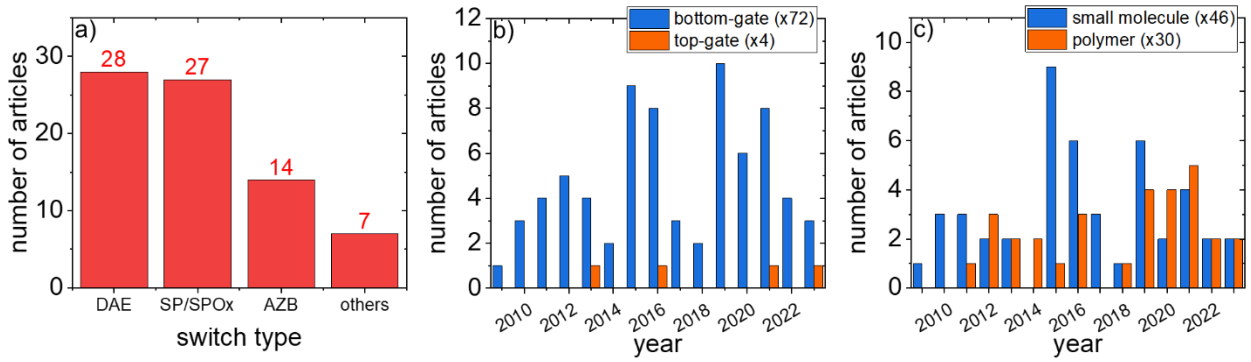

Figure 2.1: Results of the literature review concerning photoswitch-functionalized organic field-effect transistors. Number of published articles categorized by the following criteria: a) Type of photoswitch, b) type of device architecture (bottom-gate vs. top-gate) and c) type of organic semiconductor (small molecule vs. polymer). In addition, b) and c) show how the number of articles developed over time from the year of the first report in 2009 to 2023 (articles published in 2024 [138-140] were not yet taken into account). Reports that utilize both architectures or both types of semiconductors were counted in either category. A breakdown of the category "others" in panel a) is given in the main text. The following acronyms are used in panel a): DAE = diarylethene, SP = spiropyran, SPOx = spirooxazine, AZB = azobenzene.

The detailed summary of the literature review given in **Table 2.1** provides further details to each report, including the OFET architecture, type of charge transport, used semiconductor, type of photoswitch, information about how the switch was incorporated into the device and most importantly the proposed mechanism by which the switch alters the charge transport through the device.

Table 2.1: Overview of publications that report photoswitch-functionalized OFETs sorted by the mechanism of charge transport modulation. The following acronyms and abbreviations are used in the columns from left to right: BG = bottom-gate, TG = top-gate, BC = bottom-contact, TC = top-contact; p = hole transport, n = electron transport, a = ambipolar transport; DAE = diarylethene, AZB = azobenzene, DASA = donor-acceptor Stenhouse adduct, SP = spiropyran, NP = naphthopyran, SPOx = spirooxazine, AAP = arylazopyrazole, HABI = hexaarylbiimidazole; OSC = organic semiconductor, SAM = self-assembled monolayer, S/D = source/drain, SAND = self-assembled nanodielectric, PIL = polymeric ionic liquid. The nomenclature of the semiconductors was reproduced without changes.

architecture	charge transport type	semiconductor(s)	switch type	incorporation of the switch into the transistor		mechanism	reference
				separate layer	location		
BGBC	n	PCBM, ICBA	DAE	no	blended into OSC	trapping via energy levels	[141]
BGBC	a	DPPT-TT	DAE	no	permeated into OSC	trapping via energy levels	[142]
BGBC, BGTC	p, n	AZOPD	AZB	yes	switch = OSC	trapping via energy levels	[143]
BGTC	p	pentacene	DAE	yes	between dielectric and OSC	trapping via energy levels	[144]
BGBC	p	P3HT	DAE	no	blended into OSC	trapping via energy levels	[145]
BGTC, BGBC	p	P3HT, C_{12}-BTBT	DAE	no	blended into OSC	trapping via energy levels	[146]
BGBC	p	P3HT	DAE	no	blended into OSC	trapping via energy levels	[147]
BGBC	p	F8T2, MDMO-PPV, F8	DAE	no	permeated into OSC	trapping via energy levels	[148]
BGBC	p	P3HT	DAE	no	blended into OSC	trapping via energy levels	[149]
TGBC	p	P3HT	DAE	no	blended into OSC	trapping via energy levels	[150]
BGTC	p	DNTT	DAE	yes	between dielectric and OSC	trapping via energy levels	[151]
BGBC	p	DPPT-TT, PCbD-IDTTP	DAE	no	blended into OSC	trapping via energy levels	[152]
BGBC	p	ITIC	DAE	no	blended into OSC	trapping via energy levels	[153]
TGBC	p	DPP3T, DPP4T, DPPBT, IDT-BT, TIF-BT, TBIDT-BT	DAE	no	blended into OSC	trapping via energy levels	[154]
BGTC	p	CuPc	DAE	no	co-evaporated into OSC	trapping via energy levels	[155]
BGBC	p	F8BT, F8T2, P3HT, DPPT-TT, IIDDT-C3	DAE	no	blended into OSC	trapping via energy levels	[156]
BGBC	p	DPP-DTT	DAE	no	blended into OSC	trapping via energy levels	[157]
BGTC	p	pentacene	AZB	yes, no	SAM on dielectric, clusters in OSC	trapping via functional groups	[158]

BGTC	p	C_5-BTBT	AZB	no	in dielectric polymer sidechain	trapping via functional groups	[159]
BGTC	p	C_{10}-BTBT	DASA	no	blended into dielectric	trapping in dielectric	[160]
BGTC	p	pentacene	DAE	yes	SAM on nanoparticles	injection or tunneling barrier	[161]
BGBC	p	PBTTT	AZB	yes	SAM on S/D electrodes	injection or tunneling barrier	[162]
BGTC	a	BTT-DAE	DAE	yes	switch = OSC	injection or tunneling barrier	[163]
BGTC	a	DBT-DAE	DAE	yes	switch = OSC	injection or tunneling barrier	[164]
TGBC	n	P(NDI2OD-T2)	DAE	yes	SAM on S/D electrodes	injection or tunneling barrier	[165]
BGBC	n	PDIF-CN_2	AZB	yes	SAM on S/D electrodes	injection or tunneling barrier	[166]
BGBC	p	P3HT	AZB	yes	SAM on nanoparticles	injection or tunneling barrier	[167]
BGTC	p	pentacene	DAE	yes	SAM on dielectric	injection or tunneling barrier	[168]
BGBC	p	pentacene	SP	yes	SAM on S/D electrodes	injection or tunneling barrier	[169]
BGBC	p	PDAZO	AZB	yes	in OSC polymer sidechain	energetic disorder	[170]
dual gate	p	PTAA	SP	no	blended into OSC	energetic disorder	[171]
BGTC	p	PTAA	NP	no	blended into OSC	energetic disorder	[172]
BGTC	p	P3HT, PTAA	SP	no	blended into OSC	energetic disorder	[173]
BGBC	p	pDSP-1, pDSP-5	SP	yes	in OSC polymer sidechain	energetic disorder	[174]
BGTC	p	PTAA	SP, SPOx	no	blended into OSC	energetic disorder	[175]
BGBC	p	DPP4T (only in SI)	SP	no	blended into OSC	energetic disorder	[176]
BGBC	p	POMPYA 1, 2 and 3	AZB, AAP	yes	in OSC polymer sidechain	morphology	[177]
BGTC	p	APDPD	AZB	yes	part of OSC small molecule	morphology	[178]
BGTC	p	AZO-BTBT-8	AZB	yes	part of OSC small molecule	morphology	[179]
BGTC	p	stilbene oligomers M3 and M4	stilbene	yes	switch = OSC	morphology	[180]
BGBC	p	PDPYA	AAP	yes	in OSC polymer sidechain	morphology	[181]
BGTC	p	2D p-MSB (single crystal)	stilbene	yes	switch = OSC	morphology	[182]
BGTC	p, n	pentacene, F_{16}CuPc	SP	no	blended into dielectric	capacitance of dielectric	[183]
BGTC	n	P13	SP	no	blended into dielectric	capacitance of dielectric	[184]
BGTC	n	P13, P5	SP	no	blended into dielectric	capacitance of dielectric	[185]
BGTC	p	pentacene	SP	yes	in dielectric polymer sidechain	capacitance of dielectric	[186]
BGTC	p	pentacene	SP	yes	SAM on dielectric	additional built-in electric field	[187]
BGBC	p	PDPP4T, P3HT, PBTTT, PDPPDTT	HABI	no	blended into OSC	additional built-in electric field	[188]

BGTC, BGBC	p, n	pentacene, $F_{16}CuPc$	SP	yes	stamped onto OSC surface	additional built-in electric field	[137]
BGTC	p	diarylethene	DAE	yes	switch = OSC	π-conjugation	[189]
BGTC	p	DAE	DAE	yes	switch = OSC	π-conjugation	[190]
BGTC	p	DAE	DAE	yes	switch = OSC	π-conjugation	[191]
BGTC	n	C_{60}	SP	yes	between dielectric and OSC	light-induced charge transfer	[192]
BGTC	n	C_{60}	SP	yes	between dielectric and OSC	photoprogrammable OFET	[193]
BGTC	n	C_{60}	SPOx	yes	between dielectric and OSC	photoprogrammable OFET	[194]
BGTC	n	C_{60}	DAE	yes	between dielectric and OSC	photoprogrammable OFET	[195]
BGTC	p	pentacene	SP	yes	between dielectric and OSC	photoprogrammable OFET	[196]
BGTC	n	C_{60}	SPOx	yes	between dielectric and OSC	photoprogrammable OFET	[197]
BGTC	p	DBI	SPOx	yes	between dielectric and OSC	photoprogrammable OFET	[198]
BGTC	n	C_{60}	DAE	yes	between dielectric and OSC	photoprogrammable OFET	[199]
BGTC	n	C_{60}	DAE	yes	between dielectric and OSC	photoprogrammable OFET	[200]
BGTC	p	pentacene	SPOx	no	blended into dielectric	photoprogrammable OFET	[201]
BGTC	p	pentacene	SP	no	blended into dielectric	photoprogrammable OFET	[202]
BGTC	p	C_5-BTBT	AZB	no	blended into OSC	phototransistor	[203]
BGTC	p	P3HT	AZB	no	blended into dielectric	phototransistor	[204]
BGTC	n	C_{60}	SP	yes, no	between dielectric and OSC, co-evaporated into OSC	phototransistor	[205]
BGTC	n	pyrrolidinofullerene 1, C_{60}	SP	yes, yes	part of OSC small molecule, between dielectric and OSC	phototransistor	[206]
BGTC	n	pyrrolidinofullerenes 3 and 4, C_{60}	DAE	yes, yes, no	part of OSC small molecule, between dielectric and OSC, co-evaporated into OSC	phototransistor	[207]
BGTC	p	pentacene	SP	no	blended into dielectric	phototransistor	[208]
BGTC	p, n	PBTOR, N2200	AZB	yes	part of SAND	phototransistor	[209]
BGBC	p	PhF-2,3	AZB	yes	in PIL sidechain	phototransistor	[210]
BGTC	n	NDI2OD-DTYM2	SP	no	blended into OSC	other	[211]
BGTC	p	F8BT	SP	no	blended into OSC	other	[212]
BGBC	p	PANI nanowires	SP	yes	in OSC polymer sidechain	other	[213]
BGTC	p	P3HT	SP	no	blended into OSC	other	[214]

The following subchapters will describe in detail the particular mechanisms that have been reported in the literature on how photoswitches can modulate charge transports in OFETs. For illustration purposes, a graphical summary of (at least) one selected report is given for each mechanism. In some of the figures, non-essential details (e.g. color of text) were adapted in order to ensure comparability between the individual subchapters and to match the overall convention of the figures shown in Chapters 3, 4 and 5.

2.1. Charge Trapping via Energy Levels

Traps are energetic states within the bandgap of a semiconductor which are able to immobilize charge carriers and therefore result in a decrease of the density of mobile charges. Traps are ubiquitous in organic semiconductors and their presence results in lower device currents [26]. Usually, this is an undesirable phenomenon, but in the context of photoswitches, it can be harnessed to create light-responsible devices. Diarylethenes experience large changes in π-conjugation due to the isomerization between open-ring and closed-ring isomers. As a consequence, the energy of the highest occupied molecular orbital (HOMO) and the lowest unoccupied molecular orbital (LUMO) levels are shifting considerably. Through chemical design of the switch and adequate choice of the semiconductor, it is possible that the HOMO or LUMO energy level of one isomer (typically the closed-ring form) acts as a charge trap, while this is not the case for the other isomer (typically the open-ring form). Such trapping through energy levels, as schematically depicted in **Figure 2.2**, can be easily realized by blending the photoswitch into the semiconductor.

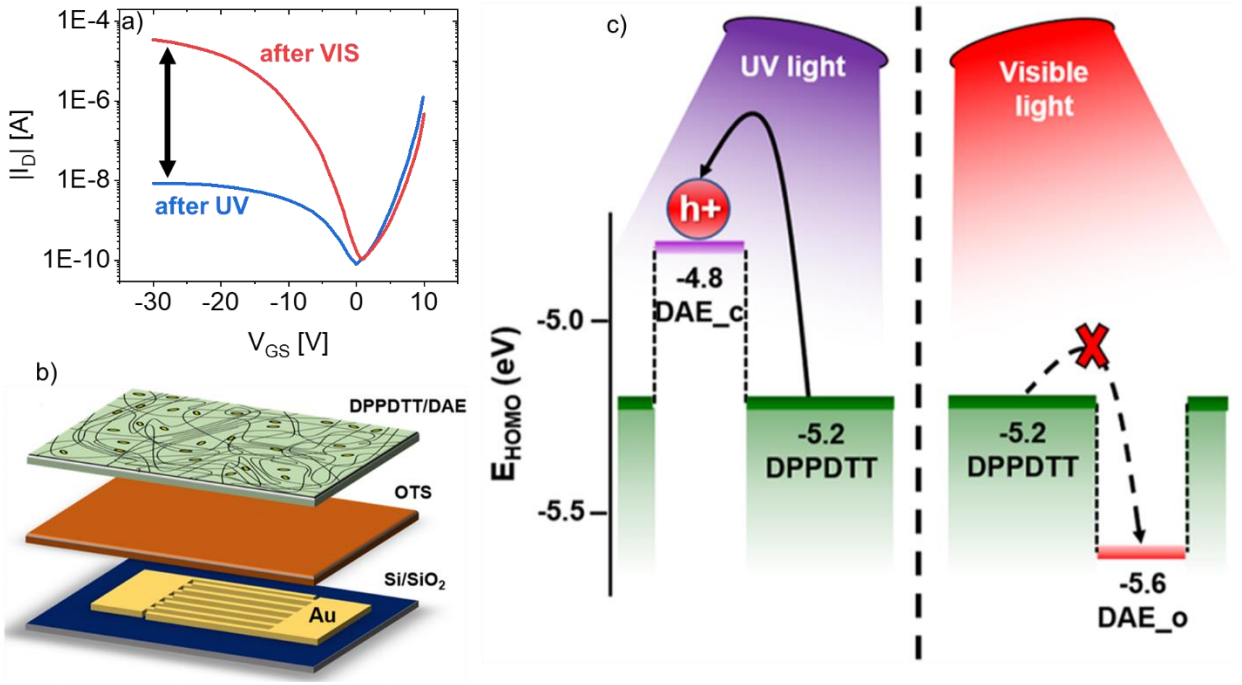

Figure 2.2: Switching of OFET characteristics due to charge trapping via energy levels. a) Reversible switching of transfer characteristics through exposure with UV and visible light. b) Transistor architecture including an active layer that is comprised of a blend of the semiconducting polymer DPPDTT and a DAE photoswitch. c) Schematic energy diagram including HOMO levels of the semiconducting polymer matrix and closed- and open-ring isomers of the photoswitch (DAE_c and DAE_o respectively). The HOMO level of DAE_c acts as a hole trap, while the HOMO level of DAE_o does not. Figures were either adapted (a) or reproduced (b, c) from [157].

By applying this strategy of light-switchable traps, it has been possible to modulate charge transport with DAE switches in p-type [144-157], n-type [141] and ambipolar [142] OFETs, allowing for innovations such as 8-bit optical memory [147], 11-bit optical-ferroelectric memory [150] and optically switchable light-emitting transistors [148]. Arlt et al. reported the same mechanism to explain their results for an azobenzene-based switch that simultaneously acts as the semiconductor in a bottom-gate bottom-contact transistor [143].

2.2. Charge Trapping via Functional Groups

In addition to a straightforward mechanism that is solely based on energy level considerations, a more complicated mechanism related to charge trapping at functional groups [158, 159] has been hypothesized. Tseng et al. applied azobenzene switches with different functional groups as self-

assembled monolayers (SAMs) or as multilayer clusters to the surface of the gate dielectric [158]. Photoexcitation of the switches resulted in threshold voltage shifts to either more positive gate-source bias for electron-withdrawing substituents (see **Figure 2.3a**) or to more negative gate-source bias for electron-donating substituents (see **Figure 2.3b**). The magnitude of these shifts could be enhanced via application of positive or negative gate-source bias pulses respectively. It was hypothesized that a light-induced charge transfer between the switch and the semiconductor occurs and that the switches with electron-withdrawing substituents act as electron traps (see **Figure 2.3c**), while the those with electron-donating substituents act as hole traps (see **Figure 2.3d**). These trapped charges cause an additional (either additive or subtractive) contribution to the gate electric field resulting in the observed threshold voltage shifts. It should be noted that the UV light-induced isomerization from the *trans*- to the *cis*-isomer of the azobenzene switches was reported to either be sterically hindered or have only a negligible effect on the transistor characteristics. A similar mechanism was reported by Smithson et al., who were able to achieve a threshold voltage shift of more than +90 V by introducing an azobenzene derivative with an electron accepting nitro group into the side chain of a dielectric polymer that is blended with a small molecule semiconductor [159]. Again, the isomerization of the photoswitch did not have a noticeable effect on the transistor characteristics.

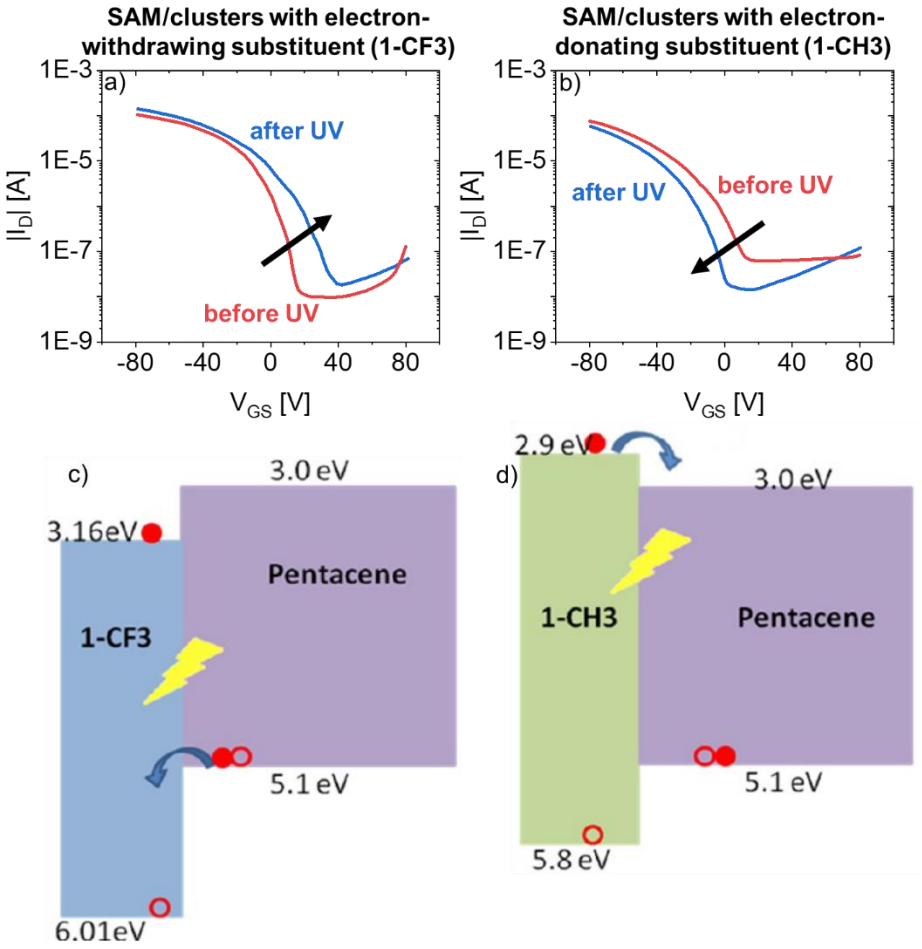

Figure 2.3: Switching of OFET characteristics due to charge trapping via functional groups. The photoswitches were applied as SAMs on the gate dielectric or as clusters within the small molecule semiconductor pentacene. Modification of transistor characteristics as a consequence of UV light exposure for devices including azobenzene photoswitches with a) electron-withdrawing and b) electron-donating substituents. Schematic energy diagrams showing the HOMO and LUMO levels of pentacene and the switches with c) electron-withdrawing substituents acting as electron traps and d) electron-donating substituents acting as hole traps. The trapped charges give rise to an additional contribution to the gate electric field resulting in a shift of the threshold voltage. Single headed arrows in panels a) and b) are only used to better indicate that UV light has opposite effects in transistors with SAMS including electron-withdrawing and electron-donating substituents. The switching is reversible in a way that the initial characteristics can be recovered after storage in the dark (data not shown). Figures were either adapted (a, b) or reproduced (c, d) from [158].

2.3. Charge Trapping in Dielectric

Chen et al. blended a multi-responsive donor-acceptor Stenhouse adduct into the polymer gate dielectric of C_{10}-BTBT OFETs and hypothesized a mechanism based on charge trapping within the dielectric [160]. This switch isomerizes from its "cyclic" to its "linear" form under elevated temperature (see **Figure 2.4a**). Since the conventional trapping through energy levels does not apply (the HOMO levels of both isomers of the switch are too deep), the authors state that the "linear" form with its extended π-conjugation serves as an effective charge trap, resulting in the degradation of transistor characteristics (see **Figure 2.4b**). The initial characteristics can be partially recovered by white light irradiation, which induces the reverse reaction to the "cyclic" form.

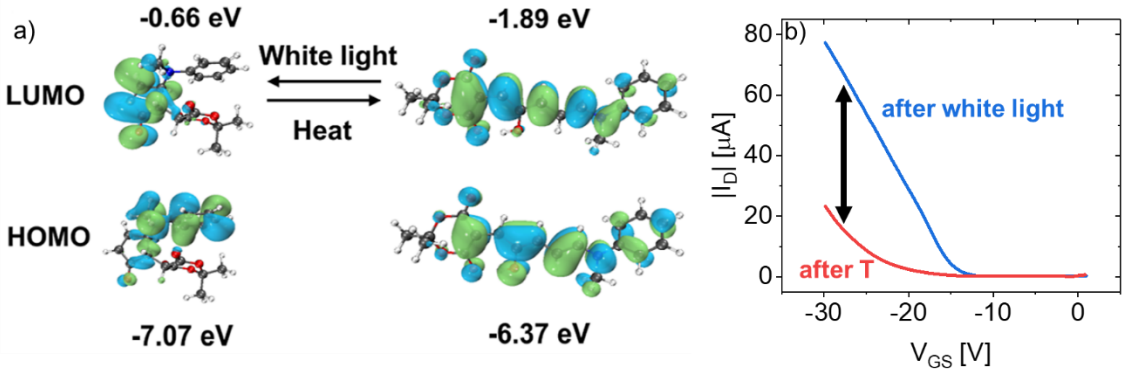

Figure 2.4: Switching of OFET characteristics due to charge trapping in the dielectric. a) Molecular structure and HOMO and LUMO energy levels of "cyclic" (left) and "linear" (right) isomers of a donor-acceptor Stenhouse adduct photoswitch. The spatial distribution of the HOMO and LUMO across both isomers of the switch is indicated. b) Reversible switching of transfer characteristics via exposure to white light and heat displayed by OFETs utilizing a blend of PMMA and the switch as gate dielectric. The deterioration of charge transport after heating was attributed to trapping through the extended π-electron system of the "linear" isomer. Figures were either reproduced (a) or adapted (b) from [160].

2.4. Injection or Tunneling Barrier

In order to ensure efficient charge injection from the source electrode into the organic semiconductor, the transport level of the semiconductor, i.e. the HOMO for p-type materials or the LUMO for n-type materials, needs to be energetically aligned with the work function of the metal electrode. A mismatch between the two will result in an injection barrier, which is a major

contributing factor to the contact resistance in OFETs [215, 216]. Since the HOMO and LUMO energy levels of photoswitches can be tuned via exposure to light, they can be used to create optically switchable injection barriers. This has been demonstrated by Mosciatti et al. by introducing a DAE-based SAM between the gold contacts and an n-type polymer semiconductor (see **Figure 2.5a**) [165]. The optical modification of the LUMO energy of the switch allowed for a transition from non-resonant to resonant tunneling of charge carriers from the source electrode into the semiconductor (see **Figure 2.5c**). As shown in **Figure 2.5b**, this resonant tunneling lead to a significant increase in drain current. Similar results using photoswitchable SAMs on gold contacts were reported for p-type polymer [162] and p-type small molecule [169] OFETs.

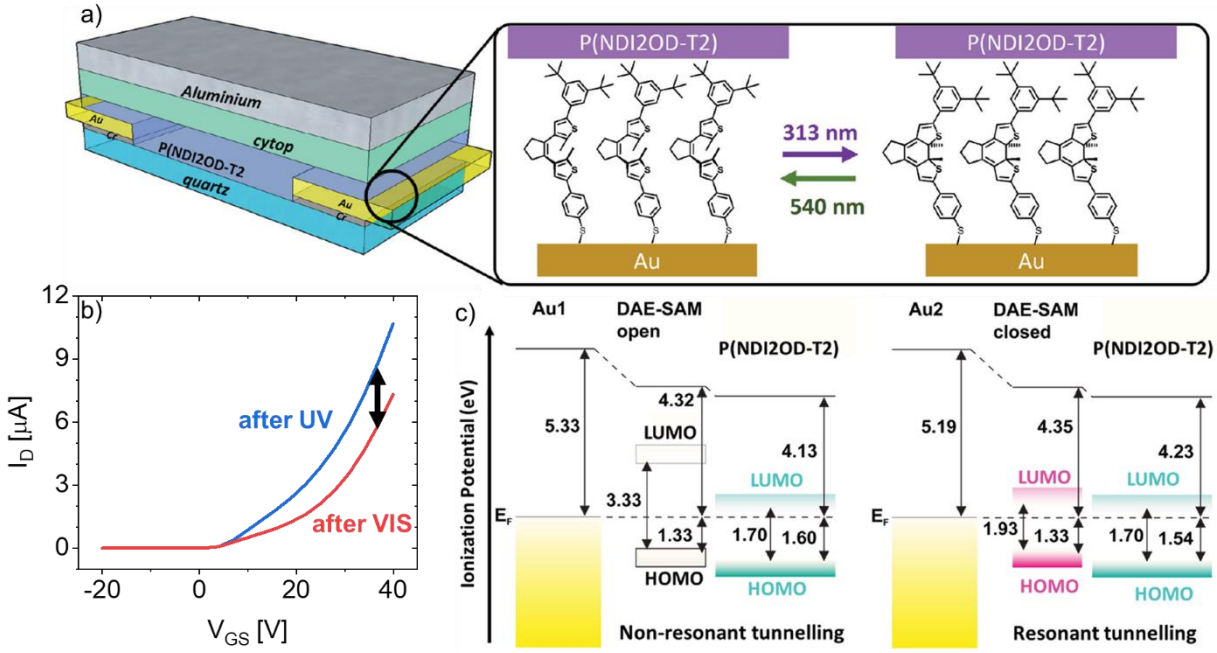

Figure 2.5: Switching of OFET characteristics due to a modification of the injection barrier between source electrode and organic semiconductor. a) Transistor architecture including a DAE-based photoswitchable SAM between gold contacts and the polymer semiconductor P(NDI2OD-T2). The molecular structures of both isomers of the switch are shown on the right side of panel a). b) Reversible switching of transfer characteristics via exposure to UV and visible light. c) Schematic energy diagrams including the work function of the gold source electrode, the HOMO and LUMO levels of the photoswitch (left: ring-open isomer; right: ring-closed isomer) and the semiconductor. The lowering of the LUMO energy for the closed-ring isomer enables charge injection through resonant tunneling. Figures were either reproduced (a, c) or adapted (b) from [165].

By utilizing such adjustable injection barriers, Kurokawa et al. achieved photoswitchable ambipolar charge transport by directly injecting either holes or electrons into semiconducting DAE

derivatives [163, 164]. It is also possible to construct floating gate memory OFETs by optically modulating charge injection/retention into/on gold nanoparticles [161] or metal oxides [168]. Raimondo et al. used azobenzene-functionalized gold nanoparticles distributed homogeneously within a poly(3-hexylthiophene) (P3HT) matrix as a hybrid active material in bottom-gate bottom-contact OFETs [167]. These devices showed higher drain current and increased hysteresis after UV light exposure which was attributed to the geometrical rearrangement of the azobenzene moieties from the *trans*- to the *cis*-form, resulting in a thinner tunneling barrier and therefore more efficient trapping/detrapping of charges on the gold nanoparticles. This mechanism is similar to the one reported for the floating gate memory OFETs [161, 168], but highlights the geometrical rearrangement of the photoswitch as the underlying principle rather than a change in the energy levels. In another work from the same group, this geometrical thinning of a tunneling barrier was found to facilitate charge injection into an n-type small molecule semiconductor, resulting in increased transistor drain current [166].

2.5. Energetic Disorder

The density of states (DOS), i.e. the energetic distribution of transport levels, is a major factor determining charge transport in all semiconducting materials. Defect-free, crystalline semiconductors have clearly defined valence and conduction band edges, which enhances carrier delocalization, and allows for high charge carrier mobilities. Due to their soft, van-der-Waals bonded nature organic materials however, are highly prone to defects that can either introduce additional states within the band gap, so-called trap states or locally cause a shift of the transport level, which results in an overall broadening of the DOS [217]. The latter effect is called energetic disorder and is highly detrimental to efficient charge transport. Energetic disorder along a polymer backbone can stem from inter- or intramolecular interactions and can be reduced e.g. by designing polymers with planar, rigid backbones and a small variation of torsional angle between the repeat units [218, 219]. On a device level, energetic disorder can be adjusted e.g. via the choice of the gate dielectric. It has been shown that large molecular dipoles present in the polymer gate dielectric can lead to a broadening of the DOS and therefore enhance carrier localization [220]. The corresponding transistor devices exhibited lower mobility, higher hysteresis and increased

threshold voltage as well as increased subthreshold swing. A theoretical study showed that this effect of dipole-induced energetic disorder is very sensitive to the distance between the dipole and the semiconductor-dielectric interface [221], which is probably the reason why the effect can be observed in some systems [220, 222], but not in others [223]. Furthermore, the authors concluded that the mechanism of Fröhlich polaron formation reported for rubrene single-crystal OFETs [224] only plays a secondary role in disordered polymer systems.

Photoswitches can be used to deliberately modify the energetic disorder of conjugated polymers and therefore alter charge transport in organic transistors. Tian et al. constructed light-responsive OFETs by covalently attaching azobenzene switches to the side chains of a diketopyrrolopyrrole (DPP)-based semiconducting polymer (see **Figure 2.6a**) [170]. These devices showed a significant decrease in drain current after UV light irradiation, which could be reversed by exposure to visible light (see **Figure 2.6b**). The authors concluded that the reversible *trans*-*cis*-isomerization of the azobenzene units was responsible for this effect, not only by affecting the crystallinity of the film and therefore the inter-chain charge transport, but also by affecting the energetic disorder along the backbone of the polymer and therefore the intra-chain charge transport. The latter effect stems from the markedly different dipole moments (around zero for the *trans*-isomer and 6.04 D for the *cis*-isomer) between both forms of the switch and the fact that only 25 % of the azobenzene moieties actually undergo the transition from *trans* to *cis*. In a subsequent publication, the same group reported similar results for another DPP-based polymer with spiropyran switches in the side chains [174]. Again, the change in the transistor characteristics was ascribed to increased energetic disorder caused by the large dipole moments of the light-induced merocyanine moieties.

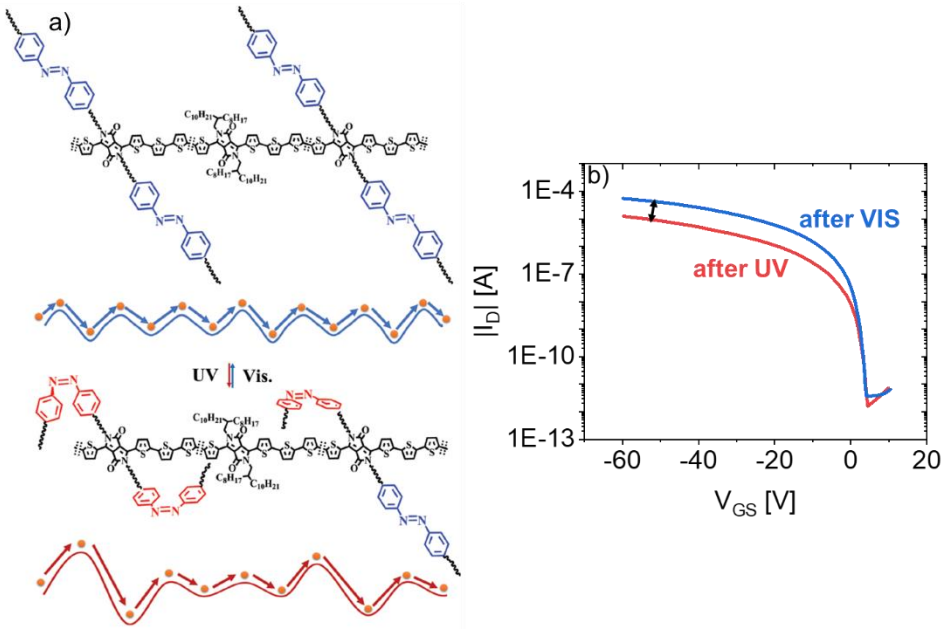

Figure 2.6: Switching of OFET characteristics due to modified energetic disorder. a) Molecular structure of a polymer semiconductor composed of a DPP-based backbone and photoswitchable azobenzene sidechains. Below the molecular structures, schematics of the potential energy landscapes along the respective backbones are given. b) Reversible switching of transfer characteristics via exposure to UV and visible light displayed by OFETs utilizing the material shown in panel a) as a photoresponsive active material. The deterioration of charge transport after UV light exposure was attributed to the enhanced energetic disorder along the polymer backbone induced by the conversion of the azobenzene moieties from the *trans*-isomer (blue) with a low dipole moment to the *cis*-isomer (red) with a large dipole moment. Figures were either reproduced (a) or adapted (b) from [170].

Instead of covalently attaching the photoswitch to the backbone of the conjugated polymer, Ishiguro et al. blended several photoswitches including spiropyran [171, 173, 175], spirooxazine [175] and naphthopyran [172] with the p-type semiconducting polymers poly(triarylamine) (PTAA) and poly(3-hexylthiophene) (P3HT). In these works, a reversible decrease in transistor drain current and field-effect mobility was observed after UV light irradiation, which has been ascribed to “scattering” of charge carriers by the merocyanine moieties. Via direct comparison between a zwitterionic and a non-ionic merocyanine (originating from a spiropyran and a spirooxazine switch respectively) it was concluded that the scattering effect (or in other words the energetic disorder effect) is more likely to be caused by the ionic moieties than the large dipole moments [175]. This hypothesis is supported by the finding that adding spiropyran alone, which already has a considerable dipole moment but no ionic moieties, does not lower the drain current of the transistor. Even though focusing mainly on the electrical conductivity in a covalent organic

framework (COF)-based device, Yang et al. reported similar results for a transistor utilizing a blend of spiropyran and a DPP-based semiconducting polymer as active material [176]. It should be noted that this mechanism works independently of the energy levels of both the semiconductor and the switch. It can be applied to all types of semiconducting polymers, which is an advantage over the previously described approach based on charge trapping via energy levels [172].

2.6. Morphology

Morphology related effects are among the most influential factors governing the performance of organic electronic devices such as organic solar cells [225, 226] and OFETs [227-229]. Obtaining precise control over the molecular arrangement of small molecule or polymer semiconductors within a thin-film is a key prerequisite for the optimization of these devices making this an active field of research [230]. Using light as a non-destructive stimulus to change the morphology of organic semiconductors during the deposition process [231] or in a thin-film [232] has been demonstrated. Inducing reversible changes in morphology with photoswitches however is challenging. Usually photoswitches are small molecules and are used at weight contents, which are too low to sufficiently affect the ordering of the surrounding matrix or other adjacent components. Nevertheless, changes in morphology induced by various photoswitches such as azobenzenes [178, 179], stilbenes [180, 182], arylazopyrazole [181] or a combination of two different switches [177] have been reported to reversibly modulate charge transport in organic field-effect transistors. Cao et al. used 2D crystals of a stilbene oligomer as a semiconductor in a bottom-gate top-contact OFET and it was observed that the device performance degraded significantly under UV light exposure (see **Figure 2.7a**) [182]. This observation was ascribed to the isomerization of the stilbene derivative from its thermodynamically stable *trans*-form to the metastable *cis*-form (see **Figure 2.7c)**, which is expected to disrupt the π-π stacking of the molecules and therefore degrade the charge transport. Interestingly, the transistor current was found to increase under UV light exposure, when studying bulk crystals of the same material (see **Figure 2.7b**). The alleged contradiction could be explained by considering that only the molecules at the surface of the crystal are able to isomerize. Charge transport in the bulk remains unaffected

by the *trans*-*cis*-isomerization and is further enhanced by the photoinduced generation of charge carriers (see **Figure 2.7d**).

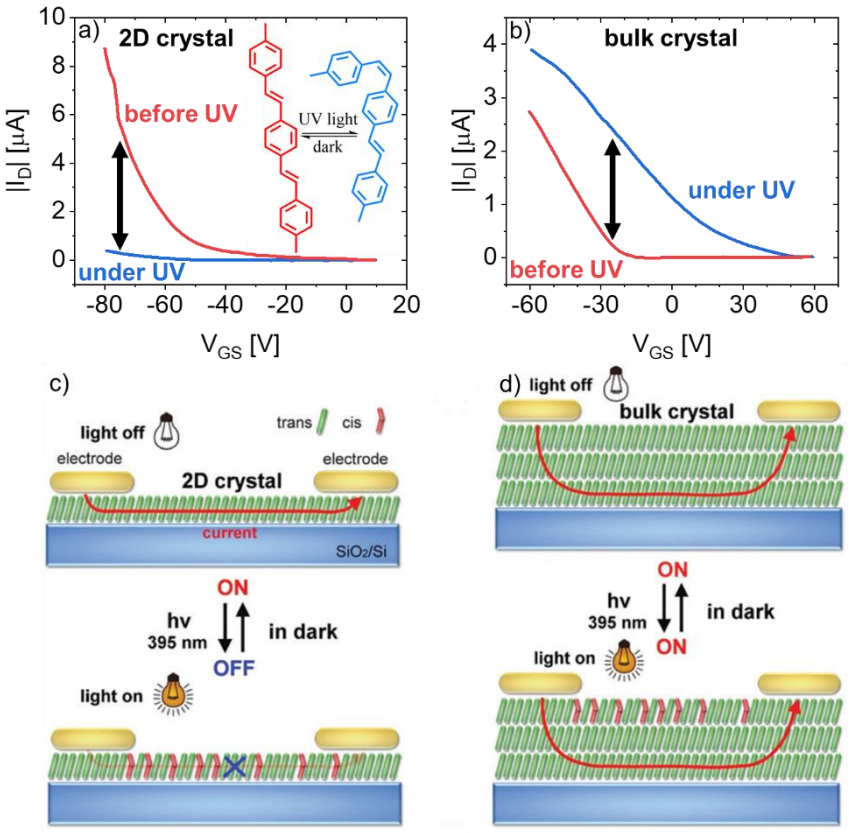

Figure 2.7: Switching of OFET characteristics due to modified morphology. Altered transfer characteristics as a consequence of UV light exposure for devices including a) 2D crystals and b) bulk crystals of semiconducting stilbene oligomer photoswitches. c) and d) Corresponding transistor architectures as well as a schematic explanation of the behavior under UV light exposure. In the 2D crystal device, charge transport deteriorates under UV, since the isomerization from *trans*- to *cis*-stilbene interrupts the crystal packing. In the bulk crystal device, the isomerization only occurs at the surface of the crystal. This does not affect the charge transport through the underlying molecular layers. Additionally, photo-generated charge carriers contribute to the overall drain current. Figures were either adapted (a, b) or reproduced (c, d) from [182].

Tian et al. successfully synthesized a photoresponsive, semiconducting polymer via the incorporation of arylazopyrazole moieties into its sidechains [181]. Instead of using the common optical stimuli of UV and visible light to induce the isomerization reactions, the authors utilized upconversion nanoparticles and the photothermal heating effect to switch an OFET using light with wavelengths of 980 nm and 808 nm respectively. To the best of my knowledge, this is the first photoswitch-functionalized organic field-effect transistor that can be switched exclusively with near-infrared light. As supported by X-ray scattering data, these optical stimuli-induced

reversible changes in the inter-chain packing, therefore affecting the crystallinity of the film. In a subsequent work, the authors combined azobenzene and arylazopyrazole side chains in one semiconducting polymer [177]. Since these photoswitchable moieties can be addressed with light of different wavelengths, OFETs made with this material showed three distinctive mobility regimes induced either by light of 365 nm, 470 nm or 560 nm wavelength. Similar to the previous report, X-ray scattering data showed that these different transport regimes are stemming from distinctive degrees of inter-chain packing. The common notion of these previously mentioned reports is that the crystallinity of the semiconductor decreases through the isomerization of the switch, which is detrimental to efficient charge carrier transport. However, also the opposite can be realized, i.e. that isomerization of a photoswitch improves crystallinity and therefore OFET performance. This has been demonstrated for an azo-functionalized liquid crystal semiconductor [178] and more recently for a self-strained azobenzene-containing benzo[*b*]benzo[4,5]thieno[2,3-*d*]thiophene (BTBT) derivative [179].

2.7. Switching the Capacitance of the Dielectric

Transistor characteristics can be modulated by altering the dielectric properties of the gate insulator. Using photoswitches, this has been realized by blending spiropyran molecules into PMMA gate dielectrics [183-185]. Shen et al. were the first to report a substantial increase of drain current as a consequence of UV light illumination in both p- and n-type transistors with a PMMA/spiropyran blend dielectric. [183]. The initial characteristics could be recovered via illumination with visible light (see **Figure 2.8a**). This modulation of transistor characteristics was attributed to the isomerization of the spiropyran photoswitches, resulting in an increase (low dipole moment spiropyran to high dipole moment merocyanine, under UV light) or decrease (high dipole moment merocyanine to low dipole moment spiropyran, under visible light) in the capacitance of the gate insulator, which could be studied directly in metal-insulator-metal devices (see **Figure 2.8b**). This direct dependence of the drain current on the capacitance of the gate dielectric can be seen in Equations 1 and 2. Furthermore, this mechanism is in line with the observation that p- and n-type transistors show the same qualitative trend (drain current increase/decrease after UV/visible light illumination). In a subsequent study, Zhang et al. were able to increase the photoswitch

content in the dielectric by covalently attaching spiropyran moieties to the side chains of a PMMA backbone [186]. The results of this study are in agreement with their previous report and therefore consolidated the mechanism of light-induced capacitance modulation (see **Figure 2.8c**).

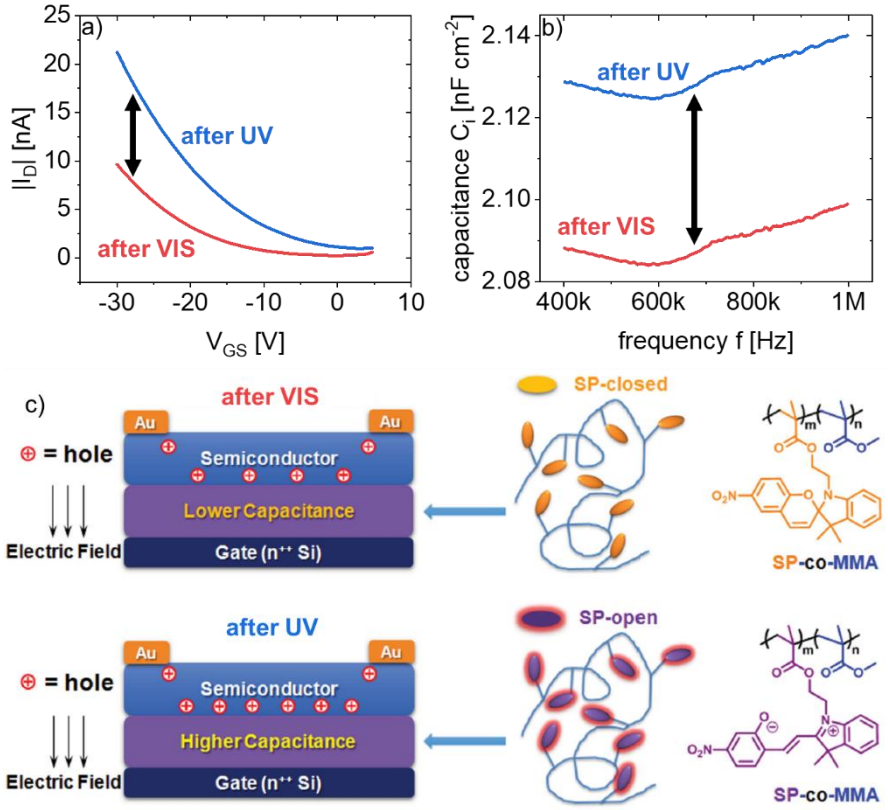

Figure 2.8: Switching of OFET characteristics due to a modification of the capacitance of the polymer gate dielectric. a) Reversible switching of transfer characteristics via exposure to UV and visible light. b) Reversible switching of the frequency-dependent capacitance of a metal-insulator-metal device via exposure to UV and visible light. c) Transistor architecture including a hybrid polymer dielectric containing photoresponsive spiropyran moieties. After UV light exposure, the dielectric shows an increased capacitance, which facilitates charge accumulation at the semiconductor-dielectric interface. The increase in capacitance has been ascribed to the conversion of the spiropyran-isomer (SP-closed, orange) with a low dipole moment to the merocyanine-isomer (SP-open, purple) with a high dipole moment. This isomerization including the corresponding molecular structures is schematically shown on the right side of panel c). Herein, the spiropyran moieties are covalently attached to a PMMA-based backbone, but it is also possible to achieve similar results by simply blending the switch into PMMA. a) and b) were adapted from [183] and c) was reproduced from [186].

2.8. Additional Built-in Electric Field

SAMs of molecules with a large dipole moment can shift the threshold voltage of organic field-effect transistors, since such an ordered arrangement of dipoles generates an additional, so-called built-in electric field [233, 234]. Depending on the direction of the dipole moments, this built-in field enhances or reduces the effect of the external gate electric field which allows for a controlled shift of transistor characteristics [235]. Zhang et al. explored this effect with pentacene OFETs employing a photoresponsive SAM, in which spiropyran switches are covalently bonded to a silicon dioxide surface via an alkyl spacer and a (3-aminopropyl)trimethoxysilane (APTMS) layer (see **Figure 2.9a**) [187]. After UV light irradiation, these devices experience a significant threshold voltage shift towards more positive gate-source bias and therefore an increase in the drain current (see **Figure 2.9b**). The initial characteristics could be recovered via visible light irradiation. Through a series of control experiments, the authors ruled out alternative mechanisms such as variations in gate dielectric capacitance, morphological effects or direct charge transfer between the photoswitch and the semiconductor. They concluded that the increased dipole moment of the merocyanine form results in an enhanced built-in electric field, which increases the charge carrier density in the transistor channel. This mechanism is schematically depicted in **Figure 2.9c**. From the direction of the threshold voltage shift, it can be concluded that the negatively charged phenoxide ion is oriented towards the semiconductor layer.

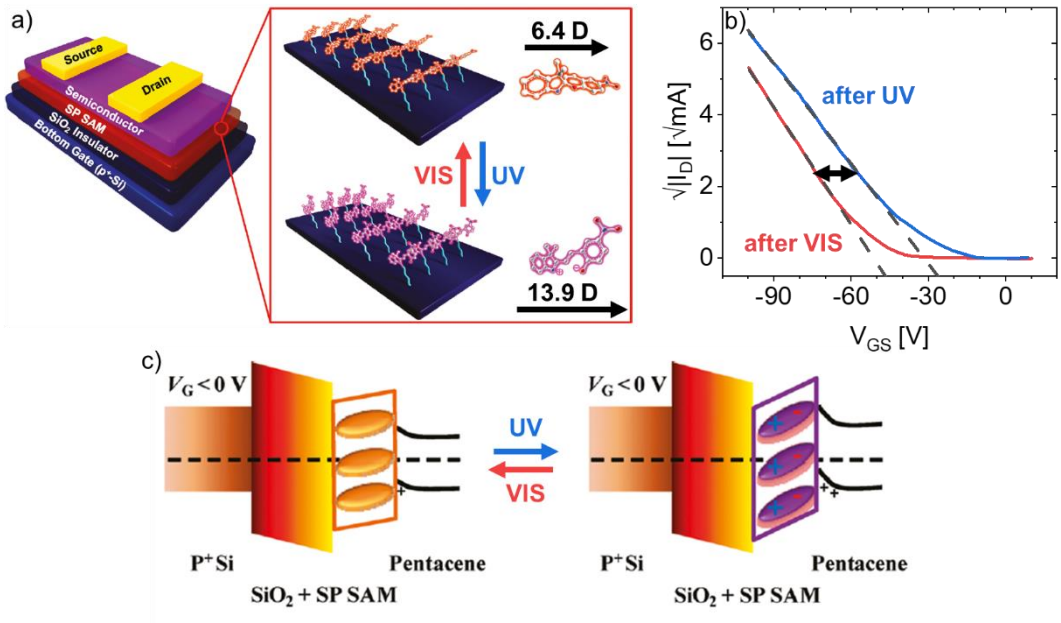

Figure 2.9: Switching of OFET characteristics due to an additional built-in electric field. a) Transistor architecture including a spiropyran-based photoswitchable SAM between the gate dielectric and the small molecule semiconductor pentacene. The molecular structures of both isomers of the switch are shown on the right side of panel a). b) Reversible switching of transfer characteristics via exposure to UV and visible light. c) Schematic energy diagrams including the gate electrode (p-doped silicon), the SAM-modified silicon dioxide gate dielectric and its interface with the semiconductor. Conversion of the low dipole moment isomer (left) to the high dipole moment isomer (right) produces an additional built-in electric field that facilitates charge accumulation at the semiconductor-dielectric interface. Figures were either reproduced (a, c) or adapted (b) from [187].

Shen et al. reported similar results (increased drain current after UV light exposure) when spiropyran switches were deposited on top of pentacene transistor channels using a poly(dimethylsiloxane) (PDMS) stamp [137]. Additionally, they observed a decrease in drain current in n-type OFETs. This observation is in agreement with the built-in electric field mechanism, since the band bending induced by spiropyran dipoles (assuming a similar orientation to the one reported by Zhang et al.) is expected to result in the accumulation/depletion of holes/electrons in the transistor channel. It is also possible to exploit the effect of the built-in electric field without complicated device fabrication steps such as SAM deposition or PDMS stamping. Liu et al. blended a hexaarylbiimidazole (HABI) derivative with various p-type semiconducting polymers and observed a significant increase in drain current after UV light exposure [188]. The light exposure caused HABI to form radicals, which can interact with defects at the semiconductor-dielectric interface, effectively stabilizing the radicals with their unpaired

electrons. The resulting built-in electric field leads to an enhanced charge carrier density within the channel.

2.9. π-Conjugation

Typical OFETs can be switched between their on- and off-states by applying an electrical bias between the source and gate electrodes. A major motivation for the utilization of photoswitches is to obtain a similar functionality through the application of light stimuli, in other words, to obtain light-gated OFETs. However, as long as the semiconductor and the photoswitch are spatially separated, it is challenging to obtain devices with efficient light-gating properties. Hayakawa et al. were able to overcome this issue by using a photoswitchable DAE derivative directly as the organic semiconductor in a bottom-gate top-contact transistor (see **Figure 2.10a**) [189]. In such a device, the drain current in the on-state could be modified over two orders of magnitude only through irradiation with light of different wavelengths (see **Figure 2.10d**). This efficient light-gating was ascribed to a large change in π-conjugation between the open-ring form and the closed-ring form of the DAE photoswitch. In the closed-ring isomer, the conjugation extends over the entire molecule, which yields a working OFET with a mobility of around 10^{-5} cm^2 V^{-1} s^{-1}. After visible light irradiation, the π-conjugation is interrupted and no field-effect behavior can be observed. Such drastic differences in conductance between both isomers are in agreement with reports on single-molecule junctions employing DAE photoswitches [236-241]. Even though the transistors reported by Hayakawa et al. show impressive switching with light, the overall performance was still poor (low mobility and large threshold voltage). However, in subsequent reports the authors were able to improve device performance, while maintaining a large degree of light-gating [190] and even extending their approach to the fabrication of an analog adder circuit through direct laser patterning of a DAE film [191].

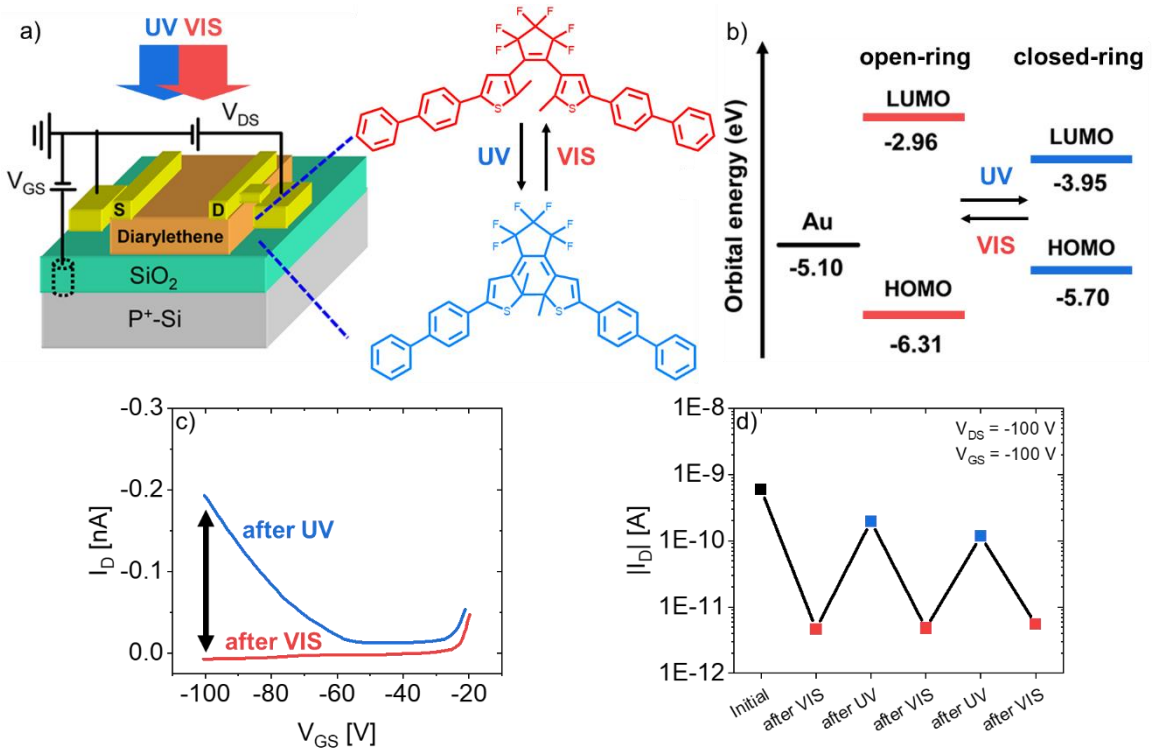

Figure 2.10: Switching of OFET characteristics due to modified π-conjugation. a) Transistor architecture including a DAE photoswitch as the semiconductor. The molecular structures of both isomers of the switch are shown on the right side of panel a). b) Schematic energy diagram including the work function of the gold contacts and the HOMO and LUMO levels of both isomers of the photoswitch. c) Reversible switching of transfer characteristics via exposure to UV and visible light. d) Reversible switching of transistor on-current over the course of three cycles. The improved charge transport properties of the closed-ring isomer were ascribed to its extended π-electron system. Figures were either reproduced (a, b) or adapted (c, d) from [189].

2.10. Light-induced Charge Transfer

In a recent article Mumyatov et al. reported the use of a novel spiropyran/merocyanine (SP/MC) salt composed of a positively charged SP/MC moiety and a negatively charged chromooxalate ion $[Cr(C_2O_4)_3)]^{3-}$ as a photochromic layer in n-type bottom-gate top-contact OFETs [192]. Through irradiation with violet (405 nm) and green (532 nm) light it was possible to reversibly tune the threshold voltage of the transistors (see **Figure 2.11**). Before clarifying the mechanism behind this device switching, it should be emphasized that this photochromic compound is thermodynamically more stable in its MC form rather than its SP form, which is in contrast to other spiropyran switches. Therefore, exposure to UV/violet light does not induce the typical isomerization from

SP to MC, but instead induces a charge transfer from the redox-active $[Cr(C_2O_4)_3)]^{3-}$ anion to the organic semiconductor C_{60} that acts as an electron acceptor. This light-induced charge transfer results in an accumulation of electrons in the transistor channel, which explains the shift of the threshold voltage towards more negative gate-source bias. In **Figure 2.11** this state of the transistor is depicted as state 1. The authors could show that this charge-separated state is stabilized by an exchange interaction between the MC moiety and the negatively charged C_{60}. The SP isomer however is not able to stabilize this state, which explains why the isomerization from MC to SP under green light (532 nm) recovers the initial transistor characteristics. This recovery of the initial state (in **Figure 2.11** either state 2 or state 0, depending on whether there is enough thermal energy to isomerize SP back to MC) occurs through an intermediate state (MC isomerized to SP) followed by the recombination of the optically separated charges. A unique aspect of this work (compared to the previous reports from the same group) is the stable charge-separated state, which can be reached without any additional programming voltage. However, applying an additional programming voltage resulted in even larger threshold voltage shifts (data not shown here) compared to the ones that were obtained by purely optical programming (as shown in **Figure 2.11**), allowing for a multistate optoelectronic OFET memory.

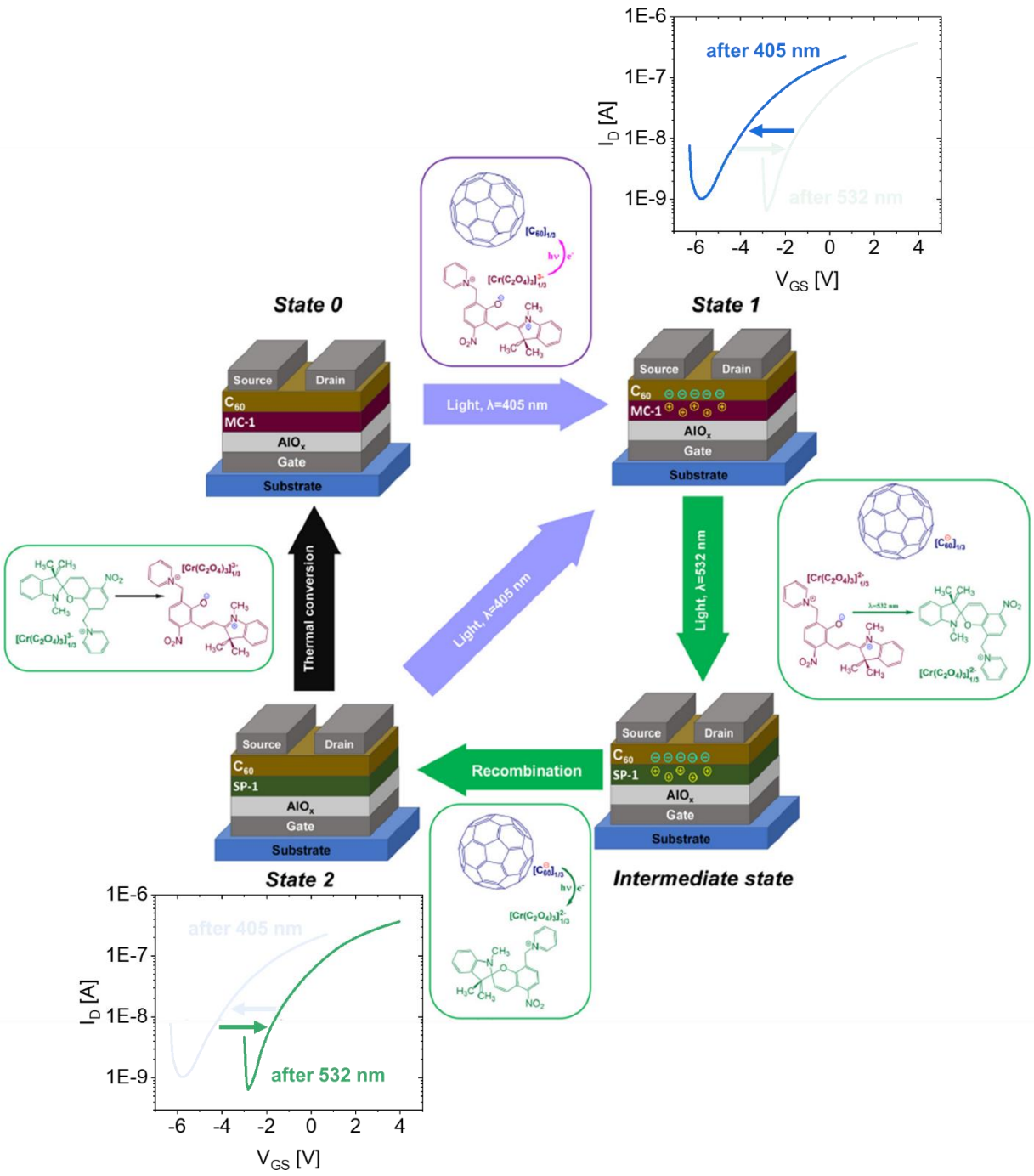

Figure 2.11: Switching of OFET characteristics due to light-induced charge transfer. The transistor utilizes a separate layer of the spiropyran/merocyanine salt SP/MC-1 as a photoresponsive component and can be switched between three distinct states (with one intermediate state between state 1 and state 2) via exposure to violet/green light (405/532 nm) or thermal stimulus. The insets are showing the molecular structures of the semiconductor C_{60} and the photoswitch salt. Additionally, the stimuli-induced molecular processes of light-induced charge transfer and isomerization of the photoswitch cation are indicated. The transfer characteristics recorded in state 1 and 2 can be reversibly interconverted via exposure to violet and green light. Figures were reproduced and adapted from [192].

2.11. Photoprogrammable OFETs, Phototransistors and Others

Another type of OFET that can employ photoswitches is the photoprogrammable transistor. In these devices, a light stimulus is applied simultaneously t a gate voltage pulse, the so-called programming voltage V_P, in order to reversibly modulate electrical characteristics. Such devices have been constructed with p-type [196, 198, 201, 202] and n-type [193-195, 197, 199, 200] small molecule semiconductors. Even though various device architectures and different types of photoswitches are used across these reports, they all show a similar result: A positive programming voltage leads to a threshold voltage shift towards more positive bias, while a negative programming voltage leads to a shift in the opposite direction (see **Figure 2.12a**). Considering that this phenomenon can only be observed when light and programming voltage are applied simultaneously (i.e. programming voltage alone is not sufficient, see **Figure 2.12b**) the following mechanism can be rationalized. Firstly, light irradiation induces excitons, which dissociate at the semiconductor-photoswitch interface. This light-induced charge separation can be observed with spectroscopic techniques [195, 199, 200] and is facilitated when the interface is composed of a strong electron acceptor on one side and a strong electron donor on the other side. In the case of an n-type OFET, application of a negative programming voltage leads to the immobilization of holes either in the bulk of the photoswitch layer, at the interface between the photoswitch and the gate dielectric or even within the bulk of the gate dielectric. The electrons remaining within the n-type semiconductor are contributing to the mobile charge carrier density. As a result, a lower gate-source bias is necessary to turn on the transistor, i.e. the threshold voltage shifts to more negative gate-source bias. This step is often called “programming” and can be reversed or “erased” by the application of light in combination with a positive programming voltage. This leads to the recombination of the previously immobilized holes with the mobile electrons in the channel and therefore results in the recovery of the initial characteristics. **Figure 2.12c** schematically depicts this mechanism for a C_{60} bottom-gate top-contact OFET. Other groups have reported similar findings for p-type OFETs [196, 201, 202], confirming the mechanism of light-induced exciton generation followed by gate-source bias-assisted charge trapping. Such photoprogrammable transistors are particularly interesting for rewritable memory applications.

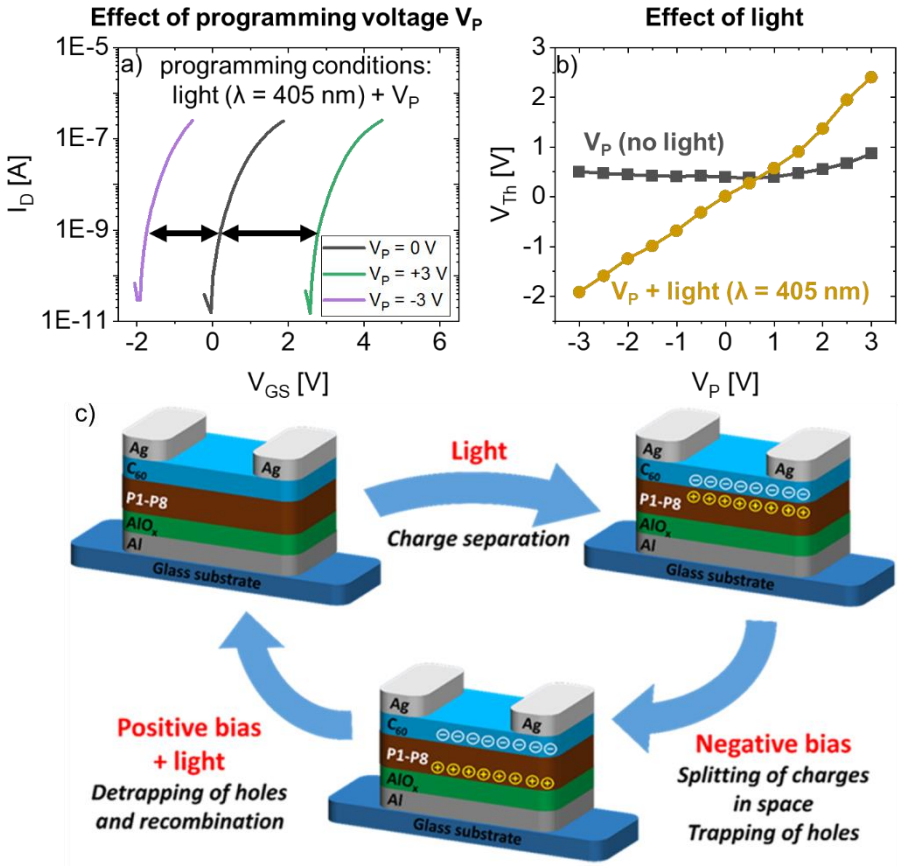

Figure 2.12: Photoprogrammable OFETs utilizing separate layers of photoswitches between the gate dielectric and the small molecule semiconductor C_{60}. a) Reversible programming of transfer characteristics via simultaneous application of light (405 nm) and programming voltage V_P. Depending on the sign of the programming voltage, the characteristics can be either shifted towards more positive gate-source bias (positive V_P) or more negative gate-source bias (negative V_P). b) Dependence of the threshold voltage on V_P. Application of V_P alone is not sufficient to shift the characteristics. c) Schematic explanation of the photoprogramming mechanism describing the individual contributions of light, negative (programming) bias and positive (programming) bias in combination with light. a) and b) were adapted from [194] and c) was reproduced from [200].

Transistors that show markedly different characteristics under illumination compared to in the dark can be used to sense light and are therefore called phototransistors. The presence of a photoswitch is not a prerequisite for these devices to operate, since it is usually the semiconductor itself, which causes the photoresponse [242]. Nevertheless, several phototransistors utilizing the additional functionality of a photoswitch have been reported [203-210]. Wu et al. e.g. were able to show that an initially UV-blind pentacene bottom-gate top-contact phototransistor could be sensitized to UV light by incorporating a spiropyran photoswitch into its polymer gate dielectric (see **Figure 2.13**) [208]. For such devices however, it can be challenging to clarify their exact working mechanism

due to the fact that semiconductor and photoswitch respond simultaneously to the light stimulus. Nevertheless, these devices are highly interesting for light-sensing applications.

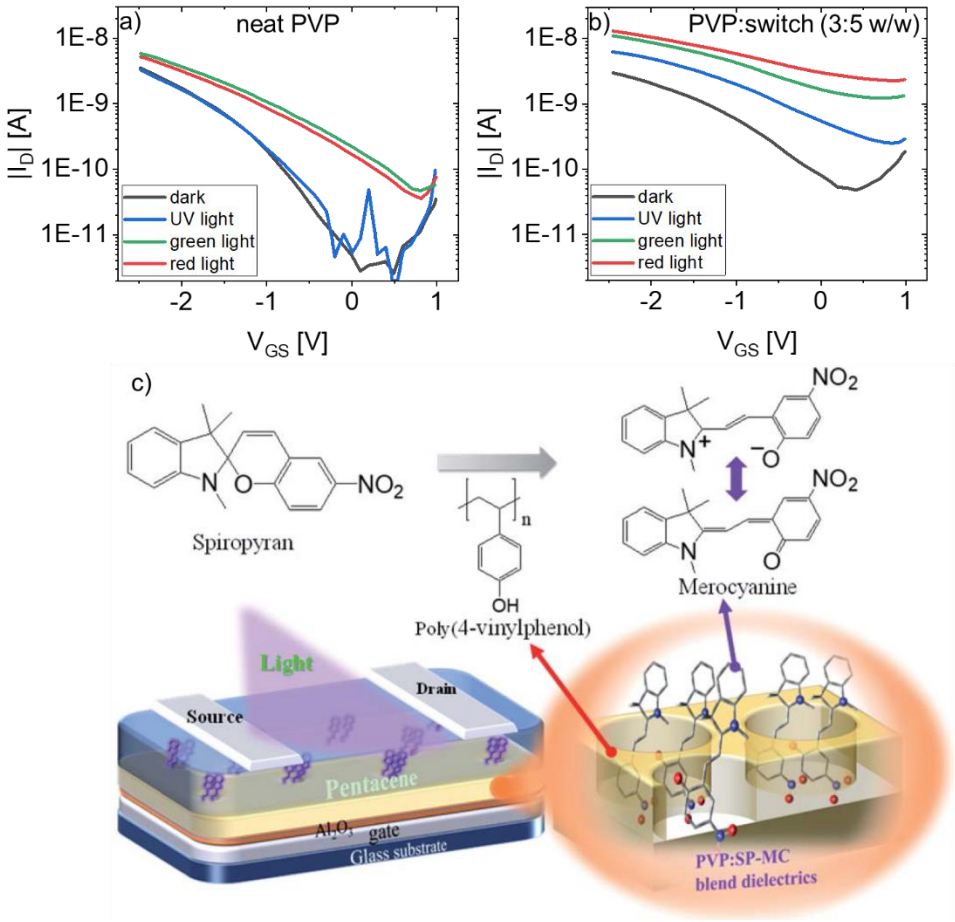

Figure 2.13: Phototransistor utilizing a blend of poly(4-vinylphenol) (PVP) and a spiropyran photoswitch as part of a double-layer bottom-gate dielectric. a) Transfer characteristics recorded in the dark or under illumination with light of various wavelengths (including UV, green and red light) for transistors with a) neat PVP films or b) blend films containing PVP and the photoswitch. c) Molecular structures of both isomers of the switch and PVP. The transistor architecture is displayed at the bottom of panel c). The addition of the photoswitch makes the phototransistor UV-responsive. Figures were either adapted (a, b) or reproduced (c) from [208].

It should be noted that some reports on OFETs utilizing photoswitches are not listed in the previous sections, either because no light-induced switching is mentioned [212], the reported field-effect is very weak [213] or because a consistent explanation is lacking [211, 214].

2.12. Photoswitches in Other Organic Electronic Devices and Outlook

Photoswitches have not only been used to modify charge transport in transistors. Abundant literature can be found reporting on the alteration of conductance in simulated [239-241, 243-252] and experimental [236-238, 253-272] single-molecule junctions, self-assembled monolayer-based junctions [273-282], multilayer junctions [283-286] or two-terminal thin-film devices [287-320], including memories of the types WORM (write once read many) [321-324], SRAM (static random-access memory) [325, 326] and RRAM (resistive random-access memory) [327], photodetectors [328-330] and OLEDs (organic light-emitting diodes) [331-336]. Other device types reported include dye-sensitized solar cells [337-340], textile-based UV sensors [341] and even superconducting electric double layer (EDL) transistors [342, 343]. It should be noted that devices using carbon nanotubes or 2D materials such as graphene or transition metal dichalcogenides as semiconductor or conductor are not included in the listing above.

Neuromorphic computing, i.e. using electronic circuits inspired by the human brain is a hot topic in organic electronics [344-346] and it is expected that new devices including photoswitches will contribute to this development [347]. Furthermore, it has already been demonstrated that artificial synapses can be realized with photoswitches in solution [348], in purely optical devices [349, 350], but also in OFETs [151, 160]. Very recently, photoswitches have also been applied for the first time to organic electrochemical transistors (OECTs) [351, 352] opening up new functionalities and design-concepts for next-generation light-switchable organic electronic devices.

Chapter 3: Reversible Switching of OFETs Employing P3HT:DHA/VHF Blends

This chapter was published in 2024 as “Reversible Switching of Light-Gated Organic Transistors Employing Dihydroazulene/Vinylheptafulvene Photo-/Thermochromic Molecules” in Advanced Electronic Materials, p. 2400455 together with [redacted], [redacted], [redacted], [redacted], [redacted], [redacted], [redacted] and [redacted].

Author contributions

[redacted] synthesized the photo-/thermochromic molecules and performed the UV/Vis absorption and NMR spectroscopy experiments in solution. [redacted] performed the GIWAXS experiments. Sten Gebel performed the remaining experiments and wrote the manuscript. [redacted] proposed the project. [redacted] and [redacted] supervised the project and corrected the manuscript. [redacted], [redacted] and [redacted] corrected the manuscript. The contribution of [redacted] is not shown here.

3.1. Introduction

Organic field-effect transistors are a promising platform for next-generation flexible electronics, including bendable displays, stretchable sensor arrays and on-skin electronics [353]. Impressive improvements in device performance of organic field-effect transistors [10], as well as operational and environmental stability [354, 355] have opened up the possibility to now focus on the development of more diversified and advanced devices [77]. Multifunctionality is highly desired for organic optoelectronic devices and can be implemented more readily compared to their inorganic counterparts due to the chemical versatility and ease of processing that is inherent to organic electronic materials. Employing photoswitches in combination with organic semiconductors is a powerful approach to optically modify electronic device characteristics and add additional functionality, i.e. responsiveness to external stimuli such as light or heat [124]. This concept facilitates a broad spectrum of photo-programmable optoelectronic devices such as photomemory [150], smart photovoltaic windows [337] or photodiodes for detection of high-

intensity ambient light overcoming early photocurrent saturation [328]. Furthermore, it enables multivalued logic, which is highly desirable due to reduced power consumption and increased information density [77, 356].

Photoswitches are molecules that undergo reversible isomerization between at least two different (meta)stable isomers upon irradiation with light. This isomerization is oftentimes visible by a change in color and also is accompanied by a change of other fundamental properties such as frontier orbital energy levels, dipole moment and/or molecular geometry [357]. As discussed in Chapter 2, the most prominent photoswitches in multifunctional organic devices to date are diarylethenes, spiropyrans/spirooxazines and azobenzenes and several review articles show that these molecules have been successfully applied in order to deliberately modify the charge transport in devices [77, 127-136].

Several approaches are reported in the literature for incorporating photoswitches into OFETs, namely 1) blending them into either the organic semiconductor [145, 146] or the dielectric [183, 202]; 2) interface modification via deposition of a self-assembled monolayer either on the source and drain contacts [162, 165] or at the semiconductor-dielectric interface [168, 187]; 3) via direct covalent incorporation into the semiconductor [177, 179] or the dielectric [186]; 4) as an interlayer between semiconductor and dielectric [195, 200]. Blending the photoswitch into semiconducting polymers is a straightforward approach for creating a photoresponsive active layer material and exploits the good solubility of the polymer and the switch in organic solvents.

A photoswitch that has been studied previously in OFETs is the non-ionic spiropyran (SP), which undergoes isomerization to the zwitterionic merocyanine (MC) under UV light. The latter has been reported to act as a charge scattering site and thus lowers the overall current running through a device [171, 173-175]. It is well known that this isomerization also leads to a considerable change in dipole moment from around 4-6 D for SP to around 14-18 D for MC [77]. This chapter focuses on a photoswitch with comparable change in dipole moment, but without the presence of any ionic species in either isomer, namely dihydroazulene (DHA)/vinylheptafulvene (VHF) switches, hence enabling to exclusively study the impact of the change in dipole moment on the transistor performance. The isomerization from DHA to VHF can be triggered with UV light and the backreaction from VHF to DHA requires thermal activation enabling a unique mixed photo-

/thermochromic system [358]. The actual dipole moments depend on the substitution pattern. However, for a given substituent, the dipole moments of the open VHF form is higher: DHA derivatives typically have dipole moments around 6-10 D, while VHF derivatives show larger dipole moments around 10-15 D [359]. Several reports have been published on how the DHA/VHF isomerization affects the conductance in single-molecule junctions [251, 252, 267-269], and on how the dipole moment of single molecules determines the interaction with electric fields [360, 361], but applications in electronic devices are still scarce [282]. Despite first reports on this particular switch in the nineteen-eighties [362-364], the potential of DHA/VHF to tune the electrical characteristics of transistors has not yet been explored. Hence, the work presented in this chapter expands the class of stimuli-responsive materials in organic electronic devices beyond the well-established diarylethenes, spiropyrans and azobenzenes, and takes advantage of the photo-/thermochromic properties of DHA/VHF switches to construct multifunctional electronic devices. Upon applying an organic semiconductor:switch blend as the active layer in an organic field-effect transistor the electrical characteristics can be reversibly switched by UV light and thermal stimuli. In order to quantify this effect, an in-depth analysis of transistor parameters is carried out and the effect of the UV light illumination dose is quantified. DHA/VHF switches with three different substituents are compared and a long-term cyclability of more than 100 illumination/annealing steps is demonstrated.

3.2. DHA/VHF Photochromism

The photo-/thermochromism of the DHA/VHF system has been reported for the first time by Daub et al. in 1984 [362]. The reversible isomerization involves a UV light-induced ring-opening reaction from DHA to VHF and a thermally-induced ring-closure reaction from VHF back to DHA. The former is typically characterized by a high quantum yield [365, 366], while the latter is relatively slow with rate constants in the range of 10^{-5} s^{-1} [365, 367]. Both isomers are not only showing different absorption and emission spectra [365, 366], but also different dipole moment [359] and single-molecule conductance [251, 252, 267-269]. In this study three different DHA/VHF derivatives were investigated for comparison: 1) DHA/VHF-Ph, with an unsubstituted phenyl ring attached to the C2 position of DHA; 2) DHA/VHF-F_2, with fluorine atoms in both

meta-positions of the phenyl ring; 3) DHA/VHF-OMe, with a methoxy group in para position. Molecular properties such as ionization potentials, electron affinities, dipole moments and frontier orbitals were determined via DFT calculations and are summarized in **Table 3.1** and **Table 3.2**.

Table 3.1: Molecular properties of the switches and polymers used in this study. Calculations were performed at the B3LYP/6-311G(d,p) level of DFT. The values for the polymers were taken from literature as indicated.

	ionization potential [eV]	electron affinity [eV]	dipole moment [D]	
			this work	[360]
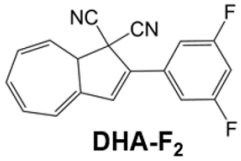 DHA-F_2	6.43	2.94	5.91	5.40
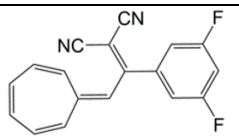 VHF-F_2	6.07	3.17	10.13	8.23
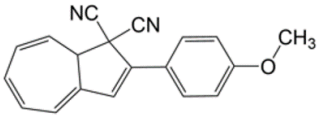 DHA-OMe	5.87	2.52	6.80	5.59
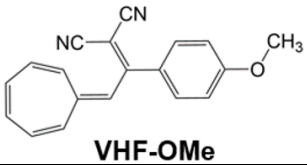 VHF-OMe	5.83	2.88	11.22	7.80
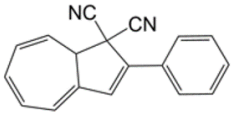 DHA-Ph	6.16	2.68	5.40	3.39
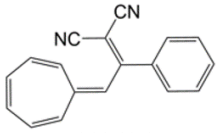 VHF-Ph	5.89	2.97	10.35	6.87
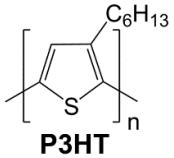 P3HT	4.9 [368]	3 [369]	-	-
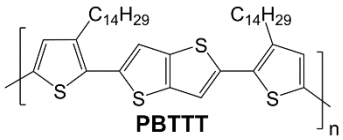 PBTTT	5.1 [370]	3.1 [371]	-	-

Table 3.2: Molecular frontier orbitals of switch molecules used in this study. Calculations were performed at the B3LYP/6-311G(d,p) level of DFT.

	HOMO	LUMO
DHA-F_2	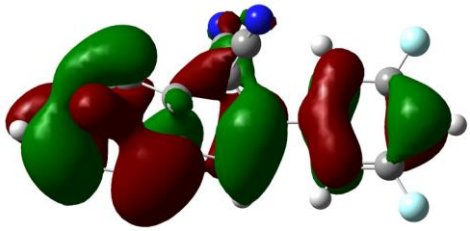	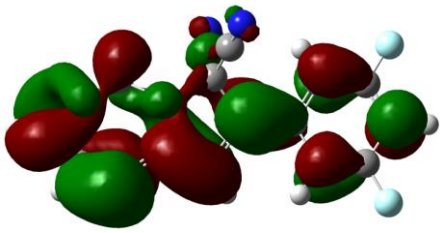
VHF-F_2	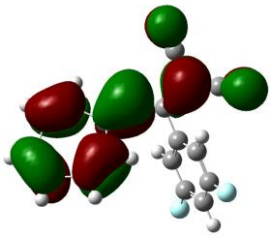	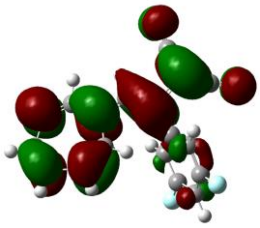
DHA-OMe	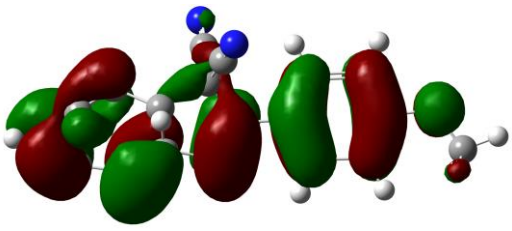	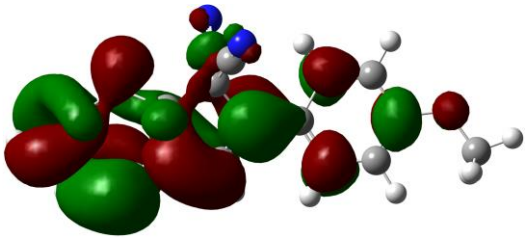
VHF-OMe	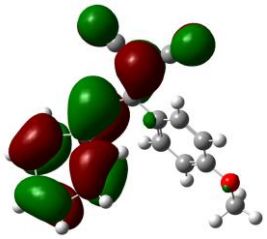	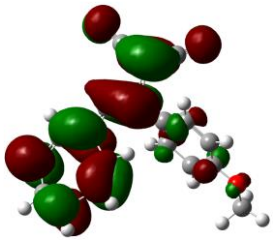
DHA-Ph	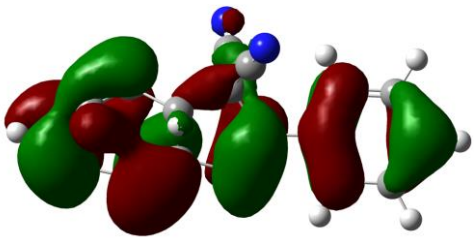	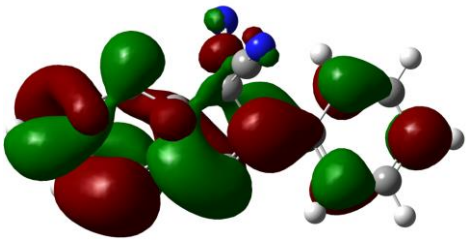
VHF-Ph	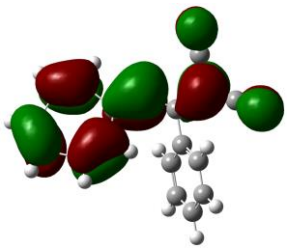	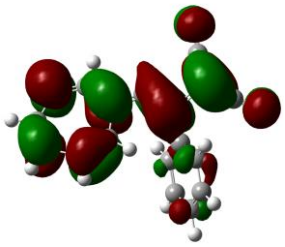

Figure 3.1a shows the molecular structure of DHA/VHF-F_2 and the characteristic color change between yellow and red upon UV light illumination or heating that can be observed in solution and in thin-films. The interconversion between both isomers in solution was studied with UV/Vis absorption and nuclear magnetic resonance (NMR) spectroscopy. As seen in **Figure 3.1b** DHA-F_2 absorbs strongly around 358 nm. With increasing UV light irradiation time, the intensity of this absorption band decreases and a new absorption band around 481 nm starts to appear. This redshift is typical for DHA/VHF compounds and is the signature of the photoinduced conversion from DHA-F_2 to VHF-F_2. Isosbestic points around 320 nm and 390 nm indicate that this conversion occurs without any side products. The thermal backreaction in the dark has been monitored using solution NMR spectroscopy. The disappearing multiplet signal of VHF-F_2 at a chemical shift of δ = 5.14-5.10 ppm and the appearing signal of DHA-F_2 at δ = 3.38 ppm indicate the completed ring-closing reaction from VHF-F_2 to DHA-F_2.

Films of DHA-F_2 show the characteristic yellow color, which turns red upon illumination with UV light (see **Figure 3.1a**). A dose as low as 100 mJ cm^{-2} is sufficient to induce this color change, which is the result of DHA transforming into VHF. The photoreaction could be reversed via thermal annealing at 90 °C for 20 min, yielding again the initial yellow colored film.

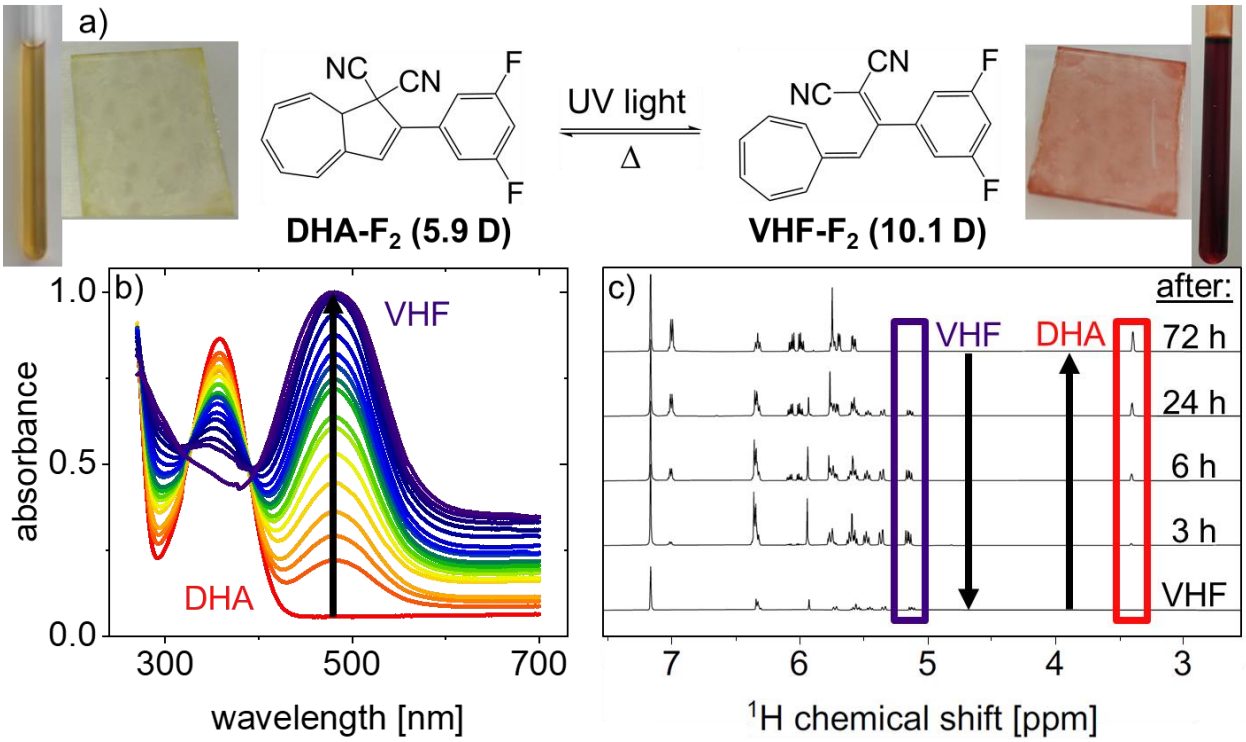

Figure 3.1: The DHA/VHF-F_2 photo-/thermochromic system. a) Molecular structures of DHA-F_2 and VHF-F_2 with the corresponding dipole moments (obtained via DFT calculations). Reversible switching between both isomers is possible via UV light illumination (DHA-F_2 to VHF-F_2) and thermal annealing (VHF-F_2 to DHA-F_2). The resulting changes in color are demonstrated in solution and thin-films. b) UV/Vis absorption spectra (in solution) indicating the transformation of DHA-F_2 (red line) to VHF-F_2 (purple line) upon UV light illumination. c) NMR spectra (in solution) showing the thermal backreaction of VHF-F_2 to DHA-F_2 at room temperature over 72 h.

3.3. Light-induced Switching of P3HT:DHA/VHF-F_2 Blend Transistors

In order to evaluate the switching capability of DHA/VHF-F_2 in OFETs, the switch was blended into solutions of the semiconducting polymer P3HT and spin coating was used to fabricate top-gate bottom-contact transistors with Cytop as gate dielectric. Electrical characteristics were recorded after applying UV light illumination and thermal stimuli. A schematic of the organic thin-film transistors and an optical microscopy image are shown in **Figure 3.2a**. Note that P3HT mainly absorbs in the visible range between 400 nm and 650 nm [372], which makes it a suitable host for the DHA-F_2 photoswitch that absorbs in the UV range.

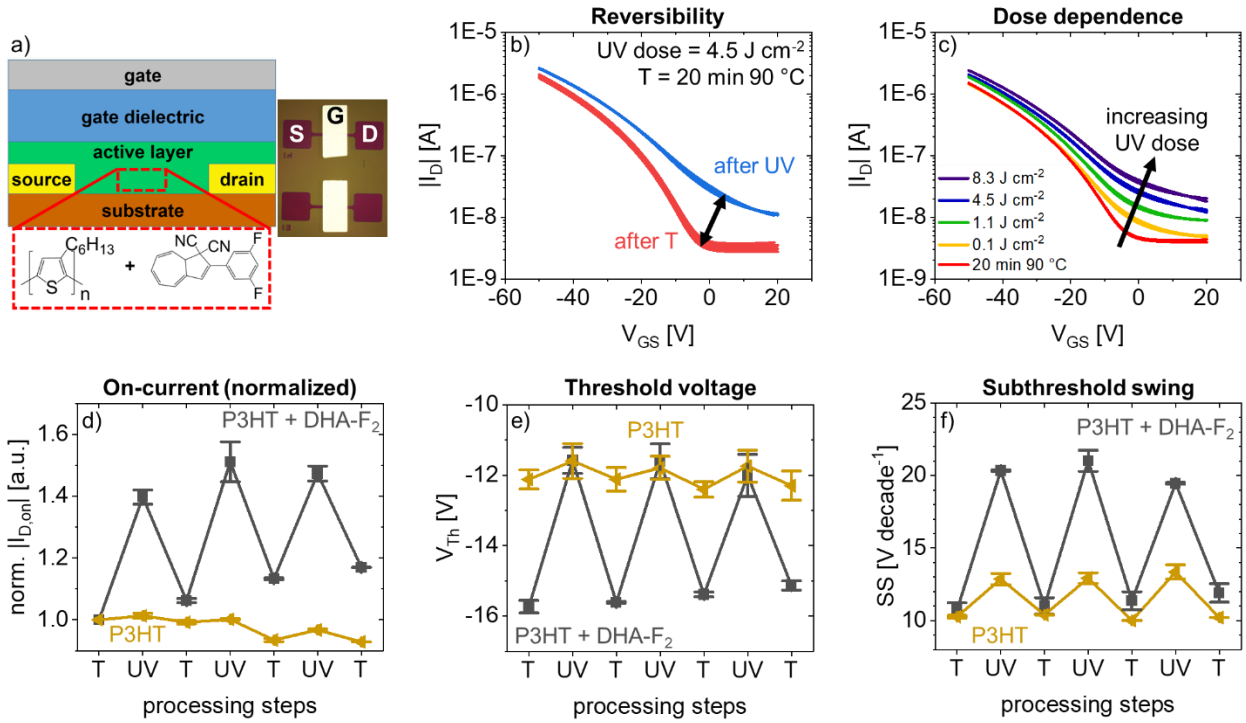

Figure 3.2: Light-gated organic transistors enabled by P3HT blends with DHA/VHF-F_2 photo-/thermochromic molecules. a) Schematic illustration of the top-gate bottom-contact OFETs with an active layer containing the organic semiconductor and the switch molecules. b) Reversible switching of transfer characteristics (V_{DS} = -50 V) of blend transistors after repeated UV light illumination (4.5 J cm^{-2}) and annealing (90 °C for 20 min). c) Dose-dependent switching of multiple electronic states (V_{DS} = -50 V). d) - f) Reversible switching of transistor parameters (d) normalized on-current, e) threshold voltage and f) subthreshold swing) extracted from transfer characteristics (V_{DS} = -50 V). UV = 4.5 J cm^{-2} and T = 90 °C for 20 min.

It is important to note that measurements were not carried out under illumination, but after switching when the light was turned off. **Figure 3.2b** shows the effect of both these stimuli on the transfer characteristics. **Figure 3.3** and **Figure 3.4** present a full set of transfer and output characteristics including gate currents (data for a reference device without switch is shown for comparison).

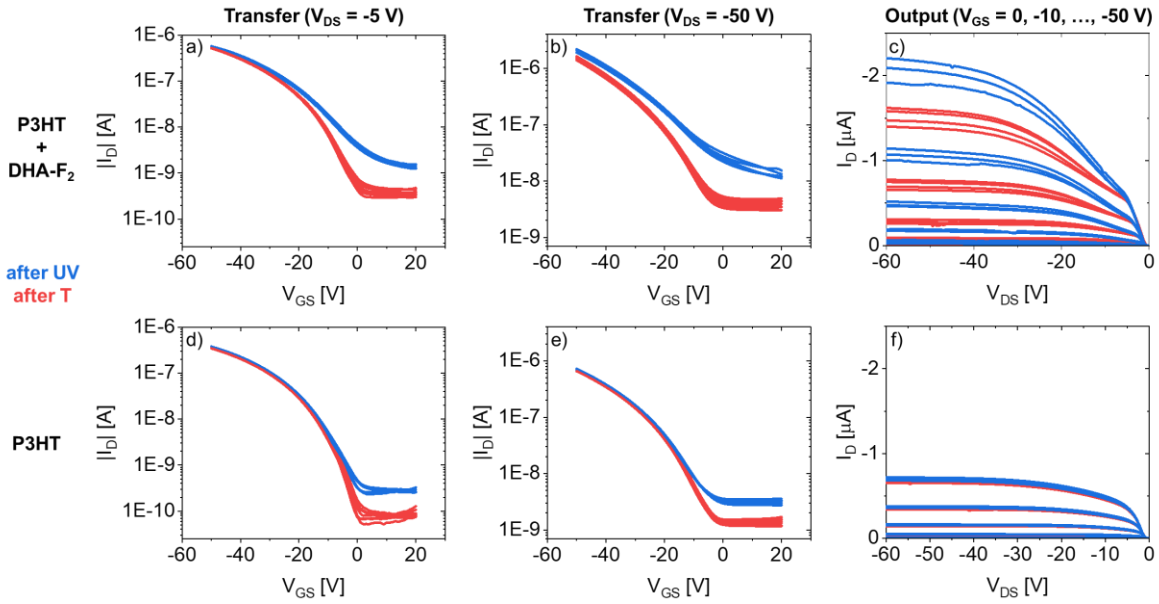

Figure 3.3: Transfer and output characteristics for a) - c) **P3HT blend device** and d) - f) **P3HT reference device** after **repeated** UV light illumination (4.5 J cm^{-2}) and annealing (90 °C for 20 min).

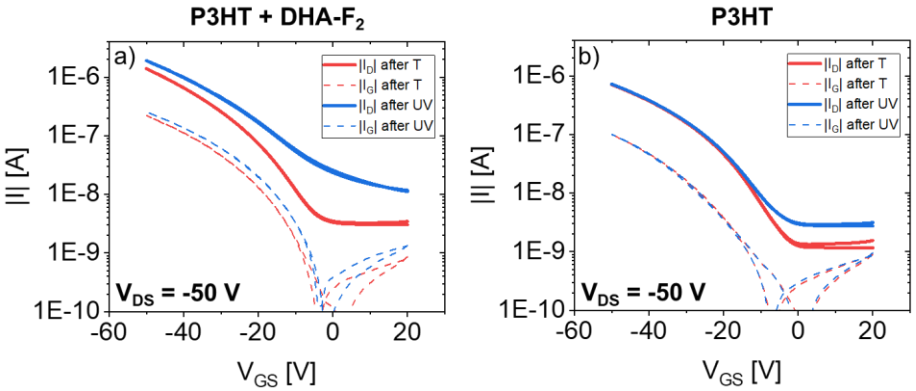

Figure 3.4: Representative transfer characteristics including drain currents $|I_D|$ and gate currents $|I_G|$ measured after UV light illumination (4.5 J cm^{-2}) and annealing (90 °C for 20 min) for a) **P3HT blend device** and b) **P3HT reference device**.

These data clearly show that switching can be observed in both transfer and output characteristics. While the transfer characteristics measured after thermal annealing show a clearly defined on-voltage around -4 V and a constant level in off-current of around 3-4 nA, the curves measured after UV light illumination feature a strongly increased off-current, a less defined on-voltage and a noticeably higher on-current. Such behavior might indicate that the VHF form of the switch acts as a dopant, while the DHA form does not (or at least to a lesser degree). A detailed discussion of

possible underlying mechanisms can be found below. **Figure 3.2c** visualizes how the magnitude of this switching effect depends on the applied UV dose. Different dose levels between 0.1 J cm^{-2} and 8.3 J cm^{-2} were applied after resetting the switching via annealing (red line). Characteristic transistor parameters such as the on/off-drain currents and subthreshold swing directly depend on the UV dose. It is hypothesized that higher UV doses lead to larger magnitude of switching, because a larger population of photoswitches is able to isomerize from DHA to VHF. Similar UV dose dependence effects have been reported in spiropyran and azobenzene-based systems [137, 166, 183] and are probably related to low isomerization quantum yields in solid state packing.

Such reversible, dose-dependent behavior is highly interesting for multi-level memory devices and can be furthermore exploited in e.g. UV sensors. For such applications, it is crucial that the same applied stimulus always causes the same response in the electrical characteristics. As shown in **Figure 3.5** and **Figure 3.6** different levels in off-current can be repeatedly written and erased in the blend devices.

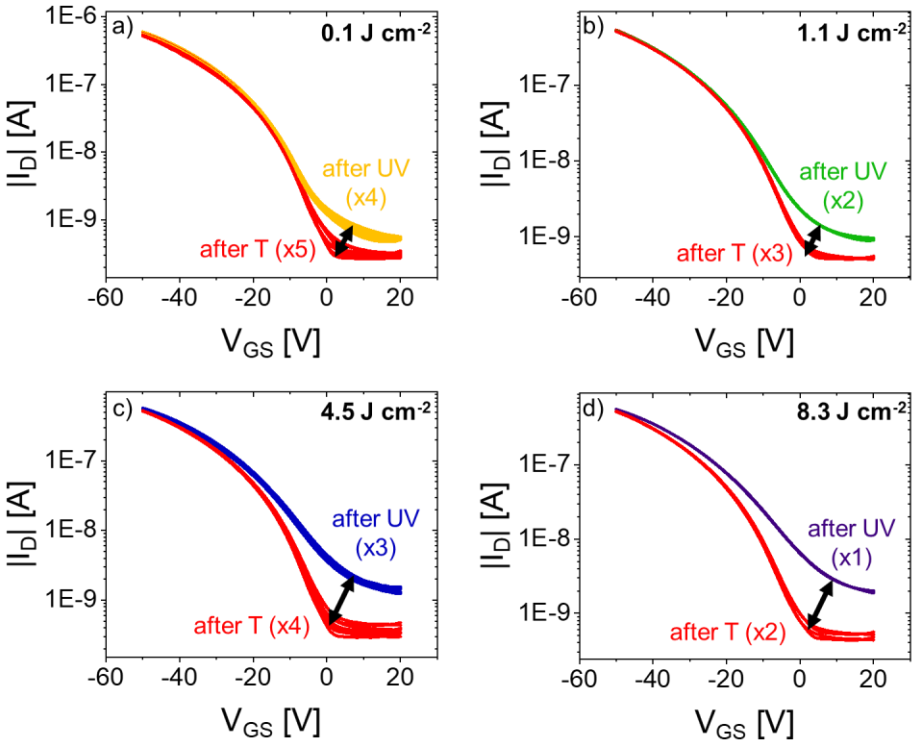

Figure 3.5: Repeated writing and erasing of transfer characteristics **(V_{DS} = -5 V)** in P3HT blend devices using UV light of various doses: a) 0.1 J cm^{-2}, b) 1.1 J cm^{-2}, c) 4.5 J cm^{-2} and d) 8.3 J cm^{-2}. Thermal annealing (T) at 90 °C for 20 min was used for erasing. The insets indicate the number of writing/erasing steps.

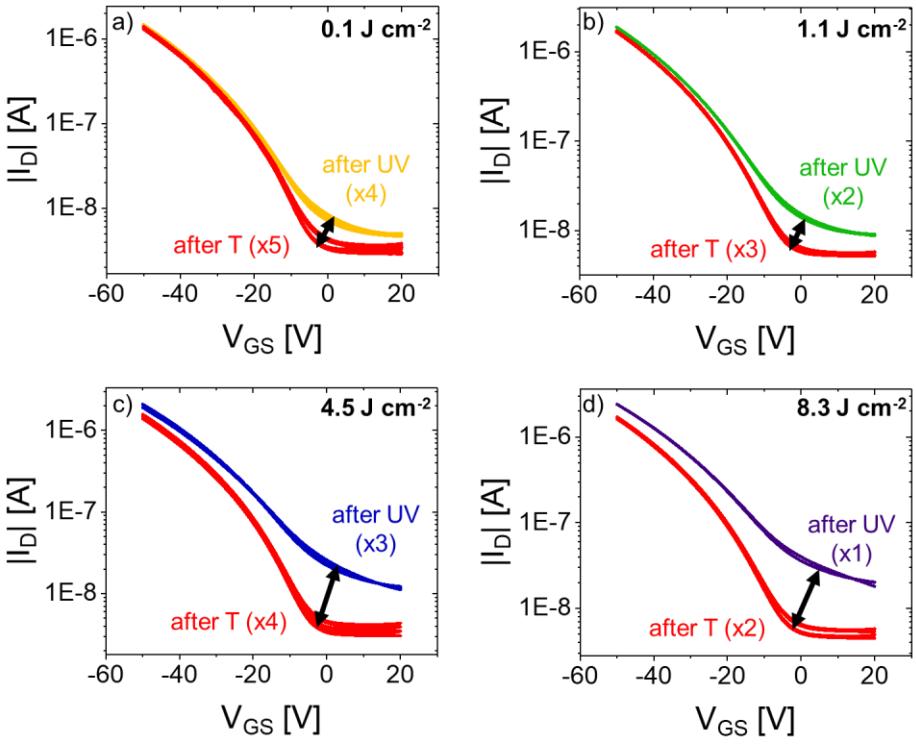

Figure 3.6: Repeated writing and erasing of transfer characteristics **(V_{DS} = -50 V)** in P3HT blend device using UV light of various doses: a) 0.1 J cm^{-2}, b) 1.1 J cm^{-2}, c) 4.5 J cm^{-2} and d) 8.3 J cm^{-2}. Thermal annealing (T) at 90 °C for 20 min was used for erasing. The insets indicate how many writing/erasing steps were performed.

Furthermore, high retention times of the individual memory states and bias stress stability are required. **Figure 3.7** shows that the UV-induced increase in off-current is sufficiently stable during 10 h of either negative or positive bias stress. This indicates that the thermal backreaction from DHA to VHF is sufficiently slow in the P3HT blend films under extended electrical bias conditions.

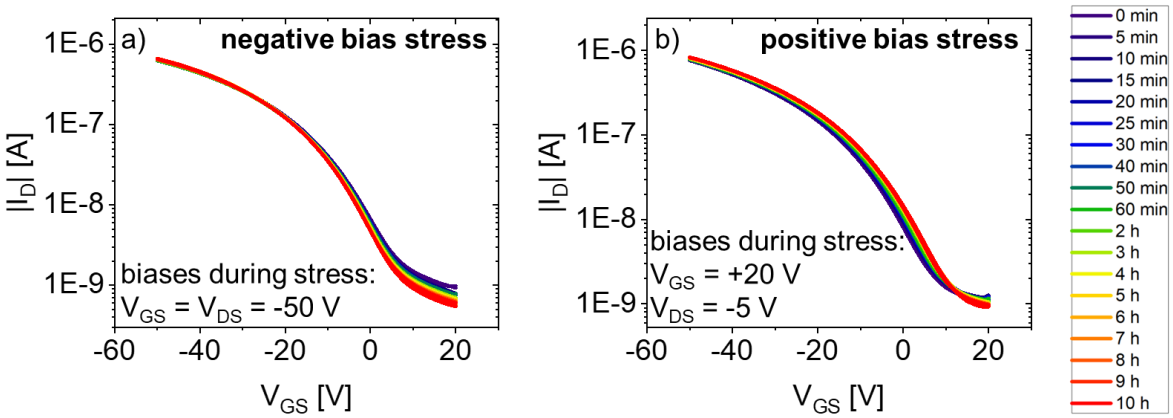

Figure 3.7: a) Negative and b) positive bias stress measurements on P3HT:VHF-F_2 blend OFETs. Total stress duration was 10 h. Prior to the measurement the transistors were irradiated with UV light (4.5 J cm^{-2}). The respective stress conditions are given in the insets. Stress conditions were paused in order to measure the transfer characteristics with V_{DS} = -5 V.

Figure 3.2d-f and **Figure 3.8** show the reversible switching of device parameters over three cycles of UV light irradiation and thermal annealing for transistors with and without switch. The general trend is that on-current ($|I_D|$ at V_{GS} = -50 V), subthreshold swing and mobility increase after UV light irradiation, while the threshold voltage shifts to more positive values.

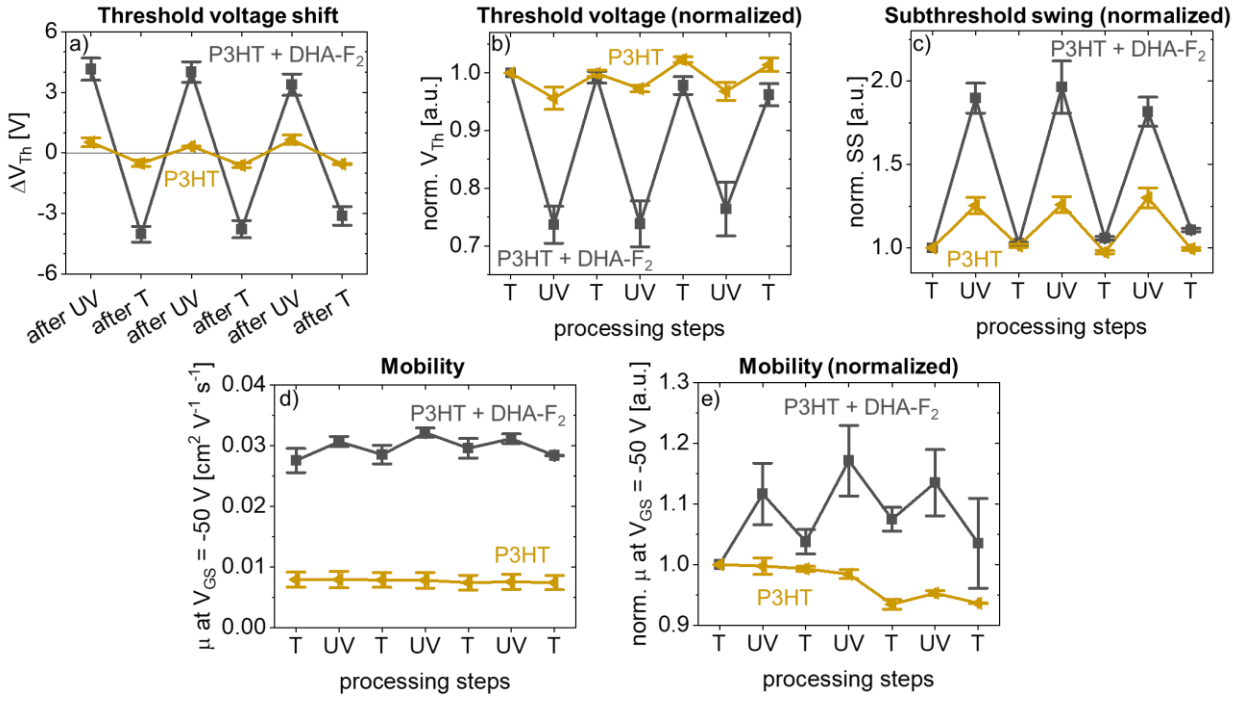

Figure 3.8: Reversible switching of transistor parameters a) threshold voltage shift, b) normalized threshold voltage, c) normalized subthreshold swing, d) mobility and e) normalized mobility extracted from transfer characteristics (V_{DS} = -50 V). UV = 4.5 J cm^{-2} and T = 90 °C for 20 min.

It is important to note that also the reference transistors show a response to the applied irradiation, even though all characteristics were measured after the light had been turned off. Such behavior has previously been reported for UV light irradiation of P3HT and PBTTT transistors under ambient conditions and was ascribed to the formation of hydrated $O_2(H_2O)_n$ clusters [373]. For this study, the OFETs were kept under glovebox conditions at all times in order to prevent atmospheric doping. However, it is impossible to fully eliminate the adverse effects of O_2 and H_2O in organic semiconductor devices with reasonable effort. If not from the atmosphere, residual O_2 and H_2O can be e.g. introduced to the devices via the polymers, switches or processing solvents [374, 375]. Regardless of the exact nature of this effect, the data indicates that this photoinduced doping effect is much smaller than the impact of the photoswitch.

3.4. Comparison of P3HT and PBTTT Blend Transistors

After having shown that DHA/VHF-F_2 switch molecules facilitate photoresponsive OFETs, a detailed study of the dose dependence of two polythiophene-based conjugated polymers was carried out. **Figure 3.9a and c** show the effect of different doses of UV light irradiation on the switching behavior of P3HT blend and PBTTT blend OFETs.

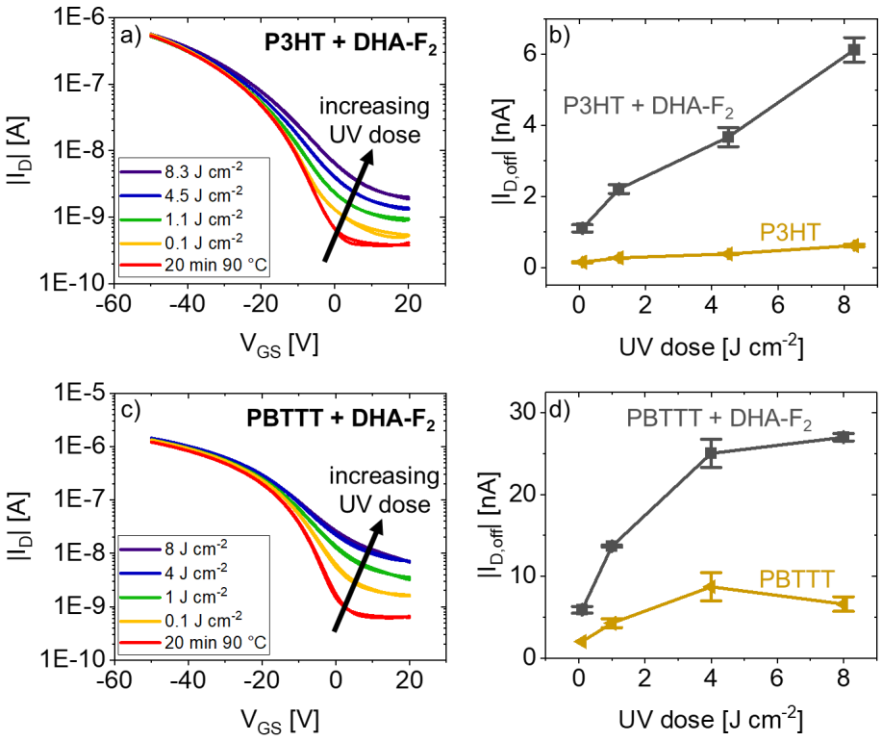

Figure 3.9: General applicability of the switch to various hosts: Dose-dependent switching of a) - b) P3HT blend and c) - d) PBTTT blend OFETs. a) and c) Dose-dependent switching of transfer characteristics (V_{DS} = -5 V). b) and d) Off-currents extracted from transfer characteristics (V_{DS} = -5 V) as a function of UV dose measured on blend and reference devices.

Figure 3.9b and d and **Figure 3.10** show the changes in off-current ($|I_D|$ at V_{GS} = 0 V) as a function of UV dose for blend and reference transistors. The increase in off-current as a consequence of illumination with UV light is significantly more pronounced for blend devices than for reference devices These results clearly show that the approach of blending DHA/VHF-F_2 into the active channel materials of OFETs is a viable strategy to obtain light-switchable devices and that this approach can be applied to different polymer hosts. Furthermore, the induced switching of OFET characteristics depends directly on the applied UV dose and can be reversed via thermal annealing.

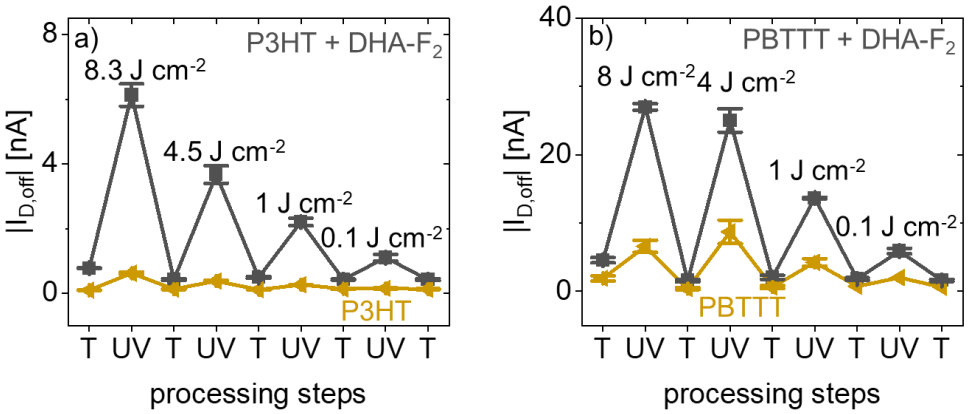

Figure 3.10: Off-currents in a) P3HT blend and b) PBTTT blend OFETs extracted from transfer characteristics (V_{DS} = -5 V) after irradiation with **different UV doses** and thermal annealing (90 °C for 20 min).

3.5. Comparison of Different DHA/VHF Switches

The photophysical behavior of DHA/VHF switches can be altered by attaching different substituents to the five-membered ring in the DHA molecule. Electron-withdrawing groups have been reported to redshift the absorption of VHF, while the opposite trend, i.e. a blueshift has been reported for electron-donating substituents [365, 376]. In order to clarify whether such substituent-effects are also affecting the stimuli-responsiveness of OFETs, two other DHA/VHF derivatives were investigated in P3HT blend OFETs. In addition to the previously discussed DHA-F_2 switch, where the substituent has electron-withdrawing character, one switch with an electron-donating methoxy group (DHA-OMe) and one with an unsubstituted phenyl ring were investigated (DHA-Ph). The molecular structures of these three photo-/thermochromic compounds are shown in **Figure 3.11a**, while the corresponding ionization potentials, electron affinities, dipole moments and frontier molecular orbitals are given in **Table 3.1** and **Table 3.2**. All three molecules enable reversible switching of the transistors upon irradiation and annealing. The normalized off-current and subthreshold swing for blend transistors are depicted in **Figure 3.11b-c**. A comparison with the reference devices shows that excellent switching can be achieved regardless of the nature of the substituent. However, based on the data it is not possible to establish a clear relationship between the nature of the substituent and the degree of optical switching. Instead, the results show that the fabrication of stimuli-responsive transistors with DHA/VHF switches is a general concept that cannot only be realized with different polymer hosts, but also with various derivatives of the

switch. Possibly, further functionalization of DHA/VHF molecules might enable the exploration of a new family of photo-/thermoresponsive optoelectronic devices.

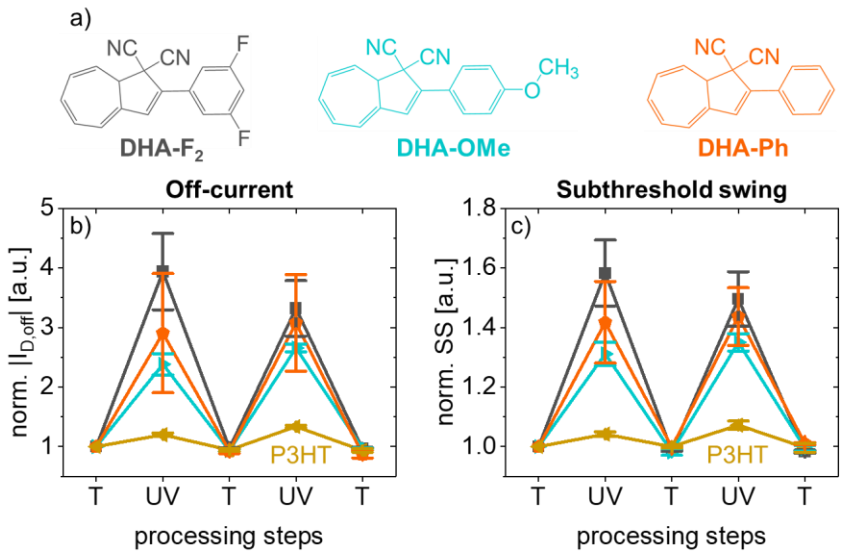

Figure 3.11: Comparison of P3HT blend devices with three different DHA/VHF derivatives. a) Molecular structures of DHA-F_2 (black, electron-withdrawing substituents), DHA-OMe (light blue, electron-donating substituent) and DHA-Ph (orange, neither electron-withdrawing or donating substituent). b) and c) Normalized transistor parameters (off-current and subthreshold swing) extracted from transfer characteristics (V_{DS} = -50 V). The colors of the lines and symbols match those used for the molecular structures.

3.6. Switching Fatigue and Improved Long-term Stability

Another important figure of merit for optically switchable OFETs is the long-term cyclability, also called switching fatigue. Diarylethene switches for example are especially resilient to switching fatigue and in some cases coloration and discoloration can be repeated for more than 10^4 times in solution [110] or in single crystals [377]. Generally, the switching capability of photochromic molecules can deteriorate when they are incorporated into a solid state matrix [378], which is one possible reason why such high cycle numbers can usually not be reported in blend systems [156]. Due to steric hindrance, it is particularly challenging to achieve sufficient isomerization when the photoswitches are blended into semi-crystalline polymer matrices [154].

In order to test the long-term cyclability of the novel P3HT blend devices, subsequent irradiation and annealing steps (both steps together comprising one cycle) were carried out and electrical

characteristics were recorded every 5 cycles. Such long-term studies, especially under applied external stimuli are very valuable in order to properly assess the reliability of such systems. **Figure 3.12** shows the evolution in off-current and mobility for blend and reference devices over the course of 50 cycles, comprising a total of 103 irradiation/annealing steps.

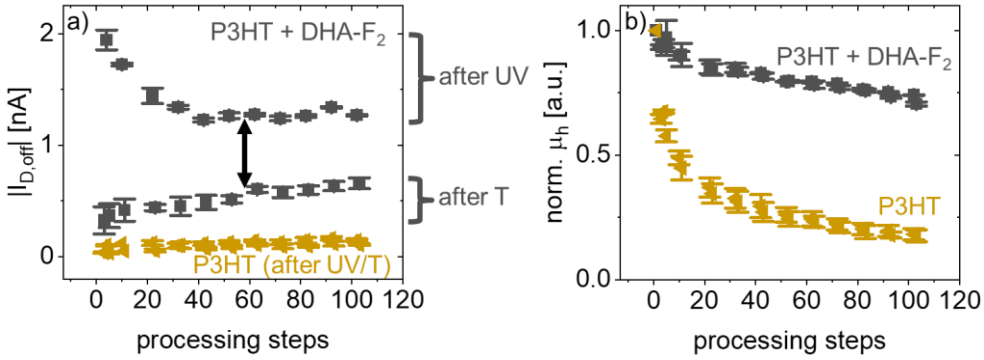

Figure 3.12: Cycling stability: Changes in transistor parameters due to repeated UV light illumination and annealing (103 steps in total, but measurements were not carried out after every step) of P3HT blend and reference OFETs. a) Off-currents and b) normalized mobilities extracted from transfer characteristics (V_{DS} = -5 V).

Full sets of transfer and output characteristics of P3HT blend and reference devices are given in **Figure 3.13** and **Figure 3.14**. Moderate switching fatigue of the blend devices manifests itself in 1) a continuous increase in off-current after annealing and 2) an initial decrease in off-current after UV light exposure during the first 40 steps, before reaching a plateau. Additionally, the decrease of the charge carrier mobility as a consequence of repeated stimulation was evaluated (see **Figure 3.12b**). Average mobilities of around 0.05 $cm^2\ V^{-1}\ s^{-1}$ and 0.04 $cm^2\ V^{-1}\ s^{-1}$ were determined for the fresh blend and reference devices. As a result of repeated UV light exposure and annealing these mobilities decreased to 71 % and 18 % of the initial value for blend and reference devices respectively. Both types of transistors were fabricated, processed and characterized side by side, the only difference being the presence/absence of the switch. Consequently, not only the increased mobility, but also its enhanced long-term stability can be ascribed to the presence of the switch within the active channel.

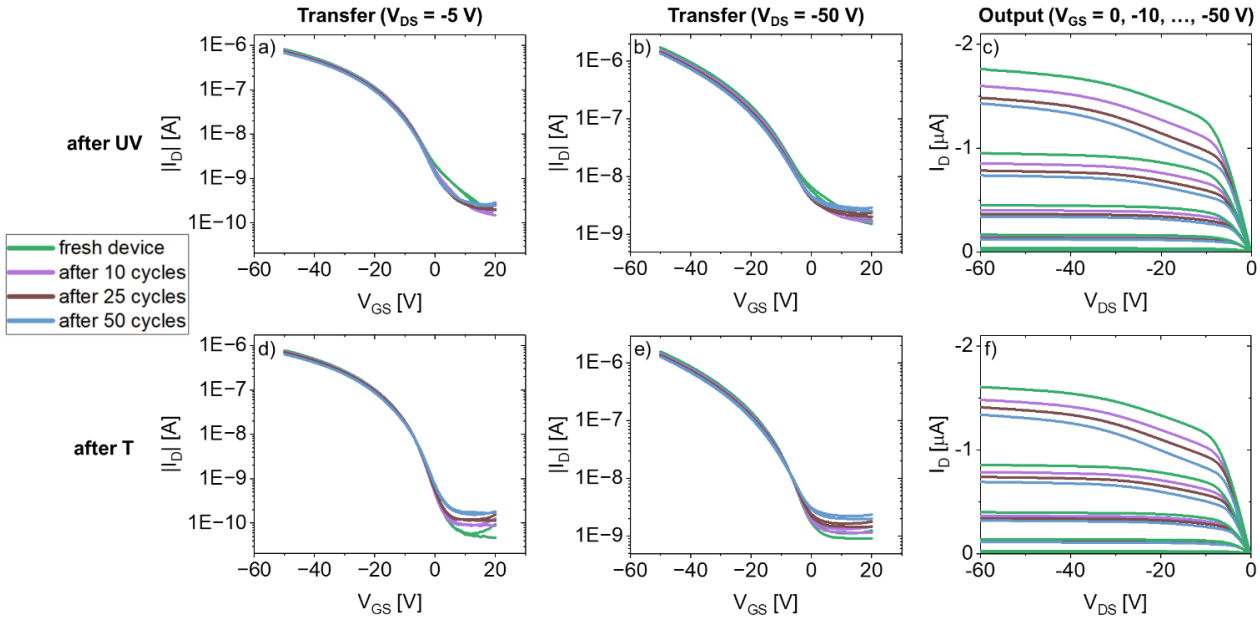

Figure 3.13: Transfer and output characteristics after a) - c) UV light irradiation (1 J cm^{-2}) and d) - f) thermal annealing (90 °C for 20 min) measured on a **P3HT blend device** before long-term cycling and after 10, 25 and 50 cycles.

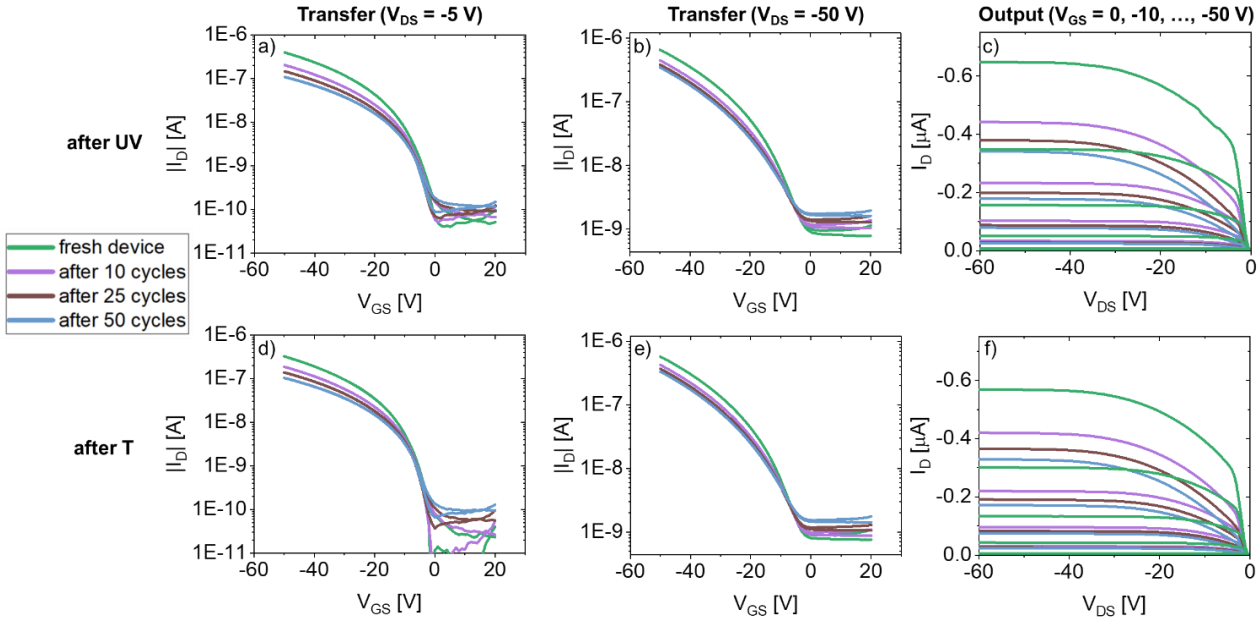

Figure 3.14: Transfer and output characteristics after a) - c) UV light irradiation (1 J cm^{-2}) and d) - f) thermal annealing (90 °C for 20 min) measured on a **P3HT reference device** before long-term cycling and after 10, 25 and 50 cycles.

To conclude this section, the key findings of Chapter 3 are summarized as follows: 1) Blending DHA/VHF switches with semiconducting polymers enables light-gated transistors. 2) The degree of switching can be precisely tuned via controlling the applied UV dose. 3) Stimuli-responsive transistors can be fabricated using various polymer hosts and derivatives of the DHA/VHF switch. This indicates the versatility of the approach. 4) The blend transistors show high resistance against switching fatigue and significantly reduced degradation of field-effect mobility as a consequence of repeated stimulation when compared to reference transistors.

3.7. Discussion

After having shown that DHA/VHF photo-/thermochromic molecules enable reversible switching and the programming of multiple states in organic blend transistors, possible underlying mechanisms need to be discussed. At first it should be noted that morphology related effects can be ruled out, since atomic force microscopy (AFM, see **Figure 3.15**) and grazing-incidence wide-angle X-ray scattering (GIWAXS, see **Figure 3.16**) data do not show any noticeable change after applied UV light and thermal stimulus.

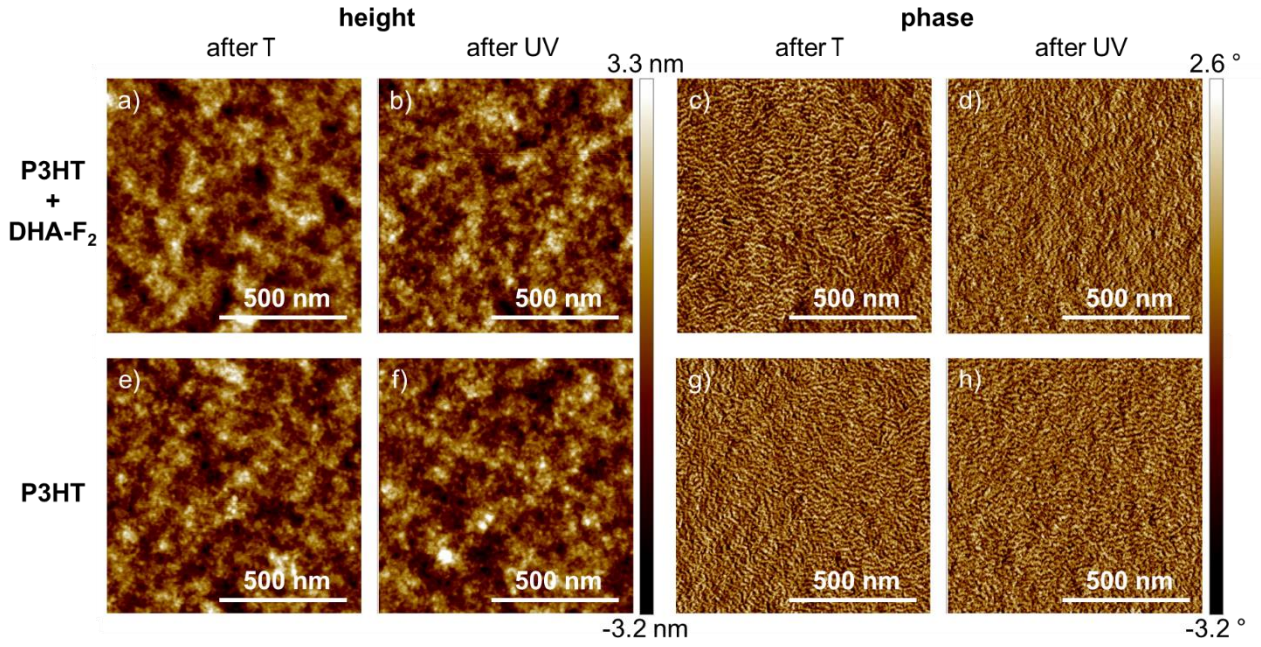

Figure 3.15: AFM images of a) - d) **P3HT blend** (with 10 wt% DHA/VHF-F_2) and e) - h) **P3HT reference** films after thermal annealing (90 °C for 20 min) and after UV irradiation (4.5 J cm^{-2}).

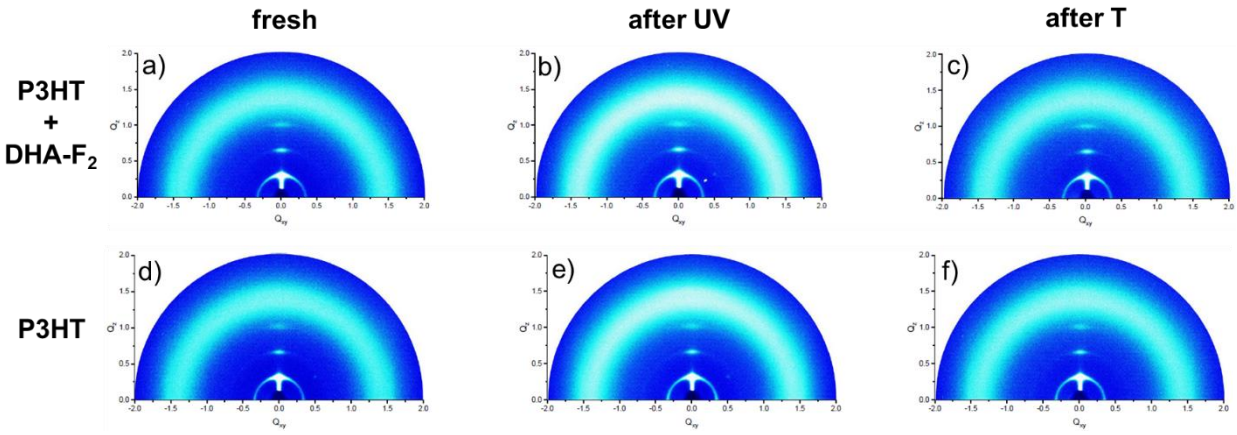

Figure 3.16: GIWAXS diffraction patterns of a) - c) **P3HT blend** (with 10 wt% DHA/VHF-F_2) and d) - f) **P3HT reference** films in the fresh state, after UV light irradiation (1 J cm^{-2}) and after thermal annealing (90 °C for 20 min).

As shown above, the blend transistors appear to be doped after UV light irradiation (increased bulk conductivity and hole mobility). Furthermore, **Figure 3.17** shows a decrease in contact resistance as well as sheet resistance after UV light exposure of the blend transistors, which is the typical signature of doping.

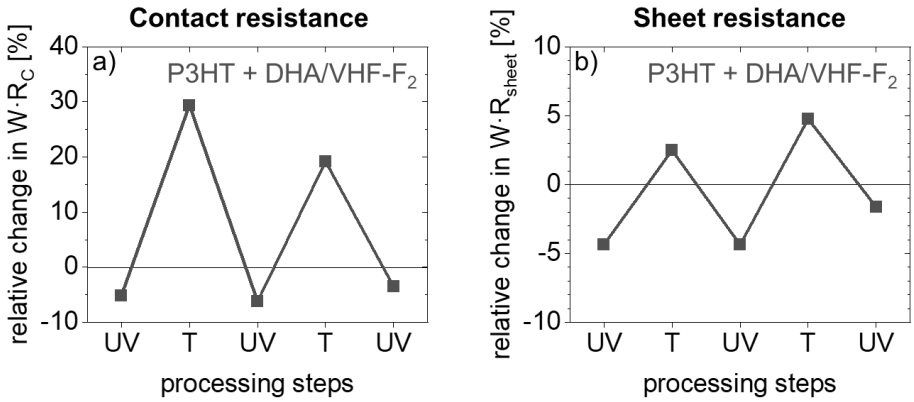

Figure 3.17: Width-normalized a) contact resistance and b) sheet resistance after UV light irradiation (1 J cm^{-2}) and thermal annealing (90 °C for 20 min) extracted for **P3HT blend devices** using the transmission line method for transistors with 30 µm, 40 µm, 50 µm and 80 µm channel length.

However, it is not yet fully clear how the UV-induced VHF derivatives can lead to doping-like effects when blended into P3HT and PBTTT. Several possible mechanisms are considered and discussed in the following: 1) Integer charge transfer; 2) (non-integer) charge transfer via

formation of a charge transfer complex; 3) dipole moment-induced photodoping; 4) VHF's dicyanovinyl group acting as an electron acceptor; 5) trap passivation.

In classical integer charge transfer doping, molecules with deep LUMOs can accept electrons from the HOMO of the organic semiconductor, creating additional holes, which contribute to the current in a device. This behavior has been reported for different organic semiconductors in combination with several dopants such as F_4TCNQ [379], $C_{60}F_{48}$ [380] or $Mo(tfd)_3$ [381]. However, neither DHA-F_2, nor VHF-F_2 are expected to act as integer charge-transfer dopants, because their electron affinities (2.94 eV for DHA-F_2 and 3.17 eV for VHF-F_2) are significantly lower than the ionization potentials of P3HT (4.9 eV [368]) and PBTTT (5.1 eV [370]). Another possible mechanism for doping to occur in organic host/guest systems is via formation of a charge transfer complex (CTC) in which the frontier orbitals of host and guest hybridize to form new occupied bonding and unoccupied antibonding orbitals [382]. These newly formed energy levels can give rise to non-integer charge transfer yielding unpaired electrons. Similar to integer charge transfer doping, these unpaired electrons can be detected with electron paramagnetic resonance (EPR) spectroscopy. In order to investigate whether doping via CTC formation could play a role, EPR spectroscopy was performed on a solution containing P3HT and VHF-F_2. The resulting EPR spectrum is shown in **Figure 3.18** and shows no sign of unpaired electrons and therefore no evidence of charge transfer between P3HT and VHF-F_2 in solution.

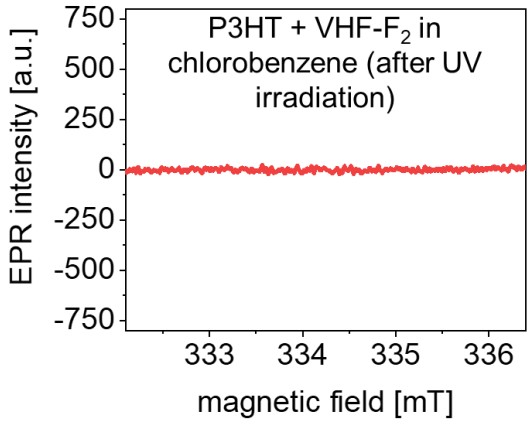

Figure 3.18: EPR spectrum of a P3HT solution (in chlorobenzene, 10 mg mL^{-1}) containing 10 wt% VHF-F_2 (after UV light illumination).

Interestingly, the close proximity of large dipoles has been reported by Balcı Leinen et al. to induce p-type doping in carbon-nanotubes [383]. The authors studied the photoresponsivity of

nanohybrids composed of single-walled carbon nanotubes wrapped with conjugated polymers with attached spiropyran moieties and observed an increase in conductivity after UV light illumination in two-terminal devices. Under UV light, spiropyran transforms into merocyanine, which is a zwitterionic molecule that has a larger dipole moment than spiropyran. The observed increase in conductivity of up to two orders of magnitude was ascribed to the large dipole moments of the merocyanine stabilizing positive charges on the nanotubes. This stabilization leads to a localized decrease in ionization potential, which in turn facilitates further doping via atmospheric contaminants such as O_2 and H_2O. Exciton splitting under illumination might also contribute to this effect. Balcı Leinen et al. suggest that the created holes are stabilized by the large dipoles of the photoswitch and electrons are quenched by atmospheric species. This mechanism is supported by two important findings: 1) The reference devices without any photoswitch also show a (smaller) response to UV light. This response is a lot less pronounced, but still occurs due to the presence of atmospheric contaminants. 2) The response to UV light is cumulative, i.e. longer exposure leads to higher degree of doping, due to the slow backreaction of merocyanine to spiropyran. Similar observations can also be found in the data presented in this chapter. **Figure 3.11** e.g. depicts a noticeable increase in drain current and subthreshold swing of the reference device upon UV light irradiation (dark yellow lines). Furthermore, the cumulative effect of UV light illumination is well in line with the observed dose-dependent modulation of transfer characteristics displayed in **Figure 3.2c** and **Figure 3.9**.

Despite differences between carbon nanotubes and conjugated polymers, the results show the same fundamental trends as the ones reported by Balcı Leinen et al. and therefore it could be plausible that similar processes are responsible for the modulations of the transistors. Furthermore, an increase in mobility and drain current caused by additives with significant molecular dipole has been previously observed for polymer transistors as well [384].

A few other reports on spiropyran/merocyanine photoswitches show increased conductivity or doping effects in small molecule or conjugated polymer-based systems, but lack a consistent explanation [211, 213]. Additionally, these reports contradict other publications, where the isomerization of spiropyran to merocyanine leads to a deterioration of charge transport [171, 173-175]. One should however keep in mind that controlled interactions, as reported by Balcı Leinen et al. might lead to different effects compared to a random distribution of photoswitches within a

semiconducting matrix and that the zwitterionic character of merocyanine adds further complexity in contrast to the DHA/VHF system.

Furthermore, the enhanced ability of the VHF isomer to act as an electron acceptor should be considered. In VHF, the dicyanovinyl group is in conjugation with the π-electron-system and acts as an electron acceptor due to its strong electronegative character, leading to a stabilization of the VHF isomer and narrowing of the bandgap [364]. Several studies showed that VHF can be more easily reduced (i.e. accept an additional electron, turning it into its radical anion) than compared to its respective DHA counterpart, making it a light-switchable π-electron acceptor [385]. This functionality has been exploited to modulate photocurrent through an electrochemical cell (higher current with VHF, since it is more readily reduced) [386, 387] or Na^+ ion-complexation in covalently attached crown ether moieties (weaker complexation with VHF due to its electron-withdrawing character) [388].

An alternative explanation for the switching of the transistor performance could be trap passivation facilitated by the VHF isomer. Nikolka et al. reported that molecular additives can improve performance and bias stress stability of organic transistors [389]. The authors suggest that additives containing strong electron-withdrawing moieties, can effectively bind water molecules through hydrogen bonds, thus reducing the number of water-related traps [390]. Interestingly, such trap passivation is mainly observed for additives that feature a dicyanovinyl group in conjugation with a π-electron-system, as present in the VHF form of the photoswitch [391].

Taking into account the increase in subthreshold swing upon UV light irradiation, it should also be considered that two effects might be superimposed. In this case, the increase in subthreshold swing could result from an increased energetic disorder caused by the large molecular dipole moments of the VHF isomers.

3.8. Conclusions

DHA/VHF switch molecules with photo-/thermoresponsive properties were blended into polythiophene-based conjugated polymers to enable novel multifunctional organic transistors, which have high prospects for applications as multi-level memory and synaptic devices. Reversible

switching of the current-voltage characteristics due to UV light irradiation and thermal annealing was demonstrated and can be attributed to the isomerization between DHA and VHF. To the best of my knowledge, this is the first time that reversible switching of transistors is achieved utilizing DHA/VHF photo-/thermochromic molecules. Transistor parameters such as drain current (in on- and off-state), threshold voltage, subthreshold swing and mobility can be modulated reversibly for three different derivatives of the DHA/VHF switches and the concept is applicable to several polymer matrices. Furthermore, the magnitude of switching depends directly on the applied UV dose enabling multi-level electronic systems. This direct correlation of applied stimulus and modulation of electrical characteristics makes these transistors promising candidates for applications in multi-level photomemories and photodetectors. Finally, a remarkably high resilience against switching fatigue over 100 steps of repeated UV light illumination and thermal annealing was demonstrated. The degradation of the field-effect mobility could be reduced through the presence of the switch.

Chapter 4: Reversible Switching of Capacitors and OFETs Employing PMMA:DHA/VHF Blends

4.1. Introduction

The increasing demand for mobile and flexible electronics and the rising interest in the "Internet of Things" promotes research on lightweight organic electronic devices and concepts where the integration of silicon chips is too expensive. Organic field-effect transistors can be used as fundamental building blocks for more advanced electronic circuits and applications on flexible foil and paper substrates [392], such as multi-level photomemories, photodetectors and neuromorphic electronics [393-395].

Here, a detailed account of reversible switching of PMMA blends with dihydroazulene/vinylheptafulvene (DHA/VHF) photo-/thermochromic molecules is given. These kind of molecular switches are promising candidates for enabling novel light-responsive organic electronic devices, since they exhibit a large change in dipole moment, but do not contain any ionic moieties (unlike the well-established spiropyrans) which are known to be detrimental for efficient charge carrier transport [171, 173, 175]. So far, however, DHA/VHF switches only received little attention in the context of stimuli-responsive organic devices and previous reports focused mostly on single-molecule junctions or devices based on self-assembled monolayers [267-269, 282]. This chapter aims to fill this gap by functionalizing PMMA gate dielectrics to enable light-programmable organic transistors.

The gate dielectric may dramatically influence morphology, energetic disorder or trapping at the semiconductor-dielectric interface and therefore charge transport and device performance [396]. In this context, the dielectric permittivity is a key material property. High permittivities for example are generally required for low voltage operation [397-399], but can also induce energetic disorder and hence lower carrier mobilities [220, 221]. Impedance spectroscopy is a commonly-used method to study dielectric properties of insulating polymers and several examples can be found in the literature where it was used to study the effect of small molecule additives, such as azo dyes or other organic chromophores, within a dielectric matrix [400-402]. Here, impedance spectroscopy was applied in a different context to investigate the isomerization of photoswitches. If the dipole moments of the two isomers of the switch differ significantly, impedance

spectroscopy will be a valuable tool to investigate the photoswitching and its effect on the dielectric properties of the insulating matrix. The reversible switching of the overall capacitance due to isomerization of photoswitches has been reported by several groups, e.g. via blending azobenzene-based photoswitches into PMMA [403] or via synthesizing spiropyran-containing dielectric copolymers [404]. However, detailed characterizations of impedance data, frequency-dependence and how the light-induced isomerization of photoswitches e.g. affects dielectric permittivity ε_r' and dielectric loss ε_r'' of light-responsive insulating blends are scarce [405]. These kinds of data could not only give further insights into underlying mechanisms, but also allow to quantify the switching capability of photochromic molecules.

In this study, it is shown that the stimulus-induced isomerization of the DHA/VHF photoswitches within the PMMA matrix can be directly observed by measuring the frequency-dependent complex electrical impedance Z^*. From the impedance spectra the switching parameters such as the complex dielectric permittivity ε_r^* and the area-normalized capacitance C_i of the gate dielectric are derived. An alternative approach to analyzing impedance data is the fitting with an equivalent circuit. This method is widely used in many fields such as electroceramics [406], battery research [407] or biosensing [408]. However, to the best of my knowledge, there is no systematic study implementing and assessing an equivalent circuit model for light-switchable organic capacitor devices. To fill this gap, an equivalent circuit fitting methodology is employed serving as an alternative approach to evaluate the switching capabilities of the DHA/VHF molecules in functioning electronic devices. Furthermore, it is demonstrated for the first time that PMMA:DHA/VHF blend gate dielectrics in organic transistors enable the control over electrical characteristics and figures of merit, by applying external stimuli such as UV light and heat. Additionally, it is shown that DHA/VHF molecular switches (unlike the established SP/MC photoswitch) exhibit excellent resistance against switching fatigue when incorporated into a PMMA dielectric.

4.2. Photoswitchable Capacitors

Three different derivatives of DHA/VHF molecular switches were blended with PMMA in order to fabricate light-switchable capacitors. **Table 3.1** shows the molecular structures of the switches,

namely DHA/VHF-Ph, DHA/VHF-OMe and DHA/VHF-F_2, including the corresponding ionization potentials, electron affinities and dipole moments. The isomerization from DHA to VHF was induced by exposure to UV light, while the backreaction from VHF to DHA was achieved via thermal annealing at 90 °C for 5 min. **Figure 4.1a** depicts the typical color change from pale yellow (DHA) to orange/red (VHF), indicating that the isomerization reaction readily occurs within the PMMA matrix. For the capacitor and transistor devices 20 nm of silver were used as semi-transparent top electrodes, allowing for high UV light transparency (see **Figure DA.2**). This switching is also evident in the obtained impedance data. In order to study the switching of the DHA/VHF molecules in the PMMA matrix, capacitors were subjected to eight switching cycles, where one cycle consists of a UV light exposure step (DHA to VHF) and one thermal annealing step (VHF to DHA). After each UV and each annealing step the impedance spectrum was measured. **Figure 4.1b-d** shows the Nyquist plot (Z'' vs. Z'), Bode plot ($|Z^*|$ vs. f) and phase angle plot (φ vs. f) for eight UV/T cycles of switching for a PMMA:DHA/VHF-Ph blend capacitor.

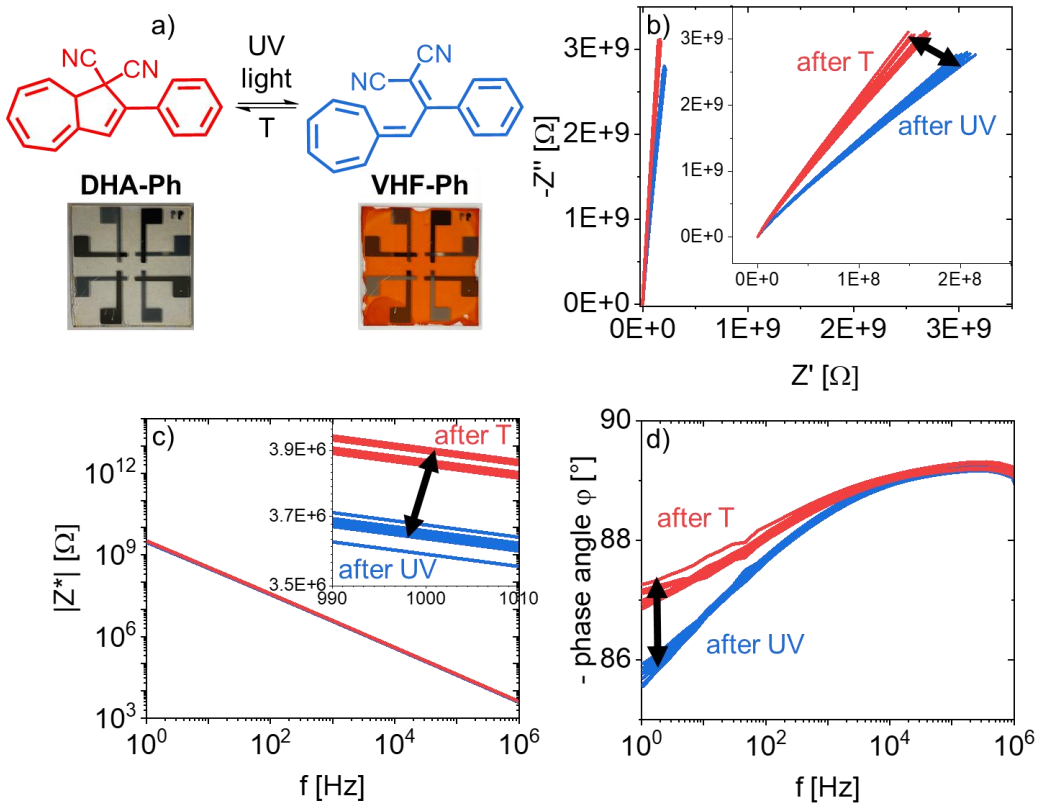

Figure 4.1: Stimuli-responsive capacitors enabled by PMMA blends with DHA/VHF-Ph photo-/thermochromic molecules. a) Molecular structure of both isomers of the switch and photographs of a substrate with four capacitor devices after thermal annealing (left, switch in DHA form) and after UV light exposure (right, switch in VHF form). b) - d) Nyquist, Bode and phase angle plot of impedance data collected for eight UV/T cycles. Blue lines: Measured after UV light exposure (5 J cm^{-2}). Red lines: Measured after thermal annealing (90 °C for 5 min). The Nyquist plot in panel b) is shown on orthonormal axes, while its inset is not. Note that phase angles of capacitors are negative per definition, which describes the scenario that the current is leading the voltage.

The corresponding data for PMMA:DHA/VHF-OMe blend, PMMA:DHA/VHF-F_2 blend and a reference capacitor without any photoswitch can be found in **Figure 4.2**.

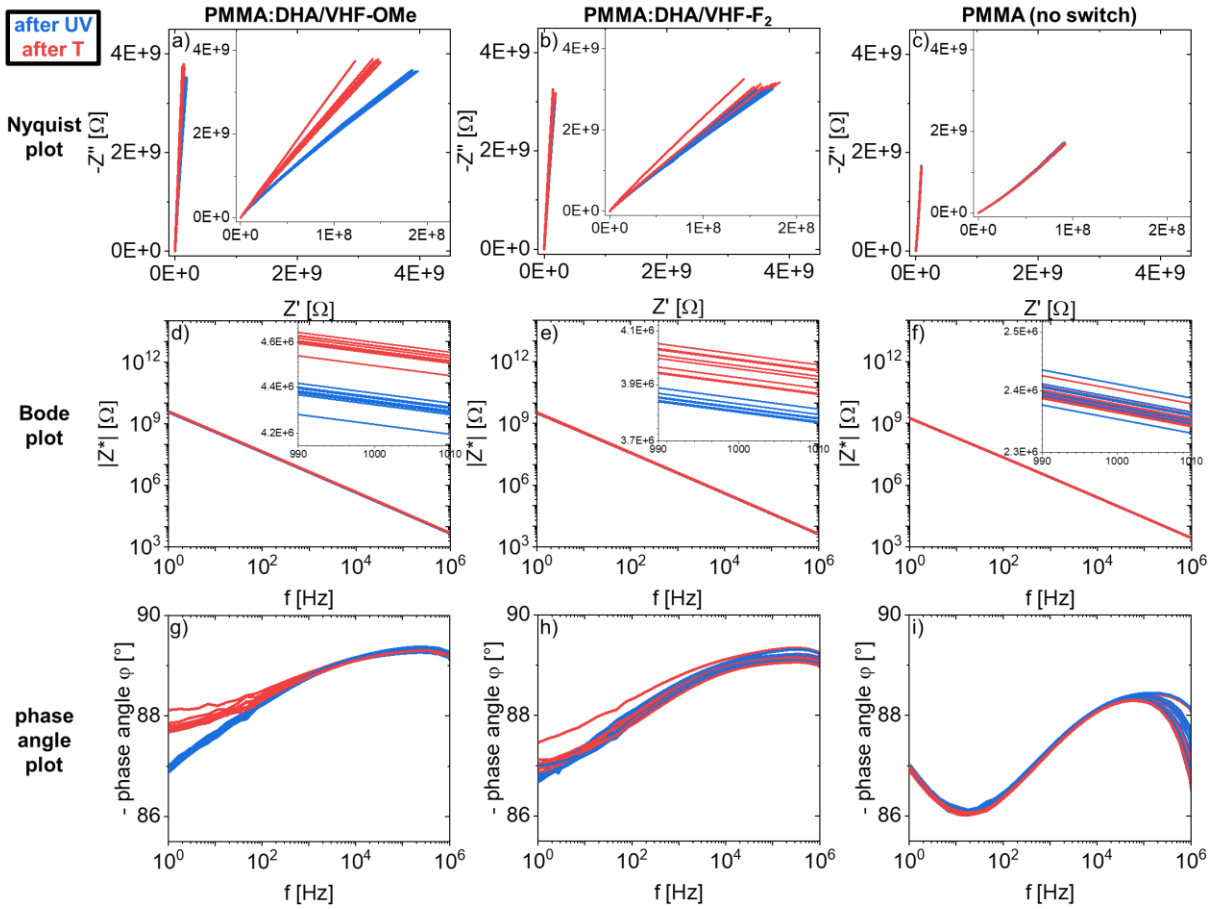

Figure 4.2: a) - c) Nyquist, d) - f) Bode and g) - i) phase angle plots of impedance data collected for eight UV/T cycles for a PMMA:DHA/VHF-OMe blend, PMMA:DHA/VHF-F_2 blend and a reference capacitor without any photoswitch. Blue lines: Measured after UV light exposure (5 J cm^{-2}). Red lines: Measured after thermal annealing (90 °C for 5 min). Note that the Nyquist plots in panels a) - c) are shown on orthonormal axes, while their insets are not.

Based on these data, the frequency-dependent complex dielectric permittivity ε_r^* was evaluated by calculating its real part ε_r', imaginary part ε_r'', modulus $|\varepsilon_r^*|$ and loss tangent $tan(\delta)$ using Equations 3 to 6, with the thickness of the dielectric d, vacuum permittivity ε_0 and area of electrode overlap A (= 1 mm^2). ε_r' and ε_r'' are sometimes referred to as dielectric permittivity and dielectric loss respectively [405]. Further information on this impedance formalism is given in the Appendix.

$$\varepsilon_r' = \frac{d}{\omega \varepsilon_0 A} \cdot \frac{-Z''}{(Z'^2 + Z''^2)} \tag{3}$$

$$\varepsilon_r'' = \frac{d}{\omega \varepsilon_0 A} \cdot \frac{Z'}{(Z'^2 + Z''^2)} \tag{4}$$

$$|\varepsilon_r^*| = \sqrt{\varepsilon_r'^2 + \varepsilon_r''^2} \tag{5}$$

$$tan(\delta) = \frac{\varepsilon_r''}{\varepsilon_r'} \tag{6}$$

Figure 4.3a-b show that both the real and imaginary part of the permittivity increase after UV light exposure.

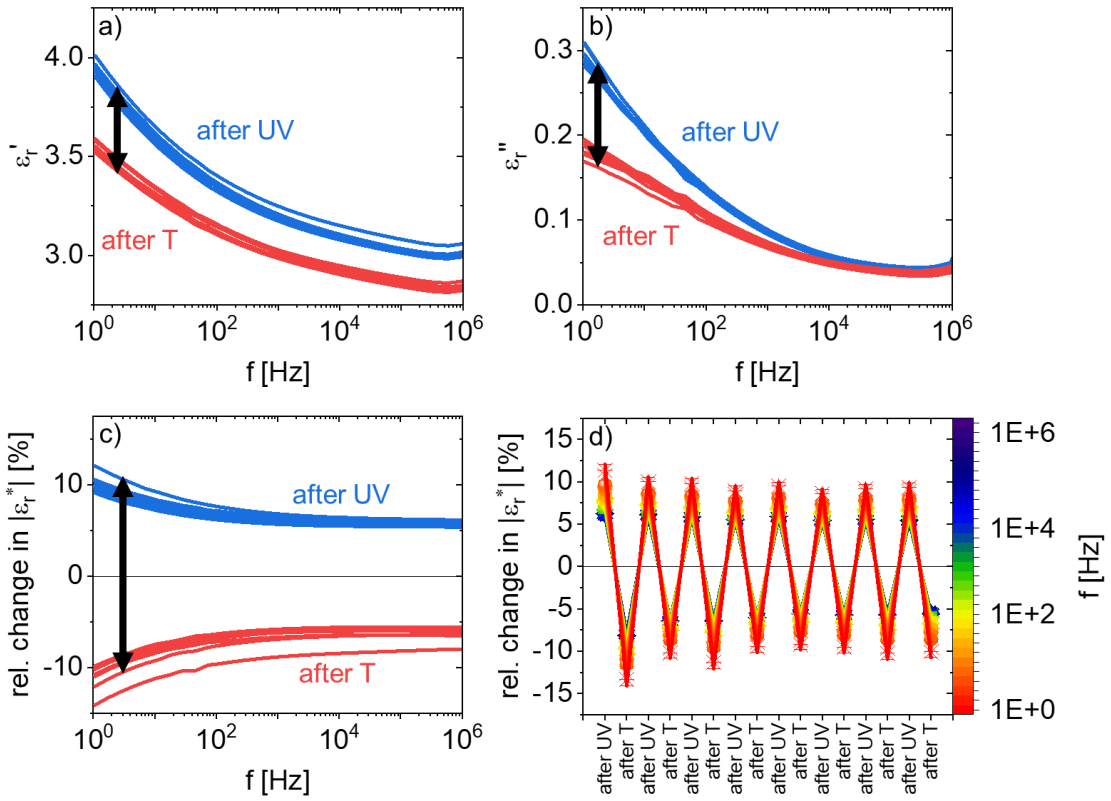

Figure 4.3: Analysis of the frequency-dependent complex permittivity ε_r*. a) - b) Real and imaginary part of ε_r*. c) Relative change in the modulus of the complex permittivity (from one processing step to the next) as a function of frequency. Blue lines: Measured after UV light exposure (5 J cm^{-2}). Red lines: Measured after thermal annealing (90 °C for 5 min). d) Relative change in the modulus of the complex permittivity over the course of eight UV/T cycles. The color coding from red to dark blue corresponds to the frequency at which the permittivity was evaluated. Note that panels c) and d) represent the same data in two different ways.

The increase in the imaginary part is more pronounced at lower frequencies. Additionally, the frequency-dependence of the modulus of the complex permittivity $|\varepsilon_r^*|$ and the loss tangent *tan(δ)* are given in **Figure 4.4**. In absolute values, $|\varepsilon_r^*|$ switches between around 3.56 and 3.96 (at f = 1 Hz), which corresponds to a switching of capacitance (per unit area) between 4.9 nF cm^{-2} and 5.4 nF cm^{-2}.

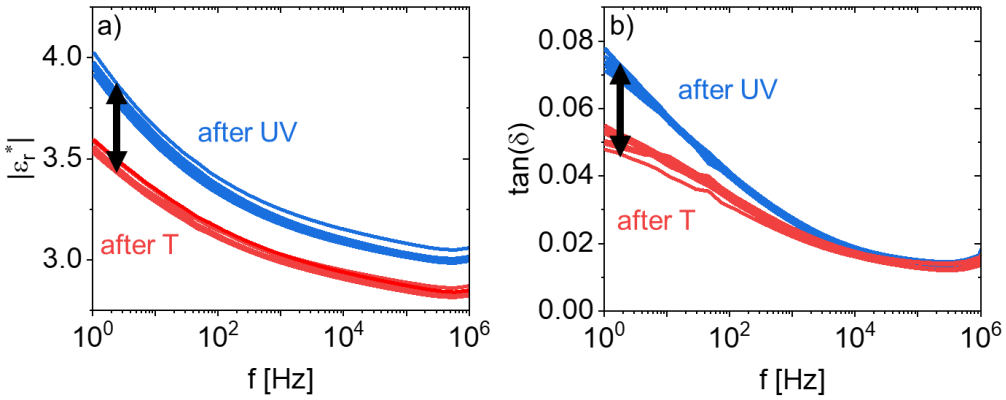

Figure 4.4: a) Modulus of complex permittivity and b) loss tangent for eight UV/T cycles of a PMMA:DHA/VHF-Ph blend capacitor as a function of frequency. Blue lines: Measured after UV light exposure (5 J cm^{-2}). Red lines: Measured after thermal annealing (90 °C for 5 min).

The frequency-independent increase in ε_r' upon UV light irradiation is related to the increased dipole moment of VHF in comparison to DHA (see **Table 3.1**) resulting in a larger polarizability of the blend. Furthermore, **Figure 4.1b** indicates a slight decrease in resistance after UV light irradiation, which is consistent with an increase in dielectric loss (see **Figure 4.4b**) and in agreement with increased single-molecule conductance of VHF [269, 358] correlated with the reduced HOMO-LUMO gap (see **Table 3.1**). The switching in ε_r'' at low frequencies could also stem from switch molecules affecting the relaxation of the PMMA side groups. It has been reported that the relaxation of the carboxymethyl (-COOCH$_3$) side groups (β relaxation mode) results in a peak in the ε_r'' spectrum between 1 and 10 Hz [400], which is in good agreement with the results shown in **Figure 4.5**. However, in the blend system with DHA/VHF this relaxation peak cannot be observed, possibly due to the fact that the presence of the switches hinders the movement of the polymer side groups, with this effect being stronger for DHA compared to VHF.

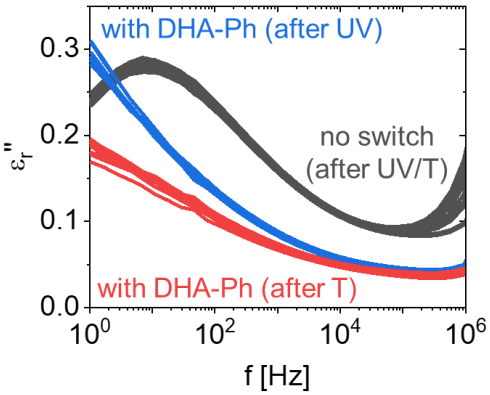

Figure 4.5: Imaginary part of ε_r* for eight UV/T cycles of a PMMA:DHA/VHF-Ph blend capacitor (same data as in **Figure 4.3b**) and a reference capacitor without any photoswitch as a function of frequency.

The results show that the contribution of ε_r' (related to the changing dipole moment of DHA/VHF) dominates the strong increase in $|\varepsilon_r^*|$ (and therefore capacitance) after UV light illumination. Similar results were reported for PMMA-based capacitors containing azobenzene [403] and spiropyran [404]. **Figure 4.3c-d** show the relative changes of $|\varepsilon_r^*|$ (from one processing step to the next) as a function of frequency and after each individual step. These results indicate that the modulus of the permittivity increases as a result of UV light exposure (consistent with the increasing dipole moment, see **Table 3.1**), while it decreases after thermal annealing. Furthermore, the changes are more pronounced at lower frequencies (due to the contribution of ε_r'') and no apparent switching fatigue (i.e. reduction in magnitude of switching) can be observed.

An alternative approach for evaluating impedance spectra is to fit the data to an equivalent circuit model in order to better understand the physical and chemical processes, which are possibly occurring during the experiment. For example, Rampi et al. reported that alkanethiol self-assembled monolayers between two opposing mercury surfaces can be modelled with an RC element (resistor and capacitor in parallel) [409]. Jin et al. used a more complicated circuit of a resistor in series with two RC elements to describe the electrochemical processes in electrochromic displays [410]. The molecules reported in that study contain photochromic diarylethene units, but their ability to photoisomerize was not investigated with impedance spectroscopy. To the best of my knowledge, there are no reports in the literature, which describe and quantify the switching of photochromic molecules using equivalent circuit fitting analysis. Here such a procedure is employed, which allows to extract dielectric permittivities from the frequency-dependent impedance data.

For this analysis an RC element model was chosen (results obtained with different models are given in the Appendix). As a first step, the impedance data is fitted with the selected model, with each fit yielding a value for the respective circuit parameters. In case of the RC element, these parameters are the fitted capacitance C (which can be converted to the area-normalized capacitance C_i) and the fitted resistance R. A representative fit result of the Nyquist plot (of data measured on a fresh PMMA:DHA/VHF-Ph capacitor sample) is given in **Figure 4.6c**, while a more detailed description of this fitting procedure and its results is provided in the Appendix. By fitting the data obtained after each processing step, it is possible to analyze how the capacitance and the resistance of the sample are affected by exposure to UV light and thermal stimulus. **Figure 4.6a-b** show that both circuit parameters of the RC model switch reversibly over the course of eight UV/T cycles. The observed switching of the resistance (i.e. lower resistance after UV light exposure) is in agreement with the increased single-molecule conductance of VHF mentioned above. With the fitted capacitance it is possible to calculate the permittivity ε_r of the sample using Equation 7. This approach of describing the sample as an ideal capacitor is an approximation justified by the large values of resistance (in the GΩ range).

$$\varepsilon_r = \frac{C_{fitted} \cdot d}{\varepsilon_0 \cdot A} \tag{7}$$

The obtained permittivities derived from the RC element model are given in **Figure 4.6d**. A comparison with the results obtained by directly analyzing the complex impedance data (at f = 1 Hz) shows that both approaches yield comparable results, underlining the validity of the fitting approach.

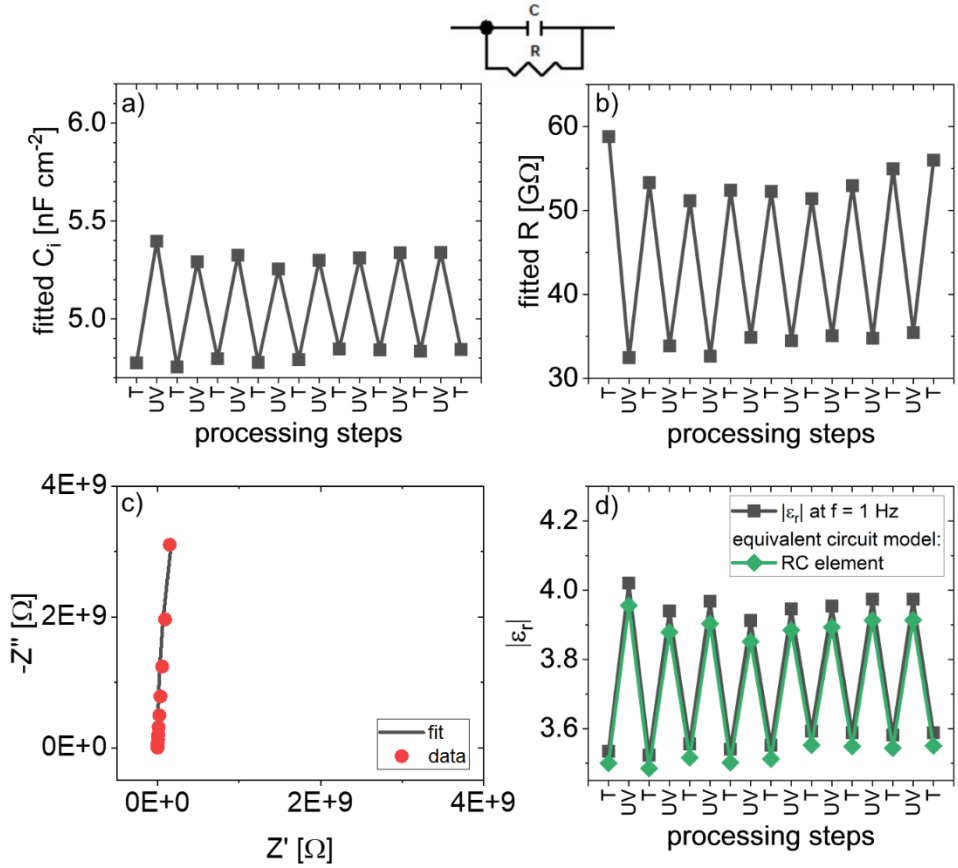

Figure 4.6: Equivalent circuit fitting analysis of impedance data from a PMMA:DHA/VHF-Ph capacitor sample acquired over the course of eight UV/T cycles using an RC element model. Fitted circuit element parameters: a) Area-normalized capacitance, b) resistance. c) Fitted (representative) Nyquist plot on orthonormal axes. Experimental data is shown as red circles and the fit result is shown as a black line. d) Resulting permittivities obtained by equivalent circuit fitting approach (green diamonds) compared to permittivities obtained by evaluating the complex frequency-dependent impedance at f = 1 Hz.

Figure 4.7 shows the switching in permittivity for PMMA blend capacitors containing three different DHA/VHF derivatives obtained via fitting with an RC element model. The largest change in permittivity is observed for blends with the unsubstituted derivative DHA/VHF-Ph, while the lowest change is observed for the fluorinated derivative DHA/VHF-F_2. This trend is in agreement with the expectation based on the calculated dipole moments of the switches (see **Table 3.1**). The differences in dipole moment of the isomers were determined as 4.95 D for DHA/VHF-Ph, 4.42 D for DHA/VHF-OMe and 4.22 D for DHA/VHF-F_2. **Figure DA.12** indicates that the same qualitative trend is obtained when other equivalent circuit models are used. All isomers demonstrate very good switching stability over multiple cycles.

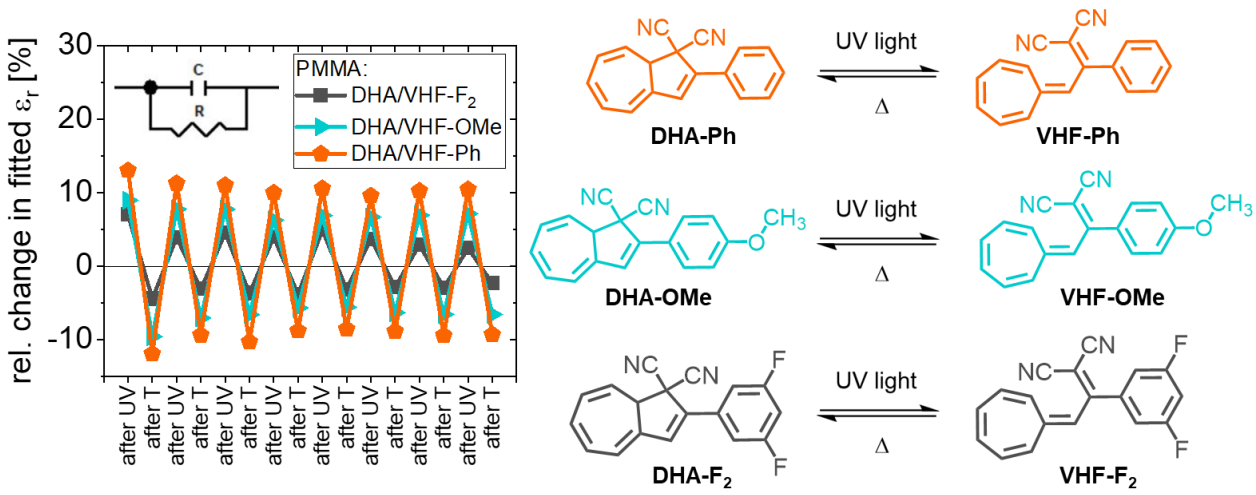

Figure 4.7: Comparing the switching in permittivity for PMMA:DHA/VHF capacitors containing three different DHA/VHF derivatives (DHA/VHF-Ph, DHA/VHF-OMe, DHA/VHF-F_2). The relative change in permittivity was determined by fitting an RC element model to impedance data collected over the course of eight UV/T cycles.

4.3. UV/Vis Absorption Spectroscopy

To study the switching fatigue, PMMA blends with DHA/VHF switches were investigated using UV/Vis absorption spectroscopy. Spectra were recorded on fresh films and after the first UV light irradiation in order to determine the characteristic absorption bands of the DHA and VHF isomers. In agreement with the literature [411] the DHA isomers showed a maximum absorption around 360-370 nm, while the VHF isomers absorbed around 470-485 nm. Additionally, the switching fatigue of the blend films was studied over the course of 20 UV/T cycles (i.e. 20 UV light exposure and 20 annealing steps). All recorded spectra are shown in **Figure 4.8**.

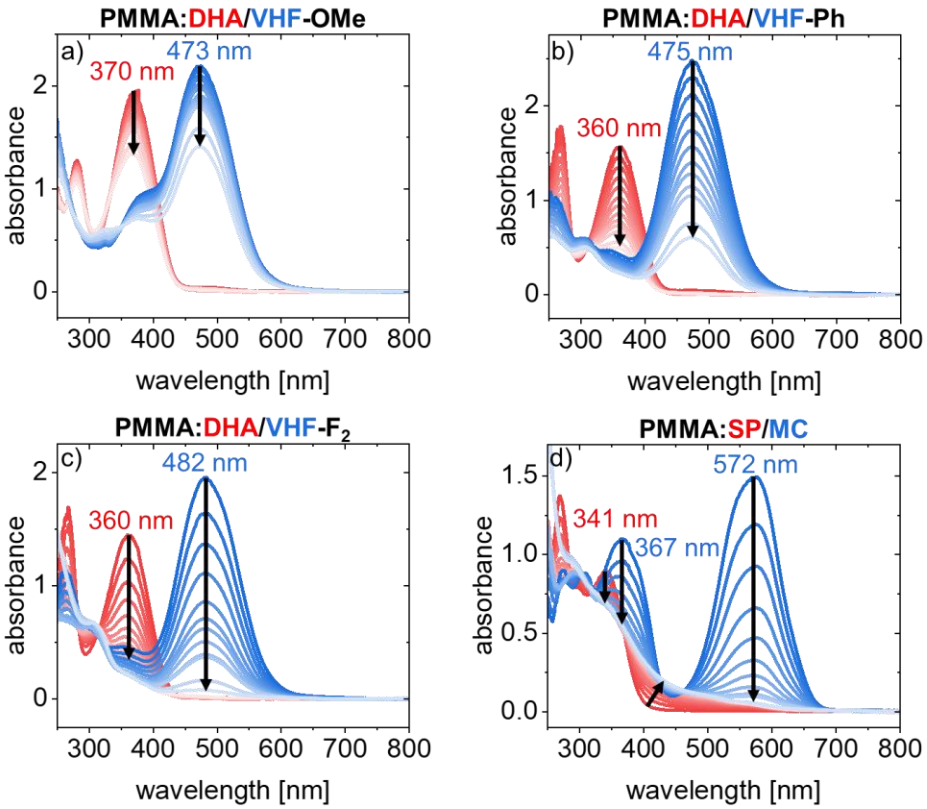

Figure 4.8: UV/Vis absorption spectra of a) PMMA:DHA/VHF-OMe blend, b) PMMA:DHA/VHF-Ph blend, c) PMMA:DHA/VHF-F_2 blend and d) PMMA:SP/MC (spiropyran/merocyanine) blend films measured over 20 UV/T cycles. Blue lines: Measured after UV light exposure (5 J cm^{-2}). Red lines: Measured after thermal annealing (90 °C for 5 min). Absorption spectra were recorded after every step for the first 10 cycles, for the 15th cycle and for the 20th cycle. The black arrows indicate the changes of the characteristic absorption features with increasing cycle number.

The absorbance of the VHF isomer at λ_{max} was used as an indicator of switching fatigue. **Figure 4.9** demonstrates that DHA/VHF-OMe shows remarkable switching stability. After 20 UV/T cycles the VHF absorption has only decreased by 35 %. Furthermore, all three DHA/VHF derivatives show superior fatigue resistance compared to the well-established spiropyran switch, which degrades almost completely within the first 10 cycles. Possibly, the DHA/VHF switches are less prone to photo-oxidation, since they exhibit higher ionization potentials than SP/MC switches (see **Table 3.1** and **Table 5.5**). Such photo-oxidation can occur as a result of the repeated UV light exposure and is known to be a major degradation path in spiropyran systems [85, 87]. Other reports indicate that spiropyrans tend to aggregate due to the presence of ionic moieties in the merocyanine form [89, 90, 412]. Neither DHA nor VHF isomers contain ionic moieties, which presumably is another reason for the improved fatigue resistance.

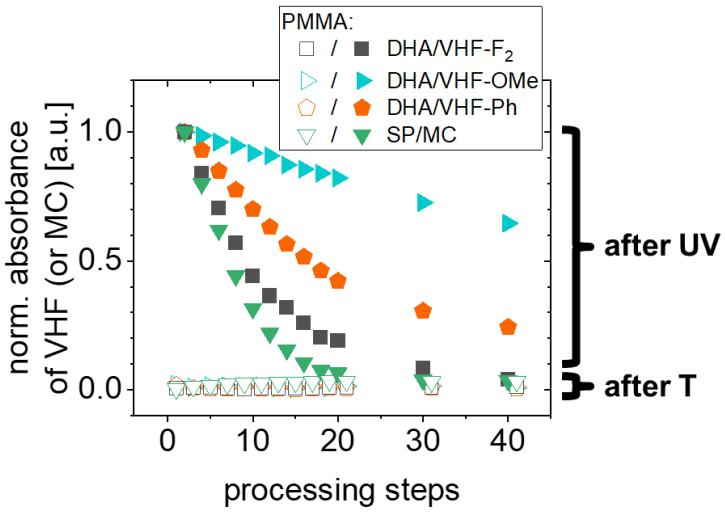

Figure 4.9: Comparing switching fatigue behavior of PMMA:DHA/VHF-OMe blend, PMMA:DHA/VHF-Ph blend, PMMA:DHA/VHF-F_2 blend and PMMA:SP/MC blend films using UV/Vis absorption spectroscopy. The graph displays the normalized absorption (measured at wavelength of maximum absorption) of VHF around 470-480 nm and MC around 570 nm respectively. Data was normalized to the absorbance measured after the first UV light illumination. Empty symbols indicate that the switch is in the DHA (or SP) form.

4.4. Photoswitchable Transistors

The first successful application of insulating polymer:photoswitch blends as gate dielectrics in OFETs was reported by Shen et al. [183]. The authors blended spiropyran molecules into PMMA and observed an increase in capacitance due to photoisomerization of the low dipole moment spiropyran to the high dipole moment merocyanine. Increased drain current in transistors was ascribed to the increase in dielectric permittivity. Lee et al. used blends of PMMA and azobenzene switches to construct UV sensors and also concluded that isomerization to the high dipole moment isomer of the photoswitch increases the capacitance of the blend dielectric, leading to a higher drain current in transistors [204]. Here, this concept of light-switchable gate dielectrics is extended for the first time to blends with DHA/VHF molecular switches. PMMA:DHA/VHF blends were applied as gate dielectrics in P3HT OFETs and device characteristics were recorded over the course of eight UV/T cycles. The resulting transfer and output characteristics for transistors with PMMA:DHA/VHF blend and unblended PMMA (as reference) dielectrics are summarized in **Figure 4.10 - Figure 4.12**. **Figure 4.10a** shows that the obtained transfer characteristics for

transistors with PMMA:DHA/VHF-OMe blend dielectric after UV and after thermal annealing can be clearly distinguished.

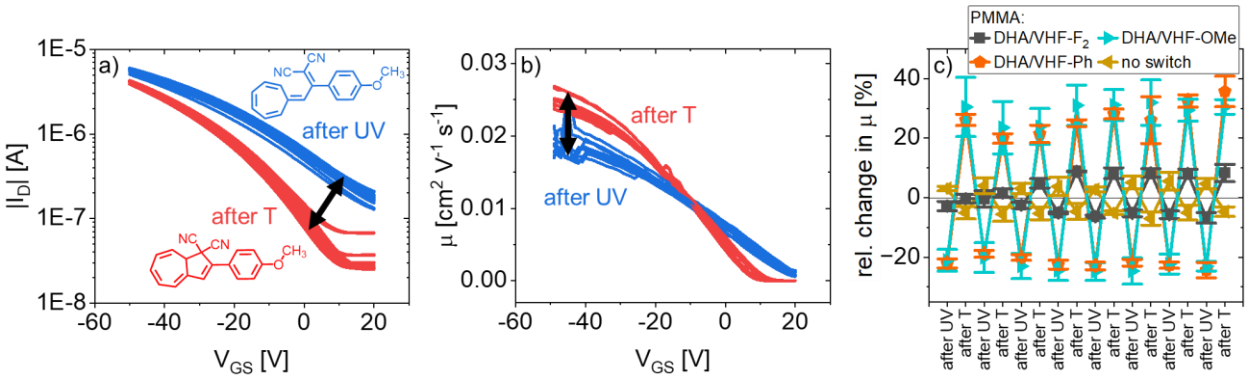

Figure 4.10: Stimuli-responsive organic transistors enabled by using PMMA blends with DHA/VHF photo-/thermochromic molecules as gate dielectrics. a) Reversible switching of transfer characteristics (V_{DS} = -50 V) in a transistor with PMMA:DHA/VHF-OMe blend dielectric measured over eight UV/T cycles. b) Gate-source bias-dependent field-effect mobilities. Blue lines: Measured after UV light exposure (5 J cm^{-2}). Red lines: Measured after thermal annealing (90 °C for 5 min). c) Reversible change in mobility (at V_{GS} = -50 V) for blends containing three different DHA/VHF derivatives (PMMA:DHA/VHF-OMe, PMMA:DHA/VHF-Ph, PMMA:DHA/VHF-F_2) and a reference device without any switch.

In contrast to previous reports employing PMMA:SP/MC blends [184, 413], these characteristics show only negligible hysteresis regardless of the state of the switch. UV light exposure leads to an increase in drain current caused by a shift of the threshold voltage (of around 15 V) towards more positive gate-source bias. Furthermore, the modulation of the transfer characteristics can be related to a change in field-effect mobility as indicated in **Figure 4.10b**. Similar behavior was observed for the blends with DHA/VHF-Ph and DHA/VHF-F_2 (see **Figure 4.11**).

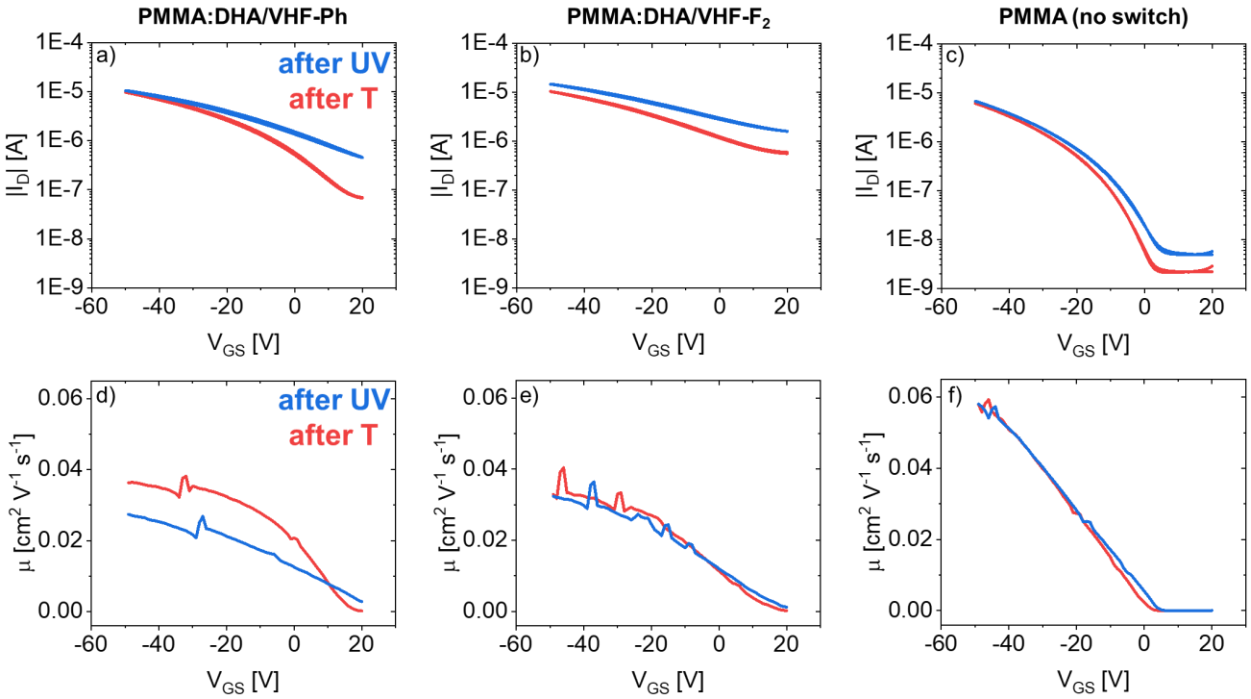

Figure 4.11: a) - c) Reversible switching of transfer characteristics (V_{DS} = -50 V) in transistors with PMMA:DHA/VHF-Ph blend, PMMA:DHA/VHF-F_2 blend and unblended PMMA dielectric. d) - f) Gate-source bias-dependent field-effect mobilities derived from the transfer characteristics (only forward sweep is shown). Blue lines: Measured after UV light exposure (5 J cm^{-2}). Red lines: Measured after thermal annealing (90 °C for 5 min).

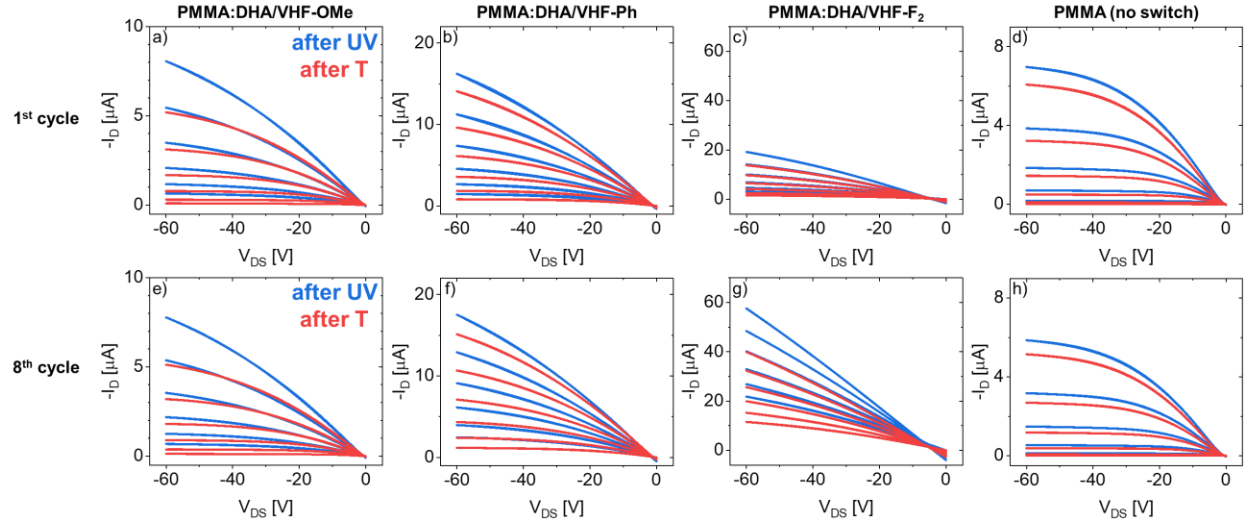

Figure 4.12: Output characteristics (V_{GS} = 0, -10, …, -50 V) of transistors with PMMA:DHA/VHF-OMe blend, PMMA:DHA/VHF-Ph blend, PMMA:DHA/VHF-F_2 blend and unblended PMMA dielectric measured during the a) - d) first and e) - h) eighth switching cycle. Blue lines: Measured after UV light exposure (5 J cm^{-2}). Red lines: Measured after thermal annealing (90 °C for 5 min).

A quantitative comparison of the stimuli-modulated field-effect mobility (determined at maximum negative gate-source bias) for blends with three different derivatives of the switch is given in **Figure 4.10c**. The area-normalized capacitances of the gate dielectrics that were used to calculate the mobilities, are summarized in **Table 4.1**.

Table 4.1: Area-normalized capacitances of PMMA:DHA/VHF blend and unblended PMMA dielectrics used in OFETs. The dielectric permittivities were obtained by fitting impedance data using an RC element as equivalent circuit. Note that area-normalized capacitances in OFETs and capacitors are not the same due to different film thicknesses.

	C_i [nF cm^{-2}]			
processing step	**PMMA: DHA/VHF-OMe**	**PMMA: DHA/VHF-Ph**	**PMMA: DHA/VHF-F_2**	**PMMA (no switch)**
1 (fresh device)	4.19	4.31	4.19	4.50
2 (UV)	4.57	4.87	4.48	4.51
3 (T)	4.13	4.29	4.28	4.61
4 (UV)	4.45	4.78	4.45	4.61
5 (T)	4.14	4.33	4.31	4.63
6 (UV)	4.46	4.81	4.50	4.64
7 (T)	4.16	4.31	4.34	4.66
8 (UV)	4.42	4.74	4.51	4.62
9 (T)	4.17	4.33	4.34	4.68
10 (UV)	4.46	4.78	4.55	4.70
11 (T)	4.21	4.37	4.41	4.73
12 (UV)	4.49	4.79	4.57	4.72
13 (T)	4.21	4.37	4.44	4.81
14 (UV)	4.50	4.82	4.57	4.79
15 (T)	4.21	4.36	4.43	4.79
16 (UV)	4.51	4.82	4.54	4.72
17 (T)	4.21	4.37	4.44	4.75

The reversible shifts of threshold voltage for all three blends are shown in **Figure 4.13**.

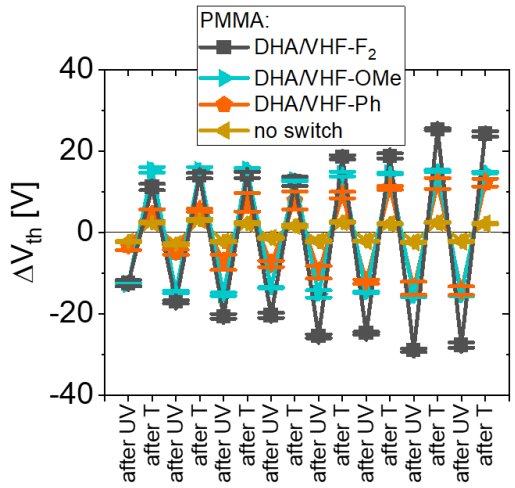

Figure 4.13: Reversible threshold voltage shifts of transistors with PMMA:DHA/VHF-F_2 blend, PMMA:DHA/VHF-OMe blend, PMMA:DHA/VHF-Ph blend and unblended PMMA dielectrics. The V_{GS} fitting range for determining the threshold voltages was chosen from -20 V to -50 V and only the forward sweep of the transfer characteristics was considered. A negative/positive ΔV_{th} indicates a decrease/increase in V_{th} (i.e. shift to more positive/negative gate-source bias).

In Chapter 3 it was possible to show that stimuli-responsive organic transistors can be fabricated by blending DHA/VHF molecular switches into the active channel (semiconductor) of the device. A reversible tuning of transfer characteristics was observed upon alternating UV light irradiation and thermal annealing. Increased on-current and a shift of threshold voltage towards more positive gate-source bias as a consequence of UV light irradiation suggested that the VHF isomer can act as a dopant, which is activated by light. Here, similar observations are reported, when incorporating DHA/VHF photoswitches into the gate dielectric, rather than the active layer. Due to the spatial separation of the switch and the semiconductor, it seems unlikely that a doping-like mechanism can occur. Hence, other effects such as a change in gate dielectric capacitance (which was observed experimentally, see above) or energetic disorder should be considered. As discussed previously, the isomerization from DHA to VHF increases the dielectric permittivity of PMMA:DHA/VHF blends and therefore yields an increase of the capacitance of the gate dielectric of the transistor. This should be expected to lead to higher drain currents, but should either not affect the threshold voltage or rather lead to a more negative threshold voltage [414]. Veres et al. reported that energetic disorder at the semiconductor-dielectric interface induced by large molecular dipoles within the dielectric leads to lower mobility and shifts the threshold voltage to more negative gate-source bias [220]. Here, a transition from the low dipole moment DHA to the high dipole moment VHF leads to a decrease in mobility and a threshold voltage shift to more

positive gate-source bias. Therefore, the changing capacitance and the energetic disorder both fail to fully explain the results and a more complicated mechanism or two simultaneous effects seem to be at place. Potential explanations include 1) interfacial mixing between the PMMA:photoswitch blend and the semiconductor and/or 2) phase separation between PMMA and the photoswitch which brings the latter in direct contact with the semiconductor. Both scenarios could potentially cause doping effects through the strong electron accepting properties of VHF [385], similar to when the switch is blended directly into the semiconductor. Alternatively, the formation of photoswitch aggregates with at least partially aligned dipole moments and the resulting built-in electric field could also cause threshold voltage shifts towards more positive gate-source bias, as observed for OFETs employing well-ordered SAM-based interfacial dipoles [233-235, 398]. In order to clarify the exact mechanism at place, further experimental studies carefully examining the microstructure of the interface will be necessary.

Furthermore, it was found that the threshold voltage shift to more positive gate-source bias can be further enhanced by applying negative bias stress over an extended period of time. **Figure 4.14** shows the changes in transfer characteristics induced by bias stress for transistors with blend dielectrics containing three different DHA/VHF derivatives. A comparison with a reference device in **Figure 4.15a and c** demonstrates that the significant increases in drain current are related to the presence of the switch molecules.

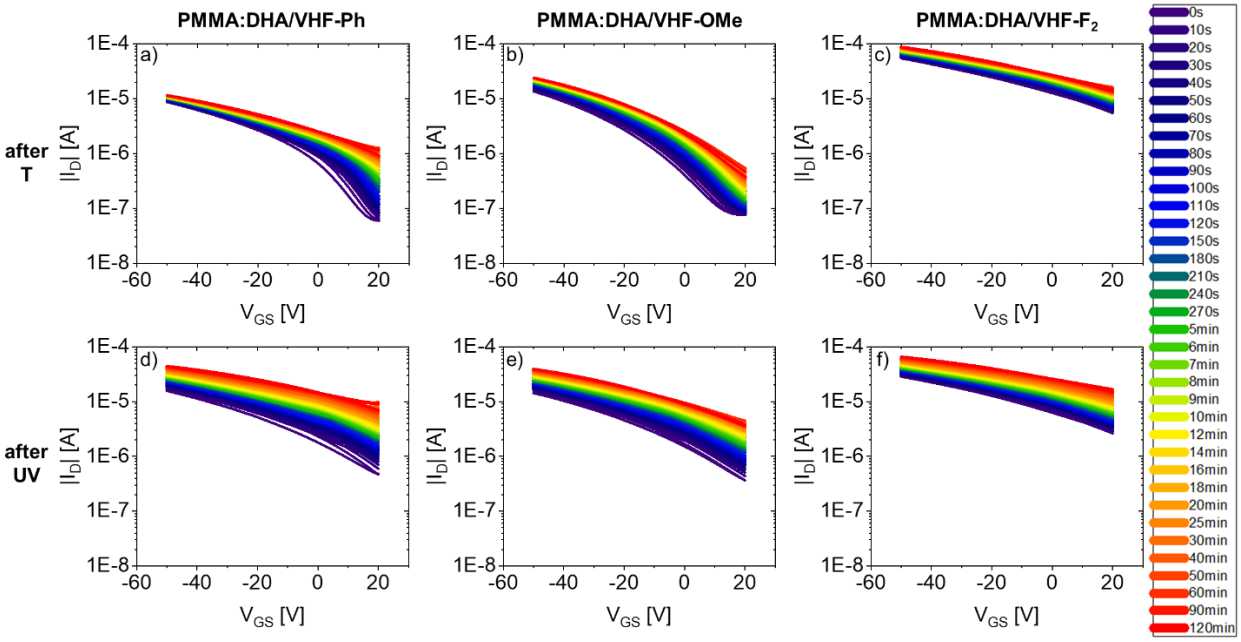

Figure 4.14: Effect of negative bias stress on transfer characteristics (V_{DS} = -50 V) of transistors with PMMA:DHA/VHF-Ph blend, PMMA:DHA/VHF-OMe blend and PMMA:DHA/VHF-F_2 blend dielectrics. Bias stress was applied for 2 h (V_{GS} = V_{DS} = -50 V) and measurements were carried out a) - c) after thermal annealing (90 °C for 5 min) and d) - f) after UV light illumination (5 J cm^{-2}). Each measurement was carried out on a transistor that had not yet been exposed to bias stress.

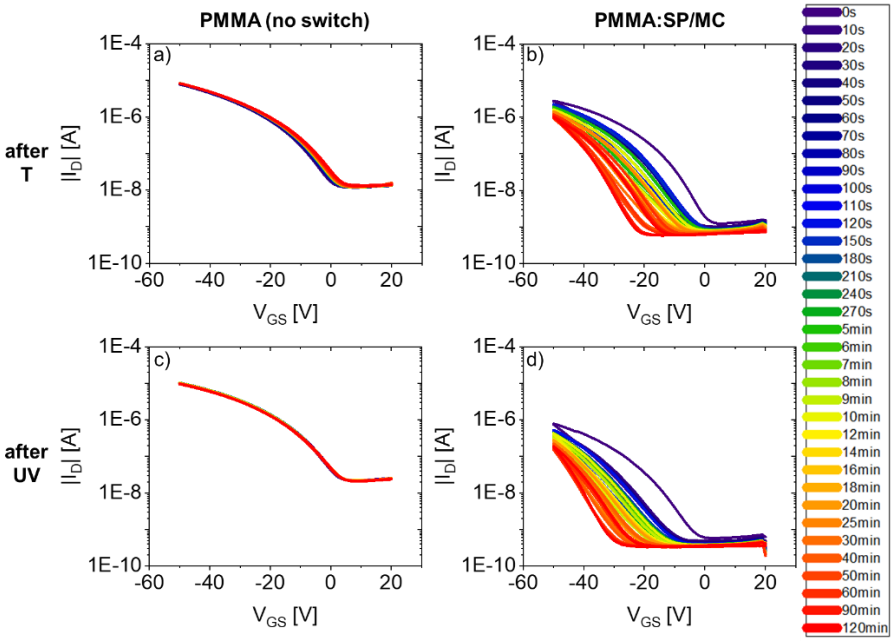

Figure 4.15: Effect of negative bias stress on transfer characteristics (V_{DS} = -50 V) of transistors with unblended PMMA and PMMA:SP/MC blend dielectrics. Bias stress was applied for 2 h (V_{GS} = V_{DS} = -50 V) and measurements were carried out a) - b) after thermal annealing (90 °C for 5 min) and c) - d) after UV light illumination (5 J cm^{-2}). Each measurement was carried out on a transistor that had not yet been exposed to bias stress.

Figure 4.16 summarizes the development of the drain current under bias stress for all transistors with DHA and VHF molecules present in the gate dielectric. The results show that the increase in drain current as a consequence of bias stress is stronger when the switch is in the VHF form, rather than in the DHA form. Such behavior could be explained by the alignment of the dipoles of the switch molecules driven by the continuously applied external field. VHFs possess larger dipole moments than their respective DHAs leading to larger built-in electric fields and therefore (as discussed previously) to shifts in threshold voltage to more positive gate-source bias, ultimately resulting in higher on-currents. Such behavior cannot be observed when PMMA gate dielectrics are blended with the well-established spiropyran switch. Spiropyran has a dipole moment of about 4-6 D and can be converted into the merocyanine form with a dipole moment of 14-18 D [77] by irradiation with UV light. In bias stress experiments both isomers of the switch cause a decrease in drain current, which is more pronounced for the merocyanine form and therefore most likely to be related to the presence of charge-trapping ionic moieties in this system (see also **Figure 4.15b and d** for the corresponding transfer characteristics).

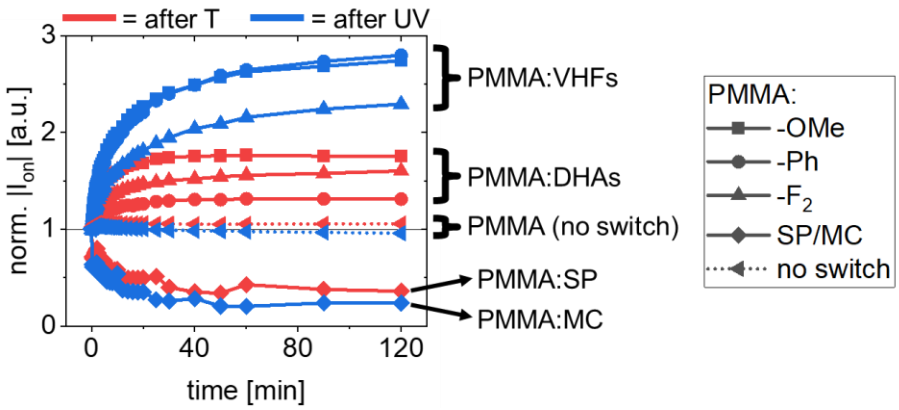

Figure 4.16: Effect of negative bias stress on transistor on-current ($|I_D|$ at V_{GS} = -50 V) measured on OFETs with PMMA:DHA/VHF (three different derivatives) blends, PMMA:SP/MC blend or unblended PMMA dielectrics. The results were normalized by the on-current of the unstressed transistor at t = 0 min. Bias stress was applied for 2 h (V_{GS} = V_{DS} = -50 V) and measurements were carried out after thermal annealing (90 °C for 5 min, red lines) and after UV light illumination (5 J cm^{-2}, blue lines). Each measurement was carried out on a transistor that had not yet been exposed to bias stress.

4.5. Conclusions

In the first part of this study, capacitors were fabricated by blending the insulating polymer PMMA with DHA/VHF photo-/thermochromic molecules. The reversible isomerization of the molecular switches could be observed in capacitors and was studied in detail by using impedance spectroscopy. In order to quantify the reversible switching of the system, the resulting impedance data was analyzed by following two different approaches: 1) Calculating the frequency-dependent complex dielectric permittivity from the real and the imaginary part of the complex impedance; 2) determination of the dielectric permittivity through equivalent circuit fitting of the complex impedance data. To the best of my knowledge, this is the first time that an equivalent circuit fitting methodology was applied to investigate the photoisomerization of molecular switches. This study shows that such a methodology is a straightforward tool to capture and accurately quantify the reversible switching of photochromic molecules in stimuli-responsive organic electronic devices.

Furthermore, the PMMA:DHA/VHF blends were successfully applied to construct light- and temperature-responsive organic transistors. It was shown that the transistor characteristics can be tuned reversibly via the isomerization of DHA/VHF molecular switches within the gate dielectric.

The charge carrier mobility in particular could be modulated by around 20-30 % by applying subsequent UV light and thermal annealing treatments. Finally, the superior resistance to switching fatigue compared to the well-established spiropyran switch was demonstrated. In agreement with Chapter 3, this study allows to conclude that DHA/VHF molecular switches and the reported reversibly switchable transistors open up new opportunities for next-generation stimuli-responsive organic electronic devices and memory applications.

Chapter 5: Reversible Switching of Capacitors and OFETs Employing PMMA:SP/MC Blends

5.1. Introduction

Key advantages of organic electronic materials are their chemical versatility, their compatibility with industrial mass-printing processes that enable low-cost fabrication of large area, as well as their mechanical properties which facilitate the development of flexible [392, 415], stretchable [416-419] and self-healable [420-422] optoelectronic devices. Transistors are essential building blocks of electronic circuits and due to intense research efforts, the mobility and stability of organic field-effect transistors has improved significantly [423, 424]. A key device parameter for sensing and memory applications is the threshold voltage, which is the gate-source bias at which a conducting channel starts to form between the source and drain electrodes [26]. Its value in organic transistors depends on several factors such as defects, impurities or interfacial roughness [16] and determines whether the transistor operates in enhancement-mode (device is in the off-state at zero gate-source bias) or depletion-mode (device is in the on-state at zero gate-source bias). The deliberate control over the threshold voltage allows for designing fast circuits with low power consumption [425]. A multitude of approaches has been reported to tune the threshold voltage of organic transistors. Strategies, which are particularly popular for the construction of transistor memory devices are the electrical poling of ferroelectric dielectrics such as polyurea [426] or P(VDF/TrFE) [427] and the use of floating gate electrodes [428] or electrets [429]. The implantation of stable charges into polymer electrets is not only possible via corona discharge [430], but also via irradiation with electron beams [431] or contact charging [432]. It is also possible to modify the architecture of the transistor, e.g. by employing a double gate structure [433], by introducing an additional buffer layer which shifts the work function of the gate electrode [434] or by using an ion-dispersed gate dielectric in which charges can be separated via electrophoresis [435]. Another method first reported by Kobayashi et al. [234] and Pernstich et al. [233] is to apply self-assembled monolayers of organosilanes or phosphonic acids [398, 414] with various functionalizations on inorganic dielectrics. This approach has been applied successfully to control the threshold voltage in unipolar [436] and complementary [235, 399] circuits. Some of the methods mentioned above have significant disadvantages such as more complicated processing (when additional layers need to be deposited) or that the threshold voltage can only be tuned during

the fabrication of the transistor (in case of SAM deposition or charge implantation via corona discharge) and cannot be changed afterwards. To overcome this issue, light can be used as an external stimulus for tuning the characteristics of already fabricated transistors. Conventional phototransistors can also show shifts in threshold voltages. However, these shifts only occur under light exposure and do not usually prevail when the irradiated device is measured again in the dark. One possibility to permanently "program" a specific threshold voltage in an organic transistor is exposure to UV light [437, 438], where excitons, formed under UV light exposure, dissociate and electrons are trapped at the semiconductor-dielectric interface, causing a significant shift of the threshold voltage towards more positive gate-source bias. However, this shift is not necessarily permanent. How quickly it reverts back to its original state depends strongly on the properties of the semiconductor-dielectric interface [439]. Marchl et al. reported another method of on-demand threshold voltage tuning on already fabricated devices. The authors used thin interlayers of photoreactive polymers to program threshold voltages in pentacene transistors and therefore turn enhancement-mode transistors into depletion-mode transistors, allowing for the construction of unipolar depletion-load-inverters [440]. A similar, but reversible methodology of harnessing the light-responsiveness of organic materials to deliberately alter OFET characteristics is the employment of photoswitches. Besides diarylethenes and azobenzenes, spiropyrans are a class of photoswitches that are already well studied in the context of light-responsive OFETs. In 2005 Guo et al. were the first to show modulation of conductance in a field-effect device through the UV light-induced isomerization of spiropyran [441]. Subsequent works demonstrated that light-responsive OFETs employing spiropyran can be realized via PDMS stamping [137], application as SAM [187], blending into a polymer gate dielectric, such as PMMA [183], blending into the active channel [214] or covalently attaching the spiropyran moiety either to the polymer chain of the dielectric [186] or the small molecule semiconductor [206]. Other studies adopting the blending approach with PMMA to create light-responsive dielectrics focused on small molecule OFETs with bottom-gate configuration [184, 185, 202].

These publications present complicated device fabrication processes or expensive synthesis schemes and exclusively focus on bottom-gate small molecule transistors. To the best of my knowledge, solution-processable polymer transistors have not yet been endowed with light-responsive properties by utilizing blends of spiropyran and insulating polymers. Therefore, this chapter examines in detail the photoresponsivity of top-gate polymer transistors functionalized

with PMMA:spiropyran dielectrics with a particular focus on the modulation of the threshold voltage induced by the isomerization of spiropyran photoswitches. Transistor characteristics can be controlled via irradiation with light, by modifying the composition of the light-responsive dielectric layer and via chemical design of the photoswitch. The latter point is addressed by examining the effect of short and long alkyl chains that are attached to the spiropyran molecule.

5.2. Threshold Voltage Shift in Polymer Transistors with PMMA:SP/MC-1 Gate Dielectrics

For this work, the commercially available spiropyran derivative 1′,3′-dihydro-1′,3′,3′-trimethyl-6-nitrospiro[2*H*-1-benzopyran-2,2′-(2*H*)-indole] (SP/MC-1) was used as a reference photoswitch (see **Figure 1.7** for chemical structure). Furthermore, three additional spiropyran/merocyanine switches (derived from SP/MC-1) with varying alkyl chain length (four, ten and sixteen carbon atoms) attached to the indoline moiety were used. In the following, these derivatives will be denoted as SP/MC-4, SP/MC-10 and SP/MC-16. As shown in **Figure 5.1a**, the characteristic color change from colorless to dark blue/purple upon UV light irradiation is also visible when SP/MC-1 is blended into PMMA films, indicating the isomerization from SP-1 to MC-1. By applying light with a wavelength of 560-580 nm, this reaction can be reversed. As an alternative, the backreaction from MC-1 to SP-1 can also be induced thermally, e.g. by annealing the film on a hot plate, allowing for a complete back-switching and color change of the whole film in only a few minutes.

Upon application of the PMMA:photoswitch blends as top-gate dielectrics in bottom-contact top-gate P3HT thin-film transistors (see **Figure 5.1c** for schematic depiction of the device) drastic changes in transistor characteristics can be induced simply by triggering the isomerization reactions between the SP and MC forms. **Figure 5.1a** shows the transfer characteristics recorded after UV light irradiation (switch is in the MC form) and after thermal annealing (switch is in the SP form).

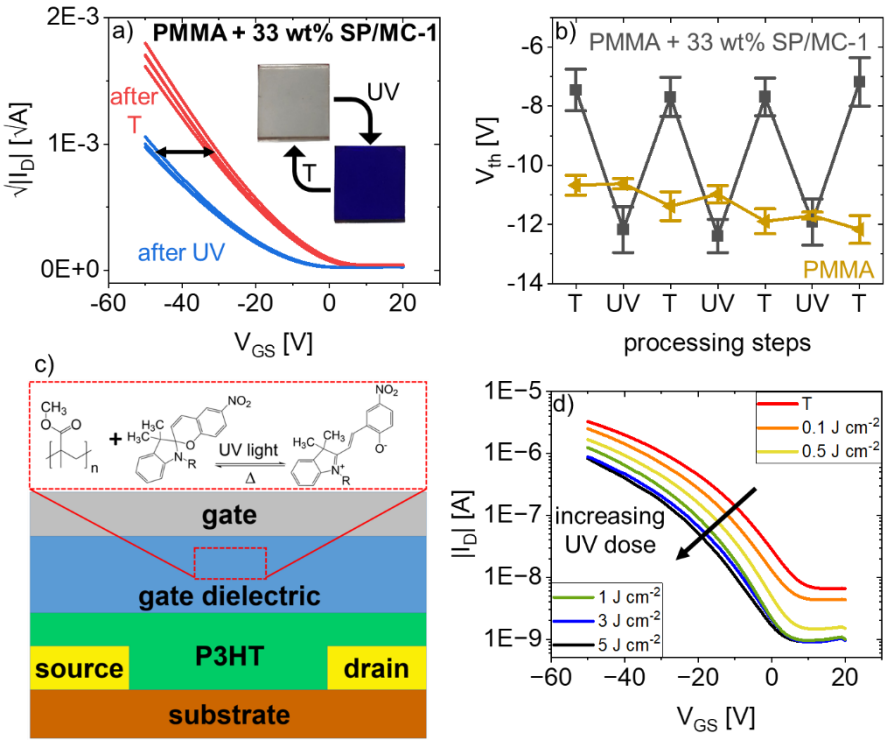

Figure 5.1: Stimuli-responsiveness of P3HT transistors employing PMMA top-gate dielectrics blended with 33 wt% SP/MC-1 photoswitch enabling on-demand control over the threshold voltage. a) Reversible switching of transfer characteristics (V_{DS} = -50 V) after repeated UV light illumination (5 J cm^{-2}) and thermal annealing (90 °C for 5 min). Inset: Characteristic color changes of a PMMA:SP/MC-1 blend film caused by the reversible isomerization of the photoswitch. b) Reversible switching of threshold voltage and comparison to reference devices. c) Schematic illustration of the OFETs with a light-responsive PMMA:spiropyran blend dielectric and the chemical structures of PMMA and of both photoisomers SP and MC, where R stands for the alkyl group, i.e. for SP/MC-1 R = CH_3. d) Dose-dependent switching of transfer characteristics (V_{DS} = -50 V).

The characteristics feature a pronounced shift in threshold voltage towards more negative gate-source bias after UV light irradiation, leading to a decrease in on-current ($|I_D|$ at V_{GS} = -50 V) from about 3 µA to 1 µA. Note that only the forward sweep of the gate-source bias is shown here. The hysteresis that can be observed during these measurements will be discussed later. The shift in threshold voltage is reversible over multiple UV/T cycles and can be ascribed to the isomerization of the photoswitch, since reference devices (with unblended PMMA as gate dielectric) are not featuring this behavior (see **Figure 5.1b**). **Figure 5.1d** shows that the magnitude of the threshold voltage shift can be controlled by the applied dose of the UV light. Hence, a specific threshold voltage can be programmed post-fabrication by tuning the UV dose. The sensitivity of the device can be separated into a low- and a high-dose regime. For low UV doses (≤ 1 J cm^{-2}) the shift is

more pronounced (i.e. the device is more sensitive) compared to higher doses (1-5 J cm^{-2}). The lower sensitivity at high doses is in line with the literature reporting a saturation in MC absorption with increasing exposure time [442, 443] or increasing number of irradiation pulses [444] due to the fact that the majority of the photoswitches has already isomerized to the MC form. **Figure 5.2** shows that the relation between threshold voltage shift and UV dose is approximately linear within these two regimes.

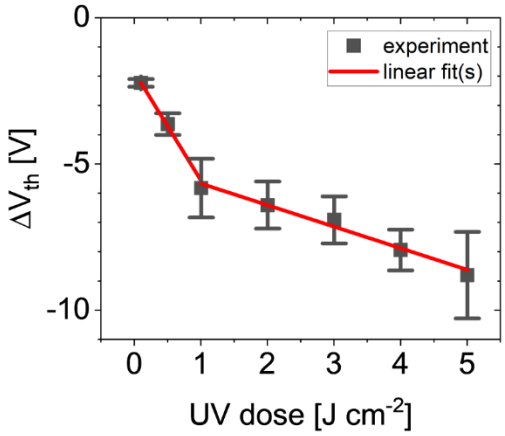

Figure 5.2: UV dose dependence of the threshold voltage shift in P3HT organic transistors employing PMMA top-gate dielectrics blended with 33 wt% SP/MC-1. The experimental data was fitted using two separate linear fits (one for doses ≤ 1 J cm^{-2} and one for doses > 1 J cm^{-2}).

At first, the effect of the amount of switches within the insulating polymer matrix was studied for the reference system PMMA:SP/MC-1. The devices were cycled several times and transistor characteristics were recorded after each stimulus. **Figure 5.3** shows the transfer characteristics (V_{DS} = -50 V) of devices with 33, 20, 10 and 0 wt% SP/MC-1 and the resulting gate-source bias-dependent hole mobilities.

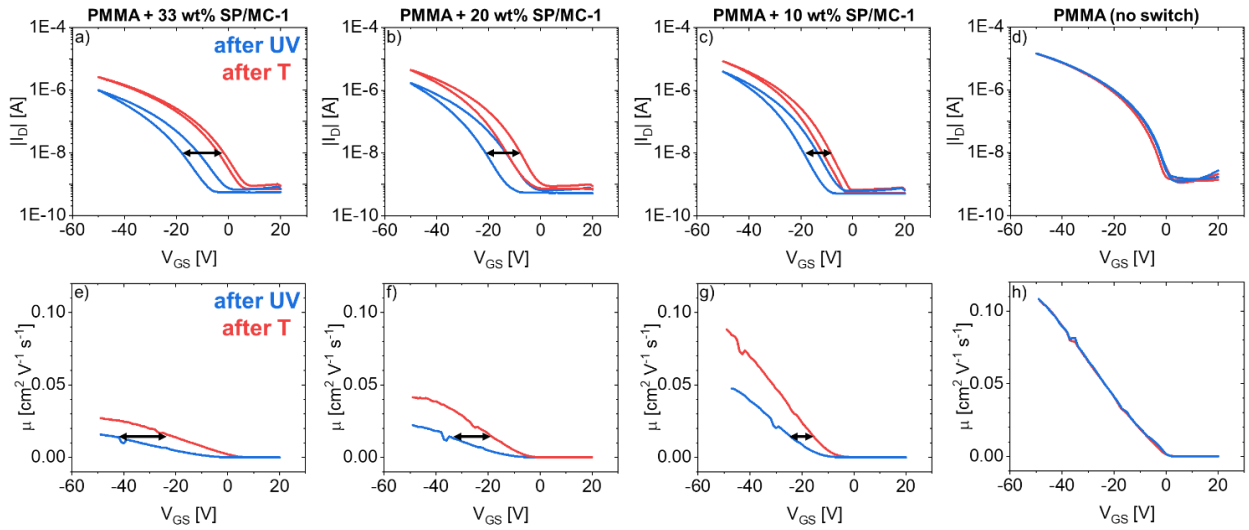

Figure 5.3: Effect of the weight content of SP/MC-1 on the switching of transistor characteristics. Reversible switching of a) - d) transfer characteristics (V_{DS} = -50 V) and e) - h) gate-source bias-dependent field-effect mobilities. Blue lines: Measured after UV light exposure (5 J cm^{-2}). Red lines: Measured after thermal annealing (90 °C for 5 min). Mobilities were only determined for the forward sweep of the gate-source bias.

Increasing the amount of SP/MC-1 within the gate dielectric leads to an increase in hysteresis of the drain current, which is especially pronounced after the UV light exposure, when the switch is in the MC form. **Figure 5.3d** shows that the repeated cycling only has a marginal effect on the reference device. When unblended PMMA is used as a dielectric, only a weak photodoping effect can be observed (similar as in the previous chapters, see **Figure 3.3e** and **Figure 4.11c**), but no significant shift in threshold voltage and no hysteresis. Similar observations were reported by Ishiguro et al. [173], who constructed a dual-gate OFET that employed a blend of P3HT and SP/MC-1 as active material. Due to vertical phase separation, photoswitches accumulated predominantly in the bottom channel, leading to a strong hysteresis and threshold voltage shifts in response to applied UV stimuli, while the photoswitch-depleted top channel showed no such effects.

The optical modulation of the threshold voltage becomes more pronounced as the weight fraction of the switch within the PMMA blend increases. Therefore, it can be concluded that the magnitude of the switching of transistor parameters, including the threshold voltage cannot only be controlled by the applied UV dose, but also by the amount of photoswitch that is incorporated into the device. Additionally, a higher content of photoswitch leads to a stronger decrease in mobility. While the reference device shows a gate-source bias-dependent mobility of around 0.1 cm^2 V^{-1} s^{-1} (at

V_{GS} = -50 V), mobilities are decreased to around 0.03 $cm^2 V^{-1} s^{-1}$ (after thermal annealing) and 0.015 $cm^2 V^{-1} s^{-1}$ (after UV light exposure) in the devices with 33 wt% SP/MC-1. These results are in line with the findings originally reported by Veres et al. that large dipole moments which are randomly oriented in the gate dielectric of polymer field-effect transistors lead to increased hysteresis and a decrease in charge carrier mobility due to energetic disorder and enhanced carrier localization [220].

In order to quantify the switching of the transistor characteristics, threshold voltages, on-currents and hole mobilities were extracted from the transfer curves in **Figure 5.3**. **Table 5.1** summarizes the absolute values of the threshold voltages and mobilities after UV light exposure and thermal annealing for transistors with PMMA:SP/MC-1 blend dielectrics.

Table 5.1: Absolute values of threshold voltages and hole mobilities (at V_{GS} = -50 V) determined for transistors with PMMA + x wt% SP/MC-1 blend top-gate dielectrics (with x = 33, 20, 10 and 0) after UV light exposure (5 J cm^{-2}) and thermal annealing (90 °C for 5 min) and the resulting average shifts between both states.

SP/MC-1 content	V_{th} [V]		av. $\lvert\Delta V_{th}\rvert$ [V]	μ [$cm^2 V^{-1} s^{-1}$]		av. $\lvert\Delta\mu\rvert$ [$cm^2 V^{-1} s^{-1}$]
	after UV	after T		after UV	after T	
33 wt%	-12.2±0.2	-7.5±0.2	4.7	0.01	0.02	0.011
20 wt%	-16.1±0.4	-13.4±0.8	2.7	0.02	0.03	0.013
10 wt%	-17.1±0.7	-15.6±0.2	1.5	0.04	0.06	0.022
0 wt%	-11.1±0.4	-11.5±0.6	0.4	0.11	0.12	0.007

In addition, **Figure 5.4** depicts the relative change in threshold voltage, on-current and mobility for transistors with PMMA:SP/MC-1 blend dielectrics and their dependence on the content of the photoswitch. These data confirm that 10 wt% of photoswitch is enough to induce the desired stimuli-responsiveness of the device. Increasing the amount of switch only enhances this effect. Again, it should be noted that the reference devices without any photoswitch also show a response to the applied stimuli. However, this effect is not only less significant, but also opposite in direction to the blend devices and can be affiliated to photodoping of the P3HT [373].

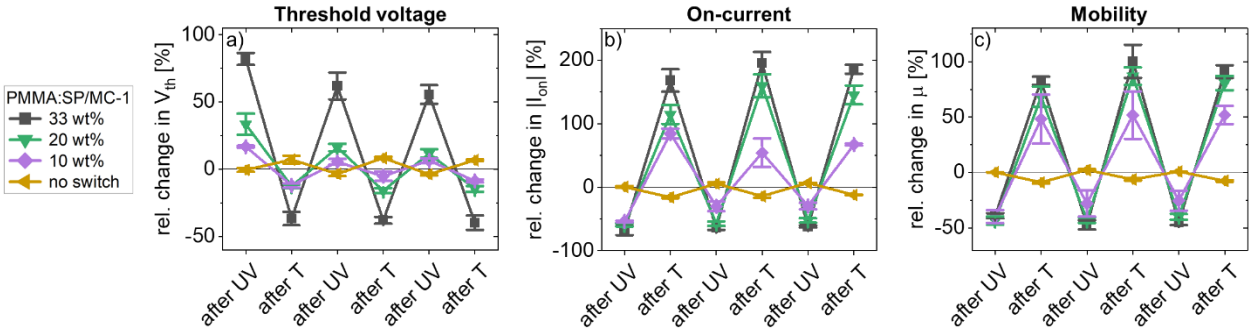

Figure 5.4: Effect of the weight content of SP/MC-1 on the reversible switching of transistor parameters. Relative changes of a) threshold voltage, b) on-current ($|I_D|$ at V_{GS} = -50 V) and c) mobilities (at V_{GS} = -50 V) induced by repeated UV light illumination (5 J cm^{-2}) and thermal annealing (90 °C for 5 min).

In these transistors, the threshold voltage shifts towards more negative gate-source bias (regardless of the intensity of the UV light and the switch content), resulting in a decrease of transistor drain current. At first sight, this finding might be surprising, since Shen et al. reported an opposite trend (increasing drain current upon UV light irradiation) in a similar experiment (PMMA:SP/MC-1 blends in pentacene bi-layer bottom-gate OFETs) [183]. The authors explained their results with the increase in capacitance of the gate dielectric which is caused by the isomerization of the low dipole moment SP-1 to the high dipole moment MC-1. Due to the higher capacitance more charges can be accumulated at the semiconductor-dielectric interface resulting in an increased carrier density and a higher transistor drain current. In order to identify possible causes for these seemingly contradictory results, a detailed analysis of the dielectric properties of the PMMA:SP/MC-n (including derivatives with alkyl chain lengths of four, ten and sixteen carbon atoms) blends was carried out using impedance spectroscopy on capacitors, UV/Vis absorption spectroscopy on thin-films and electrical characterization of polymer transistors. A further discussion is given in Section 5.4.

5.3. PMMA:SP/MC-n Blend Dielectrics

Photoswitchable Capacitors

The PMMA:SP/MC-n blend dielectrics were sandwiched between a thick bottom and a thin, semi-transparent top electrode (100 and 20 nm silver) and the frequency-dependent impedance was

measured at room temperature in a frequency-range between 1 Hz and 10^6 Hz. Measurements were conducted either after UV light irradiation (5 J cm^{-2}) or after thermal annealing (5 min 90 °C) to examine how a change between the SP and MC form of the switch are affecting the dielectric properties of the blend system. Dielectric characteristics were recorded over the course of eight cycles, where one cycle comprises a UV light irradiation and a thermal annealing step. **Figure 5.5 - Figure 5.8** summarize the Nyquist, Bode and phase angle plots that were obtained for blends with the four different derivatives SP/MC-1, -4, -10 and -16 with weight fractions of 33, 20, 10 and 0 wt%.

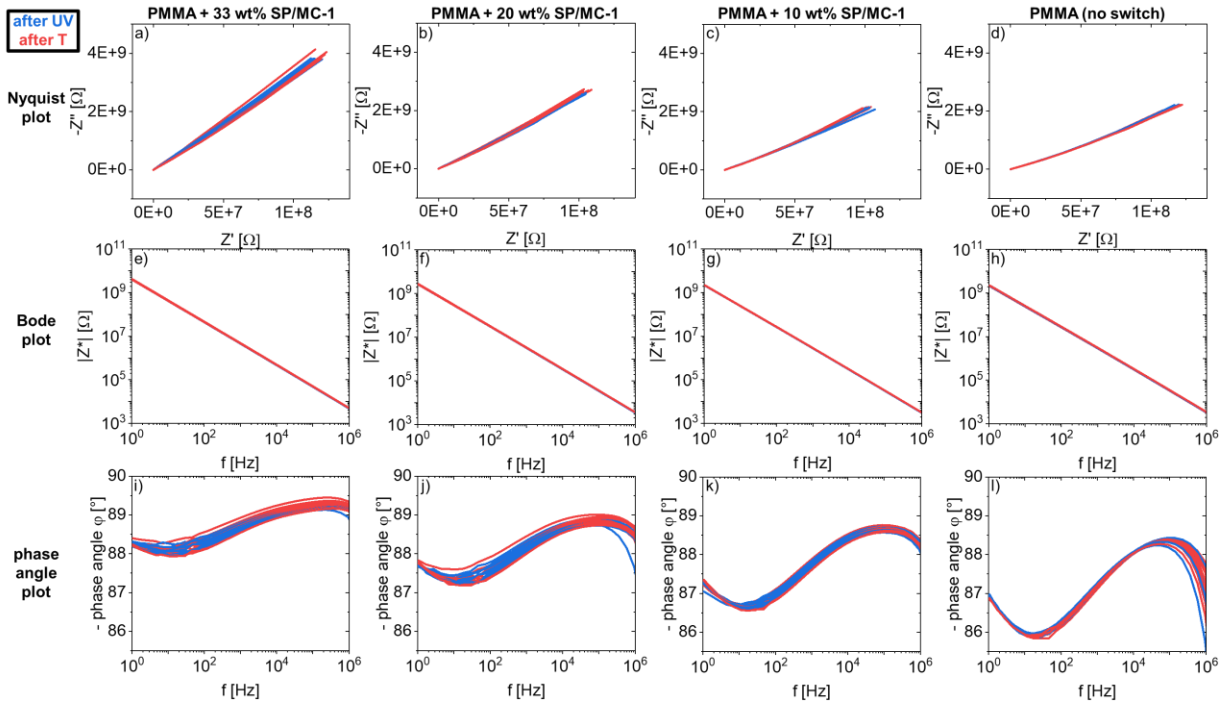

Figure 5.5: a) - d) Nyquist, e) - h) Bode and i) - l) phase angle plots of impedance data collected for eight UV/T cycles for PMMA + x wt% **SP/MC-1 blend capacitors** (with x = 33, 20, 10 and 0). Blue lines: Measured after UV light exposure (5 J cm^{-2}). Red lines: Measured after thermal annealing (90 °C for 5 min).

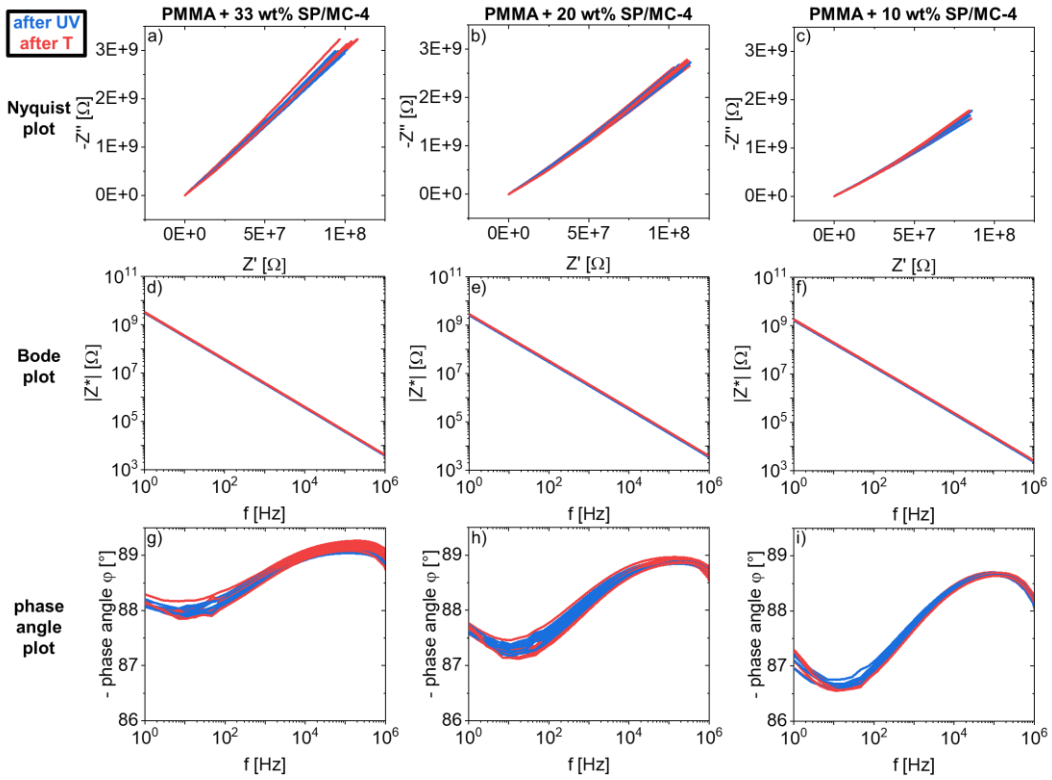

Figure 5.6: a) - c) Nyquist, d) - f) Bode and g) - i) phase angle plots of impedance data collected for eight UV/T cycles for PMMA + x wt% **SP/MC-4 blend capacitors** (with x = 33, 20 and 10). Blue lines: Measured after UV light exposure (5 J cm^{-2}). Red lines: Measured after thermal annealing (90 °C for 5 min).

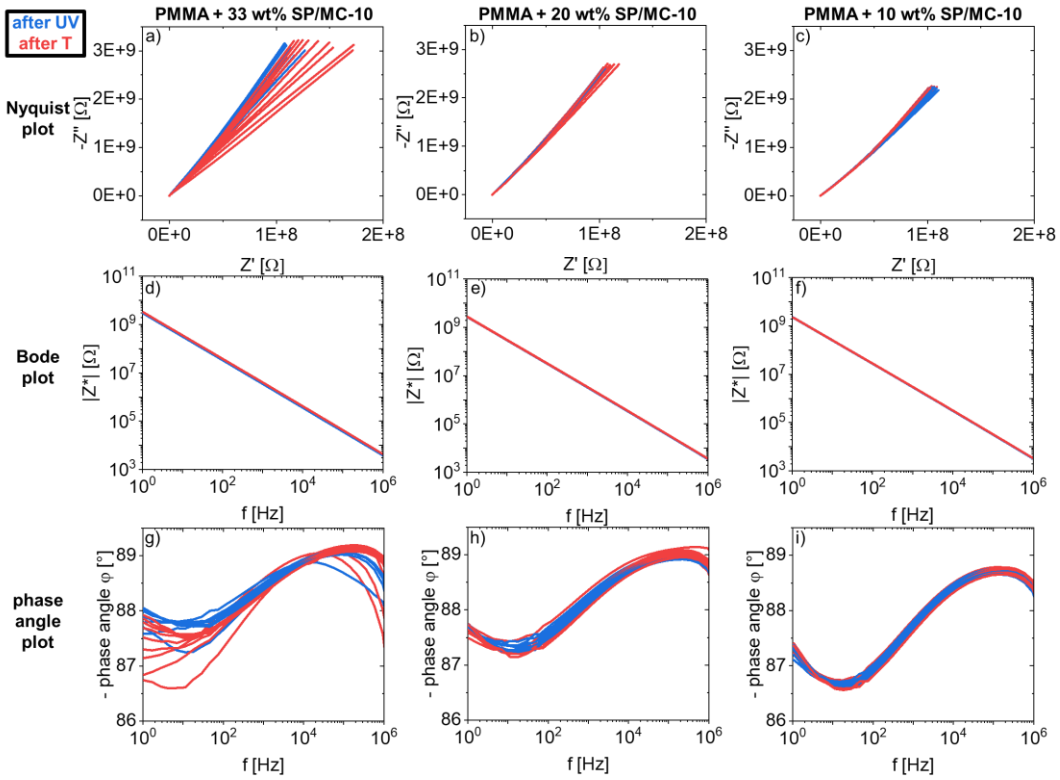

Figure 5.7: a) - c) Nyquist, d) - f) Bode and g) - i) phase angle plots of impedance data collected for eight UV/T cycles for PMMA + x wt% **SP/MC-10 blend capacitors** (with x = 33, 20 and 10). Blue lines: Measured after UV light exposure (5 J cm^{-2}). Red lines: Measured after thermal annealing (90 °C for 5 min).

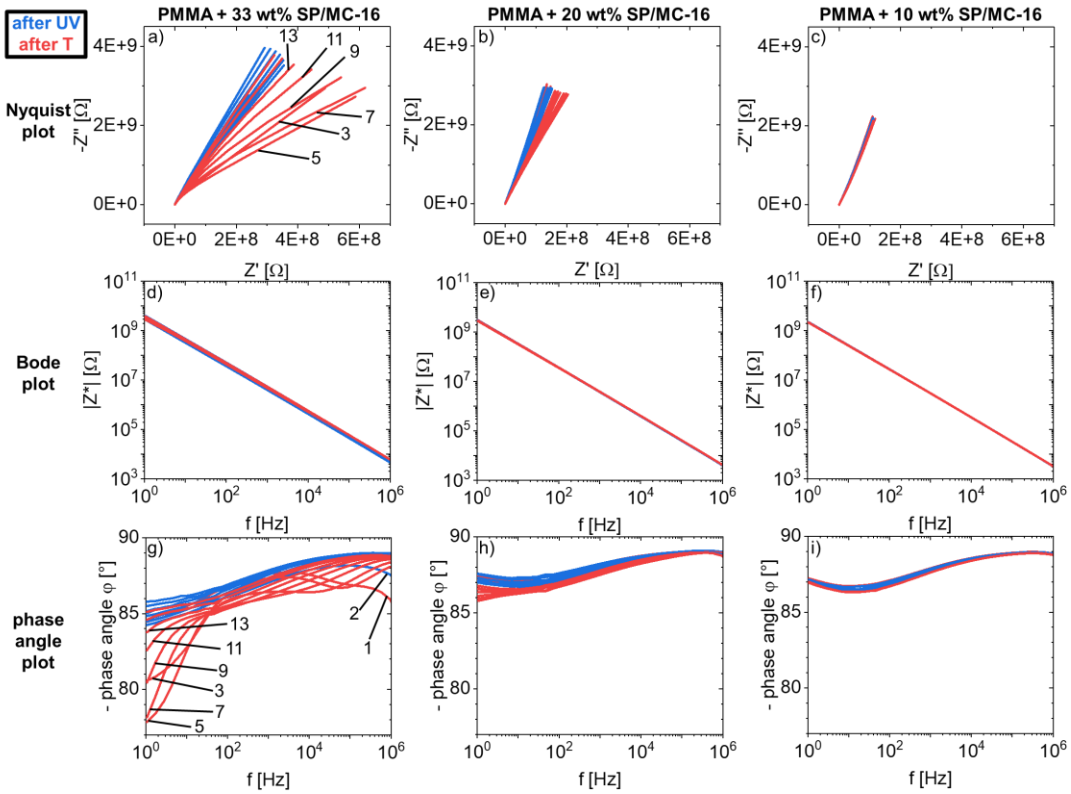

Figure 5.8: a) - c) Nyquist, d) - f) Bode and g) - i) phase angle plots of impedance data collected for eight UV/T cycles for PMMA + x wt% **SP/MC-16 blend capacitors** (with x = 33, 20 and 10). Blue lines: Measured after UV light exposure (5 J cm^{-2}). Red lines: Measured after thermal annealing (90 °C for 5 min). The numbers in panel a) and g) indicate the number of the respective measurement.

Based on the impedance data, the modulus $|\varepsilon_r^*|$ of the dielectric permittivity (as well as its real part ε_r' and its imaginary part ε_r'') and the loss tangent *tan(δ)* were calculated. **Figure 5.9** shows the relative change in $|\varepsilon_r^*|$ that is induced by the UV light and temperature stimuli, how this change depends on frequency and how it evolves due to repeated cycling.

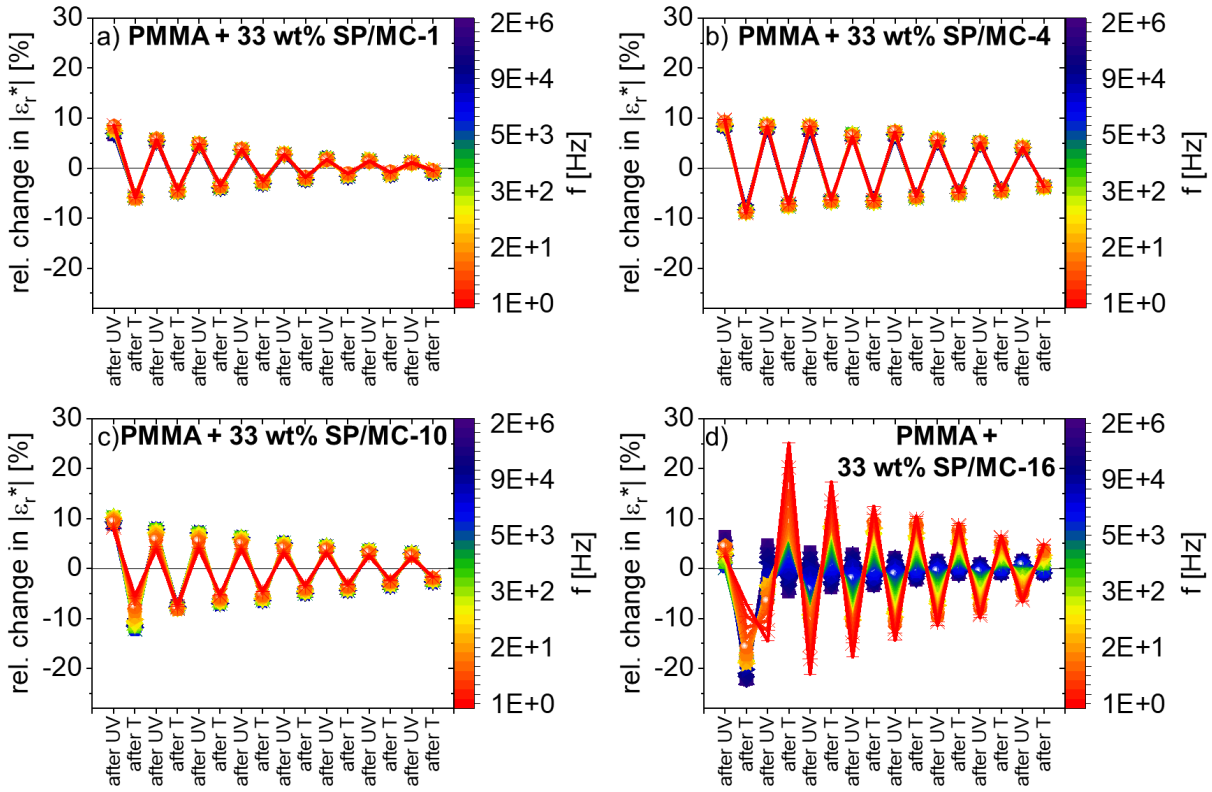

Figure 5.9: Switching of the modulus of dielectric permittivity of PMMA films blended with 33 wt% of a) SP/MC-1, b) SP/MC-4, c) SP/MC-10 and d) SP/MC-16. The changes in dielectric properties were induced by repeated UV light illumination (5 J cm^{-2}) and thermal annealing (90 °C for 5 min) over the course of eight UV/T cycles. The color scale indicates how the switching depends on the frequency of the applied electric field.

The data for PMMA blends with SP/MC-1 (see **Figure 5.9a**), indicate that the UV light irradiation (SP switches to MC) results in an increase in dielectric permittivity and that thermal annealing (MC switches to SP) leads to a decrease. Assuming that the film thickness does not change as a result of the treatments, it can be concluded that the capacitance of the sample increases by switching from SP to MC and decreases by switching back from MC to SP, which is in line with the results of Shen et al. The data also show that the magnitude of the change depends only weakly on the frequency and that it decreases with increasing cycle number, which can be ascribed to the degradation of the photoswitch, possibly due to photo-oxidation [85, 87]. The results for the blends with SP/MC-4 and -10 (see **Figure 5.9b-c**) show similar trends, but also indicate that the switching of $|\varepsilon_r^*|$ improves (larger amplitude of switching) when alkyl chains are attached to the photoswitch molecule. The average relative change in $|\varepsilon_r^*|$ during the first UV/T cycle (considering the whole frequency-range) increases from 6.7 % for the SP/MC-1 blend to 8.7 % and 10.0 % for the SP/MC-4 and SP/MC-10 blends respectively. Comparing the average relative switching between

the first and the eighth cycle allows a rough estimation of the switching fatigue in these systems. The switching decreases by 86 % in the SP/MC-1 blend, but only by 55 % and 74 % in the SP/MC-4 and SP/MC-10 blends respectively. **Figure 5.9d** shows that the SP/MC-16 blend exhibits a different, more complex behavior. Especially the pronounced frequency-dependence of the switching of $|\varepsilon_r^*|$ is striking. At high frequencies (between $3 \cdot 10^4$ Hz and $1 \cdot 10^6$ Hz) the SP/MC-16 blend follows the trend of the other systems (higher $|\varepsilon_r^*|$ after UV), but at lower frequencies ($< 3 \cdot 10^4$ Hz) this trend is reversed and the switching to the MC form (after UV) leads to a decrease of $|\varepsilon_r^*|$. To the best of my knowledge, such a frequency-dependent reversal of the switching direction of dielectric properties in insulating polymer:photoswitch blends has not been reported previously.

A more detailed comparison of the switching of the complex dielectric properties (at $f = 1$ Hz) of all blend systems is given in **Figure 5.10** and in the Appendix (**Table DA.1 - Table DA.4**).

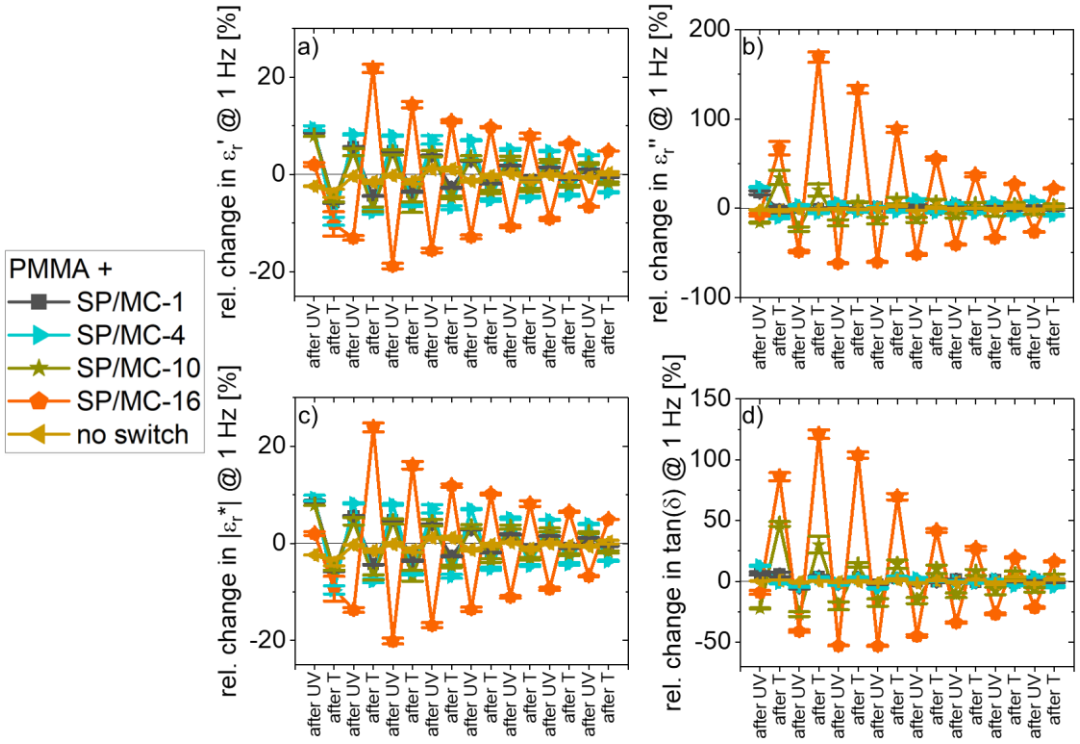

Figure 5.10: Comparing the relative switching of dielectric properties for PMMA + 33 wt% SP/MC-n blend capacitors with n = 1, 4, 10 and 16 (including reference devices without any photoswitch). The relative changes of these properties were determined by evaluating frequency-dependent impedance data (at $f = 1$ Hz) collected over the course of eight UV/T cycles (5 J cm^{-2} and 90 °C for 5 min always alternating).

From these results it can be seen that the real part of the dielectric permittivity ε_r' shows similar relative switching compared to $|\varepsilon_r^*|$ (see **Figure 5.10a and c**). This is because ε_r' typically is at least ten times larger than ε_r'' and therefore dominates the value of the modulus. It is interesting to note that the relative switching of ε_r'' is only marginal for the SP/MC-1 and -4 blends, but is more pronounced for the SP/MC-10 and -16 blends, which both show unexpected reversed switching (i.e. low-frequency permittivity decreases after UV light exposure and increases after thermal annealing, see **Figure 5.10b**). This unconventional behavior of the dielectric properties induced by the long alkyl chains is also reflected in the relative switching of the loss tangent *tan(δ)* (see **Figure 5.10d**) and the fact that the absolute values of dielectric loss become larger with increasing chain length (see **Figure 5.11**).

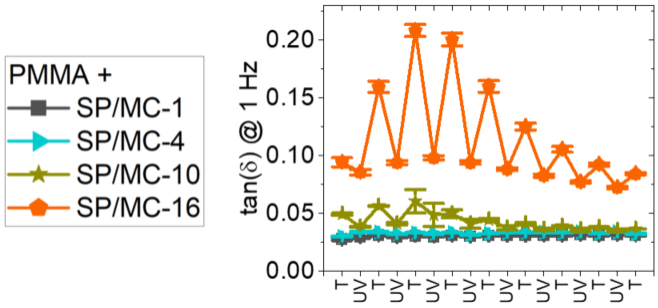

Figure 5.11: Comparing the absolute values of loss tangent *tan(δ)* for PMMA + 33 wt% SP/MC-n blend capacitors with n = 1, 4, 10 and 16. The values were determined by evaluating frequency-dependent impedance data (at f = 1 Hz) collected over the course of eight UV/T cycles (5 J cm^{-2} and 90 °C for 5 min always alternating).

The high values of dielectric loss, especially observed for the SP/MC-16 system, indicate that the presence of long alkyl chains sterically hinders dielectric relaxation phenomena, such as the reorientation of molecular dipoles (from either the SP/MC chromophores or the carboxymethyl side groups of PMMA) under alternating electric field. As an alternative approach for quantifying the switching of the dielectric permittivities of these systems, equivalent circuit fitting of the impedance data with two different models, i.e. a single capacitor and a single constant phase element (CPE), was used. The resulting fitted dielectric permittivities derived from the capacitor model (same fitting methodology as in Chapter 4, see Appendix for details) are given in **Figure 5.12**.

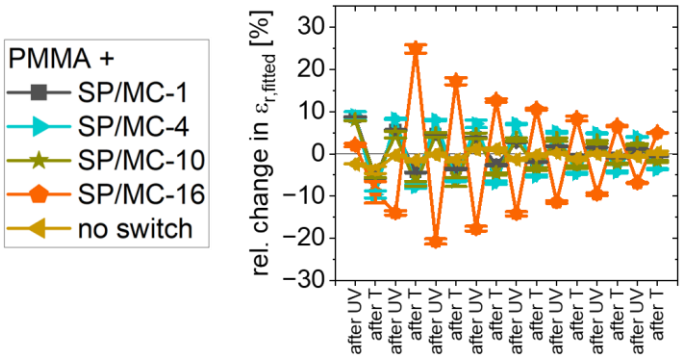

Figure 5.12: Comparing the relative switching of fitted dielectric permittivity for PMMA + 33 wt% SP/MC-n blend capacitors with n = 1, 4, 10 and 16 (including reference devices without any photoswitch). The relative change in permittivity was determined via fitting a single capacitor model to impedance data collected over the course of eight UV/T cycles (5 J cm^{-2} and 90 °C for 5 min always alternating).

Figure 5.13 shows that the permittivities determined by evaluating the frequency-dependent dielectric permittivity at 1 Hz (as given in **Figure 5.10c**) are similar to those obtained by fitting with a single capacitor model, while fitting with a single CPE model leads to an overestimation of the absolute values of permittivity and therefore also to an overestimation of the relative switching amplitudes. A similar result was obtained in Chapter 4 for the PMMA:DHA/VHF blends (see **Figure DA.9 - Figure DA.11**).

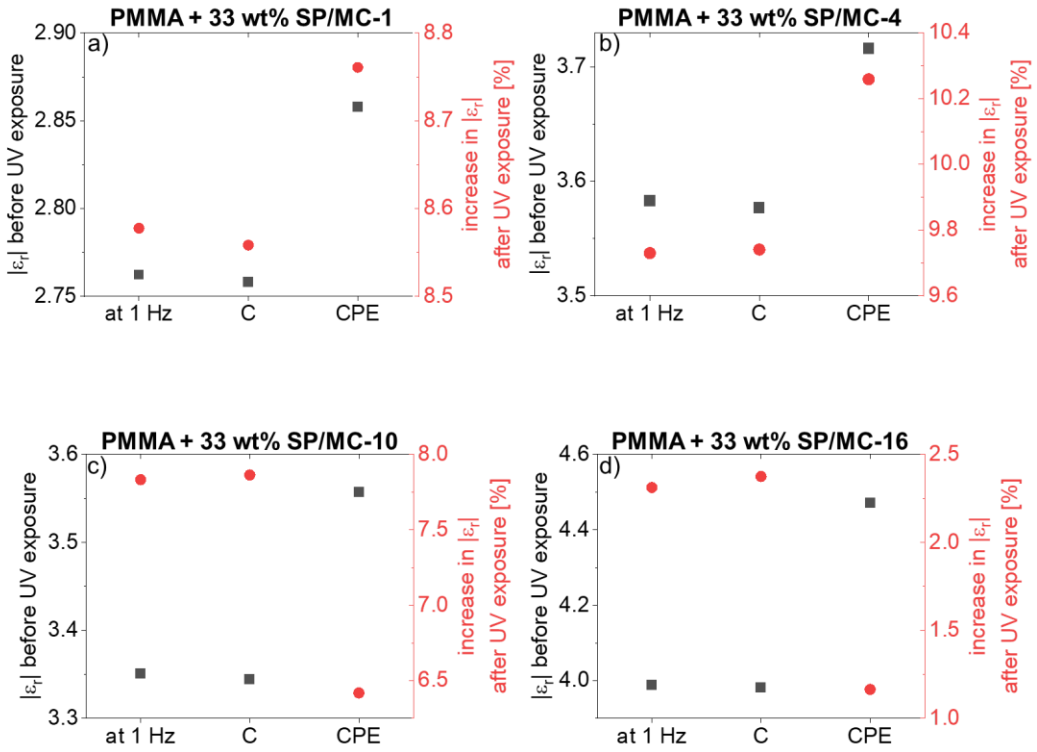

Figure 5.13: Comparing two different approaches for the determination of dielectric permittivity of PMMA + 33 wt% SP/MC-n blend capacitors. Absolute values of permittivity of fresh devices (black squares) and the relative increase in permittivity due to the first UV light exposure (red circles) for blends of PMMA with a) SP/MC-1, b) SP/MC-4, c) SP/MC-10 and d) SP/MC-16. Permittivities were either determined by evaluating the frequency-dependent impedance at f = 1 Hz or by fitting the data with an equivalent circuit model, i.e. single capacitor (C) or single constant phase element (CPE).

UV/Vis Absorption Spectroscopy

In order to investigate the effect of the alkyl chain length of the SP/MC photoswitch, PMMA blends of switches with alkyl groups containing one, four, ten or sixteen carbon atoms were prepared. Regardless of the length of the alkyl chain, all blend films showed the typical color change from colorless (SP) to dark blue/purple (MC) upon application of the UV light stimulus. The UV/Vis absorption spectra of the films in both states (see **Figure 5.14a-b and d-e**) show the typical absorption of SP around 340 nm and of MC around 580 nm.

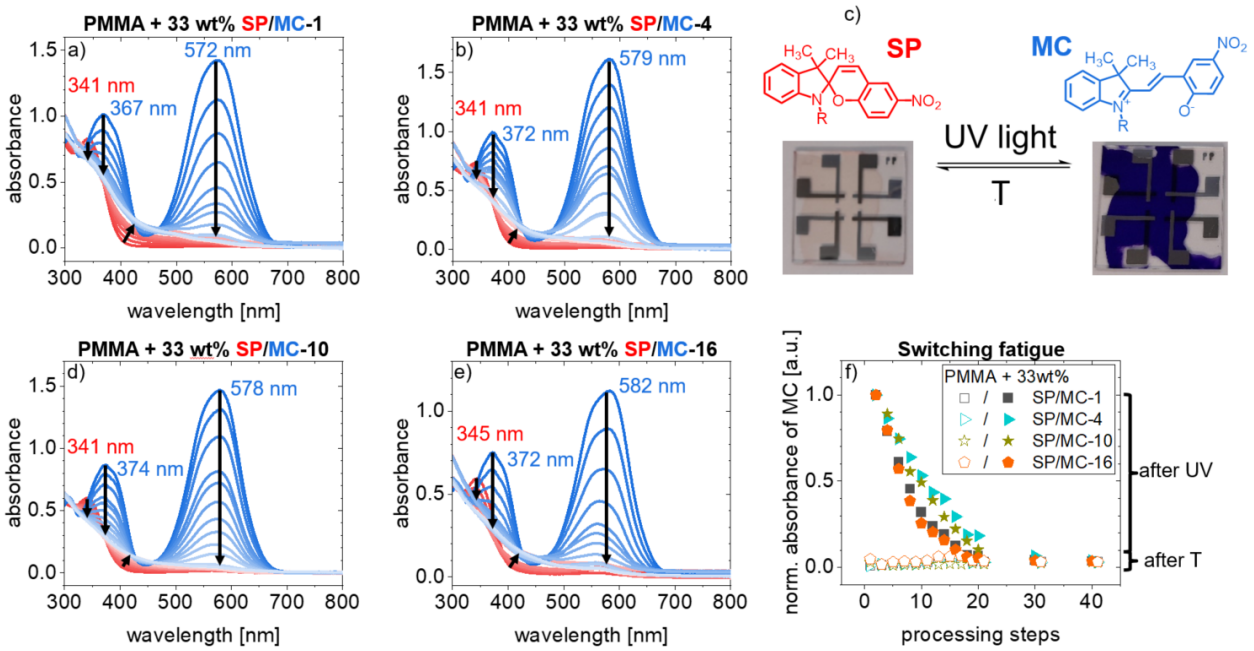

Figure 5.14: UV/Vis absorption spectra of PMMA:SP/MC-n blend films (33 wt%) measured over the course of 20 UV/T cycles. Blends with a) SP/MC-1, b) SP/MC-4, d) SP/MC-10 and e) SP/MC-16. Blue lines: Measured after UV light exposure (5 J cm^{-2}). Red lines: Measured after thermal annealing (90 °C for 5 min). The black arrows indicate the changes of the characteristic absorption features with increasing cycle number. c) Molecular structure of SP/MC-n, where R corresponds to the alkyl chain. Photographs before and after exposure to UV light demonstrating the photochromic behavior of the blends. f) Switching fatigue: Normalized absorption (measured at wavelength of maximum absorption) of MC-n around 570-580 nm. Data was normalized to the absorbance measured after the first UV light illumination. Empty symbols indicate that the switch is in the SP form.

Furthermore, the switching fatigue of the four different SP/MC-n derivatives was probed via UV/Vis absorption spectroscopy. The evolution of the absorption spectra of all blend films due to repeated cycling is displayed in **Figure 5.14a-b and d-e**. As shown in **Figure 5.14f** the ability of the PMMA blend films to colorize and decolorize deteriorates within the first 20 UV/T cycles (40 processing steps). This fatigue can most likely be ascribed to the photo-oxidation of the switches (especially considering the high UV dose of 5 J cm^{-2} per illumination step) [85, 87]. Nevertheless, the data suggest that switching fatigue occurs slower in blends with SP/MC-4 and -10 compared to blends with SP/MC-1 and -16, which is in line with the results of the impedance measurements on capacitors.

Photoswitchable Transistors

Transfer characteristics and the corresponding gate-source bias-dependent mobilities of transistors employing blends of PMMA with either SP/MC-4, -10 or -16 as functional gate dielectrics are given in **Figure 5.15 - Figure 5.17**.

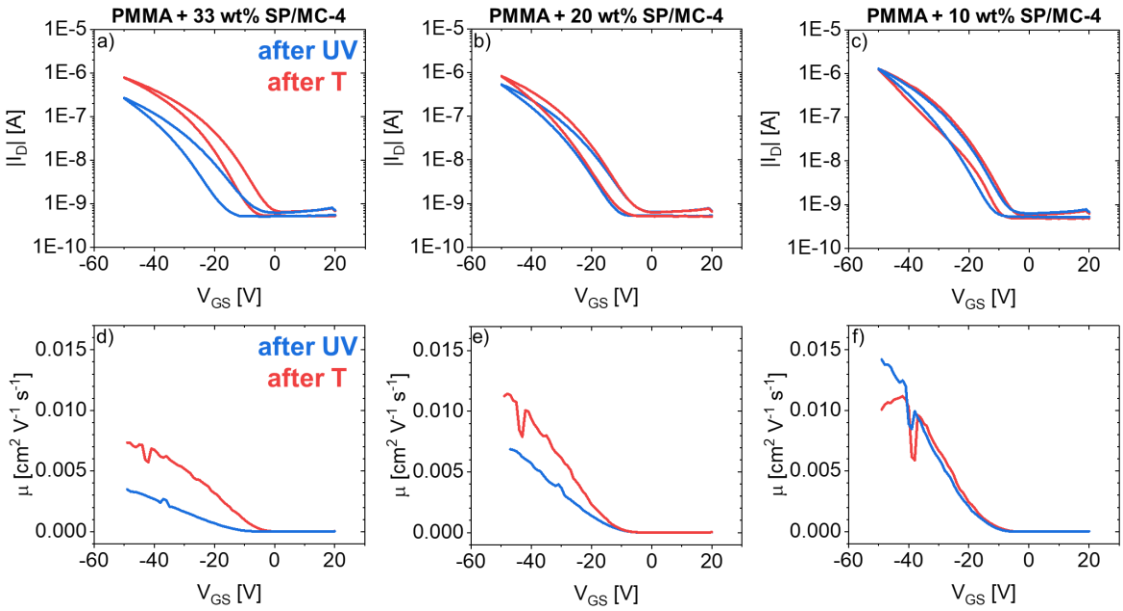

Figure 5.15: Effect of the weight content of **SP/MC-4** on the switchability of transistor characteristics. Reversible switching of a) - c) transfer characteristics (V_{DS} = -50 V) and d) - f) gate-source bias-dependent field-effect mobilities. Blue lines: Measured after UV light exposure (5 J cm^{-2}). Red lines: Measured after thermal annealing (90 °C for 5 min). Mobilities were only determined for the forward sweep of the gate-source bias.

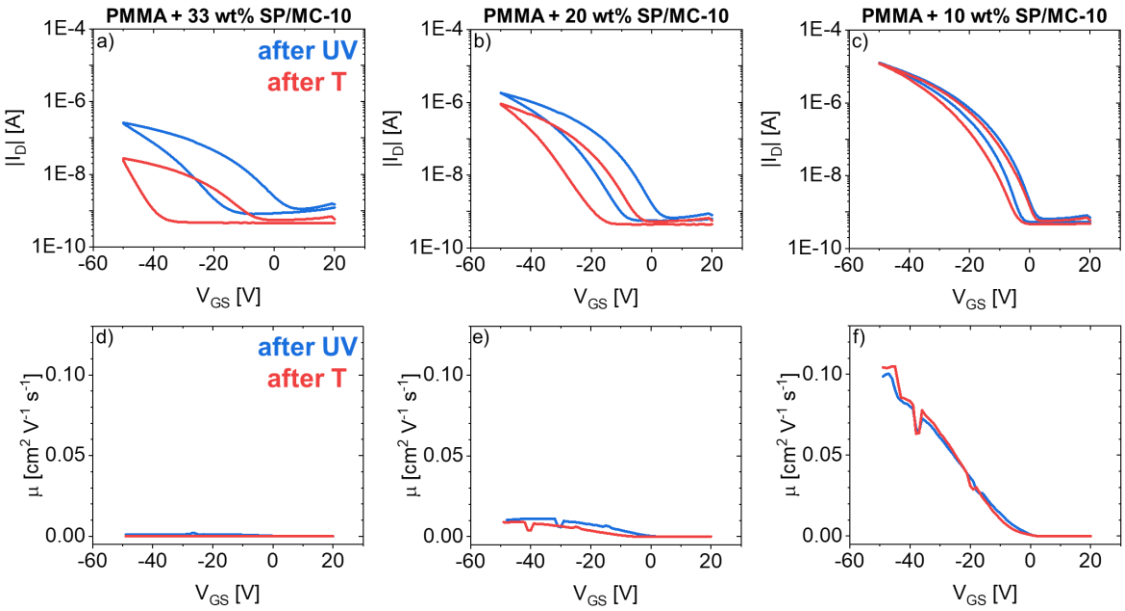

Figure 5.16: Effect of the weight content of **SP/MC-10** on the switchability of transistor characteristics. Reversible switching of a) - c) transfer characteristics (V_{DS} = -50 V) and d) - f) gate-source bias-dependent field-effect mobilities. Blue lines: Measured after UV light exposure (5 J cm^{-2}). Red lines: Measured after thermal annealing (90 °C for 5 min). Mobilities were only determined for the forward sweep of the gate-source bias.

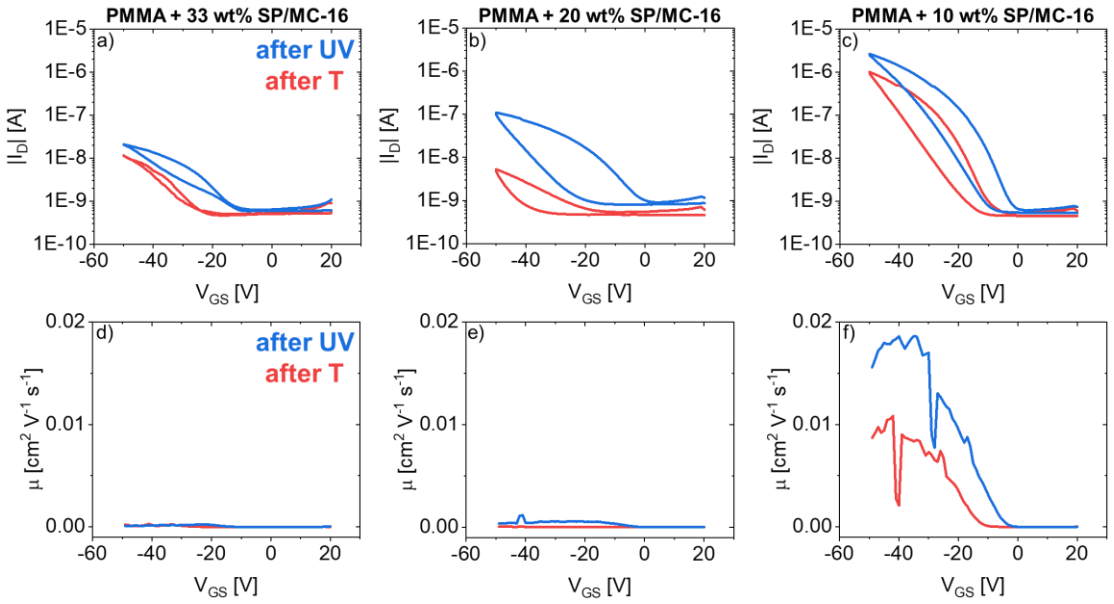

Figure 5.17: Effect of the weight content of **SP/MC-16** on the switchability of transistor characteristics. Reversible switching of a) - c) transfer characteristics (V_{DS} = -50 V) and d) - f) gate-source bias-dependent field-effect mobilities. Blue lines: Measured after UV light exposure (5 J cm^{-2}). Red lines: Measured after thermal annealing (90 °C for 5 min). Mobilities were only determined for the forward sweep of the gate-source bias.

Similar to the previous analysis for the PMMA:SP/MC-1 system, transistor figures of merit and their switching in absolute numbers was quantified and is summarized in **Table 5.2 - Table 5.4**. The relative switching of these properties is given in **Table DA.1 - Table DA.4**.

Table 5.2: Absolute values of threshold voltages and mobilities (at V_{GS} = -50 V) determined for transistors with PMMA + x wt% **SP/MC-4** blend top-gate dielectrics (with x = 33, 20 and 10) after UV light exposure (5 J cm^{-2}) and thermal annealing (90 °C for 5 min) and the resulting average shifts between both states.

SP/MC-4 content	**V_{th} [V]**		**av. $\lvert\Delta V_{th}\rvert$ [V]**	**μ [0.00X cm^2 V^{-1} s^{-1}]**		**av. $\lvert\Delta\mu\rvert$ [0.00X cm^2 V^{-1} s^{-1}]**
	after UV	**after T**		**after UV**	**after T**	
33 wt%	-14.3±0.6	-11.8±0.5	2.5	3.6±0.5	6.9±0.5	3.3
20 wt%	-16.9±0.8	-16.3±0.6	0.6	4.6±1.2	8.2±1.8	3.6
10 wt%	-17.8±0.6	-17.0±0.4	0.8	14.8±1.5	11.8±1.5	3.1

Table 5.3: Absolute values of threshold voltages and mobilities (at V_{GS} = -50 V) determined for transistors with PMMA + x wt% **SP/MC-10** blend top-gate dielectrics (with x = 33, 20 and 10) after UV light exposure (5 J cm^{-2}) and thermal annealing (90 °C for 5 min) and the resulting average shifts between both states. Values in italics indicate that large differences occurred between the individual cycles, resulting in large standard deviations.

SP/MC-10 content	**V_{th} [V]**		**av. $\|\Delta V_{th}\|$ [V]**	**μ [0.00X cm^2 V^{-1} s^{-1}]**		**av. $\|\Delta\mu\|$ [0.00X cm^2 V^{-1} s^{-1}]**
	after UV	**after T**		**after UV**	**after T**	
33 wt%	-0.1±0.7	*-3.0±4.3*	2.9	1.1±0.3	*0.6±0.6*	0.5
20 wt%	-8.2±0.4	-12.2±0.3	3.9	14.5±0.9	15.6±4.0	1.1
10 wt%	-13.2±0.5	-13.7±0.2	0.5	65.6±5.6	71.6±5.5	6.0

Table 5.4: Absolute values of threshold voltages and mobilities (at V_{GS} = -50 V) determined for transistors with PMMA + x wt% **SP/MC-16** blend top-gate dielectrics (with x = 33, 20 and 10) after UV light exposure (5 J cm^{-2}) and thermal annealing (90 °C for 5 min) and the resulting average shifts between both states. Values in italics indicate that large differences occurred between the individual cycles, resulting in large standard deviations. X indicates that the values could not be determined.

SP/MC-16 content	**V_{th} [V]**		**av. $\|\Delta V_{th}\|$ [V]**	**μ [0.0000X cm^2 V^{-1} s^{-1}]**		**av. $\|\Delta\mu\|$ [0.0000X cm^2 V^{-1} s^{-1}]**
	after UV	**after T**		**after UV**	**after T**	
33 wt%	X	X	X	*18.9±10.4*	*19.1±16.6*	0.2
20 wt%	-2.8±0.8	-14.1±3.9	11.3	56.4±8.8	*34.0±47.4*	22.4
10 wt%	-13.8±0.4	16.2±0.2	2.3	1986±110	1674±183	312

The results obtained by impedance spectroscopy of capacitors showed that the stimuli-induced isomerization of the SP/MC-n photoswitches within a PMMA matrix alters the dielectric properties of such blends. However, it was also found that these changes in properties were markedly different, depending on the length of the alkyl chain attached to the switch (see e.g. switching of ε_r'' and *tan(δ)* in **Figure 5.10b and d**). The transistor characterization confirms this notion that the SP/MC-n derivatives can cause different effects in electronic devices depending on the length of the alkyl chain. Blends with SP/MC-4 cause similar effects compared to blends with SP/MC-1, in particular a threshold voltage shift to more negative gate-source bias, resulting in a decrease in on-current after the UV light exposure. For blends with SP/MC-10 and -16 UV light exposure leads to the opposite effect, namely a threshold voltage shift to more positive gate-source bias resulting in an increase in on-current. It is unlikely that these changes in transfer characteristics are only caused by the altered capacity of the dielectric, since this fails to explain the significant hysteresis observed e.g. for blends with 33 wt% SP/MC-10 (see **Figure 5.16a**) and 20 wt%

SP/MC-16 (see **Figure 5.17b**). Opposing effects of the stimuli depending on the length of the alkyl chain can also be observed for the mobility. Devices containing SP/MC-1 and -4 show lower (higher) mobility, after UV light exposure (thermal annealing), while the same stimulus results in higher (lower) mobility in devices containing SP/MC-10 and -16. **Figure 5.18** summarizes this reversal of switching direction induced by the long alkyl chains by comparing the maximum relative changes (i.e. increase and decrease) in threshold voltage, on-current and mobility that were observed during an experiment comprising three UV/T cycles.

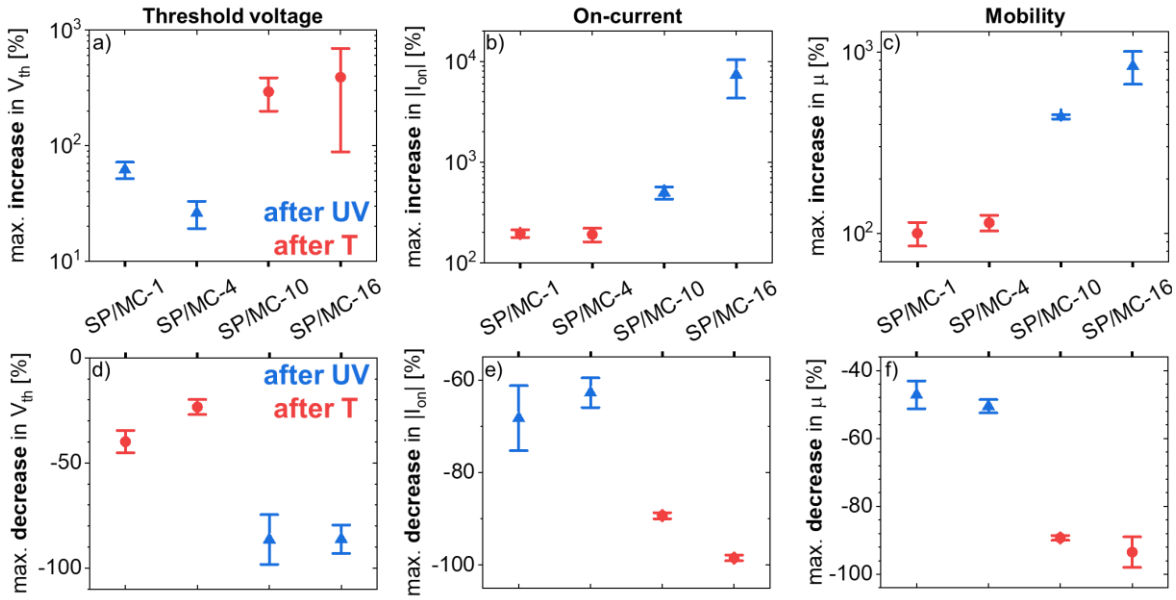

Figure 5.18: Comparison of figures of merit of transistors with PMMA:SP/MC-n dielectrics with n = 1, 4, 10 and 16 (33 wt%, only for n = 16, 20 wt%). a) - c) Maximum relative increases and d) - f) maximum relative decreases of threshold voltage, on-current ($|I_D|$ at V_{GS} = -50 V) and mobility (at V_{GS} = -50 V) that were observed over the course of three UV/T cycles.

From the data, it is clear that the mobilities are decreasing, when the content of any of the switches in the PMMA matrix is increasing. **Figure 5.19** shows the switching of the mobility for transistors with PMMA + 33, 20 and 10 wt% SP/MC-n blend dielectrics.

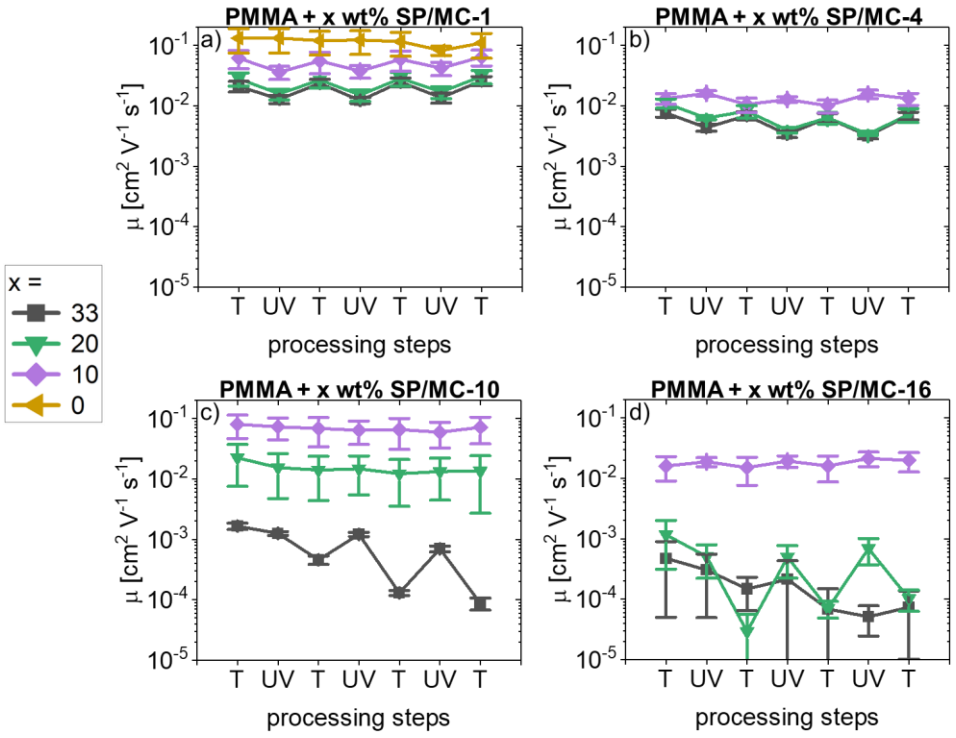

Figure 5.19: Effect of the length of the alkyl chain attached to SP/MC-n photoswitches on mobilities of organic transistors. For each derivative of the switch weight contents of 33, 20 and 10 wt% were tested. Measurements were conducted on P3HT transistors with PMMA:SP/MC-n blend top-gate dielectrics with n = a) 1, b) 4, c) 10 and d) 16.

This decrease in mobility is not surprising, since the addition of more entities with high dipole moment results in larger energetic disorder at the interface, which is detrimental to charge transport [220]. However, it is not solely the effect of the dipole moments of the SP/MC moieties, but also the attached alkyl chains are playing a significant role. This becomes especially clear upon comparing those blends with the same weight content of switch, but containing derivatives with different alkyl chain length (see **Figure 5.20**).

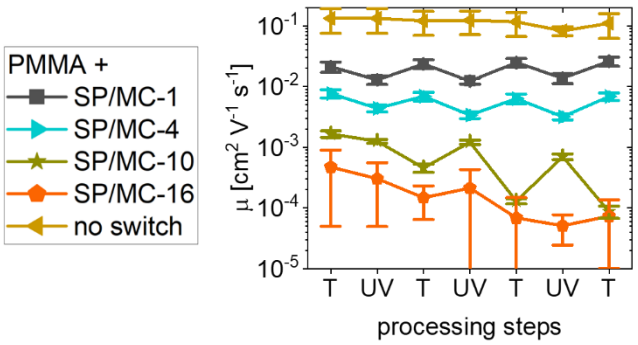

Figure 5.20: Effect of the length of the alkyl chain attached to SP/MC-n photoswitches (with n = 1, 4, 10 and 16) on mobilities of organic transistors. Direct comparison of the four derivatives of the switch obtained from measurements on P3HT transistors with PMMA + 33 wt% SP/MC-n blend top-gate dielectrics.

From this, it can be concluded that longer alkyl chains lead to lower mobilities. This is particularly striking, since the number of SP/MC moieties decreases at the same weight content, as the molecular weight of the switches increases with larger side chain. This behavior indicates that the long alkyl chains have an unexpectedly large influence on transistor characteristics and therefore might also be responsible for the unusual switching of device properties, observed in both transistor and capacitor experiments. However, this is not an electronic effect, since alkyl chains are insulating and their length does not affect the electronic properties of the SP/MC moiety. The ionization potentials, electron affinities and dipole moments given in **Table 5.5** (calculated using density functional theory) confirm this notion. Instead, a morphological effect should be considered as discussed below.

Table 5.5: Molecular properties of the SP/MC-n photoswitches. Calculations were performed at the B3LYP/6-311G(d,p) level of DFT.

	ionization potential [eV]	electron affinity [eV]	dipole moment [D]
SP-1	5.81	2.34	5.47
SP-4	5.76	2.33	5.59
SP-10	5.75	2.32	5.62
SP-16	5.75	2.32	5.57
MC-1	5.53	3.05	12.48
MC-4	5.47	3.00	12.79
MC-10	5.46	2.99	12.85
MC-16	5.46	2.99	12.87

One striking difference between the SP/MC-n derivatives with short and long alkyl chains is their ability to form crystals. Hayashida et al. reported that SP/MC-n switches can crystallize in thin-

films, but also when blended into polymer matrices such as polystyrene, PMMA and polyvinyl butyral [445, 446]. Derivatives with n = 7, 12 and 18 were observed to form ordered structures and the ability to form these crystals increased with increasing alkyl chain length. Interestingly, the photochromic properties of these materials were not affected. The isomerization between the SP and MC forms could still be readily observed, indicating that the crystals are formed predominantly via aggregation of the alkyl chains. Herein, by using X-ray diffractometry, it was possible to confirm the formation of crystals in PMMA:SP/MC-16 blends (see **Figure 5.21**).

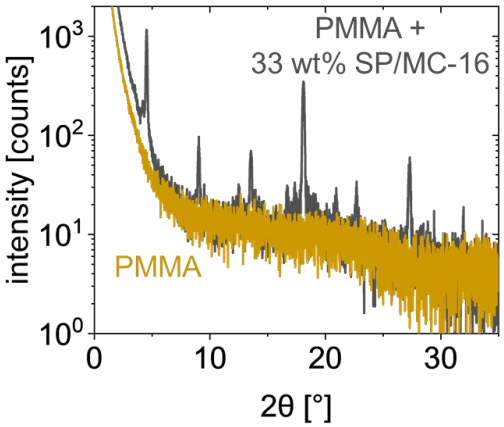

Figure 5.21: X-ray diffractograms measured on PMMA:SP/MC-16 blend and unblended PMMA films. Measurements were conducted after drying of the spin coated films.

However, the observed crystallinity is low and therefore further studies will be necessary to clarify whether the SP/MC-n crystallization could be related to the unusual switching of the transistor characteristics. Nevertheless, this study is the first to report the effect of SP/MC-n crystal formation in working electronic devices. Besides the XRD and electrical data, the formation of crystals can also be observed in the UV/Vis absorption spectra, as indicated e.g. by the significant broadening of the absorption of MC-16 at around 580 nm (see **Figure 5.14e**) which was also observed by Hayashida et al. [445].

To further evaluate the difference in transistor properties resulting from blending PMMA with SP/MC-n derivatives with different alkyl chain length, bias stress measurements were performed for transistors with PMMA:SP/MC-n gate dielectrics after UV light exposure (switch is in the MC form) and after thermal annealing (switch is in the SP form).

Typically, the on-current of an OFET decreases, when the device experiences bias stress over a prolonged period of time. This is often ascribed to mobile charges becoming trapped at the semiconductor-dielectric interface or in the bulk of the dielectric leading to a lowering of the effective gate-source bias [447, 448]. Here, this behavior was verified for a reference device with an unblended PMMA top-gate dielectric (see **Figure 5.24**, transfer characteristics not shown). Upon blending SP/MC-n molecular switches into the PMMA dielectric, the bias stress characteristics changed drastically. The changes in transfer characteristics induced by bias stress for transistors with blend dielectrics and the corresponding shifts in on-current are shown in **Figure 5.22** and **Figure 5.23** respectively.

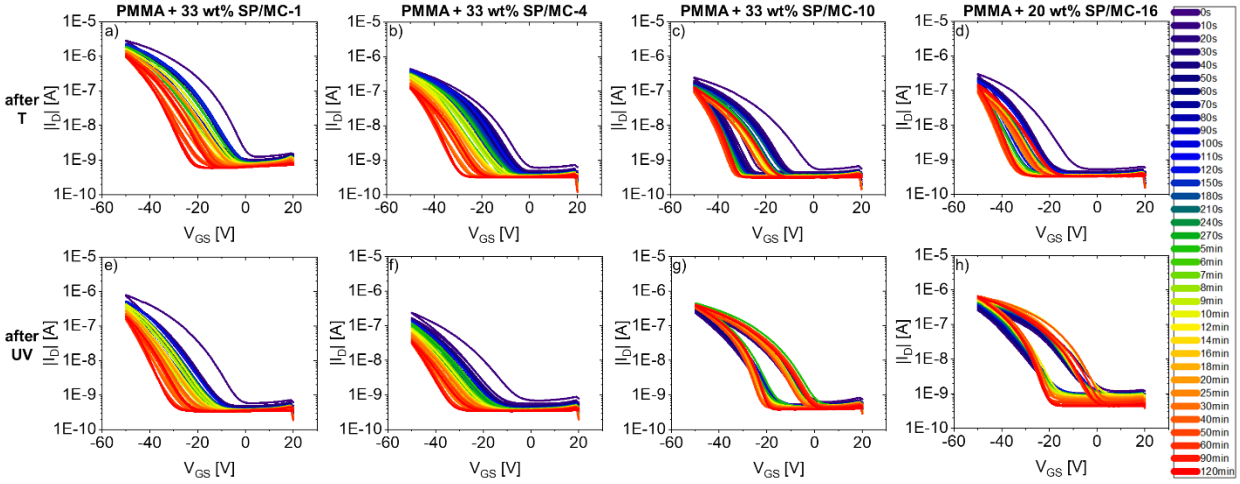

Figure 5.22: Effect of negative bias stress on transfer characteristics (V_{DS} = -50 V) of transistors with PMMA:SP/MC-n (with n = 1, 4, 10 and 16) blend dielectrics. Bias stress was applied for 2 h (V_{GS} = V_{DS} = -50 V) and measurements were carried out a) - d) after thermal annealing (90 °C for 5 min) and e) - h) after UV light illumination (5 J cm^{-2}). Each measurement was carried out on a transistor that had not yet been exposed to bias stress.

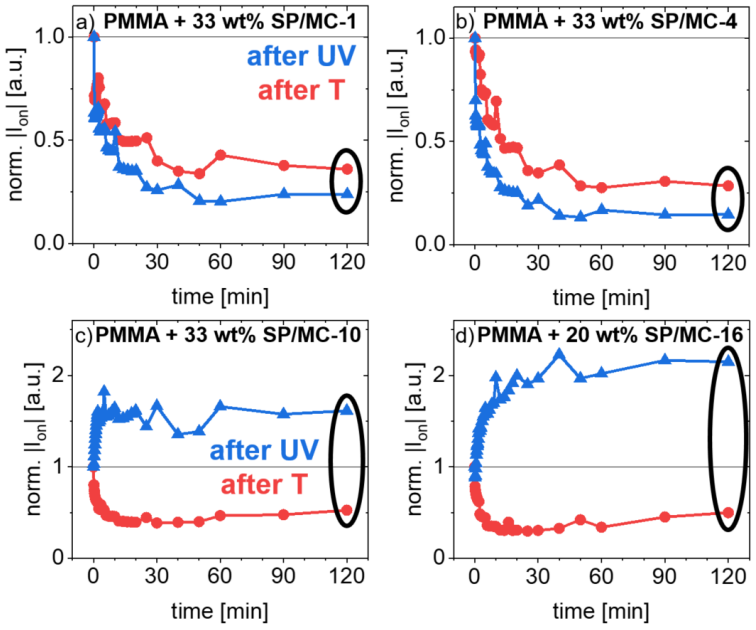

Figure 5.23: Effect of negative bias stress on transistor on-current ($|I_D|$ at V_{GS} = -50 V) measured on OFETs with PMMA:SP/MC-n blend dielectrics with n = a) 1, b) 4, c) 10 and d) 16. The results were normalized by the on-current of the unstressed transistor at t = 0 min. Bias stress was applied for 2 h (V_{GS} = V_{DS} = -50 V) and measurements were carried out after thermal annealing (90 °C for 5 min, red circles) and after UV light illumination (5 J cm^{-2}, blue triangles). Each measurement was carried out on a transistor that had not yet been exposed to bias stress. The data points marked at t = 120 min are those shown in **Figure 5.24**.

In comparison to the reference device, the decrease in on-current with increasing bias stress time occurs faster for blends with SP/MC-1 and -4. This was observed, regardless of whether the switches were in the SP or MC form and is indicative for the aforementioned charge trapping mechanism. A different observation was made for blends with SP/MC-10 and -16. In these cases, the on-current only decreased due to bias stress, when the switches were in the SP form. Surprisingly, the on-current increased during bias stress, when the switches were in the MC form. These results are summarized in **Figure 5.24**. Such behavior could be caused by trap filling. However, clarification of the exact mechanism would require further experiments. Nonetheless, these results show once again that the length of the alkyl chain of the molecular switches is a determining factor for how these molecules affect the behavior of field-effect transistors. Blending PMMA with SP/MC-n with short and long alkyl chains induces opposing behaviors in transistors.

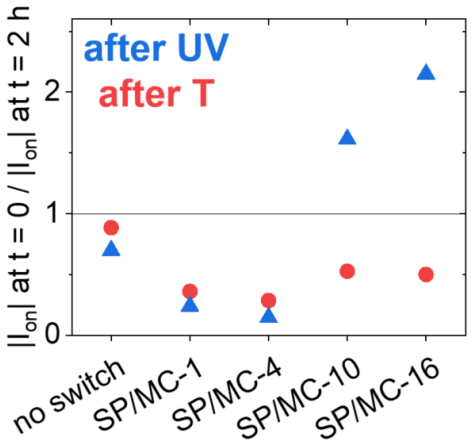

Figure 5.24: Shifts of on-current of transistors containing SP/MC-n derivatives (including a reference device without any switch) after 2 h of applied negative bias stress. Results were normalized by the on-current of the unstressed transistor at t = 0 min. The switch was either in the SP form (red circles) or the MC form (blue triangles) during the bias stress measurement. Values < 1 indicate a decrease in on-current and values > 1 indicate an increase in on-current with respect to the unstressed transistor.

5.4. Discussion

Impedance spectroscopy on capacitors confirmed that the dielectric permittivity of the PMMA:SP/MC-1 blend increases when the switch isomerizes from the SP to the MC form. Therefore, the capacitance of the gate dielectric increases, which should result in an increase in drain current as reported by Shen et al. [183]. However, this report is not in line with results presented here, which rather show a decrease in drain current after UV light exposure. Therefore, it is hypothesized that two mechanisms are relevant in the transistors with PMMA:SP/MC-1 top-gate dielectrics: The effect of the capacitance is counteracted by carrier localization/trapping caused by the presence of large dipole moments in the vicinity of the semiconductor-dielectric interface. In fact, the latter effect clearly outweighs the change in capacitance and therefore dominates the stimuli-responsiveness of the transistors. The question why the results reported here are in contrast to the findings of Shen et al. can be resolved by considering a vertical phase separation effect, similar to the one reported by Ishiguro et al. [173] for P3HT:SP/MC-1 blends. If the SP/MC-1 molecules accumulate predominantly at the bottom of the blend film, the charge localization/trapping caused by dipole moments close to the interface can only be observed in top-gate devices and not in the bottom-gate devices studied by Shen et al.

A detailed summary of the relative changes of the switchable dielectric permittivity (from impedance spectroscopy on capacitors) and of the transistor figures of merit is given in **Table DA.1 - Table DA.4**. Comparing the two types of devices clearly shows that the switching is more pronounced in transistors than in capacitors. This is in line with the previous argument that the switching of capacitors and transistors are dominated by two different effects, i.e. the switching of the capacitance and the charge localization/trapping caused by the dipole moments of the photoswitches at the semiconductor-dielectric interface.

5.5. Conclusions

The control of the threshold voltage of organic transistors post-fabrication was demonstrated by blending photo-/thermochromic spiropyran/merocyanine switches into the PMMA top-gate dielectric of polymer TFTs. Non-destructive UV light stimuli were used to alter the electrical characteristics of the transistors and therefore tune the threshold voltage in a controlled way over several volts. The pristine state is restored via a thermal stimulus. Such methodology allows for the on-demand post-fabrication control over crucial device parameters, which is a highly necessary condition for the fabrication of fast electronic circuits with low power consumption. In order to obtain a better understanding of the working mechanisms behind this behavior, the functional blends of PMMA:SP/MC-n photoswitches were thoroughly characterized using capacitor and transistor devices. Impedance spectroscopy was used to investigate the dielectric properties of the blends and their switching fatigue behavior. For the transistors, it was found that the photoresponsivity cannot only be adjusted by changing the composition of the blend dielectric, but also by changing the length of the alkyl chain that is attached to the switch. Opposite switching could be observed between blends with derivatives with short (n = 1 and 4) and long (n = 10 and 16) alkyl chains, unravelling that for SP/MC-n switches, not only the change in dipole moment, but also their ability to form ordered structures via mediation of long alkyl chains plays an important role. The chain length dependence of the switching highlights the importance of chemical design and morphological effects for the development of well-controlled stimuli-responsive devices.

Dissertation Conclusions

Employing molecular switches is a very effective approach for the fabrication of multifunctional organic field-effect transistors. These devices cannot only be controlled through the application of electrical stimuli, but also via other stimuli such as light or heat, enabling a variety of applications in the fields of sensing and memory. The underlying principle of this stimuli-responsiveness is based on the isomerization of the molecular switch, which results in altered charge transport through the device. It is a key requirement for the technological advancement of such devices to fundamentally comprehend the delicate interplay between the molecular switch and the individual components of the transistor, including the organic semiconductor, the gate dielectric and the electrodes. However, this is inherently challenging and often times a fundamental understanding for these microscopic processes is lacking, hindering further innovations in this field. Therefore, the aim of this dissertation is to gain a deeper insight into how the potential of molecular switches can be harnessed in multifunctional organic transistors and to indicate new pathways for future innovations.

In order to achieve this, first the current literature was evaluated and the numerous mechanisms by which molecular switches can alter the electrical characteristics of organic transistors were identified. This systematic overview is provided in Chapter 2 including a short summary of every mechanism. From this literature overview it was concluded that more than 90 % of the published works focus on only three families of photoswitches (i.e. diarylethenes, spirocompounds and azobenzenes). Chapters 3 and 4 go beyond these well-established molecular switches and demonstrate that dihydroazulene/vinylheptafulvene (DHA/VHF) photo-/thermochromic molecules are well suited to fabricate stimuli-responsive organic transistors. This was achieved by applying two different strategies of incorporating DHA/VHF into the transistor.

At first DHA/VHF was blended with semiconducting polythiophene-based polymers and these blends were used as transistor channel materials (Chapter 3). These transistors could be reversibly switched trough alternating exposure to UV light and heat and it was found that the magnitude of the switching depends on the applied UV dose, which makes such transistors promising candidates for UV sensing applications. In particular, the switching could be observed in several transistor figures of merit including on-current, off-current, threshold voltage and subthreshold swing.

Additionally, it was demonstrated that the stimuli-responsiveness of the transistors is maintained after up to 100 repeated UV light exposure/thermal annealing steps, indicating the high resistance of DHA/VHF against switching fatigue.

Secondly, DHA/VHF was blended with an insulating polymer and these blends were used as gate dielectric materials in transistors (Chapter 4). Before studying these blends in transistors, the switching of their dielectric properties was studied in detail in metal-insulator-metal capacitors using impedance spectroscopy. Through equivalent circuit fitting of the frequency-dependent impedance data, it was possible to capture and quantify the reversible isomerization of DHA/VHF inside the insulating polymer matrix. Upon applying these blends as dielectrics in transistors, a reversible modulation of field-effect-mobility of around 20-30 % was achieved. In agreement with the results presented in the previous chapter, DHA/VHF molecules showed excellent resistance against switching fatigue.

In Chapter 5, spiropyran/merocyanine molecular switches with different alkyl chain lengths were used to deliberately tune the electrical characteristics of organic transistors. In comparison to the works with DHA/VHF, here the threshold voltage was identified as the dominating switchable figure of merit. This approach of using light for the post-fabrication adjustment of the threshold voltage was successfully demonstrated for polythiophene-based OFETs. Additionally, it was found that attaching long alkyl chains to the switch molecules dramatically changes the stimuli-responsiveness of the transistors by reversing the direction of the switching effect.

In short, the control over electrical characteristics, as demonstrated in this dissertation, using optical and thermal stimuli allows for the construction of multi-level photomemories, photodetectors and next-generation light-switchable logic circuits. Therefore, it can be concluded that molecular switches still hold an enormous potential to push the boundaries of organic electronics. The findings presented here are paving the way for future developments such as molecular switch-embedded artificial synapses and stimuli-responsive organic electrochemical transistors, thus enabling new advancements in the fields of neuromorphic computing and biosensing.

References

1. Chiang, C.K., C.R. Fincher, Y.W. Park, A.J. Heeger, H. Shirakawa, E.J. Louis, S.C. Gau, and A.G. MacDiarmid, *Electrical Conductivity in Doped Polyacetylene.* Physical Review Letters, 1977. **39**(17): p. 1098-1101.

2. Blom, P.W.M., *Polymer Electronics: To Be or Not to Be?* Advanced Materials Technologies, 2020. **5**(6): p. 2000144.

3. Yan, C., S. Barlow, Z. Wang, H. Yan, A.K.Y. Jen, S.R. Marder, and X. Zhan, *Non-fullerene acceptors for organic solar cells.* Nature Reviews Materials, 2018. **3**(3): p. 18003.

4. Fukuda, K., K. Yu, and T. Someya, *The Future of Flexible Organic Solar Cells.* Advanced Energy Materials, 2020. **10**(25): p. 2000765.

5. Duan, L. and A. Uddin, *Progress in Stability of Organic Solar Cells.* Advanced Science, 2020. **7**(11): p. 1903259.

6. Liu, Y., C. Li, Z. Ren, S. Yan, and M.R. Bryce, *All-organic thermally activated delayed fluorescence materials for organic light-emitting diodes.* Nature Reviews Materials, 2018. **3**(4): p. 18020.

7. Song, J., H. Lee, E.G. Jeong, K.C. Choi, and S. Yoo, *Organic Light-Emitting Diodes: Pushing Toward the Limits and Beyond.* Advanced Materials, 2020. **32**(35): p. 1907539.

8. Van der Zee, B., Y. Li, G.-J.A.H. Wetzelaer, and P.W.M. Blom, *Efficiency of Polymer Light-Emitting Diodes: A Perspective.* Advanced Materials, 2022. **34**(13): p. 2108887.

9. Horowitz, G., *Organic Field-Effect Transistors.* Advanced Materials, 1998. **10**(5): p. 365-377.

10. Sirringhaus, H., *25th Anniversary Article: Organic Field-Effect Transistors: The Path Beyond Amorphous Silicon.* Advanced Materials, 2014. **26**(9): p. 1319-1335.

11. Chen, H., W. Zhang, M. Li, G. He, and X. Guo, *Interface Engineering in Organic Field-Effect Transistors: Principles, Applications, and Perspectives.* Chemical Reviews, 2020. **120**(5): p. 2879-2949.

12. Kymissis, I., *Organic Field Effect Transistors: Theory, Fabrication and Characterization*. Integrated Circuits and Systems, ed. A. Chandrakasan. 2009, New York, NY, USA: Springer Science+Business Media, LLC.

13. Köhler, A. and H. Bässler, *Electronic Processes in Organic Semiconductors: An Introduction*. 2015, Weinheim, Germany: Wiley-VCH Verlag GmbH & Co. KGaA.

14. Anthony, J.E., C.A. Arias, M. Bergsmann, G. Blanchet, E. Cantatore, M.L. Chabinyc, J.H. Daniel, G.H. Gelinck, M. Halik, M. Heuken, G. Horowitz, J. Huang, H.E.A. Huitema, H.E.

Katz, T. Kelley, H.H. Lee, D.M. de Leeuw, Y. Li, P.J.G. van Lieshout, R. Lujan, W.A. MacDonald, A.W. Marsman, E.J. Meijer, N. Meyer, S.F. Nelson, B.S. Ong, C. Ramsdale, S.E. Ready, J. Rogers, T. Sakurai, A. Salleo, C. Sele, H. Sirringhaus, T. Someya, C.J. Stonley, F.J. Touwslager, R. Treutlein, E. van Veenendaal, T. von Werne, W. Wong, Y. Wu, and L. Zhou, *Organic Electronics: Materials, Manufacturing and Applications*, ed. H. Klauk. 2006, Weinheim, Germany: Wiley-VCH Verlag GmbH & Co. KGaA.

15. Sirringhaus, H., *Device Physics of Solution-Processed Organic Field-Effect Transistors.* Advanced Materials, 2005. **17**(20): p. 2411-2425.

16. Lamport, Z.A., H.F. Haneef, S. Anand, M. Waldrip, and O.D. Jurchescu, *Tutorial: Organic field-effect transistors: Materials, structure and operation.* Journal of Applied Physics, 2018. **124**(7): p. 071101.

17. Kuik, M., G.-J.A.H. Wetzelaer, H.T. Nicolai, N.I. Craciun, D.M. De Leeuw, and P.W.M. Blom, *25th Anniversary Article: Charge Transport and Recombination in Polymer Light-Emitting Diodes.* Advanced Materials, 2014. **26**(4): p. 512-531.

18. Brütting, W., S. Berleb, and A.G. Mückl, *Device physics of organic light-emitting diodes based on molecular materials.* Organic Electronics, 2001. **2**(1): p. 1-36.

19. Schopp, N. and V.V. Brus, *A Review on the Materials Science and Device Physics of Semitransparent Organic Photovoltaics.* Energies, 2022. **15**(13).

20. Ebisawa, F., T. Kurokawa, and S. Nara, *Electrical properties of polyacetylene/polysiloxane interface.* Journal of Applied Physics, 1983. **54**(6): p. 3255-3259.

21. Tsumura, A., H. Koezuka, and T. Ando, *Macromolecular electronic device: Field-effect transistor with a polythiophene thin film.* Applied Physics Letters, 1986. **49**(18): p. 1210-1212.

22. Hu, P., X. He, and H. Jiang, *Greater than 10 cm2 V−1 s−1: A breakthrough of organic semiconductors for field-effect transistors.* InfoMat., 2021. **3**(6): p. 613-630.

23. Choi, H.H., K. Cho, C.D. Frisbie, H. Sirringhaus, and V. Podzorov, *Critical assessment of charge mobility extraction in FETs.* Nature Materials, 2018. **17**(1): p. 2-7.

24. Cheng, Z., C.-S. Pang, P. Wang, S.T. Le, Y. Wu, D. Shahrjerdi, I. Radu, M.C. Lemme, L.-M. Peng, X. Duan, Z. Chen, J. Appenzeller, S.J. Koester, E. Pop, A.D. Franklin, and C.A. Richter, *How to report and benchmark emerging field-effect transistors.* Nature Electronics, 2022. **5**(7): p. 416-423.

25. Paterson, A.F., S. Singh, K.J. Fallon, T. Hodsden, Y. Han, B.C. Schroeder, H. Bronstein, M. Heeney, I. McCulloch, and T.D. Anthopoulos, *Recent Progress in High-Mobility Organic Transistors: A Reality Check.* Advanced Materials, 2018. **30**(36): p. 1801079.

26. Haneef, H.F., A.M. Zeidell, and O.D. Jurchescu, *Charge carrier traps in organic semiconductors: a review on the underlying physics and impact on electronic devices.* Journal of Materials Chemistry C, 2020. **8**(3): p. 759-787.

27. Liu, C., Y. Xu, Y. Li, W. Scheideler, and T. Minari, *Critical Impact of Gate Dielectric Interfaces on the Contact Resistance of High-Performance Organic Field-Effect Transistors.* The Journal of Physical Chemistry C, 2013. **117**(23): p. 12337-12345.

28. Ward, J.W., H.L. Smith, A. Zeidell, P.J. Diemer, S.R. Baker, H. Lee, M.M. Payne, J.E. Anthony, M. Guthold, and O.D. Jurchescu, *Solution-Processed Organic and Halide Perovskite Transistors on Hydrophobic Surfaces.* ACS Applied Materials & Interfaces, 2017. **9**(21): p. 18120-18126.

29. Lin, C., B. Peng, J. Wu, Z. Huang, M. Chen, D. Hu, S. Ke, B.C.K. Tee, and H. Li, *Ambipolar Organic Field-Effect Transistors and Complementary Circuits Based on Single Crystals with Alcohol Treatment.* Advanced Electronic Materials, 2022. **8**(11): p. 2200557.

30. Wang, S.-J., M. Sawatzki, G. Darbandy, F. Talnack, J. Vahland, M. Malfois, A. Kloes, S. Mannsfeld, H. Kleemann, and K. Leo, *Organic bipolar transistors.* Nature, 2022. **606**(7915): p. 700-705.

31. Köhler, A. and H. Bässler, *Electronic Processes in Organic Semiconductors: An Introduction*. 2015, Wiley-VCH Verlag GmbH & Co. KGaA: Weinheim, Germany. p. 371.

32. Zaumseil, J. and H. Sirringhaus, *Electron and Ambipolar Transport in Organic Field-Effect Transistors.* Chemical Reviews, 2007. **107**(4): p. 1296-1323.

33. Bouas-Laurent, H. and H. Dürr, *Organic photochromism (IUPAC Technical Report).* Pure and Applied Chemistry, 2001. **73**(4): p. 639-665.

34. Singer, M. and A. Jäschke, *Reversibly Photoswitchable Nucleosides: Synthesis and Photochromic Properties of Diarylethene-Functionalized 7-Deazaadenosine Derivatives.* Journal of the American Chemical Society, 2010. **132**(24): p. 8372-8377.

35. Day, J.H., *Thermochromism.* Chemical Reviews, 1963. **63**(1): p. 65-80.

36. Beaujuge, P.M. and J.R. Reynolds, *Color Control in π-Conjugated Organic Polymers for Use in Electrochromic Devices.* Chemical Reviews, 2010. **110**(1): p. 268-320.

37. Reichardt, C., *Solvatochromic Dyes as Solvent Polarity Indicators.* Chemical Reviews, 1994. **94**(8): p. 2319-2358.

38. Li, E., K. Jie, M. Liu, X. Sheng, W. Zhu, and F. Huang, *Vapochromic crystals: understanding vapochromism from the perspective of crystal engineering.* Chemical Society Reviews, 2020. **49**(5): p. 1517-1544.

39. Van der Schueren, L. and K. De Clerck, *Coloration and application of pH-sensitive dyes on textile materials.* Coloration Technology, 2012. **128**(2): p. 82-90.

40. Liu, J., L. Han, J. Geng, J. Hua, and Z. Wang, *Metal-Ligand Coordination Induced Ionochromism for π-Conjugated Materials.* Frontiers in Chemistry, 2020. **8**(589106): p. 1-9.

41. Xue, P., J. Ding, P. Wang, and R. Lu, *Recent progress in the mechanochromism of phosphorescent organic molecules and metal complexes.* Journal of Materials Chemistry C, 2016. **4**(28): p. 6688-6706.

42. Koumura, N., R.W.J. Zijlstra, R.A. van Delden, N. Harada, and B.L. Feringa, *Light-driven monodirectional molecular rotor.* Nature, 1999. **401**(6749): p. 152-155.

43. Volarić, J., W. Szymanski, N.A. Simeth, and B.L. Feringa, *Molecular photoswitches in aqueous environments.* Chemical Society Reviews, 2021. **50**(22): p. 12377-12449.

44. Das, P., C.T. Kornman, I. Ghiviriga, K.A. Abboud, and R.K. Castellano, *Enlightening the Well-Controlled Photochemical Behavior of 1,1-Dicyanomethylene-3-Indanone-Functionalized π-Conjugated Molecules.* Chemistry of Materials, 2023. **35**(19): p. 8122-8134.

45. Loan, T., M. Santra, and M. Bradley, *Novel class of photochromic molecules exhibiting photo-switching in the solid state.* Frontiers in Chemistry, 2023. **11**(1205452): p. 1-9.

46. Tran Ngoc, T., N. Grabicki, E. Irran, O. Dumele, and J.F. Teichert, *Photoswitching neutral homoaromatic hydrocarbons.* Nature Chemistry, 2023. **15**(3): p. 377-385.

47. Zhang, Z., W. Wang, M. O'Hagan, J. Dai, J. Zhang, and H. Tian, *Stepping Out of the Blue: From Visible to Near-IR Triggered Photoswitches.* Angewandte Chemie International Edition, 2022. **61**(31): p. e202205758.

48. Thaggard, G.C., B.K.P. Maldeni Kankanamalage, K.C. Park, J. Haimerl, R.A. Fischer, and N.B. Shustova, *Switching in harmony: Tailoring the properties of functional materials with orthogonal stimuli.* Chemical Physics Reviews, 2024. **5**(1): p. 011305.

49. Hu, J., T. Song, M.-M. Yu, and H. Yu, *Optically Controlled Solid-to-Liquid Phase Transition Materials Based on Azo Compounds.* Chemistry of Materials, 2023. **35**(12): p. 4621-4648.

50. Zhang, H.-Y., N. Zhang, Y. Zhang, H.-H. Jiang, Y.-L. Zeng, S.-Y. Tang, P.-F. Li, Y.-Y. Tang, and R.-G. Xiong, *Ferroelectric Phase Transition Driven by Switchable Covalent Bonds.* Physical Review Letters, 2023. **130**(17): p. 176802.

51. Du, Y., C.-R. Huang, Z.-K. Xu, W. Hu, P.-F. Li, R.-G. Xiong, and Z.-X. Wang, *Photochromic Single-Component Organic Fulgide Ferroelectric with Photo-Triggered Polarization Response.* JACS Au, 2023. **3**(5): p. 1464-1471.

52. Liu, Y.-Y., Z.-Q. Liu, Y.-Q. Wang, Y. Zhou, Y. Qin, H.-P. Lv, P.-F. Li, X.-G. Chen, X.-J. Song, and Y. Ai, *Light-Driven Domain Switching on a Photochromic Ferroelectric.* Crystal Growth & Design, 2023. **23**(4): p. 2602-2608.

53. Olesińska-Mönch, M. and C. Deo, *Small-molecule photoswitches for fluorescence bioimaging: engineering and applications.* Chemical Communications, 2023. **59**(6): p. 660-669.

54. Kobauri, P., F.J. Dekker, W. Szymanski, and B.L. Feringa, *Rational Design in Photopharmacology with Molecular Photoswitches.* Angewandte Chemie International Edition, 2023. **62**(30): p. e202300681.

55. Boelke, J. and S. Hecht, *Designing Molecular Photoswitches for Soft Materials Applications.* Advanced Optical Materials, 2019. **7**(16): p. 1900404.

56. Pianowski, Z.L., *Recent Implementations of Molecular Photoswitches into Smart Materials and Biological Systems.* Chemistry – A European Journal, 2019. **25**(20): p. 5128-5144.

57. Mitscherlich, E., *Ueber das Stickstoffbenzid.* Annalen der Physik, 1834. **108**(15): p. 225-227.

58. Yager, K.G. and C.J. Barrett, *Novel photo-switching using azobenzene functional materials.* Journal of Photochemistry and Photobiology A: Chemistry, 2006. **182**(3): p. 250-261.

59. Bafana, A., S.S. Devi, and T. Chakrabarti, *Azo dyes: past, present and the future.* Environmental Reviews, 2011. **19**: p. 350-370.

60. Jerca, F.A., V.V. Jerca, and R. Hoogenboom, *Advances and opportunities in the exciting world of azobenzenes.* Nature Reviews Chemistry, 2022. **6**(1): p. 51-69.

61. Hartley, G.S., *The Cis-form of Azobenzene.* Nature, 1937. **140**(3537): p. 281-281.

62. Klajn, R., *Immobilized azobenzenes for the construction of photoresponsive materials.* Pure and Applied Chemistry, 2010. **82**(12): p. 2247-2279.

63. Lameijer, L.N., S. Budzak, N.A. Simeth, M.J. Hansen, B.L. Feringa, D. Jacquemin, and W. Szymanski, *General Principles for the Design of Visible-Light-Responsive Photoswitches: Tetra-ortho-Chloro-Azobenzenes.* Angewandte Chemie International Edition, 2020. **59**(48): p. 21663-21670.

64. Siewertsen, R., H. Neumann, B. Buchheim-Stehn, R. Herges, C. Näther, F. Renth, and F. Temps, *Highly Efficient Reversible Z−E Photoisomerization of a Bridged Azobenzene with Visible Light through Resolved S1(nπ*) Absorption Bands.* Journal of the American Chemical Society, 2009. **131**(43): p. 15594-15595.

65. Bléger, D., J. Schwarz, A.M. Brouwer, and S. Hecht, *o-Fluoroazobenzenes as Readily Synthesized Photoswitches Offering Nearly Quantitative Two-Way Isomerization with Visible Light.* Journal of the American Chemical Society, 2012. **134**(51): p. 20597-20600.

66. Weston, C.E., R.D. Richardson, P.R. Haycock, A.J.P. White, and M.J. Fuchter, *Arylazopyrazoles: Azoheteroarene Photoswitches Offering Quantitative Isomerization and Long Thermal Half-Lives.* Journal of the American Chemical Society, 2014. **136**(34): p. 11878-11881.

67. Bandara, H.M.D. and S.C. Burdette, *Photoisomerization in different classes of azobenzene.* Chemical Society Reviews, 2012. **41**(5): p. 1809-1825.

68. Cheng, H.-B., S. Zhang, J. Qi, X.-J. Liang, and J. Yoon, *Advances in Application of Azobenzene as a Trigger in Biomedicine: Molecular Design and Spontaneous Assembly.* Advanced Materials, 2021. **33**(26): p. 2007290.

69. Xu, X., J. Feng, W.-Y. Li, G. Wang, W. Feng, and H. Yu, *Azobenzene-containing polymer for solar thermal energy storage and release: Advances, challenges, and opportunities.* Progress in Polymer Science, 2024. **149**: p. 101782.

70. Taniguchi, T., T. Asahi, and H. Koshima, *Photomechanical Azobenzene Crystals.* Crystals, 2019. **9**(9): p. 437.

71. Li, Y., B. Xue, J. Yang, J. Jiang, J. Liu, Y. Zhou, J. Zhang, M. Wu, Y. Yuan, Z. Zhu, Z.J. Wang, Y. Chen, Y. Harabuchi, T. Nakajima, W. Wang, S. Maeda, J.P. Gong, and Y. Cao, *Azobenzene as a photoswitchable mechanophore.* Nature Chemistry, 2024. **16**(3): p. 446-455.

72. Decker, H. and H. Felser, *Über cyclische Oxoniumsalze aus Dicumarketon und über Spiropyranderivate.* Berichte der deutschen chemischen Gesellschaft, 1908. **41**(2): p. 2997-3007.

73. Fischer, E. and Y. Hirshberg, *Formation of coloured forms of spirans by low-temperature irradiation.* Journal of the Chemical Society, 1952: p. 4522-4524.

74. Berkovic, G., V. Krongauz, and V. Weiss, *Spiropyrans and Spirooxazines for Memories and Switches.* Chemical Reviews, 2000. **100**(5): p. 1741-1754.

75. Hirshberg, Y., *Photochromie dans la serie de la bianthrone.* Comptes Rendus Hebdomadaires Des Seances De L Academie Des Sciences, 1950. **231**(18): p. 903-904.

76. Klajn, R., *Spiropyran-based dynamic materials.* Chemical Society Reviews, 2014. **43**(1): p. 148-184.

77. Yu, S.H., S.Z. Hassan, C. So, M. Kang, and D.S. Chung, *Molecular-Switch-Embedded Solution-Processed Semiconductors.* Advanced Materials, 2023. **35**(4): p. 2203401.

78. Nam, Y.-S., I. Yoo, O. Yarimaga, I.S. Park, D.-H. Park, S. Song, J.-M. Kim, and C.W. Lee, *Photochromic spiropyran-embedded PDMS for highly sensitive and tunable optochemical gas sensing.* Chemical Communications, 2014. **50**(32): p. 4251-4254.

79. Fries, K.H., J.D. Driskell, S. Samanta, and J. Locklin, *Spectroscopic Analysis of Metal Ion Binding in Spiropyran Containing Copolymer Thin Films.* Analytical Chemistry, 2010. **82**(8): p. 3306-3314.

80. Shiraishi, Y., M. Itoh, and T. Hirai, *Thermal isomerization of spiropyran to merocyanine in aqueous media and its application to colorimetric temperature indication.* Physical Chemistry Chemical Physics, 2010. **12**(41): p. 13737-13745.

81. Lee, C.K., D.A. Davis, S.R. White, J.S. Moore, N.R. Sottos, and P.V. Braun, *Force-Induced Redistribution of a Chemical Equilibrium.* Journal of the American Chemical Society, 2010. **132**(45): p. 16107-16111.

82. Krongauz, V.A. and E.S. Goldburt, *Quasi-crystals from irradiated photochromic dyes in an applied electric field.* Nature, 1978. **271**(5640): p. 43-45.

83. Goldburt, E., F. Shvartsman, S. Fishman, and V. Krongauz, *Intramolecular interactions in photochromic spiropyran-merocyanine polymers.* Macromolecules, 1984. **17**(6): p. 1225-1230.

84. Cabrera, I., F. Shvartsman, O. Veinberg, and V. Krongauz, *Photocontraction of Liquid Spiropyran-Merocyanine Films.* Science, 1984. **226**(4672): p. 341-343.

85. Yoshida, T. and A. Morinaka, *Decomposition process of the photochromic compound spiro[1,3,3-trimethylindoline-6'-hydroxy benopyran] in the solid state under UV irradiation.* Journal of Photochemistry and Photobiology A: Chemistry, 1992. **63**(2): p. 227-234.

86. Parthenopoulos, D.A. and P.M. Rentzepis, *Three-Dimensional Optical Storage Memory.* Science, 1989. **245**(4920): p. 843-845.

87. Li, X., Y. Wang, T. Matsuura, and J. Meng, *Synthesis and Photochromic Behaviors of Spiropyrans and Spirooxazines Containing an Antioxidant Group.* Molecular Crystals and Liquid Crystals Science and Technology. Section A. Molecular Crystals and Liquid Crystals, 2000. **344**(1): p. 301-306.

88. Salemi, C., G. Giusti, and R. Guglielmetti, *DABCO effect on the photodegradation of photochromic compounds in spiro[indoline-pyran] and spiro[indoline-oxazine] series.* Journal of Photochemistry and Photobiology A: Chemistry, 1995. **86**(1): p. 247-252.

89. Matsushima, R., M. Nishiyama, and M. Doi, *Improvements in the fatigue resistances of photochromic compounds.* Journal of Photochemistry and Photobiology A: Chemistry, 2001. **139**(1): p. 63-69.

90. Radu, A., R. Byrne, N. Alhashimy, M. Fusaro, S. Scarmagnani, and D. Diamond, *Spiropyran-based reversible, light-modulated sensing with reduced photofatigue.* Journal of Photochemistry and Photobiology A: Chemistry, 2009. **206**(2): p. 109-115.

91. Yang, Y., H. Zhao, Y. Li, Y. Chen, Z. Wang, W. Wu, L. Hu, and J. Zhu, *Tuning the Photochromism of Spiropyran in Functionalized Nanoporous Silica Nanoparticles for Dynamic Anticounterfeiting Applications.* ACS Omega, 2023. **8**(18): p. 16459-16470.

92. Keyvan Rad, J., A.R. Ghomi, K. Karimipour, and A.R. Mahdavian, *Progressive Readout Platform Based on Photoswitchable Polyacrylic Nanofibers Containing Spiropyran in Photopatterning with Instant Responsivity to Acid–Base Vapors.* Macromolecules, 2020. **53**(5): p. 1613-1622.

93. Kumar, S., S. Soni, W. Danowski, I.F. Leach, S. Faraji, B.L. Feringa, P. Rudolf, and R.C. Chiechi, *Eliminating Fatigue in Surface-Bound Spiropyrans.* The Journal of Physical Chemistry C, 2019. **123**(42): p. 25908-25914.

94. Lokshin, V.A., A. Samat, and A.V. Metelitsa, *Spirooxazines: synthesis, structure, spectral and photochromic properties.* Russian Chemical Reviews, 2002. **71**(11): p. 893-916.

95. Xia, H., K. Xie, and G. Zou, *Advances in Spiropyrans/Spirooxazines and Applications Based on Fluorescence Resonance Energy Transfer (FRET) with Fluorescent Materials.* Molecules, 2017. **22**(12): p. 2236.

96. Minkin, V.I., *Photo-, Thermo-, Solvato-, and Electrochromic Spiroheterocyclic Compounds.* Chemical Reviews, 2004. **104**(5): p. 2751-2776.

97. Nigel Corns, S., S.M. Partington, and A.D. Towns, *Industrial organic photochromic dyes.* Coloration Technology, 2009. **125**(5): p. 249-261.

98. Zhang, T., X.-Y. Lou, X. Li, X. Tu, J. Han, B. Zhao, and Y.-W. Yang, *Tunable Photochromism of Spirooxazine in the Solid State: A New Design Strategy Based on the Hypochromic Effect.* Advanced Materials, 2023. **35**(11): p. 2210551.

99. Gautron, R., D. Eloy, P. Escaffre, R. Guglielmetti, E. Pottier, and P. Tardieu, *Étude par Photolyse à Éclairs Répétés de la Photodégradation et de la Colorabilité de Quelques Spiro[Indoline-Oxazines]*. Bulletin des Sociétés Chimiques Belges, 1991. **100**(4): p. 315-328.

100. Kawauchi, S., H. Yoshida, N. Yamashina, M. Ohira, S. Saeda, and M. Irie, *A New Photochromic Spiro[3H-1,4-oxazine]*. Bulletin of the Chemical Society of Japan, 1990. **63**(1): p. 267-268.

101. Kawata, S. and Y. Kawata, *Three-Dimensional Optical Data Storage Using Photochromic Materials.* Chemical Reviews, 2000. **100**(5): p. 1777-1788.

102. Ali, A.A., R. Kharbash, and Y. Kim, *Chemo- and biosensing applications of spiropyran and its derivatives - A review.* Analytica Chimica Acta, 2020. **1110**: p. 199-223.

103. Mandal, M., D. Banik, A. Karak, S.K. Manna, and A.K. Mahapatra, *Spiropyran–Merocyanine Based Photochromic Fluorescent Probes: Design, Synthesis, and Applications.* ACS Omega, 2022. **7**(42): p. 36988-37007.

104. Kozlenko, A.S., I.V. Ozhogin, A.D. Pugachev, M.B. Lukyanova, I.M. El-Sewify, and B.S. Lukyanov, *A Modern Look at Spiropyrans: From Single Molecules to Smart Materials.* Topics in Current Chemistry, 2023. **381**(8): p. 1-79.

105. Fagan, A., M. Bartkowski, and S. Giordani, *Spiropyran-Based Drug Delivery Systems.* Frontiers in Chemistry, 2021. **9**(720087): p. 1-19.

106. Jia, S., W.-K. Fong, B. Graham, and B.J. Boyd, *Photoswitchable Molecules in Long-Wavelength Light-Responsive Drug Delivery: From Molecular Design to Applications.* Chemistry of Materials, 2018. **30**(9): p. 2873-2887.

107. Mallory, F.B. and C.W. Mallory, *Photocyclization of Stilbenes and Related Molecules*, in *Organic Reactions*, W.G. Dauben, Editor. 1984, John Wiley & Sons Inc.: New York, NY, USA. p. 1-456.

108. Irie, M. and M. Mohri, *Thermally irreversible photochromic systems. Reversible photocyclization of diarylethene derivatives.* The Journal of Organic Chemistry, 1988. **53**(4): p. 803-808.

109. Takami, S., S. Kobatake, T. Kawai, and M. Irie, *Extraordinarily High Thermal Stability of the Closed-ring Isomer of 1,2-Bis(5-methyl-2-phenylthiazol-4-yl)perfluorocyclopentene.* Chemistry Letters, 2003. **32**(10): p. 892-893.

110. Hanazawa, M., R. Sumiya, Y. Horikawa, and M. Irie, *Thermally irreversible photochromic systems. Reversible photocyclization of 1,2-bis (2-methylbenzo[b]thiophen-3-yl)perfluorocyclocoalkene derivatives.* Journal of the Chemical Society, Chemical Communications, 1992(3): p. 206-207.

111. Uchida, K., Y. Nakayama, and M. Irie, *Thermally Irreversible Photochromic Systems. Reversible Photocyclization of 1,2-Bis(benzo[b]thiophen-3-yl)ethene Derivatives.* Bulletin of the Chemical Society of Japan, 1990. **63**(5): p. 1311-1315.

112. Morimoto, M. and M. Irie, *Photochromism of diarylethene single crystals: crystal structures and photochromic performance.* Chemical Communications, 2005(31): p. 3895-3905.

113. Miyasaka, H., S. Araki, A. Tabata, T. Nobuto, N. Malaga, and M. Irie, *Picosecond laser photolysis studies on photochromic reactions of 1,2-bis(2,4,5-trimethyl-3-thienyl)maleic anhydride in solutions.* Chemical Physics Letters, 1994. **230**(3): p. 249-254.

114. Tamai, N., T. Saika, T. Shimidzu, and M. Irie, *Femtosecond Dynamics of a Thiophene Oligomer with a Photoswitch by Transient Absorption Spectroscopy.* The Journal of Physical Chemistry, 1996. **100**(12): p. 4689-4692.

115. Shibata, K., K. Muto, S. Kobatake, and M. Irie, *Photocyclization/Cycloreversion Quantum Yields of Diarylethenes in Single Crystals.* The Journal of Physical Chemistry A, 2002. **106**(1): p. 209-214.

116. Yamada, T., K. Muto, S. Kobatake, and M. Irie, *Crystal Structure−Reactivity Correlation in Single-Crystalline Photochromism of 1,2-Bis(2-methyl-5-phenyl-3-thienyl)perfluorocyclopentene.* The Journal of Organic Chemistry, 2001. **66**(18): p. 6164-6168.

117. Tian, H. and S. Yang, *Recent progresses on diarylethene based photochromic switches.* Chemical Society Reviews, 2004. **33**(2): p. 85-97.

118. Nakamura, S., S. Yokojima, K. Uchida, T. Tsujioka, A. Goldberg, A. Murakami, K. Shinoda, M. Mikami, T. Kobayashi, S. Kobatake, K. Matsuda, and M. Irie, *Theoretical investigation on photochromic diarylethene: A short review.* Journal of Photochemistry and Photobiology A: Chemistry, 2008. **200**(1): p. 10-18.

119. Irie, M., T. Fukaminato, K. Matsuda, and S. Kobatake, *Photochromism of Diarylethene Molecules and Crystals: Memories, Switches, and Actuators.* Chemical Reviews, 2014. **114**(24): p. 12174-12277.

120. Cheng, H.-B., S. Zhang, E. Bai, X. Cao, J. Wang, J. Qi, J. Liu, J. Zhao, L. Zhang, and J. Yoon, *Future-Oriented Advanced Diarylethene Photoswitches: From Molecular Design to Spontaneous Assembly Systems.* Advanced Materials, 2022. **34**(16): p. 2108289.

121. Irie, M., *Diarylethenes for Memories and Switches.* Chemical Reviews, 2000. **100**(5): p. 1685-1716.

122. Saika, T., M. Irie, and T. Shimidzu, *Thiophene oligomers with a photoswitch.* Journal of the Chemical Society, Chemical Communications, 1994(18): p. 2123-2124.

123. Kudernac, T., N. Katsonis, W.R. Browne, and B.L. Feringa, *Nano-electronic switches: Light-induced switching of the conductance of molecular systems.* Journal of Materials Chemistry, 2009. **19**(39): p. 7168-7177.

124. Huang, X. and T. Li, *Recent progress in the development of molecular-scale electronics based on photoswitchable molecules.* Journal of Materials Chemistry C, 2020. **8**(3): p. 821-848.

125. Fuentes, N., A. Martín-Lasanta, L. Álvarez de Cienfuegos, M. Ribagorda, A. Parra, and J.M. Cuerva, *Organic-based molecular switches for molecular electronics.* Nanoscale, 2011. **3**(10): p. 4003-4014.

126. Chatterjee, S., S. Molla, J. Ahmed, and S. Bandyopadhyay, *Light-driven modulation of electrical conductance with photochromic switches: bridging photochemistry with optoelectronics.* Chemical Communications, 2023. **59**(85): p. 12685-12698.

127. Orgiu, E. and P. Samorì, *25th Anniversary Article: Organic Electronics Marries Photochromism: Generation of Multifunctional Interfaces, Materials, and Devices.* Advanced Materials, 2014. **26**(12): p. 1827-1845.

128. Wakayama, Y., R. Hayakawa, K. Higashiguchi, and K. Matsuda, *Photochromism for optically functionalized organic field-effect transistors: a comprehensive review.* Journal of Materials Chemistry C, 2020. **8**(32): p. 10956-10974.

129. Harvey, C.P. and J.D. Tovar, *Main-chain photochromic conducting polymers.* Polymer Chemistry, 2011. **2**(12): p. 2699-2706.

130. Tsujioka, T. and M. Irie, *Electrical functions of photochromic molecules.* Journal of Photochemistry and Photobiology C: Photochemistry Reviews, 2010. **11**(1): p. 1-14.

131. Lutsyk, P., J. Sworakowski, K. Janus, S. Nešpůrek, and A. Kochalska, *Photochromic Systems as Models for Opto-Electrical Switches.* Molecular Crystals and Liquid Crystals, 2010. **522**(1): p. 211/[511]-228/[528].

132. Ru, Y., Z. Shi, J. Zhang, J. Wang, B. Chen, R. Huang, G. Liu, and T. Yu, *Recent progress of photochromic materials towards photocontrollable devices.* Materials Chemistry Frontiers, 2021. **5**(21): p. 7737-7758.

133. Zhang, X., L. Hou, and P. Samorì, *Coupling carbon nanomaterials with photochromic molecules for the generation of optically responsive materials.* Nature Communications, 2016. **7**(1): p. 11118.

134. Zhao, Y., S. Ippolito, and P. Samorì, *Functionalization of 2D Materials with Photosensitive Molecules: From Light-Responsive Hybrid Systems to Multifunctional Devices.* Advanced Optical Materials, 2019. **7**(16): p. 1900286.

135. Fu, L.-N., B. Leng, Y.-S. Li, and X.-K. Gao, *Photoresponsive organic field-effect transistors involving photochromic molecules.* Chinese Chemical Letters, 2016. **27**(8): p. 1319-1329.

136. Xu, C., J. Zhang, W. Xu, and H. Tian, *Multifunctional organic field effect transistors constructed with photochromic molecules.* Materials Chemistry Frontiers, 2021. **5**(3): p. 1060-1075.

137. Shen, Q., Y. Cao, S. Liu, M.L. Steigerwald, and X. Guo, *Conformation-Induced Electrostatic Gating of the Conduction of Spiropyran-Coated Organic Thin-Film Transistors.* The Journal of Physical Chemistry C, 2009. **113**(24): p. 10807-10812.

138. Hassan, S.Z., J. Kwon, J. Lee, H.R. Sim, S. An, S. Lee, and D.S. Chung, *Photophore-Anchored Molecular Switch for High-Performance Nonvolatile Organic Memory Transistor.* Advanced Science, 2024: p. 2401482.

139. Yin, Z.Y., J. Yang, X. Gao, Z.D. Zhang, J.T. Ye, Z.N. Lu, C. Qian, Y.N. Zhong, J.L. Xu, and S.D. Wang, *Low-Voltage Electronic Dosimeter for Portable UV Exposure Monitoring.* IEEE Electron Device Letters, 2024: p. 1-4.

140. Li, H., Z. Shangguan, T. Li, Z.-Y. Zhang, D. Ji, and W. Hu, *Arylazopyrazole-modulated stable dual-mode phototransistors.* Science Advances, 2024. **10**(23): p. eado2329.

141. Börjesson, K., M. Herder, L. Grubert, D.T. Duong, A. Salleo, S. Hecht, E. Orgiu, and P. Samorì, *Optically switchable transistors comprising a hybrid photochromic molecule/n-type organic active layer.* Journal of Materials Chemistry C, 2015. **3**(16): p. 4156-4161.

142. Rekab, W., T. Leydecker, L. Hou, H. Chen, M. Kirkus, C. Cendra, M. Herder, S. Hecht, A. Salleo, I. McCulloch, E. Orgiu, and P. Samorì, *Phototuning Selectively Hole and Electron Transport in Optically Switchable Ambipolar Transistors.* Advanced Functional Materials, 2020. **30**(5): p. 1908944.

143. Arlt, M., A. Scheffler, I. Suske, M. Eschner, T.P.I. Saragi, J. Salbeck, and T. Fuhrmann-Lieker, *Bipolar redox behaviour, field-effect mobility and transistor switching of the low-molecular azo glass AZOPD.* Physical Chemistry Chemical Physics, 2010. **12**(41): p. 13828-13834.

144. Yoshida, M., K. Suemori, S. Uemura, S. Hoshino, N. Takada, T. Kodzasa, and T. Kamata, *Development of Field-Effect Transistor-Type Photorewritable Memory Using Photochromic Interface Layer.* Japanese Journal of Applied Physics, 2010. **49**: p. 04DK09.

145. Orgiu, E., N. Crivillers, M. Herder, L. Grubert, M. Pätzel, J. Frisch, E. Pavlica, D.T. Duong, G. Bratina, A. Salleo, N. Koch, S. Hecht, and P. Samorì, *Optically switchable transistor via energy-level phototuning in a bicomponent organic semiconductor.* Nature Chemistry, 2012. **4**(8): p. 675-679.

146. Gemayel, M.E., K. Börjesson, M. Herder, D.T. Duong, J.A. Hutchison, C. Ruzié, G. Schweicher, A. Salleo, Y. Geerts, S. Hecht, E. Orgiu, and P. Samorì, *Optically switchable transistors by simple incorporation of photochromic systems into small-molecule semiconducting matrices.* Nature Communications, 2015. **6**(1): p. 6330.

147. Leydecker, T., M. Herder, E. Pavlica, G. Bratina, S. Hecht, E. Orgiu, and P. Samorì, *Flexible non-volatile optical memory thin-film transistor device with over 256 distinct levels based on an organic bicomponent blend.* Nature Nanotechnology, 2016. **11**(9): p. 769-775.

148. Hou, L., X. Zhang, G.F. Cotella, G. Carnicella, M. Herder, B.M. Schmidt, M. Pätzel, S. Hecht, F. Cacialli, and P. Samorì, *Optically switchable organic light-emitting transistors.* Nature Nanotechnology, 2019. **14**(4): p. 347-353.

149. Carroli, M., D.T. Duong, E. Buchaca-Domingo, A. Liscio, K. Börjesson, M. Herder, V. Palermo, S. Hecht, N. Stingelin, A. Salleo, E. Orgiu, and P. Samorì, *The Role of Morphology in Optically Switchable Transistors Based on a Photochromic Molecule/p-Type Polymer Semiconductor Blend.* Advanced Functional Materials, 2020. **30**(20): p. 1907507.

150. Carroli, M., A.G. Dixon, M. Herder, E. Pavlica, S. Hecht, G. Bratina, E. Orgiu, and P. Samorì, *Multiresponsive Nonvolatile Memories Based on Optically Switchable Ferroelectric Organic Field-Effect Transistors.* Advanced Materials, 2021. **33**(14): p. 2007965.

151. Shi, Q., D. Liu, S. Dai, and J. Huang, *A Wavelength-Tunable Multi-Functional Transistor with Visible-Light Detection and Inverse Photomemory for Logic Gate and Retina Emulation.* Advanced Optical Materials, 2021. **9**(20): p. 2100654.

152. Yu, S.H., S.Z. Hassan, S. Lee, B. Lim, and D.S. Chung, *Boosting photoprogramming performance of molecular-switch-embedded organic transistors via structural optimization of polymer semiconductors.* Journal of Materials Chemistry C, 2023. **11**(4): p. 1560-1568.

153. Hassan, S.Z., S.H. Yu, C. So, D. Moon, and D.S. Chung, *End-Functionalization of Diarylethene for Opto-Electronic Switching with High Fatigue Resistance.* Chemistry of Materials, 2021. **33**(1): p. 403-412.

154. Chen, Y., H. Wang, H. Chen, W. Zhang, S. Xu, M. Pätzel, C. Ma, C. Wang, I. McCulloch, S. Hecht, and P. Samorì, *Quasi-1D Polymer Semiconductor–Diarylethene Blends: High Performance Optically Switchable Transistors.* Advanced Functional Materials, 2023. **33**(46): p. 2305494.

155. Qian, Y., W. Li, W. Li, X. Xu, Z. Lin, L. Xie, M. Yi, and W. Huang, *Reversible Optical and Electrical Switching of Air-Stable OFETs for Nonvolatile Multi-Level Memories and Logic Gates.* Advanced Electronic Materials, 2015. **1**(12): p. 1500230.

156. Hou, L., T. Leydecker, X. Zhang, W. Rekab, M. Herder, C. Cendra, S. Hecht, I. McCulloch, A. Salleo, E. Orgiu, and P. Samorì, *Engineering Optically Switchable Transistors with Improved Performance by Controlling Interactions of Diarylethenes in Polymer Matrices.* Journal of the American Chemical Society, 2020. **142**(25): p. 11050-11059.

157. Hassan, S.Z., J. Song, S.H. Yu, and D.S. Chung, *Critical Factors of Diarylethene for a High-Performance Photoprogrammable Polymer Transistor: Crystallographic Compatibility, Quantum Yield, and Fatigue Resistance.* Chemistry of Materials, 2021. **33**(18): p. 7546-7557.

158. Tseng, C.-W., D.-C. Huang, and Y.-T. Tao, *Electric Bistability Induced by Incorporating Self-Assembled Monolayers/aggregated Clusters of Azobenzene Derivatives in Pentacene-Based Thin-Film Transistors.* ACS Applied Materials & Interfaces, 2012. **4**(10): p. 5483-5491.

159. Smithson, C.S., Y. Wu, T. Wigglesworth, and S. Zhu, *A More Than Six Orders of Magnitude UV-Responsive Organic Field-Effect Transistor Utilizing a Benzothiophene Semiconductor and Disperse Red 1 for Enhanced Charge Separation.* Advanced Materials, 2015. **27**(2): p. 228-233.

160. Chen, X., S. Zheng, B. Liang, X. Wu, D. Wang, Y. Dong, W. Huang, Y. Liu, X. Yu, J. Shen, S. Feng, C.-C. Chang, and W. Huang, *Realizing a Brain-Like Transistor Memory with Triple Data-Storage Modes by One Single Smart Molecular Dopant in the Dielectric Layer.* Chemistry of Materials, 2023. **35**(7): p. 2808-2819.

161. Yuan, S.-H., D.-C. Huang, and Y.-T. Tao, *Photochromic Dithienylethene Monolayer-Modified Gold Nanoparticles as a Tunable Floating Gate in the Fabrication of Nonvolatile Organic Memory.* ACS Applied Materials & Interfaces, 2022. **14**(5): p. 7102-7108.

162. Yu, S.H., S.Z. Hassan, G.-H. Nam, S. An, B. Kang, and D.S. Chung, *Consideration of Azobenzene-Based Self-Assembled Monolayer Deposition Conditions for Maximizing Optoelectronic Switching Performances.* Chemistry of Materials, 2021. **33**(15): p. 5991-6002.

163. Kurokawa, Y., R. Hayakawa, S. Shimada, K. Higashiguchi, Y. Noguchi, K. Matsuda, and Y. Wakayama, *Ambipolar carrier transport in an optically controllable diarylethene thin film transistor.* Organic Electronics, 2019. **64**: p. 205-208.

164. Kurokawa, Y., R. Hayakawa, S. Shimada, K. Tanaka, K. Higashiguchi, Y. Noguchi, K. Matsuda, and Y. Wakayama, *Photocontrollable ambipolar transistors with π-conjugated diarylethene photochromic channels.* Japanese Journal of Applied Physics, 2019. **58**: p. SDDH03.

165. Mosciatti, T., M.G. del Rosso, M. Herder, J. Frisch, N. Koch, S. Hecht, E. Orgiu, and P. Samorì, *Light-Modulation of the Charge Injection in a Polymer Thin-Film Transistor by Functionalizing the Electrodes with Bistable Photochromic Self-Assembled Monolayers.* Advanced Materials, 2016. **28**(31): p. 6606-6611.

166. Crivillers, N., E. Orgiu, F. Reinders, M. Mayor, and P. Samorì, *Optical Modulation of the Charge Injection in an Organic Field-Effect Transistor Based on Photochromic Self-Assembled-Monolayer-Functionalized Electrodes.* Advanced Materials, 2011. **23**(12): p. 1447-1452.

167. Raimondo, C., N. Crivillers, F. Reinders, F. Sander, M. Mayor, and P. Samorì, *Optically switchable organic field-effect transistors based on photoresponsive gold nanoparticles blended with poly(3-hexylthiophene).* Proceedings of the National Academy of Sciences, 2012. **109**(31): p. 12375-12380.

168. Chen, H., N. Cheng, W. Ma, M. Li, S. Hu, L. Gu, S. Meng, and X. Guo, *Design of a Photoactive Hybrid Bilayer Dielectric for Flexible Nonvolatile Organic Memory Transistors.* ACS Nano, 2016. **10**(1): p. 436-445.

169. Zhang, H., H. Chen, W. Ma, J. Hui, S. Meng, W. Xu, D. Zhu, and X. Guo, *Photocontrol of charge injection/extraction at electrode/semiconductor interfaces for high-photoresponsivity organic transistors.* Journal of Materials Chemistry C, 2016. **4**(23): p. 5289-5296.

170. Tian, J., L. Fu, Z. Liu, H. Geng, Y. Sun, G. Lin, X. Zhang, G. Zhang, and D. Zhang, *Optically Tunable Field Effect Transistors with Conjugated Polymer Entailing Azobenzene Groups in the Side Chains.* Advanced Functional Materials, 2019. **29**(12): p. 1807176.

171. Ishiguro, Y., R. Hayakawa, T. Yasuda, T. Chikyow, and Y. Wakayama, *Unique Device Operations by Combining Optical-Memory Effect and Electrical-Gate Modulation in a*

Photochromism-Based Dual-Gate Transistor. ACS Applied Materials & Interfaces, 2013. **5**(19): p. 9726-9731.

172. Ishiguro, Y., M. Frigoli, R. Hayakawa, T. Chikyow, and Y. Wakayama, *Improved thermal stability in photochromism-based optically controllable organic thin film transistor.* Organic Electronics, 2014. **15**(9): p. 1891-1895.

173. Ishiguro, Y., R. Hayakawa, T. Chikyow, and Y. Wakayama, *Optically Controllable Dual-Gate Organic Transistor Produced via Phase Separation between Polymer Semiconductor and Photochromic Spiropyran Molecules.* ACS Applied Materials & Interfaces, 2014. **6**(13): p. 10415-10420.

174. Ma, J., J. Tian, Z. Liu, D. Shi, X. Zhang, G. Zhang, and D. Zhang, *Multi-Stimuli-Responsive Field-Effect Transistor with Conjugated Polymer Entailing Spiropyran in the Side Chains.* CCS Chemistry, 2020. **2**(2): p. 632-641.

175. Ishiguro, Y., R. Hayakawa, T. Chikyow, and Y. Wakayama, *Optical switching of carrier transport in polymeric transistors with photochromic spiropyran molecules.* Journal of Materials Chemistry C, 2013. **1**(17): p. 3012-3016.

176. Yang, Y., A.P. Sandra, A. Idström, C. Schäfer, M. Andersson, L. Evenäs, and K. Börjesson, *Electroactive Covalent Organic Framework Enabling Photostimulus-Responsive Devices.* Journal of the American Chemical Society, 2022. **144**(35): p. 16093-16100.

177. Tian, J., Z. Liu, C. Wu, W. Jiang, L. Chen, D. Shi, X. Zhang, G. Zhang, and D. Zhang, *Simultaneous Incorporation of Two Types of Azo-Groups in the Side Chains of a Conjugated D–A Polymer for Logic Control of the Semiconducting Performance by Light Irradiation.* Advanced Materials, 2021. **33**(8): p. 2005613.

178. Chen, Y., C. Li, X. Xu, M. Liu, Y. He, I. Murtaza, D. Zhang, C. Yao, Y. Wang, and H. Meng, *Thermal and Optical Modulation of the Carrier Mobility in OTFTs Based on an Azo-anthracene Liquid Crystal Organic Semiconductor.* ACS Applied Materials & Interfaces, 2017. **9**(8): p. 7305-7314.

179. Li, M., J. Zheng, X. Wang, R. Yu, Y. Wang, Y. Qiu, X. Cheng, G. Wang, G. Chen, K. Xie, and J. Tang, *Light-responsive self-strained organic semiconductor for large flexible OFET sensing array.* Nature Communications, 2022. **13**(1): p. 4912.

180. Karimi-Alavijeh, H., F. Panahi, and A. Gharavi, *Photo-switching effect in stilbene organic field effect transistors.* Journal of Applied Physics, 2014. **115**(9): p. 093706.

181. Tian, J., Z. Liu, W. Jiang, D. Shi, L. Chen, X. Zhang, G. Zhang, C.-a. Di, and D. Zhang, *A Conjugated Polymer Containing Arylazopyrazole Units in the Side Chains for Field-Effect Transistors Optically Tunable by Near Infra-Red Light.* Angewandte Chemie International Edition, 2020. **59**(33): p. 13844-13851.

182. Cao, M., Z. Cai, X. Chen, K. Yi, and D. Wei, *Photo-switchable field-effect transistors based on two-dimensional stilbene oligomer crystals.* Journal of Materials Chemistry C, 2017. **5**(37): p. 9597-9601.

183. Shen, Q., L. Wang, S. Liu, Y. Cao, L. Gan, X. Guo, M.L. Steigerwald, Z. Shuai, Z. Liu, and C. Nuckolls, *Photoactive Gate Dielectrics.* Advanced Materials, 2010. **22**(30): p. 3282-3287.

184. Lutsyk, P., K. Janus, J. Sworakowski, G. Generali, R. Capelli, and M. Muccini, *Photoswitching of an n-Type Organic Field Effect Transistor by a Reversible Photochromic Reaction in the Dielectric Film.* The Journal of Physical Chemistry C, 2011. **115**(7): p. 3106-3114.

185. Lutsyk, P., K. Janus, J. Sworakowski, A. Kochalska, and S. Nešpůrek, *Kinetic study of light-driven processes in photochromic dye-doped polymers used as gate insulators in photoswitchable organic field effect transistors.* Chemical Physics, 2012. **404**: p. 22-27.

186. Zhang, H., J. Hui, H. Chen, J. Chen, W. Xu, Z. Shuai, D. Zhu, and X. Guo, *Synergistic Photomodulation of Capacitive Coupling and Charge Separation Toward Functional Organic Field-Effect Transistors with High Responsivity.* Advanced Electronic Materials, 2015. **1**(9): p. 1500159.

187. Zhang, H., X. Guo, J. Hui, S. Hu, W. Xu, and D. Zhu, *Interface Engineering of Semiconductor/Dielectric Heterojunctions toward Functional Organic Thin-Film Transistors.* Nano Letters, 2011. **11**(11): p. 4939-4946.

188. Liu, Y., Y. Yang, D. Shi, M. Xiao, L. Jiang, J. Tian, G. Zhang, Z. Liu, X. Zhang, and D. Zhang, *Photo-/Thermal-Responsive Field-Effect Transistor upon Blending Polymeric Semiconductor with Hexaarylbiimidazole toward Photonically Programmable and Thermally Erasable Memory Device.* Advanced Materials, 2019. **31**(44): p. 1902576.

189. Hayakawa, R., K. Higashiguchi, K. Matsuda, T. Chikyow, and Y. Wakayama, *Optically and Electrically Driven Organic Thin Film Transistors with Diarylethene Photochromic Channel Layers.* ACS Applied Materials & Interfaces, 2013. **5**(9): p. 3625-3630.

190. Hayakawa, R., M. Petit, K. Higashiguchi, K. Matsuda, T. Chikyow, and Y. Wakayama, *Interface engineering for improving optical switching in a diarylethene-channel transistor.* Organic Electronics, 2015. **21**: p. 149-154.

191. Tsuruoka, T., R. Hayakawa, K. Kobashi, K. Higashiguchi, K. Matsuda, and Y. Wakayama, *Laser Patterning of Optically Reconfigurable Transistor Channels in a Photochromic Diarylethene Layer.* Nano Letters, 2016. **16**(12): p. 7474-7480.

192. Mumyatov, A.V., L.A. Frolova, L.G. Gutsev, E.A. Khakina, N.A. Sanina, S.M. Aldoshin, and P.A. Troshin, *A light-triggered molecular switch for an efficient OFET-based organic memory device.* Journal of Materials Chemistry C, 2023. **11**(3): p. 963-969.

193. Frolova, L.A., A.A. Rezvanova, B.S. Lukyanov, N.A. Sanina, P.A. Troshin, and S.M. Aldoshin, *Design of rewritable and read-only non-volatile optical memory elements using photochromic spiropyran-based salts as light-sensitive materials.* Journal of Materials Chemistry C, 2015. **3**(44): p. 11675-11680.

194. Frolova, L.A., P.A. Troshin, D.K. Susarova, A.V. Kulikov, N.A. Sanina, and S.M. Aldoshin, *Photoswitchable organic field-effect transistors and memory elements comprising an interfacial photochromic layer.* Chemical Communications, 2015. **51**(28): p. 6130-6132.

195. Frolova, L.A., A.A. Rezvanova, V.Z. Shirinian, A.G. Lvov, A.V. Kulikov, M.M. Krayushkin, and P.A. Troshin, *OFET-Based Memory Devices Operating via Optically and Electrically Modulated Charge Separation between the Semiconductor and 1,2-bis(Hetaryl)ethene Dielectric Layers.* Advanced Electronic Materials, 2016. **2**(3): p. 1500219.

196. Jeong, Y.J., E.J. Yoo, L.H. Kim, S. Park, J. Jang, S.H. Kim, S.W. Lee, and C.E. Park, *Light-responsive spiropyran based polymer thin films for use in organic field-effect transistor memories.* Journal of Materials Chemistry C, 2016. **4**(23): p. 5398-5406.

197. Rezvanova, A.A., L.A. Frolova, and P.A. Troshin, *Design of optical memory elements based on n-type organic field-effect transistors comprising a light-sensitive spirooxazine layer.* Mendeleev Communications, 2016. **26**(1): p. 26-28.

198. Leshanskaya, L.I., I.V. Klimovich, D.D. Dashitsyrenova, L.A. Frolova, E.S. Ershova, V.A. Sergeeva, V.Y. Tabakov, S.V. Kostyuk, K.A. Lyssenko, and P.A. Troshin, *Dibenzoindigo: A Nature-Inspired Biocompatible Semiconductor Material for Sustainable Organic Electronics.* Advanced Optical Materials, 2017. **5**(9): p. 1601033.

199. Dashitsyrenova, D.D., A.G. Lvov, L.A. Frolova, A.V. Kulikov, N.N. Dremova, V.Z. Shirinian, S.M. Aldoshin, M.M. Krayushkin, and P.A. Troshin, *Molecular structure–electrical performance relationship for OFET-based memory elements comprising unsymmetrical photochromic diarylethenes.* Journal of Materials Chemistry C, 2019. **7**(23): p. 6889-6894.

200. Obrezkov, F.A., D.D. Dashitsyrenova, A.G. Lvov, D.Y. Volyniuk, V.Z. Shirinian, P. Stadler, J.V. Grazulevicius, N.S. Sariciftci, S.M. Aldoshin, M.M. Krayushkin, and P.A. Troshin, *Light-Sensitive Material Structure–Electrical Performance Relationship for Optical Memory Transistors Incorporating Photochromic Dihetarylethenes.* ACS Applied Materials & Interfaces, 2020. **12**(29): p. 32987-32993.

201. Kang, M., A.-N. Cha, S.-A. Lee, S.-K. Lee, S. Bae, D.-Y. Jeon, J.-M. Hong, S. Fabiano, M. Berggren, and T.-W. Kim, *Light-sensitive charge storage medium with spironaphthooxazine molecule-polymer blends for dual-functional organic phototransistor memory.* Organic Electronics, 2020. **78**: p. 105554.

202. Lv, J.-J., X. Gao, L.-X. Zhang, Y. Feng, J.-L. Xu, J. Xiao, B. Dong, and S.-D. Wang, *Visible-blind UV monitoring with a photochromic charge trapping layer in organic field-effect transistors.* Applied Physics Letters, 2019. **115**(11): p. 113302.

203. Smithson, C.S., D. Ljubic, Y. Wu, and S. Zhu, *The effect of azobenzene derivatives on UV-responsive organic thin-film transistors with a 2,7-dipentylbenzo[b]benzo[4,5]thieno[2,3-d]thiophene semiconductor.* Journal of Materials Chemistry C, 2015. **3**(31): p. 8090-8096.

204. Lee, K.E., J.U. Lee, D.G. Seong, M.-K. Um, and W. Lee, *Highly Sensitive Ultraviolet Light Sensor Based on Photoactive Organic Gate Dielectrics with an Azobenzene Derivative.* The Journal of Physical Chemistry C, 2016. **120**(40): p. 23172-23179.

205. Tuktarov, A.R., R.B. Salikhov, A.A. Khuzin, I.N. Safargalin, I.N. Mullagaliev, O.V. Venidiktova, T.M. Valova, V.A. Barachevsky, and U.M. Dzhemilev, *Optically controlled field effect transistors based on photochromic spiropyran and fullerene C60 films.* Mendeleev Communications, 2019. **29**(2): p. 160-162.

206. Tuktarov, A.R., R.B. Salikhov, A.A. Khuzin, N.R. Popod'ko, I.N. Safargalin, I.N. Mullagaliev, and U.M. Dzhemilev, *Photocontrolled organic field effect transistors based on the fullerene C60 and spiropyran hybrid molecule.* RSC Advances, 2019. **9**(13): p. 7505-7508.

207. Khuzin, A.A., A.R. Tuktarov, O.V. Venidiktova, V.A. Barachevsky, I.N. Mullagaliev, T.R. Salikhov, R.B. Salikhov, L.M. Khalilov, L.L. Khuzina, and U.M. Dzhemilev, *Hybrid Molecules Based on Fullerene C60 and Dithienylethenes. Synthesis and Photochromic Properties. Optically Controlled Organic Field-Effect Transistors.* Photochemistry and Photobiology, 2022. **98**(4): p. 815-822.

208. Wu, R.-J., Y.-L. Hsu, W.-Y. Chou, and H.-L. Cheng, *Enhancing functionalities of organic ultraviolet-visible phototransistors incorporating spiropyran-merocyanine photochromic materials.* Journal of Materials Chemistry A, 2021. **9**(39): p. 22522-22532.

209. Senanayak, S.P., V.K. Sangwan, J.J. McMorrow, K. Everaerts, Z. Chen, A. Facchetti, M.C. Hersam, T.J. Marks, and K.S. Narayan, *Self-Assembled Photochromic Molecular Dipoles for High-Performance Polymer Thin-Film Transistors.* ACS Applied Materials & Interfaces, 2018. **10**(25): p. 21492-21498.

210. Scheuermann, A.M., H. Wakidi, A.T. Lill, S. Oh, L.C. Llanes, C.A. D'Ambra, S. Antoine, M. Wang, M.L. Chabinyc, T.-Q. Nguyen, J. Read de Alaniz, and C.M. Bates, *Multiwavelength Photodetectors Based on an Azobenzene Polymeric Ionic Liquid.* ACS Applied Polymer Materials, 2021. **3**(10): p. 5125-5133.

211. Fu, L.-N., B. Leng, Y.-S. Li, and X.-K. Gao, *Photoresponsive n-channel organic field-effect transistors based on a tri-component active layer.* Chinese Chemical Letters, 2018. **29**(1): p. 175-178.

212. Liu, C.-F., H. Lin, S.-S. Li, H. Xie, J.-L. Zhang, D.-Z. Ji, Y. Yan, X. Liu, and W.-Y. Lai, *Smart Responsive Photoelectric Organic Modulator Integrated with Versatile Optoelectronic Characteristics.* Advanced Functional Materials, 2022. **32**(17): p. 2111276.

213. Bardavid, Y., I. Goykhman, D. Nozaki, G. Cuniberti, and S. Yitzchaik, *Dipole Assisted Photogated Switch in Spiropyran Grafted Polyaniline Nanowires.* The Journal of Physical Chemistry C, 2011. **115**(7): p. 3123-3128.

214. Li, Y., H. Zhang, C. Qi, and X. Guo, *Light-driven photochromism-induced reversible switching in P3HT–spiropyran hybrid transistors.* Journal of Materials Chemistry, 2012. **22**(10): p. 4261-4265.

215. Waldrip, M., O.D. Jurchescu, D.J. Gundlach, and E.G. Bittle, *Contact Resistance in Organic Field-Effect Transistors: Conquering the Barrier.* Advanced Functional Materials, 2020. **30**(20): p. 1904576.

216. Shi, Y., J. Liu, Y. Hu, W. Hu, and L. Jiang, *Effect of contact resistance in organic field-effect transistors.* Nano Select, 2021. **2**(9): p. 1661-1681.

217. Karki, A., G.-J.A.H. Wetzelaer, G.N.M. Reddy, V. Nádaždy, M. Seifrid, F. Schauer, G.C. Bazan, B.F. Chmelka, P.W.M. Blom, and T.-Q. Nguyen, *Unifying Energetic Disorder from Charge Transport and Band Bending in Organic Semiconductors.* Advanced Functional Materials, 2019. **29**(20): p. 1901109.

218. Xiao, M., X. Ren, K. Ji, S. Chung, X. Shi, J. Han, Z. Yao, X. Tao, S.J. Zelewski, M. Nikolka, Y. Zhang, Z. Zhang, Z. Wang, N. Jay, I. Jacobs, W. Wu, H. Yu, Y. Abdul Samad, S.D. Stranks, B. Kang, K. Cho, J. Xie, H. Yan, S. Chen, and H. Sirringhaus, *Achieving ideal transistor characteristics in conjugated polymer semiconductors.* Science Advances, 2023. **9**(22): p. eadg8659.

219. Bronstein, H., C.B. Nielsen, B.C. Schroeder, and I. McCulloch, *The role of chemical design in the performance of organic semiconductors.* Nature Reviews Chemistry, 2020. **4**(2): p. 66-77.

220. Veres, J., S.D. Ogier, S.W. Leeming, D.C. Cupertino, and S. Mohialdin Khaffaf, *Low-k Insulators as the Choice of Dielectrics in Organic Field-Effect Transistors.* Advanced Functional Materials, 2003. **13**(3): p. 199-204.

221. Richards, T., M. Bird, and H. Sirringhaus, *A quantitative analytical model for static dipolar disorder broadening of the density of states at organic heterointerfaces.* The Journal of Chemical Physics, 2008. **128**(23): p. 234905.

222. Merari Masillamani, A., E. Orgiu, and P. Samorì, *Effect of the molecular weight of the polymer gate dielectric on the performances of solution-processed ambipolar OTFTs.* Journal of Materials Chemistry C, 2013. **1**(46): p. 7725-7730.

223. Yan, H., Z. Chen, Y. Zheng, C. Newman, J.R. Quinn, F. Dötz, M. Kastler, and A. Facchetti, *A high-mobility electron-transporting polymer for printed transistors.* Nature, 2009. **457**(7230): p. 679-686.

224. Hulea, I.N., S. Fratini, H. Xie, C.L. Mulder, N.N. Iossad, G. Rastelli, S. Ciuchi, and A.F. Morpurgo, *Tunable Fröhlich polarons in organic single-crystal transistors.* Nature Materials, 2006. **5**(12): p. 982-986.

225. Lee, H., C. Park, D.H. Sin, J.H. Park, and K. Cho, *Recent Advances in Morphology Optimization for Organic Photovoltaics.* Advanced Materials, 2018. **30**(34): p. 1800453.

226. Zhao, F., C. Wang, and X. Zhan, *Morphology Control in Organic Solar Cells.* Advanced Energy Materials, 2018. **8**(28): p. 1703147.

227. Zhi, D., E. Zhang, B. Zhang, and F. Zhang, *Advances in morphology control of organic semiconductor enabled organic transistor-based chemical sensors.* Molecular Systems Design & Engineering, 2022. **7**(6): p. 553-568.

228. Riera-Galindo, S., F. Leonardi, R. Pfattner, and M. Mas-Torrent, *Organic Semiconductor/Polymer Blend Films for Organic Field-Effect Transistors.* Advanced Materials Technologies, 2019. **4**(9): p. 1900104.

229. Virkar, A.A., S. Mannsfeld, Z. Bao, and N. Stingelin, *Organic Semiconductor Growth and Morphology Considerations for Organic Thin-Film Transistors.* Advanced Materials, 2010. **22**(34): p. 3857-3875.

230. Rivnay, J., S.C.B. Mannsfeld, C.E. Miller, A. Salleo, and M.F. Toney, *Quantitative Determination of Organic Semiconductor Microstructure from the Molecular to Device Scale.* Chemical Reviews, 2012. **112**(10): p. 5488-5519.

231. Sørensen, M.K., A.S. Gertsen, R.P. Fornari, B. Zhou, X. Zhang, P.U. Jepsen, E. Stanzani, S. Yun, M. Fernández Castro, M. Schwartzkopf, A. Koutsioubas, P. de Silva, M. Espindola-Rodriguez, L.T. Kuhn, and J.W. Andreasen, *Manipulating Organic Semiconductor Morphology with Visible Light.* Advanced Functional Materials, 2023. **33**(10): p. 2212835.

232. Chae, S., A. Yi, H.H. Lee, J. Choi, and H.J. Kim, *Laser-induced orientation transformation of a conjugated polymer thin film with enhanced vertical charge transport.* Journal of Materials Chemistry C, 2018. **6**(35): p. 9374-9382.

233. Pernstich, K.P., S. Haas, D. Oberhoff, C. Goldmann, D.J. Gundlach, B. Batlogg, A.N. Rashid, and G. Schitter, *Threshold voltage shift in organic field effect transistors by dipole monolayers on the gate insulator.* Journal of Applied Physics, 2004. **96**(11): p. 6431-6438.

234. Kobayashi, S., T. Nishikawa, T. Takenobu, S. Mori, T. Shimoda, T. Mitani, H. Shimotani, N. Yoshimoto, S. Ogawa, and Y. Iwasa, *Control of carrier density by self-assembled monolayers in organic field-effect transistors.* Nature Materials, 2004. **3**(5): p. 317-322.

235. Zschieschang, U., F. Ante, M. Schlörholz, M. Schmidt, K. Kern, and H. Klauk, *Mixed Self-Assembled Monolayer Gate Dielectrics for Continuous Threshold Voltage Control in Organic Transistors and Circuits.* Advanced Materials, 2010. **22**(40): p. 4489-4493.

236. Jia, C., J. Wang, C. Yao, Y. Cao, Y. Zhong, Z. Liu, Z. Liu, and X. Guo, *Conductance Switching and Mechanisms in Single-Molecule Junctions.* Angewandte Chemie International Edition, 2013. **52**(33): p. 8666-8670.

237. Jia, C., A. Migliore, N. Xin, S. Huang, J. Wang, Q. Yang, S. Wang, H. Chen, D. Wang, B. Feng, Z. Liu, G. Zhang, D.-H. Qu, H. Tian, M.A. Ratner, H.Q. Xu, A. Nitzan, and X. Guo, *Covalently bonded single-molecule junctions with stable and reversible photoswitched conductivity.* Science, 2016. **352**(6292): p. 1443-1445.

238. Kim, Y., T.J. Hellmuth, D. Sysoiev, F. Pauly, T. Pietsch, J. Wolf, A. Erbe, T. Huhn, U. Groth, U.E. Steiner, and E. Scheer, *Charge Transport Characteristics of Diarylethene Photoswitching Single-Molecule Junctions.* Nano Letters, 2012. **12**(7): p. 3736-3742.

239. Huang, J., Q. Li, H. Su, and J. Yang, *Transport properties through diarylethene derivatives between carbon nanotube electrodes: A theoretical study.* Chemical Physics Letters, 2009. **479**(1): p. 120-124.

240. Odell, A., A. Delin, B. Johansson, I. Rungger, and S. Sanvito, *Investigation of the Conducting Properties of a Photoswitching Dithienylethene Molecule.* ACS Nano, 2010. **4**(5): p. 2635-2642.

241. Motta, C., M.I. Trioni, G.P. Brivio, and K.L. Sebastian, *Conductance of a photochromic molecular switch with graphene leads.* Physical Review B, 2011. **84**(11): p. 113408.

242. Huang, X., D. Ji, H. Fuchs, W. Hu, and T. Li, *Recent Progress in Organic Phototransistors: Semiconductor Materials, Device Structures and Optoelectronic Applications.* ChemPhotoChem, 2020. **4**(1): p. 9-38.

243. del Valle, M., R. Gutiérrez, C. Tejedor, and G. Cuniberti, *Tuning the conductance of a molecular switch.* Nature Nanotechnology, 2007. **2**(3): p. 176-179.

244. Ghosh, S., P. Roy, A. Pramanik, and P. Sarkar, *Photoinduced conductance and carrier switching in homoannulene ester derivatives: A theoretical exploration.* Computational and Theoretical Chemistry, 2024. **1233**: p. 114509.

245. Nemnes, G.A. and C. Visan, *Electron transport properties of fulgide-based photochromic switches.* RSC Advances, 2015. **5**(33): p. 26438-26442.

246. Tsuji, Y. and R. Hoffmann, *Frontier Orbital Control of Molecular Conductance and its Switching.* Angewandte Chemie International Edition, 2014. **53**(16): p. 4093-4097.

247. Xia, C.-J., K. Gao, D.-H. Zhang, M. Yang, and F.-L. Feng, *Conductance switching in single light-sensitive molecular device with carbon nanotube electrodes.* Journal of Applied Physics, 2014. **116**(8): p. 083704.

248. You, J., J. He, M.-M. Yin, L.-M. Tang, K.-Q. Chen, and Z.-Q. Fan, *The E–Z photo-isomerization switching behavior in single molecular device with carbon nanotube electrodes.* Computational Materials Science, 2012. **65**: p. 203-206.

249. Zhao, P., P. Wang, Z. Zhang, C. Fang, Y. Wang, Y. Zhai, and D. Liu, *Electronic transport properties of a diarylethene-based molecular switch with single-walled carbon nanotube electrodes: The effect of chirality.* Solid State Communications, 2009. **149**(23): p. 928-931.

250. Xu, G., X. Tan, and D. Ren, *Thermal Spin Transport Properties in Diarylethene-Based Molecule Devices.* Advances in Condensed Matter Physics, 2022. **2022**: p. 2149190.

251. Olsen, S.T., T. Hansen, M.B. Nielsen, M.A. Ratner, and K.V. Mikkelsen, *Stepwise "Dark Photoswitching" of Photochromic Dimers in a Junction.* The Journal of Physical Chemistry C, 2017. **121**(6): p. 3163-3170.

252. Xia, C.-J., A.-Y. Yang, B.-Q. Zhang, Y.H. Su, Z.-Y. Tu, and J. Wang, *Effect of the anchoring groups on the switching behaviour of the dihydroazulene/vinylheptafulvene molecular junction with zigzag-edged graphene nanoribbons electrodes.* Molecular Physics, 2017. **115**(14): p. 1606-1613.

253. Dulić, D., S.J. van der Molen, T. Kudernac, H.T. Jonkman, J.J.D. de Jong, T.N. Bowden, J. van Esch, B.L. Feringa, and B.J. van Wees, *One-Way Optoelectronic Switching of Photochromic Molecules on Gold.* Physical Review Letters, 2003. **91**(20): p. 207402.

254. Ghasemi, S., L. Ornago, Z. Liasi, M.B. Johansen, T.J. von Buchwald, A.E. Hillers-Bendtsen, S. van der Poel, H. Hölzel, Z. Wang, F.M. Amombo Noa, L. Öhrström, K.V. Mikkelsen, H.S.J. van der Zant, S. Lara-Avila, and K. Moth-Poulsen, *Exploring the impact of select anchor groups for norbornadiene/quadricyclane single-molecule switches.* Journal of Materials Chemistry C, 2023. **11**(44): p. 15412-15418.

255. He, J., F. Chen, P.A. Liddell, J. Andréasson, S.D. Straight, D. Gust, T.A. Moore, A.L. Moore, J. Li, O.F. Sankey, and S.M. Lindsay, *Switching of a photochromic molecule on gold electrodes: single-molecule measurements.* Nanotechnology, 2005. **16**(6): p. 695.

256. Kim, Y., A. Garcia-Lekue, D. Sysoiev, T. Frederiksen, U. Groth, and E. Scheer, *Charge Transport in Azobenzene-Based Single-Molecule Junctions.* Physical Review Letters, 2012. **109**(22): p. 226801.

257. Kim, Y., S.G. Bahoosh, D. Sysoiev, T. Huhn, F. Pauly, and E. Scheer, *Inelastic electron tunneling spectroscopy of difurylethene-based photochromic single-molecule junctions.* Beilstein Journal of Nanotechnology, 2017. **8**: p. 2606-2614.

258. Martin, S., W. Haiss, S.J. Higgins, and R.J. Nichols, *The Impact of E−Z Photo-Isomerization on Single Molecular Conductance.* Nano Letters, 2010. **10**(6): p. 2019-2023.

259. Rashid, U., E. Chatir, L. Medrano Sandonas, P.A. Sreelakshmi, A. Dianat, R. Gutierrez, G. Cuniberti, S. Cobo, and V. Kaliginedi, *Dithienylethene-Based Single Molecular*

Photothermal Linear Actuator. Angewandte Chemie International Edition, 2023. **62**(16): p. e202218767.

260. Roldan, D., V. Kaliginedi, S. Cobo, V. Kolivoska, C. Bucher, W. Hong, G. Royal, and T. Wandlowski, *Charge Transport in Photoswitchable Dimethyldihydropyrene-Type Single-Molecule Junctions.* Journal of the American Chemical Society, 2013. **135**(16): p. 5974-5977.

261. Sendler, T., K. Luka-Guth, M. Wieser, Lokamani, J. Wolf, M. Helm, S. Gemming, J. Kerbusch, E. Scheer, T. Huhn, and A. Erbe, *Light-Induced Switching of Tunable Single-Molecule Junctions.* Advanced Science, 2015. **2**(5): p. 1500017.

262. Tam, E.S., J.J. Parks, W.W. Shum, Y.-W. Zhong, M.E.B. Santiago-Berríos, X. Zheng, W. Yang, G.K.L. Chan, H.D. Abruña, and D.C. Ralph, *Single-Molecule Conductance of Pyridine-Terminated Dithienylethene Switch Molecules.* ACS Nano, 2011. **5**(6): p. 5115-5123.

263. Taniguchi, M., Y. Nojima, K. Yokota, J. Terao, K. Sato, N. Kambe, and T. Kawai, *Self-Organized Interconnect Method for Molecular Devices.* Journal of the American Chemical Society, 2006. **128**(47): p. 15062-15063.

264. Tebikachew, B.E., H.B. Li, A. Pirrotta, K. Börjesson, G.C. Solomon, J. Hihath, and K. Moth-Poulsen, *Effect of Ring Strain on the Charge Transport of a Robust Norbornadiene–Quadricyclane-Based Molecular Photoswitch.* The Journal of Physical Chemistry C, 2017. **121**(13): p. 7094-7100.

265. Whalley, A.C., M.L. Steigerwald, X. Guo, and C. Nuckolls, *Reversible Switching in Molecular Electronic Devices.* Journal of the American Chemical Society, 2007. **129**(42): p. 12590-12591.

266. Xin, N., C. Hu, H. Al Sabea, M. Zhang, C. Zhou, L. Meng, C. Jia, Y. Gong, Y. Li, G. Ke, X. He, P. Selvanathan, L. Norel, M.A. Ratner, Z. Liu, S. Xiao, S. Rigaut, H. Guo, and X. Guo, *Tunable Symmetry-Breaking-Induced Dual Functions in Stable and Photoswitched Single-Molecule Junctions.* Journal of the American Chemical Society, 2021. **143**(49): p. 20811-20817.

267. Broman, S.L., S. Lara-Avila, C.L. Thisted, A.D. Bond, S. Kubatkin, A. Danilov, and M.B. Nielsen, *Dihydroazulene Photoswitch Operating in Sequential Tunneling Regime: Synthesis and Single-Molecule Junction Studies.* Advanced Functional Materials, 2012. **22**(20): p. 4249-4258.

268. Huang, C., M. Jevric, A. Borges, S.T. Olsen, J.M. Hamill, J.-T. Zheng, Y. Yang, A. Rudnev, M. Baghernejad, P. Broekmann, A.U. Petersen, T. Wandlowski, K.V. Mikkelsen, G.C. Solomon, M. Brøndsted Nielsen, and W. Hong, *Single-molecule detection of dihydroazulene photo-thermal reaction using break junction technique.* Nature Communications, 2017. **8**(1): p. 15436.

269. Lara-Avila, S., A.V. Danilov, S.E. Kubatkin, S.L. Broman, C.R. Parker, and M.B. Nielsen, *Light-Triggered Conductance Switching in Single-Molecule Dihydroazulene/Vinylheptafulvene Junctions.* The Journal of Physical Chemistry C, 2011. **115**(37): p. 18372-18377.

270. Zhang, N., W.-Y. Lo, A. Jose, Z. Cai, L. Li, and L. Yu, *A Single-Molecular AND Gate Operated with Two Orthogonal Switching Mechanisms.* Advanced Materials, 2017. **29**(28): p. 1701248.

271. Meng, F., Y.-M. Hervault, Q. Shao, B. Hu, L. Norel, S. Rigaut, and X. Chen, *Orthogonally modulated molecular transport junctions for resettable electronic logic gates.* Nature Communications, 2014. **5**(1): p. 3023.

272. Meng, L., N. Xin, C. Hu, J. Wang, B. Gui, J. Shi, C. Wang, C. Shen, G. Zhang, H. Guo, S. Meng, and X. Guo, *Side-group chemical gating via reversible optical and electric control in a single molecule transistor.* Nature Communications, 2019. **10**(1): p. 1450.

273. Kim, D., H. Jeong, H. Lee, W.-T. Hwang, J. Wolf, E. Scheer, T. Huhn, H. Jeong, and T. Lee, *Flexible Molecular-Scale Electronic Devices Composed of Diarylethene Photoswitching Molecules.* Advanced Materials, 2014. **26**(23): p. 3968-3973.

274. Kim, D., H. Jeong, W.-T. Hwang, Y. Jang, D. Sysoiev, E. Scheer, T. Huhn, M. Min, H. Lee, and T. Lee, *Reversible Switching Phenomenon in Diarylethene Molecular Devices with Reduced Graphene Oxide Electrodes on Flexible Substrates.* Advanced Functional Materials, 2015. **25**(37): p. 5918-5923.

275. Koo, J., Y. Jang, L. Martin, D. Kim, H. Jeong, K. Kang, W. Lee, J. Kim, W.-T. Hwang, D. Xiang, E. Scheer, M. Kabdulov, T. Huhn, F. Pauly, and T. Lee, *Unidirectional Real-Time Photoswitching of Diarylethene Molecular Monolayer Junctions with Multilayer Graphene Electrodes.* ACS Applied Materials & Interfaces, 2019. **11**(12): p. 11645-11653.

276. Kronemeijer, A.J., H.B. Akkerman, T. Kudernac, B.J. van Wees, B.L. Feringa, P.W.M. Blom, and B. de Boer, *Reversible Conductance Switching in Molecular Devices.* Advanced Materials, 2008. **20**(8): p. 1467-1473.

277. Mativetsky, J.M., G. Pace, M. Elbing, M.A. Rampi, M. Mayor, and P. Samorì, *Azobenzenes as Light-Controlled Molecular Electronic Switches in Nanoscale Metal−Molecule−Metal Junctions.* Journal of the American Chemical Society, 2008. **130**(29): p. 9192-9193.

278. Nguyen, D.T., M. Freitag, C. Gutheil, K. Sotthewes, B.J. Tyler, M. Böckmann, M. Das, F. Schlüter, N.L. Doltsinis, H.F. Arlinghaus, B.J. Ravoo, and F. Glorius, *An Arylazopyrazole-Based N-Heterocyclic Carbene as a Photoswitch on Gold Surfaces: Light-Switchable Wettability, Work Function, and Conductance.* Angewandte Chemie International Edition, 2020. **59**(32): p. 13651-13656.

279. Smaali, K., S. Lenfant, S. Karpe, M. Oçafrain, P. Blanchard, D. Deresmes, S. Godey, A. Rochefort, J. Roncali, and D. Vuillaume, *High On−Off Conductance Switching Ratio in*

Optically-Driven Self-Assembled Conjugated Molecular Systems. ACS Nano, 2010. **4**(4): p. 2411-2421.

280. Uchida, K., Y. Yamanoi, T. Yonezawa, and H. Nishihara, *Reversible On/Off Conductance Switching of Single Diarylethene Immobilized on a Silicon Surface.* Journal of the American Chemical Society, 2011. **133**(24): p. 9239-9241.

281. Zhang, X., Y. Wen, Y. Li, G. Li, S. Du, H. Guo, L. Yang, L. Jiang, H. Gao, and Y. Song, *Molecularly Controlled Modulation of Conductance on Azobenzene Monolayer-Modified Silicon Surfaces.* The Journal of Physical Chemistry C, 2008. **112**(22): p. 8288-8293.

282. Li, T., M. Jevric, J.R. Hauptmann, R. Hviid, Z. Wei, R. Wang, N.E.A. Reeler, E. Thyrhaug, S. Petersen, J.A.S. Meyer, N. Bovet, T. Vosch, J. Nygård, X. Qiu, W. Hu, Y. Liu, G.C. Solomon, H.G. Kjaergaard, T. Bjørnholm, M.B. Nielsen, B.W. Laursen, and K. Nørgaard, *Ultrathin Reduced Graphene Oxide Films as Transparent Top-Contacts for Light Switchable Solid-State Molecular Junctions.* Advanced Materials, 2013. **25**(30): p. 4164-4170.

283. Bakkar, A., F. Lafolet, D. Roldan, E. Puyoo, D. Jouvenot, G. Royal, E. Saint-Aman, and S. Cobo, *Bidirectional light-induced conductance switching in molecular wires containing a dimethyldihydropyrene unit.* Nanoscale, 2018. **10**(12): p. 5436-5441.

284. Taherinia, D. and C.D. Frisbie, *Photoswitchable Hopping Transport in Molecular Wires 4 nm in Length.* The Journal of Physical Chemistry C, 2016. **120**(12): p. 6442-6449.

285. Hnid, I., A. Grempka, A. Khettabi, X. Sun, J.C. Lacroix, F. Lafolet, and S. Cobo, *Combining Photomodulation and Rectification in Coordination Molecular Wires Based on Dithienylethene Molecular Junctions.* The Journal of Physical Chemistry C, 2020. **124**(48): p. 26304-26309.

286. Hnid, I., D. Frath, F. Lafolet, X. Sun, and J.-C. Lacroix, *Highly Efficient Photoswitch in Diarylethene-Based Molecular Junctions.* Journal of the American Chemical Society, 2020. **142**(17): p. 7732-7736.

287. Choi, H., H. Lee, Y. Kang, E. Kim, S.O. Kang, and J. Ko, *Photochromism and Electrical Transport Characteristics of a Dyad and a Polymer with Diarylethene and Quinoline Units.* The Journal of Organic Chemistry, 2005. **70**(21): p. 8291-8297.

288. Nešpůrek, S., J. Sworakowski, C. Combellas, G. Wang, and M. Weiter, *A molecular device based on light controlled charge carrier mobility.* Applied Surface Science, 2004. **234**(1): p. 395-402.

289. Matsui, N. and T. Tsujioka, *Carrier mobility of photochromic diarylethene amorphous films.* Organic Electronics, 2014. **15**(10): p. 2264-2269.

290. Tsujioka, T., M. Shimizu, and E. Ishihara, *Organic bistable memory characteristics with a photochromic diarylethene layer.* Applied Physics Letters, 2005. **87**(21): p. 213506.

291. Tsujioka, T. and H. Kondo, *Organic bistable molecular memory using photochromic diarylethene.* Applied Physics Letters, 2003. **83**(5): p. 937-939.

292. Tsujioka, T. and K. Masuda, *Electrical carrier-injection and transport characteristics of photochromic diarylethene films.* Applied Physics Letters, 2003. **83**(24): p. 4978-4980.

293. Tsujioka, T., I. Onishi, and D. Natsume, *Photocurrent switching method based on photoisomerization of diarylethene layer for nondestructive readout of photochromic optical memory.* Applied Optics, 2010. **49**(20): p. 3894-3899.

294. Tsujioka, T., T. Sasa, and Y. Kakihara, *Nonvolatile organic memory based on isomerization of diarylethene molecules by electrical carrier injection.* Organic Electronics, 2012. **13**(4): p. 681-686.

295. Tsujioka, T., N. Iefuji, A. Jiapaer, M. Irie, and S. Nakamura, *Hole-injection isomerization of photochromic diarylethene for organic molecular memory.* Applied Physics Letters, 2006. **89**(22): p. 222102.

296. Hayakawa, R., K. Higashiguchi, K. Matsuda, T. Chikyow, and Y. Wakayama, *Photoisomerization-Induced Manipulation of Single-Electron Tunneling for Novel Si-Based Optical Memory.* ACS Applied Materials & Interfaces, 2013. **5**(21): p. 11371-11376.

297. Shallcross, R.C., P. Zacharias, A. Köhnen, P.O. Körner, E. Maibach, and K. Meerholz, *Photochromic Transduction Layers in Organic Memory Elements.* Advanced Materials, 2013. **25**(3): p. 469-476.

298. Shallcross, R.C., P.O. Körner, E. Maibach, A. Köhnen, and K. Meerholz, *A Photochromic Diode With a Continuum of Intermediate States: Towards High Density Multilevel Storage.* Advanced Materials, 2013. **25**(34): p. 4807-4813.

299. Tsujioka, T. and N. Matsui, *Electrical characterization of photochromic diarylethene films consisting of extraordinarily large crystallites.* Journal of Materials Chemistry C, 2014. **2**(18): p. 3589-3596.

300. Körner, P.O., R.C. Shallcross, E. Maibach, A. Köhnen, and K. Meerholz, *Optical and electrical multilevel storage in organic memory passive matrix arrays.* Organic Electronics, 2014. **15**(12): p. 3688-3693.

301. Kim, E. and H.W. Lee, *Photo-induced electrical switching through a mainchain polymer.* Journal of Materials Chemistry, 2006. **16**(14): p. 1384-1389.

302. Chatterjee, S., M.S. Hossain, S. Molla, and S. Bandyopadhyay, *Modulation of conductance using light-induced morphological change of a layered π-structure.* Journal of Materials Chemistry C, 2022. **10**(40): p. 14993-14999.

303. Ghosh, S., M.S. Hossain, S. Chatterjee, S.A. Rahaman, and S. Bandyopadhyay, *Light-Gated Modulation of Electronic Mobility of a Dihydropyrene-Based Photochromic*

Coordination Polymer. ACS Applied Materials & Interfaces, 2020. **12**(47): p. 52983-52991.

304. Guo, X., D. Zhang, G. Yu, M. Wan, J. Li, Y. Liu, and D. Zhu, *Reversible Photoregulation of the Electrical Conductivity of Spiropyran-Doped Polyaniline for Information Recording and Nondestructive Processing.* Advanced Materials, 2004. **16**(7): p. 636-640.

305. Ikeda, M., N. Tanifuji, H. Yamaguchi, M. Irie, and K. Matsuda, *Photoswitching of conductance of diarylethene-Au nanoparticle network.* Chemical Communications, 2007(13): p. 1355-1357.

306. Kawai, T., Y. Nakashima, and M. Irie, *A Novel Photoresponsive π-Conjugated Polymer Based on Diarylethene and its Photoswitching Effect in Electrical Conductivity.* Advanced Materials, 2005. **17**(3): p. 309-314.

307. Matsuda, K., H. Yamaguchi, T. Sakano, M. Ikeda, N. Tanifuji, and M. Irie, *Conductance Photoswitching of Diarylethene−Gold Nanoparticle Network Induced by Photochromic Reaction.* The Journal of Physical Chemistry C, 2008. **112**(43): p. 17005-17010.

308. van der Molen, S.J., J. Liao, T. Kudernac, J.S. Agustsson, L. Bernard, M. Calame, B.J. van Wees, B.L. Feringa, and C. Schönenberger, *Light-Controlled Conductance Switching of Ordered Metal−Molecule−Metal Devices.* Nano Letters, 2009. **9**(1): p. 76-80.

309. Pakula, C., V. Zaporojtchenko, T. Strunskus, D. Zargarani, R. Herges, and F. Faupel, *Reversible light-controlled conductance switching of azobenzene-based metal/polymer nanocomposites.* Nanotechnology, 2010. **21**(46): p. 465201.

310. Toyama, T., K. Higashiguchi, T. Nakamura, H. Yamaguchi, E. Kusaka, and K. Matsuda, *Photoswitching of Conductance of Diarylethene–Gold Nanoparticle Network Based on the Alteration of π-Conjugation.* The Journal of Physical Chemistry Letters, 2016. **7**(11): p. 2113-2118.

311. Lu, H., H. Huang, J. Yang, Z. Zheng, X. Dong, L. Zhao, C. Xu, J. Hu, H. Liu, Y. Qian, J.-Q. Wang, and J. Lin, *Incorporating Photochromic Viologen Derivative to Unprecedentedly Boost UV Sensitivity in Photoelectrochromic Hydrogel.* ACS Sensors, 2023. **8**(4): p. 1609-1615.

312. Yu, X.-Q., M.-S. Wang, and G.-C. Guo, *Single-Component Photochromic Smart Semiconductor with Photoswitchable Fast Bidirectional Electron Transfer.* Advanced Functional Materials, 2023. **33**(14): p. 2212907.

313. Saha, M., S. Chatterjee, M.S. Hossain, A. Ghude, and S. Bandyopadhyay, *Modulation of Electronic Mobility of a One-Dimensional Coordination Polymeric Molecular Wire with Light.* Chemistry – An Asian Journal, 2019. **14**(24): p. 4659-4664.

314. Tsujioka, T., Y. Hamada, K. Shibata, A. Taniguchi, and T. Fuyuki, *Nondestructive readout of photochromic optical memory using photocurrent detection.* Applied Physics Letters, 2001. **78**(16): p. 2282-2284.

315. Taniguchi, A., T. Tsujioka, Y. Hamada, K. Shibata, and T. Fuyuki, *Carrier Injection/Transport Characteristics of Photochromic Diarylethene Film.* Japanese Journal of Applied Physics, 2001. **40**(12): p. 7029-7030.

316. Tsujioka, T., K. Masui, and F. Otoshi, *Photocurrent detection from photochromic diarylethene film.* Applied Physics Letters, 2004. **85**(15): p. 3128-3130.

317. Yamamoto, K. and T. Tsujioka, *Isomerization structure of photochromic diarylethene film based on electrical carrier injection.* Materials Letters, 2016. **179**: p. 158-161.

318. Tsujioka, T., D. Natsume, and I. Onishi, *Nondestructive Readout of Photochromic Memory using Photocurrent Switching.* Proceedings of the Joint International Symposium on Optical Memory and Optical Data Storage, 2011: p. OTuD16.

319. Tsujioka, T., *Electrical Molecular Memory Using Diarylethene Derivatives.* Molecular Crystals and Liquid Crystals, 2005. **431**(1): p. 391-395.

320. Tsujioka, T. and K. Yamamoto, *Elemental isomerization processes for a photochromic diarylethene film based on carrier injection toward all-electrically operable organic memory.* Japanese Journal of Applied Physics, 2016. **55**(6): p. 061602.

321. Liu, Q., K. Jiang, Y. Wen, J. Wang, J. Luo, and Y. Song, *High-performance optoelectrical dual-mode memory based on spiropyran-containing polyimide.* Applied Physics Letters, 2010. **97**(25): p. 253304.

322. Seok, W.C., S.H. Son, T.K. An, S.H. Kim, and S.W. Lee, *Photo-enhanced polymer memory device based on polyimide containing spiropyran.* Electronic Materials Letters, 2016. **12**(4): p. 537-544.

323. Tsujioka, T., M. Nobunaga, and M. Dohi, *In-plane electrical bistability of photochromic diarylethene/Cu composite film.* Organic Electronics, 2015. **26**: p. 144-150.

324. Tsujioka, T. and K. Hoshimoto, *Minute Organic Memory Fabricated by Laser Scanning and Selective Metal-Vapor Deposition of a Diarylethene–Cu Composite Film.* Advanced Electronic Materials, 2019. **5**(1): p. 1800491.

325. Wong, C.-L., M. Ng, E.Y.-H. Hong, Y.-C. Wong, M.-Y. Chan, and V.W.-W. Yam, *Photoresponsive Dithienylethene-Containing Tris(8-hydroxyquinolinato)aluminum(III) Complexes with Photocontrollable Electron-Transporting Properties for Solution-Processable Optical and Organic Resistive Memory Devices.* Journal of the American Chemical Society, 2020. **142**(28): p. 12193-12206.

326. Wong, C.-L., Y.-H. Cheng, C.-T. Poon, and V.W.-W. Yam, *Synthesis, Photophysical, Photochromic, and Photomodulated Resistive Memory Studies of Dithienylethene-Containing Copper(I) Diimine Complexes.* Inorganic Chemistry, 2020. **59**(20): p. 14785-14795.

327. Ling, H., K. Tan, Q. Fang, X. Xu, H. Chen, W. Li, Y. Liu, L. Wang, M. Yi, R. Huang, Y. Qian, L. Xie, and W. Huang, *Light-Tunable Nonvolatile Memory Characteristics in Photochromic RRAM.* Advanced Electronic Materials, 2017. **3**(8): p. 1600416.

328. Kang, M., S.Z. Hassan, S.-M. Ko, C. Choi, J. Kim, S.K.R. Parumala, Y.-H. Kim, Y.H. Jang, J. Yoon, D.-W. Jee, and D.S. Chung, *A Molecular-Switch-Embedded Organic Photodiode for Capturing Images against Strong Backlight.* Advanced Materials, 2022. **34**(17): p. 2200526.

329. Geng, Y., Y. Zhao, J. Zhao, Y. Zhai, M. Yuan, X.-D. Wang, H. Gao, J. Feng, Y. Wu, and L. Jiang, *Optical and electrical modulation in ultraviolet photodetectors based on organic one-dimensional photochromic arrays.* SmartMat., 2021. **2**(3): p. 388-397.

330. Tsujioka, T., M. Yamamoto, K. Shoji, and K. Tani, *Efficient carrier separation from a photochromic diarylethene layer.* Photochemical & Photobiological Sciences, 2010. **9**(2): p. 157-161.

331. Andersson, P., N.D. Robinson, and M. Berggren, *Switchable Charge Traps in Polymer Diodes.* Advanced Materials, 2005. **17**(14): p. 1798-1803.

332. Zacharias, P., M.C. Gather, A. Köhnen, N. Rehmann, and K. Meerholz, *Photoprogrammable Organic Light-Emitting Diodes.* Angewandte Chemie International Edition, 2009. **48**(22): p. 4038-4041.

333. Qian, Y., X. Xu, W. Li, J. Wang, B. Wei, Q. Wei, X. Yan, W. Hu, Y. Lu, L. Xie, X. Zhang, and W. Huang, *Photo-induced storage and mask-free arbitrary micro-patterning in solution-processable and simple-structured photochromic organic light-emitting diodes.* Organic Electronics, 2015. **26**: p. 476-480.

334. Zhang, Z., X. Liu, Z. Li, Z. Chen, F. Zhao, F. Zhang, and C.H. Tung, *A Smart Light-Controlled Carrier Switch in an Organic Light Emitting Device.* Advanced Functional Materials, 2008. **18**(2): p. 302-307.

335. Ligorio, G., G.F. Cotella, A. Bonasera, N. Zorn Morales, G. Carnicella, B. Kobin, Q. Wang, N. Koch, S. Hecht, E.J.W. List-Kratochvil, and F. Cacialli, *Modulating the luminance of organic light-emitting diodes via optical stimulation of a photochromic molecular monolayer at transparent oxide electrode.* Nanoscale, 2020. **12**(9): p. 5444-5451.

336. Cotella, G.F., A. Bonasera, G. Carnicella, A. Minotto, S. Hecht, and F. Cacialli, *Diarylethenes in Optically Switchable Organic Light-Emitting Diodes: Direct Investigation of the Reversible Charge Carrier Trapping Process.* Advanced Optical Materials, 2022. **10**(2): p. 2101116.

337. Huaulmé, Q., V.M. Mwalukuku, D. Joly, J. Liotier, Y. Kervella, P. Maldivi, S. Narbey, F. Oswald, A.J. Riquelme, J.A. Anta, and R. Demadrille, *Photochromic dye-sensitized solar cells with light-driven adjustable optical transmission and power conversion efficiency.* Nature Energy, 2020. **5**(6): p. 468-477.

338. Andrés Castán, J.-M., V.M. Mwalukuku, A.J. Riquelme, J. Liotier, Q. Huaulmé, J.A. Anta, P. Maldivi, and R. Demadrille, *Photochromic spiro-indoline naphthoxazines and naphthopyrans in dye-sensitized solar cells.* Materials Chemistry Frontiers, 2022. **6**(20): p. 2994-3005.

339. Mwalukuku, V.M., J. Liotier, A.J. Riquelme, Y. Kervella, Q. Huaulmé, A. Haurez, S. Narbey, J.A. Anta, and R. Demadrille, *Strategies to Improve the Photochromic Properties and Photovoltaic Performances of Naphthopyran Dyes in Dye-Sensitized Solar Cells.* Advanced Energy Materials, 2023. **13**(8): p. 2203651.

340. Simpang, A.I., A. Ghifari, S.-Y. Han, D. Hayati, D.X. Long, Y.H. Jang, and J. Hong, *Metal-free Organic Dyes Featuring an Azobenzene Bridge for Photochromic Dye-Sensitized Solar Cells.* ChemistrySelect, 2023. **8**(20): p. e202204571.

341. Zhang, J., J. Zhou, Q. Zhou, W. Wu, H. Zhang, X. Lin, Q. Luo, J. Cao, and H. Ma, *Light-driven textile sensors with potential application of UV detection.* RSC Advances, 2023. **13**(8): p. 5266-5272.

342. Suda, M., R. Kato, and H.M. Yamamoto, *Light-induced superconductivity using a photoactive electric double layer.* Science, 2015. **347**(6223): p. 743-746.

343. Suda, M., N. Takashina, S. Namuangruk, N. Kungwan, H. Sakurai, and H.M. Yamamoto, *N-Type Superconductivity in an Organic Mott Insulator Induced by Light-Driven Electron-Doping.* Advanced Materials, 2017. **29**(33): p. 1606833.

344. Tuchman, Y., T.N. Mangoma, P. Gkoupidenis, Y. van de Burgt, R.A. John, N. Mathews, S.E. Shaheen, R. Daly, G.G. Malliaras, and A. Salleo, *Organic neuromorphic devices: Past, present, and future challenges.* MRS Bulletin, 2020. **45**(8): p. 619-630.

345. van de Burgt, Y., A. Melianas, S.T. Keene, G. Malliaras, and A. Salleo, *Organic electronics for neuromorphic computing.* Nature Electronics, 2018. **1**(7): p. 386-397.

346. Gkoupidenis, P., Y. Zhang, H. Kleemann, H. Ling, F. Santoro, S. Fabiano, A. Salleo, and Y. van de Burgt, *Organic mixed conductors for bioinspired electronics.* Nature Reviews Materials, 2024. **9**(2): p. 134-149.

347. He, L., Z. Yang, Z. Wang, T. Leydecker, and E. Orgiu, *Organic multilevel (opto)electronic memories towards neuromorphic applications.* Nanoscale, 2023. **15**(27): p. 11434-11456.

348. Sharma, D., D. Rao, and B. Saha, *A photonic artificial synapse with a reversible multifaceted photochromic compound.* Nanoscale Horizons, 2023. **8**(4): p. 543-549.

349. Rhim, S.-Y., G. Ligorio, F. Hermerschmidt, J. Hildebrandt, M. Pätzel, S. Hecht, and E.J.W. List-Kratochvil, *Using Active Surface Plasmons in a Multibit Optical Storage Device to Emulate Long-Term Synaptic Plasticity.* physica status solidi (a), 2020. **217**(20): p. 2000354.

350. Rhim, S.-Y., G. Ligorio, F. Hermerschmidt, M. Pätzel, M. Herder, S. Hecht, and E.J.W. List-Kratochvil, *Reversible training of waveguide-based AND/OR gates for optically driven artificial neural networks using photochromic molecules.* Journal of Physics D: Applied Physics, 2022. **55**(4): p. 044002.

351. Turetta, N., W. Danowski, L. Cusin, P.A. Livio, R. Hallani, I. McCulloch, and P. Samorì, *A photo-responsive organic electrochemical transistor.* Journal of Materials Chemistry C, 2023. **11**(24): p. 7982-7988.

352. Corrado, F., U. Bruno, M. Prato, A. Carella, V. Criscuolo, A. Massaro, M. Pavone, A.B. Muñoz-García, S. Forti, C. Coletti, O. Bettucci, and F. Santoro, *Azobenzene-based optoelectronic transistors for neurohybrid building blocks.* Nature Communications, 2023. **14**(1): p. 6760.

353. Wang, C., Y. Liu, and Y. Guo, *Intrinsically flexible organic phototransistors for bioinspired neuromorphic sensory system.* Wearable Electronics, 2024. **1**: p. 41-52.

354. Nguyen, M., U. Kraft, W.L. Tan, I. Dobryden, K. Broch, W. Zhang, H.-I. Un, D. Simatos, D. Venkateshavaran, I. McCulloch, P.M. Claesson, C.R. McNeill, and H. Sirringhaus, *Improving OFF-State Bias-Stress Stability in High-Mobility Conjugated Polymer Transistors with an Antisolvent Treatment.* Advanced Materials, 2023. **35**(16): p. 2205377.

355. Iqbal, H.F., Q. Ai, K.J. Thorley, H. Chen, I. McCulloch, C. Risko, J.E. Anthony, and O.D. Jurchescu, *Suppressing bias stress degradation in high performance solution processed organic transistors operating in air.* Nature Communications, 2021. **12**(1): p. 2352.

356. Jeon, Y., S. Kim, J. Seo, and H. Yoo, *Contributions of Light to Novel Logic Concepts Using Optoelectronic Materials.* Small Methods, 2024. **8**(2): p. 2300391.

357. Goulet-Hanssens, A., F. Eisenreich, and S. Hecht, *Enlightening Materials with Photoswitches.* Advanced Materials, 2020. **32**(20): p. 1905966.

358. Broman, S.L. and M.B. Nielsen, *Dihydroazulene: from controlling photochromism to molecular electronics devices.* Physical Chemistry Chemical Physics, 2014. **16**(39): p. 21172-21182.

359. Plaquet, A., B. Champagne, F. Castet, L. Ducasse, E. Bogdan, V. Rodriguez, and J.-L. Pozzo, *Theoretical investigation of the dynamic first hyperpolarizability of DHA–VHF molecular switches.* New Journal of Chemistry, 2009. **33**(6): p. 1349-1356.

360. Au-Yeung, K.H., T. Kühne, O. Aiboudi, S. Sarkar, O. Guskova, D.A. Ryndyk, T. Heine, F. Lissel, and F. Moresco, *STM-induced ring closure of vinylheptafulvene molecular dipole switches on Au(111).* Nanoscale Advances, 2022. **4**(20): p. 4351-4357.

361. Kühne, T., K.H. Au-Yeung, F. Eisenhut, O. Aiboudi, D.A. Ryndyk, G. Cuniberti, F. Lissel, and F. Moresco, *STM induced manipulation of azulene-based molecules and nanostructures: the role of the dipole moment.* Nanoscale, 2020. **12**(48): p. 24471-24476.

362. Daub, J., T. Knöchel, and A. Mannschreck, *Photosensitive Dihydroazulenes with Chromogenic Properties.* Angewandte Chemie International Edition in English, 1984. **23**(12): p. 960-961.

363. Gierisch, S. and J. Daub, *Lichtsensitive Dihydroazulene: Alternativer Syntheseweg – Einfluß von Alkylsubstituenten im Fünfring auf das photochrome Verhalten.* Chemische Berichte, 1989. **122**(1): p. 69-75.

364. Daub, J., S. Gierisch, U. Klement, T. Knöchel, G. Maas, and U. Seitz, *Lichtinduzierte reversible Reaktionen: Synthesen und Eigenschaften photochromer 1,1-Dicyan-1,8a-dihydroazulene und thermochromer 8-(2,2-Dicyanvinyl)heptafulvene.* Chemische Berichte, 1986. **119**(8): p. 2631-2646.

365. Görner, H., C. Fischer, S. Gierisch, and J. Daub, *Dihydroazulene/vinylheptafulvene photochromism: Effects of substituents, solvent, and temperature in the photorearrangement of dihydroazulenes to vinylheptafulvenes.* The Journal of Physical Chemistry, 1993. **97**(16): p. 4110-4117.

366. Görner, H., C. Fischer, and J. Daub, *Photoreaction of dihydroazulenes into vinylheptafulvenes: photochromism of nitrophenyl-substituted derivatives.* Journal of Photochemistry and Photobiology A: Chemistry, 1995. **85**(3): p. 217-224.

367. Broman, S.L., S.L. Brand, C.R. Parker, M.Å. Petersen, C.G. Tortzen, A. Kadziola, K. Kilså, and M.B. Nielsen, *Optimized synthesis and detailed NMR spectroscopic characterization of the 1,8a-dihydroazulene-1,1-dicarbonitrile photoswitch.* ARKIVOC, 2011(9): p. 51-67.

368. Lyon, J.E., A.J. Cascio, M.M. Beerbom, R. Schlaf, Y. Zhu, and S.A. Jenekhe, *Photoemission study of the poly(3-hexylthiophene)/Au interface.* Applied Physics Letters, 2006. **88**(22): p. 222109.

369. Nicolai, H.T., M. Kuik, G.A.H. Wetzelaer, B. de Boer, C. Campbell, C. Risko, J.L. Brédas, and P.W.M. Blom, *Unification of trap-limited electron transport in semiconducting polymers.* Nature Materials, 2012. **11**(10): p. 882-887.

370. McCulloch, I., M. Heeney, C. Bailey, K. Genevicius, I. MacDonald, M. Shkunov, D. Sparrowe, S. Tierney, R. Wagner, W. Zhang, M.L. Chabinyc, R.J. Kline, M.D. McGehee, and M.F. Toney, *Liquid-crystalline semiconducting polymers with high charge-carrier mobility.* Nature Materials, 2006. **5**(4): p. 328-333.

371. Cochran, J.E., M.J.N. Junk, A.M. Glaudell, P.L. Miller, J.S. Cowart, M.F. Toney, C.J. Hawker, B.F. Chmelka, and M.L. Chabinyc, *Molecular Interactions and Ordering in Electrically Doped Polymers: Blends of PBTTT and F4TCNQ.* Macromolecules, 2014. **47**(19): p. 6836-6846.

372. Fei, Z., P. Boufflet, S. Wood, J. Wade, J. Moriarty, E. Gann, E.L. Ratcliff, C.R. McNeill, H. Sirringhaus, J.-S. Kim, and M. Heeney, *Influence of Backbone Fluorination in*

Regioregular Poly(3-alkyl-4-fluoro)thiophenes. Journal of the American Chemical Society, 2015. **137**(21): p. 6866-6879.

373. Zhuo, J.-M., L.-H. Zhao, R.-Q. Png, L.-Y. Wong, P.-J. Chia, J.-C. Tang, S. Sivaramakrishnan, M. Zhou, E.C.W. Ou, S.-J. Chua, W.-S. Sim, L.-L. Chua, and P.K.H. Ho, *Direct Spectroscopic Evidence for a Photodoping Mechanism in Polythiophene and Poly(bithiophene-alt-thienothiophene) Organic Semiconductor Thin Films Involving Oxygen and Sorbed Moisture.* Advanced Materials, 2009. **21**(46): p. 4747-4752.

374. Ruan, X., S. Cheng, W. Deng, Y. Tan, Z. Lu, J. Shi, X. Zhang, and J. Jie, *Insights into the Origins of Minority Carrier Traps in Solution-Processed Organic Semiconductors and Their Effects on Transistor Photostability.* Advanced Electronic Materials, 2022. **8**(10): p. 2200355.

375. Simatos, D., I.E. Jacobs, I. Dobryden, M. Nguyen, A. Savva, D. Venkateshvaran, M. Nikolka, J. Charmet, L.J. Spalek, M. Gicevičius, Y. Zhang, G. Schweicher, D.J. Howe, S. Ursel, J. Armitage, I.B. Dimov, U. Kraft, W. Zhang, M. Alsufyani, I. McCulloch, R.M. Owens, P.M. Claesson, T.P.J. Knowles, and H. Sirringhaus, *Effects of Processing-Induced Contamination on Organic Electronic Devices.* Small Methods, 2023. **7**(11): p. 2300476.

376. Broman, S.L., M. Jevric, and M.B. Nielsen, *Linear Free-Energy Correlations for the Vinylheptafulvene Ring Closure: A Probe for Hammett σ Values.* Chemistry – A European Journal, 2013. **19**(29): p. 9542-9548.

377. Jean-Ruel, H., R.R. Cooney, M. Gao, C. Lu, M.A. Kochman, C.A. Morrison, and R.J.D. Miller, *Femtosecond Dynamics of the Ring Closing Process of Diarylethene: A Case Study of Electrocyclic Reactions in Photochromic Single Crystals.* The Journal of Physical Chemistry A, 2011. **115**(45): p. 13158-13168.

378. Gonzalez, A., E.S. Kengmana, M.V. Fonseca, and G.G.D. Han, *Solid-state photoswitching molecules: structural design for isomerization in condensed phase.* Materials Today Advances, 2020. **6**: p. 100058.

379. Ma, L., W.H. Lee, Y.D. Park, J.S. Kim, H.S. Lee, and K. Cho, *High performance polythiophene thin-film transistors doped with very small amounts of an electron acceptor.* Applied Physics Letters, 2008. **92**(6): p. 063310.

380. Paterson, A.F., N.D. Treat, W. Zhang, Z. Fei, G. Wyatt-Moon, H. Faber, G. Vourlias, P.A. Patsalas, O. Solomeshch, N. Tessler, M. Heeney, and T.D. Anthopoulos, *Small Molecule/Polymer Blend Organic Transistors with Hole Mobility Exceeding 13 cm2 V−1 s−1.* Advanced Materials, 2016. **28**(35): p. 7791-7798.

381. Tiwari, S.P., W.J. Potscavage, T. Sajoto, S. Barlow, S.R. Marder, and B. Kippelen, *Pentacene organic field-effect transistors with doped electrode-semiconductor contacts.* Organic Electronics, 2010. **11**(5): p. 860-863.

382. Scaccabarozzi, A.D., A. Basu, F. Aniés, J. Liu, O. Zapata-Arteaga, R. Warren, Y. Firdaus, M.I. Nugraha, Y. Lin, M. Campoy-Quiles, N. Koch, C. Müller, L. Tsetseris, M. Heeney,

and T.D. Anthopoulos, *Doping Approaches for Organic Semiconductors.* Chemical Reviews, 2022. **122**(4): p. 4420-4492.

383. Balcı Leinen, M., P. Klein, F.L. Sebastian, N.F. Zorn, S. Adamczyk, S. Allard, U. Scherf, and J. Zaumseil, *Spiropyran-Functionalized Polymer–Carbon Nanotube Hybrids for Dynamic Optical Memory Devices and UV Sensors.* Advanced Electronic Materials, 2020. **6**(11): p. 2000717.

384. Chen, M.-N., C.-Y. Ke, A. Nyayachavadi, H. Zhao, M.U. Ocheje, M. Mooney, Y.-T. Li, X. Gu, G.-S. Liou, S. Rondeau-Gagné, and Y.-C. Chiu, *Facile Blending Strategy for Boosting the Conjugated Polymer Semiconductor Transistor's Mobility.* ACS Applied Materials & Interfaces, 2023. **15**(46): p. 53755-53764.

385. Gobbi, L., P. Seiler, F. Diederich, V. Gramlich, C. Boudon, J.-P. Gisselbrecht, and M. Gross, *Photoswitchable Tetraethynylethene-Dihydroazulene Chromophores.* Helvetica Chimica Acta, 2001. **84**(4): p. 743-777.

386. Daub, J., C. Fischer, S. Gierisch, and J. Set, *Novel Multichromophoric Dyes for Chemical, and Physical Switching.* Molecular Crystals and Liquid Crystals Science and Technology. Section A. Molecular Crystals and Liquid Crystals, 1992. **217**(1): p. 177-185.

387. Daub, J., J. Salbeck, T. Knöchel, C. Fischer, H. Kunkely, and K.M. Rapp, *Light-Sensitive Molecular Building Blocks with Electron Transfer Activity: Synthesis and Properties of a Photochemically Switchable, Dicyanovinyl-Substituted Furan.* Angewandte Chemie International Edition in English, 1989. **28**(11): p. 1494-1496.

388. Fischer, C. and J. Daub, *Crown Ether-Bearing Dihydroazulenes: Synthesis and Photochromism of a Benzo[15]crown-5 Derivative.* Chemische Berichte, 1993. **126**(7): p. 1631-1634.

389. Nikolka, M., I. Nasrallah, B. Rose, M.K. Ravva, K. Broch, A. Sadhanala, D. Harkin, J. Charmet, M. Hurhangee, A. Brown, S. Illig, P. Too, J. Jongman, I. McCulloch, J.-L. Bredas, and H. Sirringhaus, *High operational and environmental stability of high-mobility conjugated polymer field-effect transistors through the use of molecular additives.* Nature Materials, 2017. **16**(3): p. 356-362.

390. Nikolka, M., G. Schweicher, J. Armitage, I. Nasrallah, C. Jellett, Z. Guo, M. Hurhangee, A. Sadhanala, I. McCulloch, C.B. Nielsen, and H. Sirringhaus, *Performance Improvements in Conjugated Polymer Devices by Removal of Water-Induced Traps.* Advanced Materials, 2018. **30**(36): p. 1801874.

391. Armitage, J., L.J. Spalek, M. Nguyen, M. Nikolka, I.E. Jacobs, L. Marañón, I. Nasrallah, G. Schweicher, I. Dimov, D. Simatos, I. McCulloch, C.B. Nielsen, G. Conduit, and H. Sirringhaus, *Fragment Graphical Variational AutoEncoding for Screening Molecules with Small Data.* arXiv [physics.data-an], 2019.

392. Kraft, U., T. Zaki, F. Letzkus, J.N. Burghartz, E. Weber, B. Murmann, and H. Klauk, *Low-Voltage, High-Frequency Organic Transistors and Unipolar and Complementary Ring Oscillators on Paper*. Advanced Electronic Materials, 2019. **5**(2): p. 1800453.

393. Lee, S., S. Kim, and H. Yoo, *Contribution of Polymers to Electronic Memory Devices and Applications.* Polymers, 2021. **13**(21): p. 3774.

394. Wakayama, Y., R. Hayakawa, and H.-S. Seo, *Recent progress in photoactive organic field-effect transistors.* Science and Technology of Advanced Materials, 2014. **15**(2): p. 024202.

395. Milvich, J., T. Zaki, M. Aghamohammadi, R. Rödel, U. Kraft, H. Klauk, and J.N. Burghartz, *Flexible low-voltage organic phototransistors based on air-stable dinaphtho[2,3-b:2',3'-f]thieno[3,2-b]thiophene (DNTT).* Organic Electronics, 2015. **20**: p. 63-68.

396. Wang, Y., X. Huang, T. Li, L. Li, X. Guo, and P. Jiang, *Polymer-Based Gate Dielectrics for Organic Field-Effect Transistors.* Chemistry of Materials, 2019. **31**(7): p. 2212-2240.

397. Ortiz, R.P., A. Facchetti, and T.J. Marks, *High-k Organic, Inorganic, and Hybrid Dielectrics for Low-Voltage Organic Field-Effect Transistors.* Chemical Reviews, 2010. **110**(1): p. 205-239.

398. Kraft, U., U. Zschieschang, F. Ante, D. Kälblein, C. Kamella, K. Amsharov, M. Jansen, K. Kern, E. Weber, and H. Klauk, *Fluoroalkylphosphonic acid self-assembled monolayer gate dielectrics for threshold-voltage control in low-voltage organic thin-film transistors.* Journal of Materials Chemistry, 2010. **20**(31): p. 6416-6418.

399. Kraft, U., M. Sejfić, M.J. Kang, K. Takimiya, T. Zaki, F. Letzkus, J.N. Burghartz, E. Weber, and H. Klauk, *Flexible Low-Voltage Organic Complementary Circuits: Finding the Optimum Combination of Semiconductors and Monolayer Gate Dielectrics.* Advanced Materials, 2015. **27**(2): p. 207-214.

400. Kalogeras, I.M., E.R. Neagu, and A. Vassilikou-Dova, *Free-Space and Intermolecular Interaction Effects on the Local-Chain Rotational Relaxation Dynamics in Dye + Polymer Lasing Materials.* Macromolecules, 2004. **37**(3): p. 1042-1053.

401. Shi, W., C. Fang, Q. Pan, X. Sun, Q. Gu, D. Xu, and J. Yu, *Dielectric relaxation of poled polymer DCNP/PMMA.* Reactive and Functional Polymers, 2000. **44**(2): p. 177-182.

402. Lei, D., J. Runt, A. Safari, and R.E. Newnham, *Dielectric properties of azo dye-poly(methyl methacrylate) mixtures.* Macromolecules, 1987. **20**(8): p. 1797-1801.

403. Zaporojtchenko, V., C. Pakula, S.W. Basuki, T. Strunskus, D. Zargarani, R. Herges, and F. Faupel, *Reversible light-induced capacitance switching of azobenzene ether/PMMA blends.* Applied Physics A, 2011. **102**(2): p. 421-427.

404. Gagliardi, M., F. Pignatelli, and V. Mattoli, *Light-induced capacitance switching in spiropyran-based capacitors.* Sensors and Actuators A: Physical, 2020. **302**: p. 111804.

405. Luo, D. and L. Deng, *Dielectric characteristic of photoinduced isomerization in azo-dye doped polymeric matrices.* Applied Physics Letters, 2006. **88**(18): p. 181104.

406. Irvine, J.T.S., D.C. Sinclair, and A.R. West, *Electroceramics: Characterization by Impedance Spectroscopy.* Advanced Materials, 1990. **2**(3): p. 132-138.

407. Gaddam, R.R., L. Katzenmeier, X. Lamprecht, and A.S. Bandarenka, *Review on physical impedance models in modern battery research.* Physical Chemistry Chemical Physics, 2021. **23**(23): p. 12926-12944.

408. Randviir, E.P. and C.E. Banks, *A review of electrochemical impedance spectroscopy for bioanalytical sensors.* Analytical Methods, 2022. **14**(45): p. 4602-4624.

409. Rampi, M.A., O.J.A. Schueller, and G.M. Whitesides, *Alkanethiol self-assembled monolayers as the dielectric of capacitors with nanoscale thickness.* Applied Physics Letters, 1998. **72**(14): p. 1781-1783.

410. Jin, H., J. Tian, S. Wang, T. Tan, Y. Xiao, and X. Li, *Novel photochromic and electrochromic diarylethenes bearing triphenylamine units.* RSC Advances, 2014. **4**(32): p. 16839-16848.

411. Torres-Pierna, H., C. Roscini, A. Vlasceanu, S.L. Broman, M. Jevric, M. Cacciarini, and M.B. Nielsen, *Photochromism of dihydroazulene-based polymeric thin films.* Dyes and Pigments, 2017. **145**: p. 359-364.

412. Abe, S., Y. Nishimura, I. Yamazaki, and N. Ohta, *Remarkable Electric Field Effect on the Absorption Intensity of a Molecular Aggregate of Photomerocyanine in a PMMA Polymer Film.* Chemistry Letters, 1999. **28**(2): p. 165-166.

413. Brohmann, M., S. Wieland, S. Angstenberger, N.J. Herrmann, J. Lüttgens, D. Fazzi, and J. Zaumseil, *Guiding Charge Transport in Semiconducting Carbon Nanotube Networks by Local Optical Switching.* ACS Applied Materials & Interfaces, 2020. **12**(25): p. 28392-28403.

414. Aghamohammadi, M., R. Rödel, U. Zschieschang, C. Ocal, H. Boschker, R.T. Weitz, E. Barrena, and H. Klauk, *Threshold-Voltage Shifts in Organic Transistors Due to Self-Assembled Monolayers at the Dielectric: Evidence for Electronic Coupling and Dipolar Effects.* ACS Applied Materials & Interfaces, 2015. **7**(41): p. 22775-22785.

415. Buga, C.S. and J.C. Viana, *A Review on Materials and Technologies for Organic Large-Area Electronics.* Advanced Materials Technologies, 2021. **6**(6): p. 2001016.

416. Kraft, U., F. Molina-Lopez, D. Son, Z. Bao, and B. Murmann, *Ink Development and Printing of Conducting Polymers for Intrinsically Stretchable Interconnects and Circuits.* Advanced Electronic Materials, 2020. **6**(1): p. 1900681.

417. Volkert, C., R. Colucci, R. Berger, P. Besenius, P.W.M. Blom, and U. Kraft, *Transfer-printing of patterned PEDOT:PSS structures for bendable, stretchable and biodegradable electronics.* Journal of Materials Chemistry C, 2024. **12**(11): p. 3865-3872.

418. Zhao, C., J. Park, S.E. Root, and Z. Bao, *Skin-inspired soft bioelectronic materials, devices and systems.* Nature Reviews Bioengineering, 2024. **2**(8): p. 671-690.

419. Wang, X., Y. Liu, Q. Chen, Y. Yan, Z. Rao, Z. Lin, H. Chen, and T. Guo, *Recent advances in stretchable field-effect transistors.* Journal of Materials Chemistry C, 2021. **9**(25): p. 7796-7828.

420. Son, D., J. Kang, O. Vardoulis, Y. Kim, N. Matsuhisa, J.Y. Oh, J.W.F. To, J. Mun, T. Katsumata, Y. Liu, A.F. McGuire, M. Krason, F. Molina-Lopez, J. Ham, U. Kraft, Y. Lee, Y. Yun, J.B.H. Tok, and Z. Bao, *An integrated self-healable electronic skin system fabricated via dynamic reconstruction of a nanostructured conducting network.* Nature Nanotechnology, 2018. **13**(11): p. 1057-1065.

421. Ocheje, M.U., B.P. Charron, A. Nyayachavadi, and S. Rondeau-Gagné, *Stretchable electronics: recent progress in the preparation of stretchable and self-healing semiconducting conjugated polymers.* Flexible and Printed Electronics, 2017. **2**(4): p. 043002.

422. Vo, N.T.P., T.U. Nam, M.W. Jeong, J.S. Kim, K.H. Jung, Y. Lee, G. Ma, X. Gu, J.B.H. Tok, T.I. Lee, Z. Bao, and J.Y. Oh, *Autonomous self-healing supramolecular polymer transistors for skin electronics.* Nature Communications, 2024. **15**(1): p. 3433.

423. Zhu, Z., Y. Guo, and Y. Liu, *Application of organic field-effect transistors in memory.* Materials Chemistry Frontiers, 2020. **4**(10): p. 2845-2862.

424. Torsi, L., M. Magliulo, K. Manoli, and G. Palazzo, *Organic field-effect transistor sensors: a tutorial review.* Chemical Society Reviews, 2013. **42**(22): p. 8612-8628.

425. Klauk, H., D.J. Gundlach, and T.N. Jackson, *Fast organic thin-film transistor circuits.* IEEE Electron Device Letters, 1999. **20**(6): p. 289-291.

426. Sakai, H., Y. Takahashi, and H. Murata, *Organic field effect transistors with dipole-polarized polymer gate dielectrics for control of threshold voltage.* Applied Physics Letters, 2007. **91**(11): p. 113502.

427. Naber, R.C.G., C. Tanase, P.W.M. Blom, G.H. Gelinck, A.W. Marsman, F.J. Touwslager, S. Setayesh, and D.M. de Leeuw, *High-performance solution-processed polymer ferroelectric field-effect transistors.* Nature Materials, 2005. **4**(3): p. 243-248.

428. Baeg, K.-J., Y.-Y. Noh, H. Sirringhaus, and D.-Y. Kim, *Controllable Shifts in Threshold Voltage of Top-Gate Polymer Field-Effect Transistors for Applications in Organic Nano Floating Gate Memory.* Advanced Functional Materials, 2010. **20**(2): p. 224-230.

429. Chou, Y.-H., H.-C. Chang, C.-L. Liu, and W.-C. Chen, *Polymeric charge storage electrets for non-volatile organic field effect transistor memory devices.* Polymer Chemistry, 2015. **6**(3): p. 341-352.

430. Huang, C., J.E. West, and H.E. Katz, *Organic Field-Effect Transistors and Unipolar Logic Gates on Charged Electrets from Spin-On Organosilsesquioxane Resins.* Advanced Functional Materials, 2007. **17**(1): p. 142-153.

431. Deshmukh, K.D., K. Reuter, H. Kempa, J.E. West, and H.E. Katz, *Tuning of threshold voltage in organic field-effect transistors with hydrophobic gate dielectric using monoenergetic low-energy electron beams and triode corona.* Applied Physics Letters, 2009. **95**(11): p. 113307.

432. Reuter, K., H. Kempa, K.D. Deshmukh, H.E. Katz, and A.C. Hübler, *Full-swing organic inverters using a charged perfluorinated electret fabricated by means of mass-printing technologies.* Organic Electronics, 2010. **11**(1): p. 95-99.

433. Iba, S., T. Sekitani, Y. Kato, T. Someya, H. Kawaguchi, M. Takamiya, T. Sakurai, and S. Takagi, *Control of threshold voltage of organic field-effect transistors with double-gate structures.* Applied Physics Letters, 2005. **87**(2): p. 023509.

434. Khim, D., E.-Y. Shin, Y. Xu, W.-T. Park, S.-H. Jin, and Y.-Y. Noh, *Control of Threshold Voltage for Top-Gated Ambipolar Field-Effect Transistor by Gate Buffer Layer*. ACS Applied Materials & Interfaces, 2016. **8**(27): p. 17416-17420.

435. Sakai, H., K. Konno, and H. Murata, *Tuning of threshold voltage of organic field-effect transistors by space charge polarization.* Applied Physics Letters, 2009. **94**(7): p. 073304.

436. Huang, C., H.E. Katz, and J.E. West, *Solution-Processed Organic Field-Effect Transistors and Unipolar Inverters Using Self-Assembled Interface Dipoles on Gate Dielectrics.* Langmuir, 2007. **23**(26): p. 13223-13231.

437. Choi, J.-M., W. Choi, S. Lee, and S. Im, *Controlling the electrical properties of pentacene-based organic inverter by ultraviolet.* Synthetic Metals, 2008. **158**(21): p. 1072-1076.

438. Iqbal, M.J., T. Afzal, M.Z. Iqbal, B.S. Almutairi, M. Nadeem, H. Haq, F. Irshad, M.A. Raza, S. Riaz, and S. Naseem, *On the optical tuning of the threshold voltage for DPPDTT-based organic field effect transistors.* Journal of Materials Research, 2023.

439. Choi, J.-M., D.K. Hwang, J.M. Hwang, J.H. Kim, and S. Im, *Ultraviolet-enhanced device properties in pentacene-based thin-film transistors.* Applied Physics Letters, 2007. **90**(11): p. 113515.

440. Marchl, M., M. Edler, A. Haase, A. Fian, G. Trimmel, T. Griesser, B. Stadlober, and E. Zojer, *Tuning the Threshold Voltage in Organic Thin-Film Transistors by Local Channel Doping Using Photoreactive Interfacial Layers.* Advanced Materials, 2010. **22**(47): p. 5361-5365.

441. Guo, X., L. Huang, S. O'Brien, P. Kim, and C. Nuckolls, *Directing and Sensing Changes in Molecular Conformation on Individual Carbon Nanotube Field Effect Transistors.* Journal of the American Chemical Society, 2005. **127**(43): p. 15045-15047.

442. Vilanove, R., H. Hervet, H. Gruler, and F. Rondelez, *Photochromism of monolayers of poly(methylmethacrylate) having spirobenzopyran side groups.* Macromolecules, 1983. **16**(5): p. 825-831.

443. Karcher, M., C. Rüdt, C. Elsäßer, and P. Fumagalli, *Switching of nonfunctionalized spiropyran thin films on single crystalline MgO(100).* Journal of Applied Physics, 2007. **102**(8): p. 084904.

444. Suzuki, M., T. Asahi, and H. Masuhara, *Photochromic reactions of crystalline spiropyrans and spirooxazines induced by intense femtosecond laser excitation.* Physical Chemistry Chemical Physics, 2002. **4**(2): p. 185-192.

445. Hayashida, S., H. Sato, and S. Sugawara, *Photochromic Evaporated Films of Spiropyrans with Long Alkyl Chains.* Japanese Journal of Applied Physics, 1985. **24**(11R): p. 1436.

446. Hayashida, S., H. Sato, and S. Sugawara, *Photo-Induced Wettability Change in Films Containing Spiropyran Microcrystals.* Polymer Journal, 1986. **18**(3): p. 227-235.

447. Mathijssen, S.G.J., M.-J. Spijkman, A.-M. Andringa, P.A. van Hal, I. McCulloch, M. Kemerink, R.A.J. Janssen, and D.M. de Leeuw, *Revealing Buried Interfaces to Understand the Origins of Threshold Voltage Shifts in Organic Field-Effect Transistors.* Advanced Materials, 2010. **22**(45): p. 5105-5109.

448. Park, S., S.H. Kim, H.H. Choi, B. Kang, and K. Cho, *Recent Advances in the Bias Stress Stability of Organic Transistors.* Advanced Functional Materials, 2020. **30**(20): p. 1904590.

449. Yildiz, I., S. Impellizzeri, E. Deniz, B. McCaughan, J.F. Callan, and F.M. Raymo, *Supramolecular Strategies To Construct Biocompatible and Photoswitchable Fluorescent Assemblies.* Journal of the American Chemical Society, 2011. **133**(4): p. 871-879.

450. Simatos, D., L.J. Spalek, U. Kraft, M. Nikolka, X. Jiao, C.R. McNeill, D. Venkateshvaran, and H. Sirringhaus, *The effect of the dielectric end groups on the positive bias stress stability of N2200 organic field effect transistors.* APL Materials, 2021. **9**(4): p. 041113.

451. Kalb, W.L., T. Mathis, S. Haas, A.F. Stassen, and B. Batlogg, *Organic small molecule field-effect transistors with Cytop™ gate dielectric: Eliminating gate bias stress effects.* Applied Physics Letters, 2007. **90**(9).

452. Umeda, T., D. Kumaki, and S. Tokito, *High air stability of threshold voltage on gate bias stress in pentacene TFTs with a hydroxyl-free and amorphous fluoropolymer as gate insulators.* Organic Electronics, 2008. **9**(4): p. 545-549.

453. Schmidt, R. and A.W. Brinkman, *Studies of the Temperature and Frequency Dependent Impedance of an Electroceramic Functional Oxide NTC Thermistor.* Advanced Functional Materials, 2007. **17**(16): p. 3170-3174.

454. Shoar Abouzari, M.R., F. Berkemeier, G. Schmitz, and D. Wilmer, *On the physical interpretation of constant phase elements.* Solid State Ionics, 2009. **180**(14): p. 922-927.

455. Orazem, M.E., B. Tribollet, V. Vivier, S. Marcelin, N. Pébère, A.L. Bunge, E.A. White, D.P. Riemer, I. Frateur, and M. Musiani, *Interpretation of Dielectric Properties for Materials showing Constant-Phase-Element (CPE) Impedance Response.* ECS Transactions, 2013. **45**(13): p. 15.

456. Gateman, S.M., O. Gharbi, H. Gomes de Melo, K. Ngo, M. Turmine, and V. Vivier, *On the use of a constant phase element (CPE) in electrochemistry.* Current Opinion in Electrochemistry, 2022. **36**: p. 101133.

457. Zoltowski, P., *On the electrical capacitance of interfaces exhibiting constant phase element behaviour.* Journal of Electroanalytical Chemistry, 1998. **443**(1): p. 149-154.

458. Hirschorn, B., M.E. Orazem, B. Tribollet, V. Vivier, I. Frateur, and M. Musiani, *Constant-Phase-Element Behavior Caused by Resistivity Distributions in Films.* ECS Transactions, 2010. **28**(24): p. 77.

459. Hirschorn, B., M.E. Orazem, B. Tribollet, V. Vivier, I. Frateur, and M. Musiani, *Constant-Phase-Element Behavior Caused by Resistivity Distributions in Films: II. Applications.* Journal of The Electrochemical Society, 2010. **157**(12): p. C458.

Dissertation Appendix

Experimental Details

Materials and Solution Preparation

DHA/VHF molecular switches were synthesized by [redacted] as described in the literature [360]. The molecular switch SP/MC-1 was purchased from Sigma-Aldrich (product number 273619), while the synthesis of the other three SP/MC-n derivatives with alkyl chain lengths of four, ten and sixteen carbon atoms was accomplished by S. Brand via a modified procedure adapted from previous reports [449]. Regioregular poly(3-hexylthiophene-2,5-diyl) (P3HT, product number 445703, molecular weight = 50-100 kDa), poly[2,5-bis(3-tetradecylthiophen-2-yl)thieno[3,2-b]thiophene] (PBTTT, product number 753971, molecular weight > 50 kDa) and poly(methyl methacrylate) (PMMA, product numbers 200336 and 445746, average molecular weight = 15 kDa used for PMMA:DHA/VHF blends in Chapter 4 and 350 kDa used for PMMA:SP/MC-n blends in Chapter 5) were purchased from Sigma Aldrich and used without further purification.

Chapter 3

Stock solutions were prepared with anhydrous chlorobenzene (P3HT, 15 mg mL^{-1}) and anhydrous dichlorobenzene (PBTTT, 7 mg mL^{-1}) in a nitrogen-filled glovebox and stirred over night at 60 °C. DHA/VHF was dissolved in the same solvent as the polymer (10 mg mL^{-1}) and stirring was performed over night at room temperature. Solutions for spin coating were prepared by adding either switch stock solution (for blend devices) or pure solvent (for reference devices) to the polymer stock solution. Final polymer concentrations were 10 mg mL^{-1} for P3HT and 5 mg mL^{-1} for PBTTT solutions. The DHA/VHF content of the blend solutions was 10 wt%. Cytop (CTL-809M) was purchased from AGC Chemicals and used in a volume ratio polymer-solution:solvent of 3:1 [450].

Chapter 4

PMMA stock solutions were prepared with anhydrous trichloromethane (80 mg mL^{-1}, for capacitor and UV/Vis absorption spectroscopy experiments) or anhydrous ethyl acetate (120 mg mL^{-1}, for transistor experiments). For the photoswitch stock solutions, the solvent was chosen to match the solvent of PMMA (35-40 mg mL^{-1} in anhydrous trichloromethane or

52-60 mg mL^{-1} in anhydrous ethyl acetate). PMMA and switch solutions were prepared in air and stirred over night at room temperature, while P3HT solutions (10 mg mL^{-1} in anhydrous chlorobenzene) were prepared in a nitrogen-filled glovebox and stirred over night at 60 °C. The final PMMA solutions (40 mg polymer mL^{-1} in anhydrous trichloromethane or 60 mg polymer mL^{-1} (80 mg polymer mL^{-1} for PMMA-only reference) in anhydrous ethyl acetate) were prepared by adding either switch stock solution or additional solvent (for reference devices) to the PMMA stock solution and were stirred for 2 h at room temperature prior to spin coating. The molar fraction of photoswitch (with respect to a single PMMA repeat unit) in these solutions was 14.6 mol% (i.e. 14.6 switch molecules in proportion to 100 PMMA repeat units), resulting in the following mass fractions: 30.44 wt% (DHA-Ph), 32.89 wt% (DHA-OMe) and 33.33 wt% (DHA-F_2).

Chapter 5

PMMA and photoswitch stock solutions were prepared with anhydrous acetone (60 mg mL^{-1} and 30 mg mL^{-1} respectively). PMMA and switch solutions were prepared in air and stirred over night at room temperature, while P3HT solutions (10 mg mL^{-1} in anhydrous chlorobenzene) were prepared in a nitrogen-filled glovebox and stirred over night at 60 °C. The final PMMA solutions (30 mg polymer mL^{-1}) were prepared by adding either switch stock solution or additional solvent (for reference devices) to the PMMA stock solution and were stirred for 2 h at room temperature prior to spin coating. The resulting mass fractions of the photoswitches in these solutions were either 33, 20, 10 or 0 wt%.

Device Fabrication

Capacitors and top-gate bottom-contact transistors were fabricated on glass substrates. Prior to bottom electrode deposition, the substrates were cleaned via sonicating in ultrapure water (5 min), acetone and isopropanol (both 10 min). After drying the substrates in an oven (10 min at 140 °C) a UV/ozone treatment was applied for 20 min. Capacitor bottom electrodes (5 nm chromium/100 nm silver) and transistor source and drain electrodes (2 nm chromium/30 nm gold, channel length = 30 μm, channel width = 1 mm) were thermally evaporated through shadow

masks in vacuum (< 10^{-7} mbar). The transistor substrates were exposed to 20 min UV/ozone treatment prior to deposition of the organic semiconductor layer. Semiconductor:switch blend solutions (or the pure semiconductor solutions) were spin coated at 1500 rpm for 30 s to yield 35 nm (P3HT) or 20 nm (PBTTT) thin-films. Organic semiconductor films were annealed for 30 min at 150 °C (P3HT) or 180 °C (PBTTT) to remove residual solvent.

For the transistors presented in Chapter 3, a Cytop gate dielectric was spin coated at 2000 rpm for 20 s on top of the annealed semiconductor film and annealed at 90 °C for 20 min to yield a 500 nm thick dielectric layer. **Figure DA.1** shows that the capacitance of the Cytop dielectric is frequency independent between 1-10^5 Hz and that the dielectric permittivity matches well with the literature value of 2.1 [451, 452]. The area-normalized gate dielectric capacitance was calculated to be 3.7 nF cm^{-2}. Finally, 70 nm of aluminum were evaporated through a shadow mask onto the Cytop as top-gate electrodes.

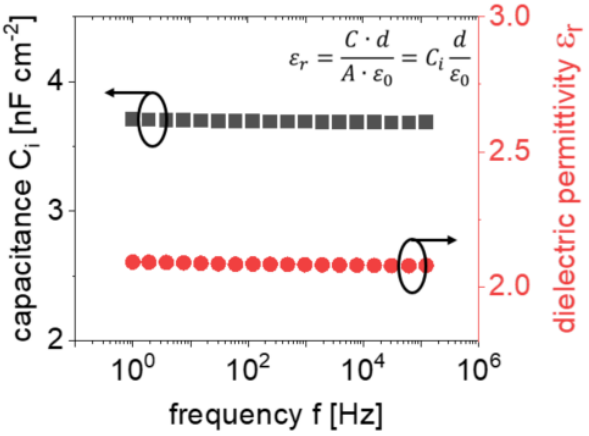

Figure DA.1: Dielectric properties of Cytop dielectric measured on a d = 500 nm thin-film sandwiched between two gold electrodes. The overlap area of the electrodes was measured as A = 0.84 mm^2 using a Bruker DektakXT profilometer. C-f measurement was conducted using a Novocontrol Alpha-A frequency analyzer. The dielectric permittivity of Cytop was calculated using the formula given in the inset and found to match well with the reported literature value of 2.1 [451, 452].

For the devices presented in Chapters 4 and 5 PMMA:photoswitch blends or pure PMMA dielectrics were spin coated either on top of the bottom electrode (capacitors) or the P3HT film (OFETs) at 2000 rpm for 60 s. This yielded films with a thickness of 600-650 nm/710-730 nm (trichloromethane/ethyl acetate, with switch) and 460 nm/700 nm (trichloromethane/ethyl acetate, no switch) in the case of DHA/VHF (Chapter 4) and 610-680 nm (33 wt% switch), 480-600 nm

(20 wt% switch), 440-550 nm (10 wt% switch) and 400-450 nm (no switch) in the case of SP/MC-n (Chapter 5). All PMMA and PMMA:photoswitch films were annealed at 90 °C for 20 min. Finally, 20 nm of silver were evaporated through a shadow mask onto the dielectric as semi-transparent top electrodes to ensure high transparency for UV light (see **Figure DA.2**). For the capacitors, the area of electrode overlap *A* is 1 mm^2.

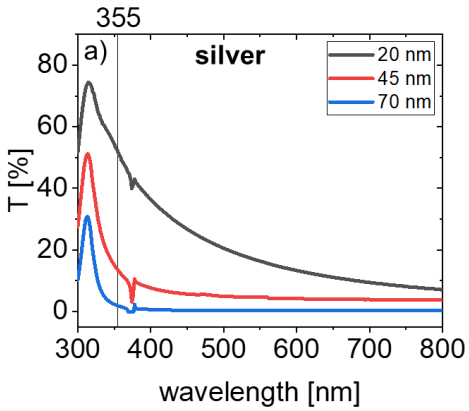

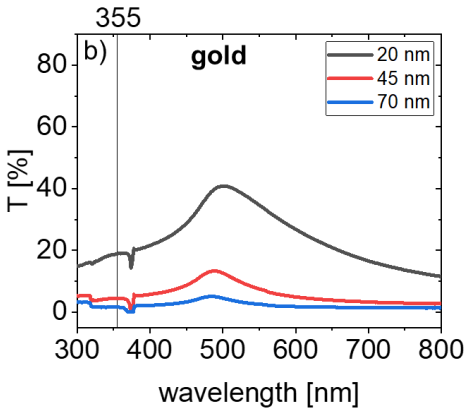

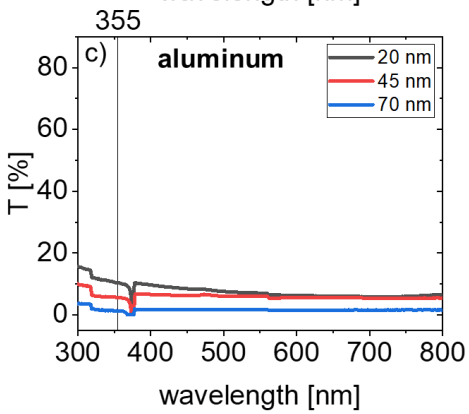

d)
Transmittance at 355 nm [%]

thickness / metal	20 nm	45 nm	70 nm
silver	52	13	2
gold	19	4	2
aluminum	10	6	1

Figure DA.2: UV/Vis absorption spectra of various metal films with different thicknesses (20 nm, 45 nm and 70 nm): a) Silver, b) gold, c) aluminum. d) Transmittance of the metal films at 355 nm (i.e. the wavelength of maximum emission of the UV light source). These measurements were carried out in order to identify the best configuration for semi-transparent top electrodes for capacitor and OFET devices.

All fabrication steps from deposition of the bottom electrodes onwards were carried out in a nitrogen-filled glovebox.

UV/T Treatments

All thin-film samples and devices (transistors and capacitors) were illuminated using a Dymax ECE 2000 flood lamp (13 mW cm^{-2} at 320-390 nm) and the dose was monitored using a Dymax Accu-Cal 50 UV dose meter. Thermal switching (from VHF to DHA or from MC to SP) was carried out on a hot plate at 90 °C for 20 min (Chapter 3) or 5 min (Chapters 4 and 5). All illumination/annealing steps were carried out in a nitrogen-filled glovebox.

Transistor Characterization

All transistors were characterized in the dark (i.e. after UV light/heat-induced switching) in a nitrogen-filled glovebox using a Keithley 4200-SCS semiconductor parameter analyzer. Transistor figures of merit, i.e. threshold voltage, subthreshold swing and field-effect mobility were derived from transfer characteristics following the common procedures described in the literature [16]. For the determination of the threshold voltage transfer characteristics were fitted for V_{GS} between -30 V and -50 V (Chapter 3) and for V_{GS} between -20 V and -50 V (Chapters 4 and 5). Due to the significant hysteresis in the transfer characteristics at high mass fractions of the SP/MC-n photoswitches (Chapter 5) the field-effect mobility and the threshold voltage were extracted from the forward V_{GS} sweep (from +20 V to -50 V) only.

For the transistor bias stress measurements presented in Chapters 4 and 5 constant bias stress was applied for 2 h (cumulative) between drain and source electrodes (V_{DS} = -50 V) and gate and source electrodes (V_{GS} = -50 V). During this time the bias stress was only paused at various time intervals (after 10, 20, 30, 40, 50, 60, 70, 80, 90, 100, 110, 120, 150, 180, 210, 240, 270, 300, 360, 420, 480, 540, 600, 720, 840, 960, 1080, 1200, 1500, 1800, 2400, 3000, 3600, 5400 and 7200 s) to record (in total 36) transfer characteristics (sweeping V_{GS} from +20 V to -50 V to +20 V, V_{DS} = -50 V).

Capacitor Characterization via Impedance Spectroscopy

Impedance spectra were recorded in the dark under ambient conditions using a Novocontrol Alpha-A impedance analyzer with a ZG4 test interface and measurements were carried out in air by applying an AC voltage of 1 V rms and sweeping the angular frequency from 10^6 Hz to 1 Hz (35 data points with equal logarithmic spacing). EISSA (Electrochemical Impedance Spectroscopy Spectrum Analyzer) software was used for fitting of the impedance data. The details of the fitting procedure, equations and further information on the impedance formalism that was adapted in this dissertation can be found below.

Characterization of DHA/VHF in Solution

Thermal conversion of VHF-F_2 to DHA-F_2 was monitored via solution ^{1}H NMR at room temperature using deuterated benzene as a solvent. The first spectrum was recorded for pure VHF-F_2 and all subsequent spectra were recorded after keeping the solution in the dark for 3, 6, 24 and 72 h respectively. These measurements were performed by [redacted].

For the UV/Vis absorption spectroscopy DHA-F_2 was dissolved in acetonitrile. Before the measurement the sample was irradiated outside of the spectrometer, using a UV lamp (500 μW cm^{-2}) equipped with a monochromator selecting 365 nm. Spectra were acquired after 2, 7, 10, 13, 17, 22, 30, 40, 60, 70, 85, 100, 125, 150, 175 and 200 s of irradiation. These measurements were performed by [redacted].

Electron paramagnetic resonance (EPR) spectroscopy was performed on a chlorobenzene solution containing P3HT (10 mg mL^{-1}) and 10 wt% of VHF-F_2 (weight fraction calculated from the amount of polymer). Before the measurement, the solution had been irradiated with UV light.

UV/Vis Absorption Spectroscopy

Thin-film samples for UV/Vis absorption measurements were fabricated by depositing the PMMA:photoswitch blends on cleaned glass substrates. Substrate cleaning and deposition of the

blends was performed under the same conditions as for the preparation of capacitor and transistor devices. All blend films were exposed to 20 UV light illumination (5 J cm^{-2}) and 20 thermal annealing (90 °C for 5 min) steps (UV and T always alternating). For the fatigue analysis, absorption spectra were recorded after every step for the first 10 cycles, for the 15th cycle and for the 20th cycle.

DFT Studies

Optimized structures and frontier molecular orbitals of the photo-/thermochromic molecules used in this dissertation were calculated at the B3LYP/6-311G(d,p) level of density functional theory (DFT) using Gaussian09.

Impedance Spectroscopy Formalism

The impedance was determined by applying a time-dependent AC voltage signal $U(\omega,t)$ of defined angular frequency ω and amplitude U_0 and measuring the amplitude I_0 and phase angle φ of the current response signal $I(\omega,t)$ (see Equations 8 and 9).

$$U(\omega, t) = U_0 cos(\omega t) \tag{8}$$

$$I(\omega, t) = I_0 cos(\omega t + \varphi) \tag{9}$$

Following Equations 10 to 12 the modulus of the complex impedance $|Z^*|$, its real part Z' and its imaginary part Z'' are calculated.

$$|Z^*| = \frac{U_0}{I_0} = \sqrt{Z'^2 + Z''^2} \tag{10}$$

$$Z' = |Z^*|cos(\varphi) \quad (11)$$

$$Z'' = |Z^*|sin(\varphi) \quad (12)$$

These quantities were determined over a wide range of frequencies *f* (between 1 Hz and 10^6 Hz). The relation between frequency and angular frequency is given by $\omega = 2\pi f$. The real part ε_r', imaginary part ε_r'' and modulus $|\varepsilon_r^*|$ of the complex dielectric permittivity ε_r^* and the loss tangent $tan(\delta)$ were calculated following Equations 3 to 6. The mathematical description of this impedance formalism was adapted from [453].

Equivalent Circuit Fitting Analysis

To the best of my knowledge, this dissertation provides the first detailed account of analyzing impedance data of light-switchable capacitors using equivalent circuit fitting. Therefore, a detailed summary of the fitting results using different circuit models is presented in the following. The software EISSA (Electrochemical Impedance Spectroscopy Spectrum Analyzer) was used for performing the equivalent circuit analysis. Firstly, a fitting algorithm and a fitting function need to be selected. For this analysis the Levenberg-Marquardt algorithm was used. Available fitting functions are labelled as "unweighted", "amplitude" and "parametric". The exact mathematical expressions behind these functions can be found in the documentation of the EISSA software (www.abc.chemistry.bsu.by/vi/analyser/). The results presented below (see **Figure DA.3 - Figure DA.5**) reveal that the unweighted fitting function yields more accurate fits than the amplitude and the parametric fitting functions, regardless of which model is used. Therefore, the unweighted function was used for the equivalent circuit fitting analysis. In order to identify the best fitting routine, three different equivalent circuit models were used to fit a representative impedance spectrum of a fresh PMMA:DHA/VHF-Ph capacitor sample. The tested models included a single capacitor, a single constant phase element (CPE) and an RC element (resistor and capacitor in parallel). These different models were tested in combination with the three different fitting functions and the overall accuracy of the fit was evaluated based on three aspects: 1) Match of

fitting results with experimental results depicted in Nyquist, Bode and phase angle plots; 2) fitting errors of the parameters of the individual circuit elements; 3) statistics of the fitted model (i.e. r^2 values). The EISSA software provides all of this information after the fit has successfully converged. **Figure DA.3 - Figure DA.5** show these fitting results for the three models tested using the three different fitting functions. It should be noted that Nyquist plots are shown on non-orthonormal axes to highlight the differences in fit results.

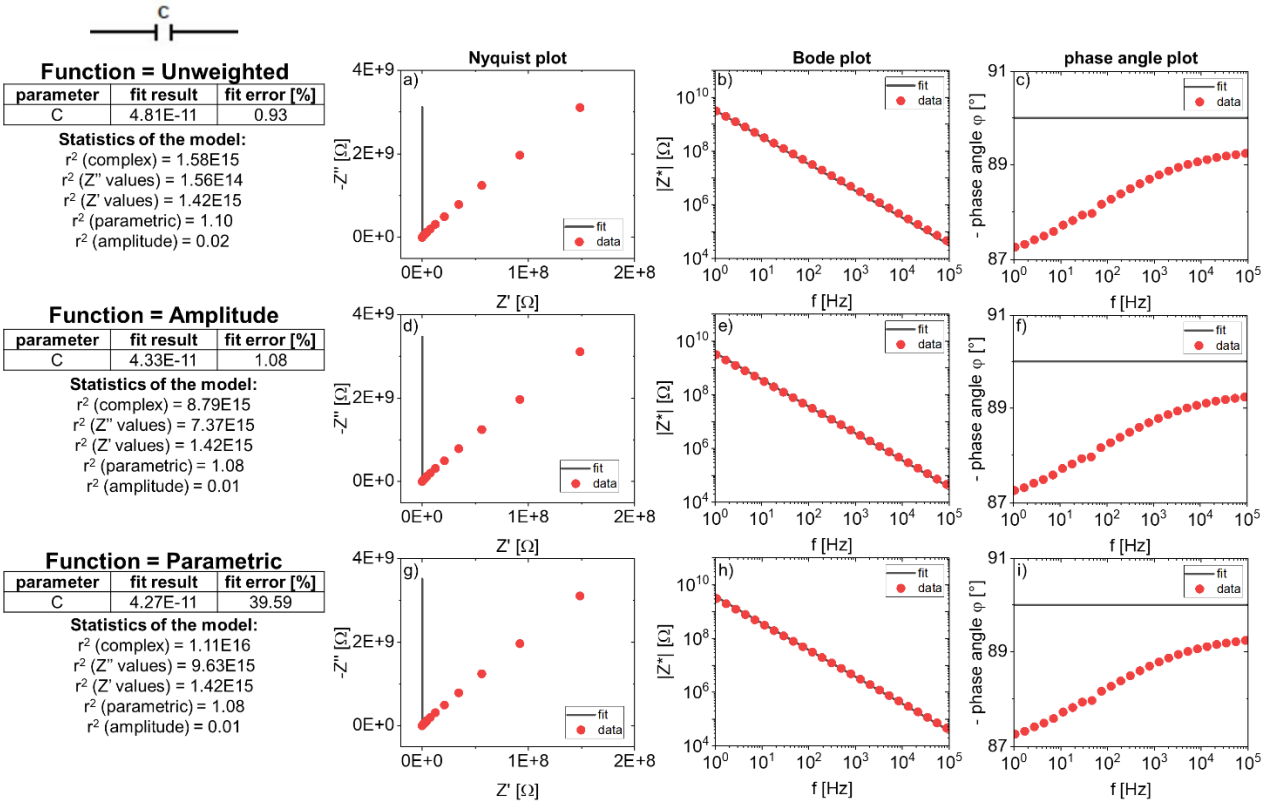

Figure DA.3: Fit results obtained by using a **single capacitor** as the equivalent circuit in combination with different fitting functions. a) - c) Unweighted, d) - f) amplitude and g) - i) parametric. The information provided includes fitting errors, model statistics and fits of Nyquist (on non-orthonormal axes), Bode and phase angle plots.

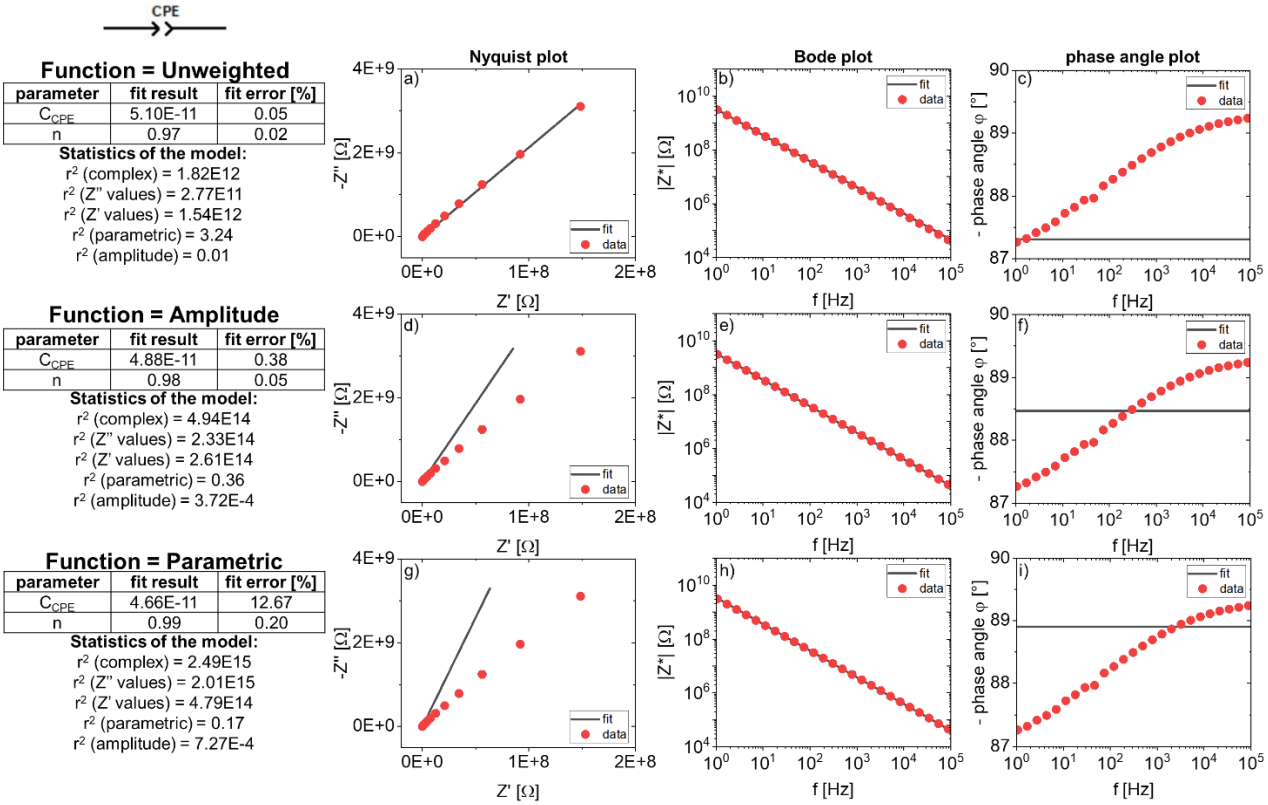

Figure DA.4: Fit results obtained by using a **single CPE** as the equivalent circuit in combination with different fitting functions. a) - c) Unweighted, d) - f) amplitude and g) - i) parametric. The information provided includes fitting errors, model statistics and fits of Nyquist (on non-orthonormal axes), Bode and phase angle plots.

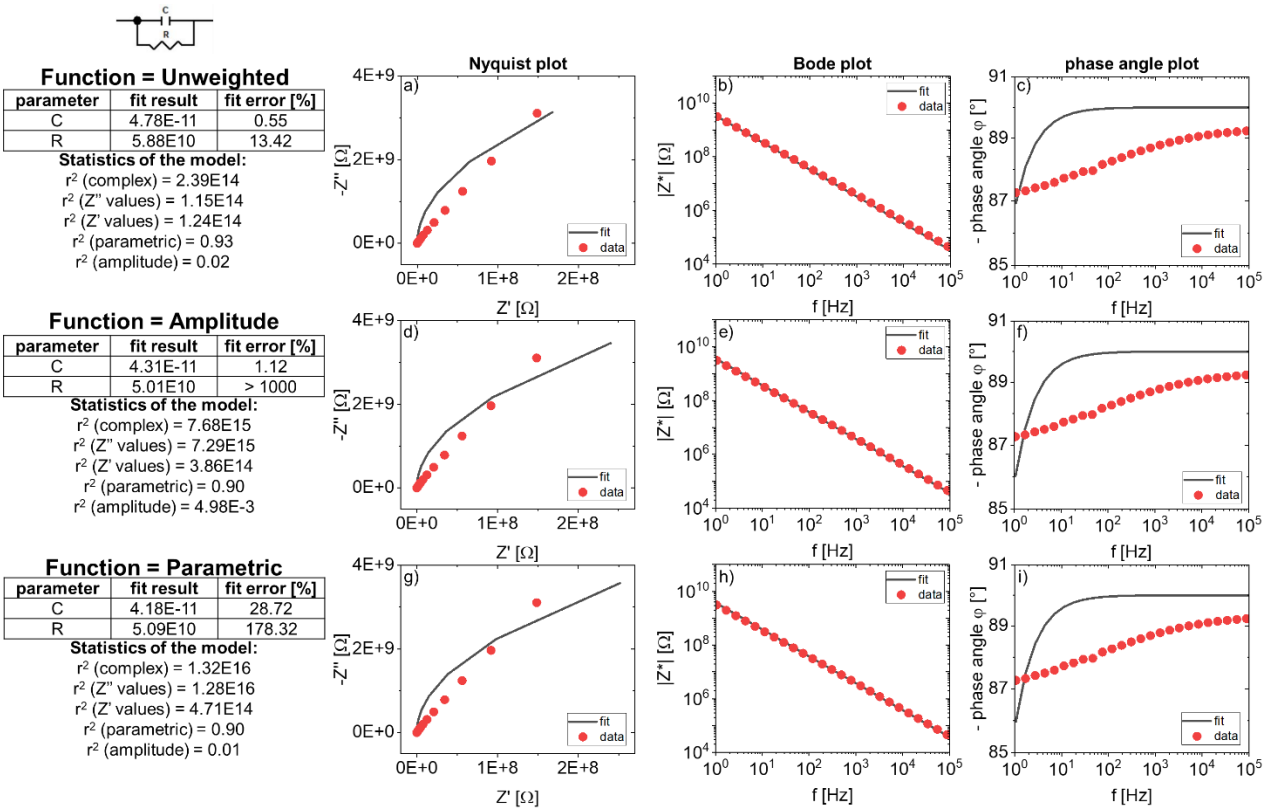

Figure DA.5: Fit results obtained by using an **RC element** as the equivalent circuit in combination with different fitting functions. a) - c) Unweighted, d) - f) amplitude and g) - i) parametric. The information provided includes fitting errors, model statistics and fits of Nyquist (on non-orthonormal axes), Bode and phase angle plots.

These data suggest that all models yield satisfying fits for the Bode plots (impedance). However, this is only the case due to the log-log scale of the plot. When plotting the phase angles on a lin-log scale however, it becomes apparent, that φ cannot be reproduced properly by any of the models. Whether the low-frequency regime of the Nyquist plot can be fitted accurately or not, depends on the model and on the fitting function used. **Figure DA.3a** shows that a single capacitor is not able to appropriately reproduce the experimental Nyquist plot. This is mostly because *Z'* of an ideal capacitor is zero, which is not the case for the measured capacitors. Instead, the Nyquist plot can be roughly fitted using a semicircle arch, which is the typical impedance behavior of an RC element. As indicated in **Figure DA.5a**, using this model still only yields a poor fitting of the experimental data. **Figure DA.4a** shows that by using a single CPE as equivalent circuit, the Nyquist plot can be fitted more accurately. **Figure DA.6** summarizes the fits of the Nyquist plot (on orthonormal axes) that were obtained with the three different circuit models.

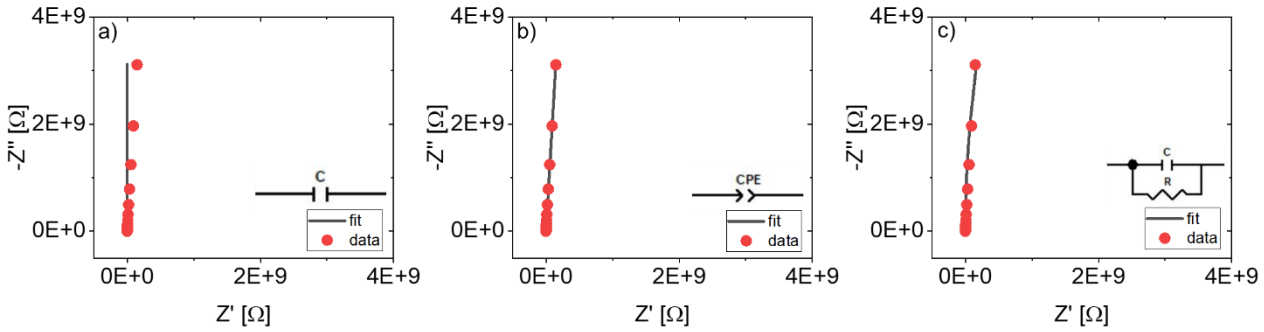

Figure DA.6: Fitting a (representative) Nyquist plot with different equivalent circuit models. a) Single capacitor, b) single CPE and c) RC element (same as **Figure 4.6c**). Experimental data is shown as red circles and the fit result is shown as a black line. The data used for the fitting is the same for all circuits and was measured on a fresh PMMA:DHA/VHF-Ph capacitor.

It can be concluded that the model containing a single CPE yields a more accurate fit than the ones with ideal capacitors (single capacitor and RC element). The more detailed evaluation of fitting errors and model statistics shown above confirms this notion, since the CPE model also leads to lower fitting errors and lower r^2 values. However, it should also be considered that a CPE is only a mathematical construct to take into account non-idealities, which usually occur in experimental impedance data. The complex impedance of a CPE can be expressed as given by Equation 13 where C_{CPE} is the specific capacitance with unit Fs^{n-1} and n is the critical exponent (dimensionless). The constant phase angle φ_{CPE} can be calculated using Equation 14. When $n = 1$, the CPE can be considered as an ideal capacitor [454]. CPEs are readily used in equivalent circuit fitting analyses in the literature, but their use generally comes at the expense that the physical interpretation of the circuit becomes non-trivial [454-456].

$$Z^*_{CPE} = \frac{1}{(i\omega)^n \cdot C_{CPE}} \tag{13}$$

$$\varphi_{CPE} = -90° \cdot n \tag{14}$$

The analysis above shows that by using relatively simple equivalent circuit models, satisfying fits for Nyquist and Bode plots can be achieved. However, the phase angle cannot be reproduced by any of these models.

As a next step, the three equivalent circuit models were used to fit the impedance spectra of a PMMA:DHA/VHF-Ph capacitor that were acquired over the course of eight UV/T cycles (i.e. 17 processing steps, including the fresh device). **Figure 4.6a-b** and **Figure DA.7 - Figure DA.8** show the results for the fitted parameters of the different circuit models. In short, all three models are able to capture the reversible switching of the system. This is particularly intriguing since the resulting accuracy of the fits differs significantly between the individual models. Depending on the circuit elements that were used in the model, the resulting switching can be quantified by either capacitances *C*, specific capacitances C_{CPE}, critical exponents *n* or resistances *R*. The overall trends are consistent with the expectation that UV light exposure and therefore the isomerization from the low dipole moment isomer (DHA) to the high dipole moment isomer (VHF) leads to an increase in capacitance/specific capacitance. Similar results were reported for PMMA-based capacitors containing azobenzene [403] and spiropyran [404] switches. At the same time this isomerization causes a decrease in resistance (see **Figure 4.6b**) which is in agreement with the increased single-molecule conductance of VHF (compared to DHA) due to a lower bandgap [269, 358]. It is interesting to note that this effect is also reflected in the critical exponent *n* (see **Figure DA.8b**), i.e. a decrease in resistance correlates with an increase in the non-ideality of the capacitance, since *n* shows a larger deviation from the ideal case ($n = 1$).

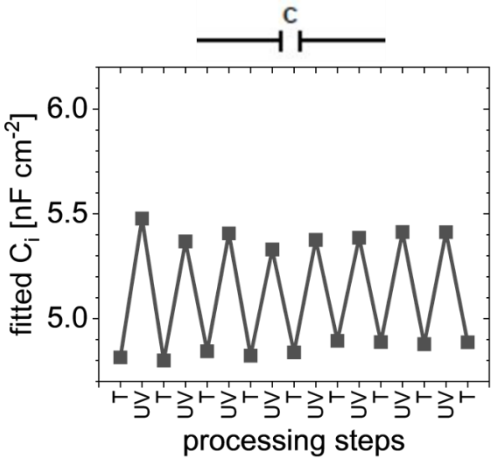

Figure DA.7: Fitted area-normalized capacitance that was obtained by using a **single capacitor** as equivalent circuit to fit impedance data from a PMMA:DHA/VHF-Ph capacitor sample acquired over the course of eight UV/T cycles.

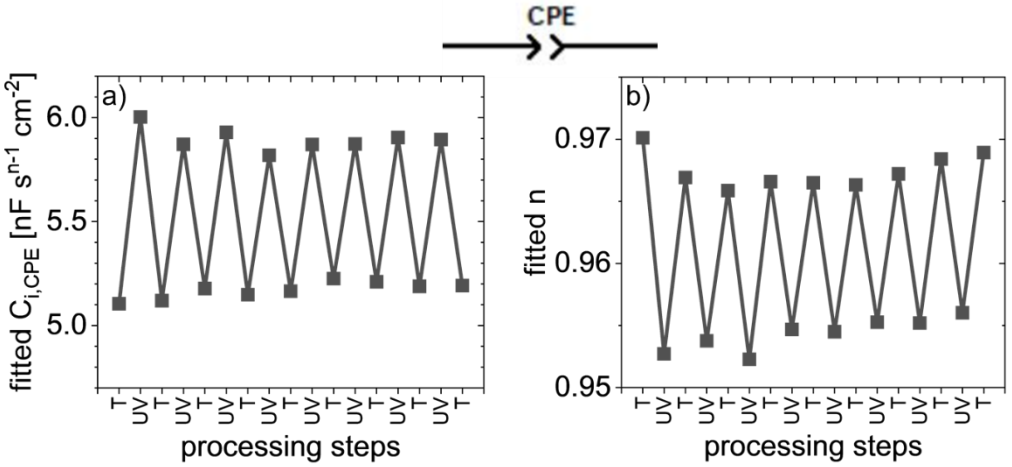

Figure DA.8: Fitted circuit element parameters that were obtained by using a **single CPE** as equivalent circuit to fit impedance data from a PMMA:DHA/VHF-Ph capacitor sample acquired over the course of eight UV/T cycles. a) Area-normalized specific capacitance, b) critical exponent. Note that the exponent *n* of the unit in panel a) corresponds to the critical exponent.

As the final step of this analysis, the permittivities were calculated using fitted capacitances and fitted specific capacitances. This is straightforward for those equivalent circuit models that contain capacitors. In this case, the permittivities can be calculated directly using Equation 7, since the film thickness *d* and the area of electrode overlap *A* are known.

The physical interpretation of the CPE model however, is not trivial and different approaches for determining capacitances from CPE parameters are used in the literature [455]. Here, the substitution approach is applied where the specific capacitance C_{CPE} is assumed to be equal to the capacitance *C*. This approach is ignoring the fact that C_{CPE} and *C* have different units and is usually applied when the critical exponent is larger than 0.9 [455].

Figure DA.9 shows a comparison between dielectric permittivities of the fresh device and the relative change in permittivity due to the first UV light exposure that were determined by either evaluating the frequency-dependent dielectric permittivity at low frequency (i.e. $|\varepsilon_r|$ at $f = 1$ Hz) or via the equivalent circuit fitting analysis.

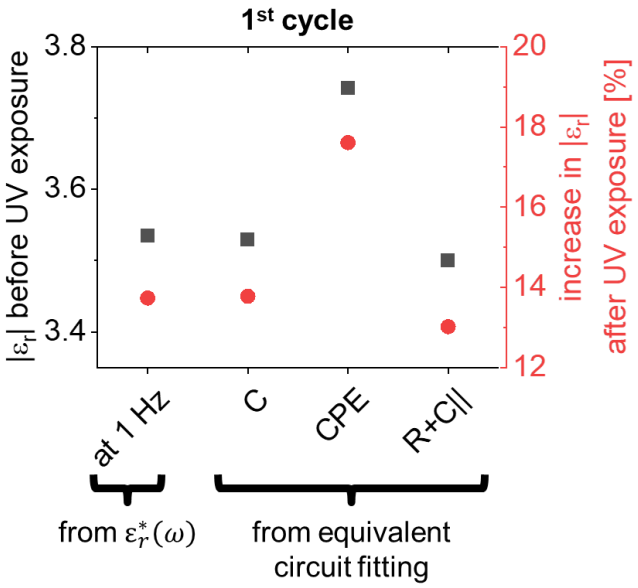

Figure DA.9: Comparing different approaches for the determination of dielectric permittivity of a PMMA:DHA/VHF-Ph capacitor. Absolute values of permittivity (black squares) of fresh capacitor and the relative increase in permittivity due to the first UV light exposure (red circles). Permittivities were obtained by either evaluating the frequency-dependent impedance at $f = 1$ Hz or by fitting the impedance data with various equivalent circuit models (i.e. single capacitor, single CPE and RC element).

This comparison shows that the values obtained by evaluating the frequency-dependent dielectric permittivity at $f = 1$ Hz are in good agreement with the values determined using either a single capacitor or an RC element as an equivalent circuit. It is also important to note that the values resulting from the single CPE equivalent circuit are higher than those derived from circuits containing ideal capacitors. **Figure DA.10** and **Figure DA.11** indicate that these findings are not only valid for the first UV/T cycle, but also for the following seven cycles.

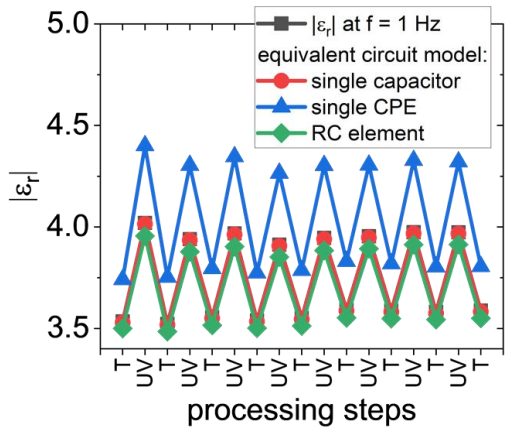

Figure DA.10: Comparing different approaches for the determination of dielectric permittivity of a PMMA:DHA/VHF-Ph capacitor. Permittivities were obtained by evaluating the frequency-dependent impedance at $f = 1$ Hz (black squares) and by fitting various equivalent circuit models (single capacitor (red circles), single CPE (blue triangles) and RC element (green diamonds)) to impedance data recorded over the course of eight UV/T cycles. Data shown with black squares and green diamonds is the same as shown in **Figure 4.6d**.

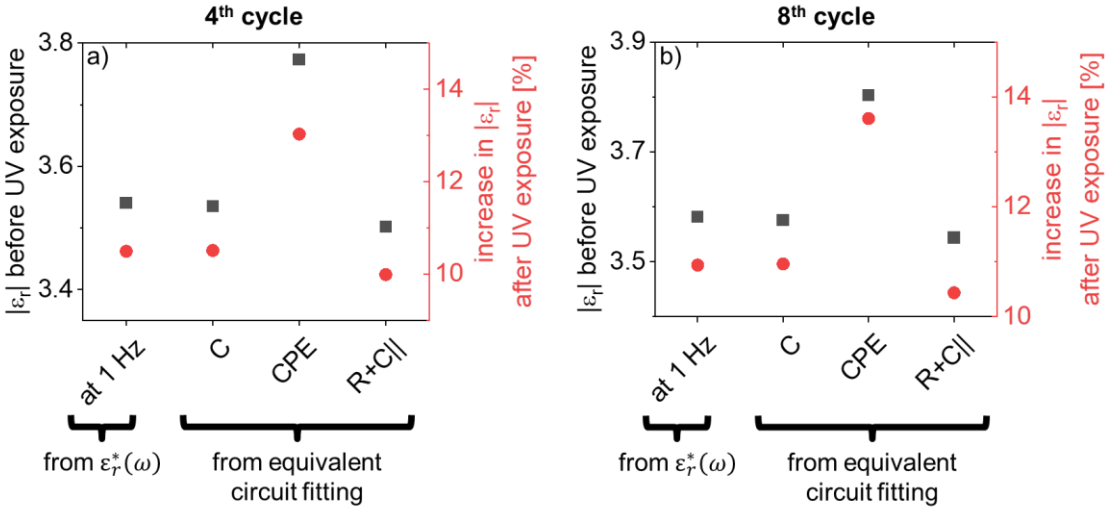

Figure DA.11: Comparing different approaches for the determination of dielectric permittivity of a PMMA:DHA/VHF-Ph capacitor. Absolute values of permittivity (black squares) and the relative increase in permittivity due to UV light exposure (red circles) during the a) fourth and b) eighth cycle. Permittivities were obtained by either evaluating the frequency-dependent impedance at $f = 1$ Hz or by fitting the impedance data with various equivalent circuit models (i.e. single capacitor, single CPE and RC element).

This analysis indicates that the fitting with a non-ideal circuit (single CPE) leads to an overestimation of the resulting permittivities. Although all values of the critical exponent *n* exceed

0.95, it may not be appropriate to use the substitution approach ($C \approx C_{CPE}$) as it is recognized as a rough approximation causing a significant error [457]. This observation is in line with the results of Orazem et al. who reported that this simple approach leads to unreasonably high permittivities. Instead, the authors recommend to use the more complicated formalism developed by Hirschorn et al. [458, 459].

To conclude this section, it can be stated that the permittivities derived from the single CPE equivalent circuit have a large error, even though the fit of the impedance spectrum is more accurate compared to the circuits containing ideal capacitors. By using a single capacitor or an RC element as an equivalent circuit, the resulting accuracy of the fit is lower, but the permittivities derived from these models are less likely to be overestimated, which is also indicated by the good agreement with the values derived by evaluating the frequency-dependent dielectric permittivity at f = 1 Hz.

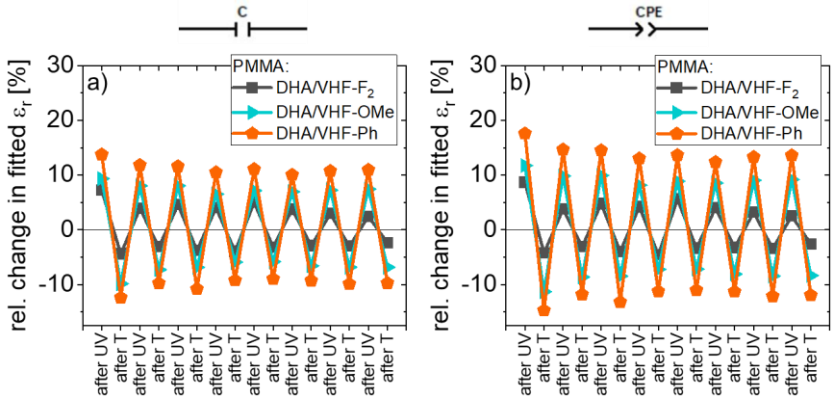

Figure DA.12: Comparing the switching of dielectric permittivity for PMMA:DHA/VHF capacitors containing three different DHA/VHF derivatives. The relative change in permittivity was determined via fitting various equivalent circuit models to impedance data collected over the course of eight UV/T cycles. a) Single capacitor and b) single CPE. Equivalent results after fitting with an RC element are shown in **Figure 4.7**.

Relative Switching of Capacitors and Transistors with PMMA:SP/MC-n Dielectrics

Table DA.1: Relative changes in dielectric permittivity and transistor figures of merit determined for capacitors and transistors with PMMA + x wt% **SP/MC-1** blend dielectrics (with x = 33, 20, 10 and 0) after UV light exposure (5 J cm^{-2}) and thermal annealing (90 °C for 5 min).

SP/MC-1 content	relative change in … [%]											
	ε_r' at 1 Hz		ε_r" at 1 Hz		$\lvert\varepsilon_r^*\rvert$ at 1 Hz		tan(δ) at 1 Hz		$\lvert I_{on}\rvert$		μ	
	after UV	after T	after UV	after T	after UV	after T	after UV	after T	after UV	after T	after UV	after T
33 wt%	5.6±0.1	-4.4±0.1	1.2±0.3	-0.2±0.2	5.6±0.1	-4.4±0.1	-5.3±1.0	3.9±0.8	-68±7.0	195±17	-47±4.1	100±15
20 wt%	4.8±0.1	-3.7±0.01	8.1±0.8	-4.4±0.2	4.8±0.1	-3.7±0.01	3.9±0.9	-2.7±0.2	-59±2.4	160±18	-43±3.7	87±7.9
10 wt%	1.3±0.04	-0.9±0.1	1.7±0.3	-2.3±0.1	1.3±0.04	-1.0±0.1	2.7±0.3	-3.2±0.2	-54±1.3	84±8	-40±5.8	52±8.2
0 wt%	1.1±0.1	-1.5±0.3	-0.9±0.1	2.8±0.7	1.1±0.1	-1.5±0.3	-1.1±0.2	1.6±0.4	7±0.1	-16±1	2.4±0.7	-8.8±1.0

Table DA.2: Relative changes in dielectric properties and transistor figures of merit determined for capacitors and transistors with PMMA + x wt% **SP/MC-4** blend dielectrics (with x = 33, 20 and 10) after UV light exposure (5 J cm^{-2}) and thermal annealing (90 °C for 5 min).

SP/MC-4 content	relative change in … [%]											
	ε_r' at 1 Hz		ε_r" at 1 Hz		$\lvert\varepsilon_r^*\rvert$ at 1 Hz		tan(δ) at 1 Hz		$\lvert I_{on}\rvert$		μ	
	after UV	after T	after UV	after T	after UV	after T	after UV	after T	after UV	after T	after UV	after T
33 wt%	8.2±0.1	-7.7±0.4	5.6±1.2	-5.1±1.1	8.2±0.1	-7.7±0.4	-5.7±0.4	3.3±1.1	-63±3.2	191±29	-51±2.0	115±11
20 wt%	4.7±0.1	-6.2±0.3	5.8±0.1	-9.2±0.6	4.7±0.1	-6.2±0.3	-2.1±0.2	-3.2±0.4	-63±6.2	204±63	-50±8.5	108±47
10 wt%	-2.3±0.1	-3.1±0.5	2.9±0.1	-6.8±1.3	-2.3±0.1	-3.1±0.5	1.6±0.1	-3.8±1.0	38±23	-24±19	60±22	-35±12

Table DA.3: Relative changes in dielectric properties and transistor figures of merit determined for capacitors and transistors with PMMA + x wt% **SP/MC-10** blend dielectrics (with x = 33, 20 and 10) after UV light exposure (5 J cm^{-2}) and thermal annealing (90 °C for 5 min). X indicates that the values could not be determined.

	relative change in … [%]											
SP/MC-10 content	**ε_r' at 1 Hz**		**ε_r" at 1 Hz**		**$\lvert\varepsilon_r^*\rvert$ at 1 Hz**		**tan(δ) at 1 Hz**		**$\lvert I_{on}\rvert$**		**μ**	
	after UV	**after T**	**after UV**	**after T**	**after UV**	**after T**	**after UV**	**after T**	**after UV**	**after T**	**after UV**	**after T**
33 wt%	4.6±0.8	-7.1±0.5	-24±2.5	20±6.7	4.5±0.8	-7.1±0.5	-27±1.9	30±6.9	497±69	-89±0.7	439±12	-89±0.7
20 wt%	4.0±0.1	-3.6±0.1	2.6±0.9	-2.5±0.6	4.0±0.1	-3.6±0.1	-6.1±1.1	2.4±0.4	126±108	-54±14	-32±2.3	-21±3.0
10 wt%	2.7±0.9	-1.8±0.03	6.3±1.9	-5.6±0.1	2.7±0.9	-1.9±0.03	3.5±1.1	-3.8±0.1	X	22±14	-8.1±5.0	19±2.8

Table DA.4: Relative changes in dielectric properties and transistor figures of merit determined for capacitors and transistors with PMMA + x wt% **SP/MC-16** blend dielectrics (with x = 33, 20 and 10) after UV light exposure (5 J cm^{-2}) and thermal annealing (90 °C for 5 min). X indicates that the values could not be determined.

	relative change in … [%]											
SP/MC-16 content	**ε_r' at 1 Hz**		**ε_r" at 1 Hz**		**$\lvert\varepsilon_r^*\rvert$ at 1 Hz**		**tan(δ) at 1 Hz**		**$\lvert I_{on}\rvert$**		**μ**	
	after UV	**after T**	**after UV**	**after T**	**after UV**	**after T**	**after UV**	**after T**	**after UV**	**after T**	**after UV**	**after T**
33 wt%	-19±0.6	22±0.9	-62±0.5	169±6	-20±0.6	24±0.9	-53±0.5	121±3	235±118	-93±3.9	X	X
20 wt%	-4.2±0.3	4.9±0.5	-30±1.5	52±4.6	-4.3±0.3	5.1±0.5	-27±1.4	45±3.9	7343±3034	-99±0.6	2409±1333	-93±4.5
10 wt%	-0.8±0.3	0.9±0.3	-2.9±0.3	2.8±0.8	-0.8±0.3	0.9±0.3	-3.0±0.5	2.0±0.8	99±66	-34±23	51±47	-21±21

List of Publications

1. Gebel, S., [redacted], [redacted], [redacted], [redacted], [redacted], [redacted], [redacted] and [redacted], *Reversible Switching of Light-Gated Organic Transistors Employing Dihydroazulene/Vinylheptafulvene Photo-/Thermochromic Molecules.* Advanced Electronic Materials, 2024: p. 2400455.

2. Gebel, S., [redacted], [redacted], [redacted] and [redacted], *Reversible Switching Through Irradiation of Capacitors and Organic Transistors Employing Dihydroazulene/Vinylheptafulvene:PMMA Blend Dielectrics.* In preparation.

3. Gebel, S., [redacted], [redacted], [redacted] and [redacted], *Adjustable Threshold Voltage in Organic Transistors Enabled by Light-Switchable Gate Dielectrics.* In preparation.

List of Conferences

Oral Presentations

1. Gebel, S., [redacted], [redacted], [redacted] and [redacted], *Reversible Switching of Organic Transistors Employing Photochromic Molecules.* 25th International Conference on Science and Technology of Synthetic Metals (ICSM) in Glasgow, United Kingdom (July 2022).

2. Gebel, S., [redacted], [redacted], [redacted] and [redacted], *Reversible Switching of Organic Transistors Employing Photochromic Molecules.* 15th International Symposium on Functional π-Electron Systems (Fπ) in Raleigh, North Carolina, United States of America (June 2023).

3. Gebel, S., [redacted], [redacted], [redacted] and [redacted], *Reversible Switching in Capacitors and Organic Transistors Employing Dihydroazulene/Vinylheptafulvene Photochromic Switches.* 2024 Materials Research Society (MRS) Spring Meeting & Exhibit in Seattle, Washington, United States of America (April 2024).

Poster Presentations

1. Gebel, S., [redacted], [redacted], [redacted] and [redacted], *Reversible Switching of Organic Transistors Employing a Photochromic Molecule.* MPI-P Poster Day in Mainz, Germany (November 2021).

2. Gebel, S., [redacted], [redacted], [redacted], [redacted], [redacted], [redacted] [redacted] and [redacted], *Switching Organic Transistors with Light.* MPI-P Poster Day in Mainz, Germany (November 2023).

3. Gebel, S., [redacted], [redacted], [redacted], [redacted] and [redacted], *Chain Length Dependent, Reversible Switching of Spiropyran-PMMA Blend Dielectric for Light-Gated Organic Transistors.* 2024 Materials Research Society (MRS) Spring Meeting & Exhibit in Seattle, Washington, United States of America (April 2024).

4. [redacted]* and Gebel, S.*, [redacted], [redacted] and [redacted], *Chain Length Dependent, Reversible Switching of Spiropyran-PMMA Blend Dielectric for Light-Gated Organic Transistors.* 26th International Conference on Science and Technology of Synthetic Electronic Materials (ICSM) in Dresden, Germany (*shared first authorship, June 2024).

5. Gebel, S., [redacted], [redacted] and [redacted], *Reversible Light-Induced Switching in Capacitors and Organic Transistors Employing Dihydroazulene/Vinylheptafulvene Photochromic Switches.* 26th International Conference on Science and Technology of Synthetic Electronic Materials (ICSM) in Dresden, Germany (June 2024).

6. [redacted]* and Gebel, S.*, [redacted], [redacted] and [redacted], *Reversible Switching of Spiropyran-PMMA Blend Dielectric for Light-Gated Organic Transistors.* MPI-P Poster Day in Mainz, Germany (*shared first authorship,November 2024).